MOLECULAR MECHANISMS OF IL-1 RECEPTOR ACTIVATION

A thesis submitted to The University of Manchester for the degree of Doctor of Philosophy in the Faculty of Life Sciences

2014

Adriana Barba-Montoya

Table of Contents

LIST OF FIGURES 6

LIST OF TABLES 8

ABSTRACT 9

DECLARATION 10

COPYRIGHT STATEMENT 11

ABBREVIATION LIST 12

ACKNOWLEDGMENTS 14

1 INTRODUCTION 16

1.1 INFLAMMATION 16
1.2 ACIDOSIS AND INFLAMMATION 16
1.3 IL-1 FAMILY 17
1.3.1 BIOLOGICAL ACTIVITY OF THE IL-1 FAMILY 18
1.3.2 IL-1 SIGNALLING PATHWAYS 21
1.3.3 EARLY STUDIES OF IL-1 LIGANDS 23
1.3.4 MOLECULAR STRUCTURE OF IL-1 LIGANDS 24
1.3.5 IL-1 BINDING STUDIES 28
1.3.7 MOLECULAR STRUCTURE OF IL-1RI 34
1.3.8 MOLECULAR STRUCTURE OF IL-1RACP 35
1.4 BIOPHYSICAL APPROACHES TO STUDY PROTEINS 40
1.4.1 CIRCULAR DICHROISM 41
1.4.2 NUCLEAR MAGNETIC RESONANCE SPECTROSCOPY 43
1.4.3 FLUORESCENCE SPECTROSCOPY 45
1.4.4 STATIC LIGHT SCATTERING 47

2 AIMS 49

3 MATERIALS AND METHODS 50

3.1 MATERIALS 50
3.2 BIOINFORMATICS 50
3.3 MOLECULAR BIOLOGY 50
3.3.1 CONSTRUCTS AND PLASMID VECTORS 50
3.3.2 *E. COLI* STRAINS 51
3.3.3 *KLUYVEROMYCES LACTIS* COMPETENT CELLS 52
3.3.4 TRANSFORMATION OF BACTERIAL COMPETENT CELLS 52
3.4 RECOMBINANT PROTEIN EXPRESSION IN BACTERIA 52
3.4.1 ISOLATION OF PLASMIDS FROM BACTERIAL CELLS 52
3.4.2 TRANSFORMATION OF BACTERIAL EXPRESSING CELLS 53
3.4.3 PROTEIN EXPRESSION OPTIMISATION 53

3.4.4 Recombinant protein expression in large volume cultures 54
3.4.5 Harvesting protein from bacteria culture 54
3.5 Recombinant protein expression in yeast 55
3.5.1 Isolation of plasmids from bacteria cells 55
3.5.2 Transformation of yeast cells 55
3.5.3 Expression trials in yeast cells 56
3.5.4 Recombinant protein expression in yeast cells 56
3.5.5 Harvesting protein from yeast culture 57
3.6 Protein Analysis 57
3.6.1 Analysis by SDS-PAGE 57
3.6.2 Analysis by Bis-Tris SDS-PAGE 58
3.6.3 Protein Identification by Mass Spectrometry 59
3.6.4 Recombinant protein quantification using A_{280} 59
3.6.5 SEC- multi-angle laser light scattering (MALLS) 60

3.7 PROTEIN PURIFICATION 60

3.7.1 Immobilised metal affinity chromatography 60
3.7.2 Ion exchange chromatography 61
3.7.3 Size-exclusion chromatography 62
3.7.4 Concentration of protein samples 63
3.7.5 Dialysis 63
3.8 Cell culture 64
3.8.1 Maintenance of bEND5 cells 64
3.8.2 Passaging bEND5 cells 64
3.8.3 Isolation of primary murine cortical neurons 65
3.8.4 Maintenance of primary neurons 65
3.9 Biophysical studies 66
3.9.1 ^{1}H- Nuclear Magnetic Resonance 66
3.9.2 Circular Dichroism 66
3.9.3 Intrinsic Fluorescence and Static Light Scattering 68
3.9.4 Analytical Ultracentrifugation 68
3.10 IL-1 bioactivity 68
3.10.1 IL-1 bioactivity in bEND5 cells 68
3.10.2 IL-1 bioactivity in primary cortical neurons 69
3.10.3 Effects of pH on IL-1 bioactivity in bEND5 cells 70
3.10.4 Effects of temperature on IL-1 bioactivity in bEND5 cells 70
3.10.5 ELISA 70
3.11 Graphs plot and statistical analyses 71

4 RESULTS: BIOPHYSICAL AND FUNCTIONAL CHARACTERISATION OF IL-1α AND IL-1β 72

4.1 Sequence analysis of IL-1α and IL-1β 72
4.2 IL-1 Expression 78
4.2.1 IL-1α expression in *E. coli* 78
4.2.2 IL-1β expression in *E. coli* 80
4.3 IL-1 purification 82
4.3.1 IL-1α purification 82
4.3.2 IL-1β purification 85
4.4 IL-1 characterization 88

4.4.1 IL-1 SEC-MALLS ANALYSIS 88
4.4.2 CIRCULAR DICHROISM 91
4.4.4 IL-1 ^{1}H-NMR 94
4.5 BACKGROUND ON IL-1 BIOACTIVITY 97
4.5.1 IL-1 BIOACTIVITY IN ENDOTHELIAL CELLS 98
4.5.2 IL-1 BIOACTIVITY IN NEURONES 101

SUMMARY OF BIOPHYSICAL AND FUNCTIONAL CHARACTERISATION OF IL-1α AND IL-1β 103

5 RESULTS: EXPRESSION AND CHARACTERISATION OF IL-1RACP AND IL-1RI 104

5.1 BACKGROUND 104
5.2 ANALYSIS OF IL-1RACP AND IL-1RI SEQUENCES CLONED INTO PET-15B AND PKLAC2 105
5.3 IL-1 RECEPTORS EXPRESSION IN *E.COLI* 116
5.3.1 IL-1RACP EXPRESSION IN *E. COLI* 116
5.3.2 IL-1RI EXPRESSION IN *E.COLI* 119
5.3.3 SUMMARY OF IL-1 RI AND IL-1RACP EXPRESSION IN *E. COLI* 121
5.4 IL-1RACP AND IL-1RI EXPRESSION IN YEAST 123
5.4.1 IL-1RACP EXPRESSION IN *K. LACTIS* 124
5.5 IL-1RACP PURIFICATION 127
5.4.1 ANION EXCHANGE PURIFICATION 128
5.5.2 SEC PURIFICATION 130
5.5.3 IMAC PURIFICATION 132
5.6 IL-1RACP CHARACTERISATION BY SEC-MALLS 133
5.7 SUMMARY OF THE RESULTS OF IL-1RI AND IL-1RACP EXPRESSION, PURIFICATION AND CHARACTERISATION 135

6 RESULTS: EFFECTS OF PH AND TEMPERATURE ON IL-1 137

6.1 EFFECTS OF PH IN THERMAL STABILITY 138
6.1.1 ACIDIC PH INFLUENCES THERMAL STABILITY OF IL-1β SECONDARY STRUCTURE BUT NOT IL-1α. 138
6.1.2 IL-1β INTRINSIC FLUORESCENCE DIFFERS AT ACIDIC PH 142
6.1.3 COLLOIDAL STABILITY OF IL-1 144
6.1.4 PH 6.2 HAS AN EFFECT ON IL-1β HYDRODYNAMIC PROPERTIES 149
6.1.5 EFFECTS OF PH ON IL-1α AND IL-1β THERMAL STABILITY CHARACTERISED BY ^{1}H-NMR 151
6.2 IL-1 BIOACTIVITY AT PH 6.2 157
6.3 IL-1 BIOACTIVITY AT 40°C 160

7 DISCUSSION 163

7.1 A COMPARATIVE STUDY OF IL-1α AND IL-1β 163
7.1.1 RECOMBINANT EXPRESSION OF IL-1α AND IL-1β 163
7.1.2 BIOPHYSICAL AND BIOLOGICAL CHARACTERISATION OF IL-1α AND IL-1β 166
7.1.3 DIFFERENTIAL EFFECTS OF IL-1α AND IL-1β ON DIFFERENT CELL TYPES 168
7.2 RECOMBINANT EXPRESSION OF IL-1RI AND IL-1RACP 175
7.2.1 HETEROLOGOUS EXPRESSION OF IL-1RI AND IL-1RACP IN *E. COLI* 176
7.2.2 HETEROLOGOUS EXPRESSION OF IL-1RI AND IL-1RACP 178
7.3 EFFECTS OF TEMPERATURE AND PH ON IL-1 STABILITY AND BIOACTIVITY 183
7.3.1 IL-1β BUT NOT IL-1α STABILITY IS PH-DEPENDENT 185

7.3 PRELIMINARY STUDIES OF EFFECTS OF TEMPERATURE AND PH ON IL-1α AND IL-1β BIOACTIVITY 190
7.4 CONCLUDING REMARKS 192

REFERENCES 193

APPENDIX 1: PLASMIDS AND SEQUENCES 207

APPENDIX 2: *E. COLI* STRAINS AND MEDIA 212

APPENDIX 3: BUFFERS AND SOLUTIONS 214

APPENDIX 4: SUPPLEMENTARY MATERIAL 219

List Of Figures

Figure 1.1 Signalling Pathways Activated By IL-1 22
Figure 1.2. Processing Of IL-1 Precursors 25
Figure 1.3 Molecular Structure Of IL-1β 26
Figure 1.4 Molecular Structure Of IL-1α 27
Figure 1.5 Cartoon Diagram Of IL-1RI/IL-1β Complex 29
Figure 1.6 Cartoon diagram representing interactions between IL-1RI and IL-1β 31
Figure 1.7 Cartoon diagram of the crystal structure of IL-1RI/IL-1B/IL-1RAcP complex in two views 38
Figure 1.8 Cartoon diagram representing interactions in the IL-1RI/IL-1B/IL-1RAcP ternary complex 39
Figure 1.9 Cartoon diagram representing interactions in the IL-1RII/IL-1B/IL-1RAcP ternary complex 40
Figure 1.10 Circular Dichroism 42

Figure 4.1 Vector And Construct Sequences Of Human Mature IL-1α 76
Figure 4.2 Vector And Construct Sequences Of Human Mature IL-1β 77
Figure 4.3 IL-1a Expression Trials In T7 Express *Lysy* Cells 79
Figure 4.4 Soluble and insoluble expression of IL-1α in T7 Express LysY cells 80
Figure 4.5 IL-1β Expression Trials In Origami B DE3 Cells 81
Figure 4.6 IMAC Purification Of IL-1α 83
Figure 4.7 SEC Purification Of IL-1α 84
Figure 4.8 IMAC Purification Of IL-1β 86
Figure 4.9 SEC Purification Of IL-1β 87
Figure 4.10 SEC-MALLS Analysis Of IL-1α 89
Figure 4.11 SEC-MALLS Analysis Of IL-1β 90
Figure 4.12 Circular Dichroism Analysis Of IL-1α Purified From *E.Coli* 92
Figure 4.13 Circular Dichroism Analysis Of IL-1β Purified From *E.Coli* 93
Figure 4.14 IL-1α And IL-1β Models Showing Aromatic Amino Acids Position 94
Figure 4.15 ^{1}H-NMR Spectrum Of IL-1α 96
Figure 4.16 ^{1}H-NMR Spectrum Of IL-1β 97
Figure 4.17 IL-1α And IL-1β Bioactivity In Bend5 Cells 100
Figure 4.18 IL-1α And IL-1β Bioactivity In Neurones 102

Figure 5.1 Construct sequences of the extracellular domain of human IL-1RAcP cloned into pET-15B vector 108
Figure 5.2 Construct sequences of the extracellular domain of human IL-1RAcP cloned into pKLAC2 vector 109
Figure 5.3 Construct sequences of the extracellular domain of human IL-1RAcP cloned into pKLAC2 vector with 6 x His tag 110
Figure 5.4 Construct sequences of the extracellular domain of human IL-1RI cloned into pET-15B vector 111
Figure 5.5 Construct Sequences Of The Extracellular Domain Of Human IL-1RI Cloned Into pKLAC2 Vector 112
Figure 5.6 10% SDS-PAGE Analysis Of IL-1RAcP Expression Trials In Shuffle

T7 EXPRESS *LYSY* CELLS 118
FIGURE 5.7 10% SDS-PAGE ANALYSIS OF IL-1RACP SOLUBLE AND INSOLUBLE EXPRESSION IN SHUFFLE T7 EXPRESS *LYSY* 119
FIGURE 5.8 10% SDS-PAGE ANALYSIS OF IL-1RI EXPRESSION TRIALS IN SHUFFLE T7 EXPRESS 121
FIGURE 5.9 IL-1RACP EXPRESSION IN *K. LACTIS* 125
FIGURE 5.10 IL-1RACP-HIS EXPRESSION IN *K. LACTIS* 125
FIGURE 5.11 GLYCOSYLATED PROTEIN STAINING OF IL-1RACP AND IL-1RACP-HIS CONSTRUCTS EXPRESSION 127
FIGURE 5.12 IL-1RI EXPRESSION IN *K. LACTIS* 128
FIGURE 5.13 ANION EXCHANGE CHROMATOGRAPHY OF IL-1RACP 130
FIGURE 5.14 SEC PURIFICATION OF IL-1RACP 131
FIGURE 5.15 IMAC PURIFICATION OF IL-1RACP-HIS 133
FIGURE 5.16 SEC-MALS ANALYSIS OF IL-1RACP 134

FIGURE 6.1 β-SHEET CONTENT PREDICTION OF IL-1α AND IL-1βAT INCREASING TEMPERATURES UNDER DIFFERENT PH CONDITIONS 139
FIGURE 6.2 EFFECTS OF PH IN THERMAL STABILITY OF IL-1α AND IL-1β 141
FIGURE 6.3 EFFECTS OF TEMPERATURE AND PH ON IL-1α AND IL-1β CONFORMATION 143
FIGURE 6.4 EFFECTS OF PH ON IL-1α SLS AND T_{AGG} AT 266 NM 145
FIGURE 6.5 EFFECTS OF PH ON IL-1α SLS AND T_{AGG} AT 473 NM 146
FIGURE 6.6 EFFECTS OF PH ON IL-1β SLS AND T_{AGG} AT 266 NM 147
FIGURE 6.7 EFFECTS OF PH ON IL-1β SLS AND T_{AGG} AT 473 NM 148
FIGURE 6.8 EFFECTS OF PH ON IL-1α AND IL-1β SEDIMENTATION 150
FIGURE 6.9 IL-1α TEMPERATURE-DEPENDENT ^{1}H-NMR OF METHYL REGION AT PH 5.5 152
FIGURE 6.10 IL-1α TEMPERATURE-DEPENDENT ^{1}H-NMR OF METHYL REGION AT PH 7.5 153
FIGURE 6.11 IL-1β TEMPERATURE-DEPENDENT ^{1}H-NMR OF METHYL REGION AT PH 5.5 155
FIGURE 6.12 IL-1β TEMPERATURE-DEPENDENT ^{1}H-NMR OF METHYL REGION AT PH 7.5 156
FIGURE 6.13 TEMPERATURE-DEPENDENCE OF INTENSITY OF SIX ARBITRARY CHOSEN EXAMPLE SIGNALS AT DIFFERENT PH 157
FIGURE 6.14 EFFECTS OF PH ON IL-1α AND IL-1β BIOACTIVITY 159
FIGURE 6.15 EFFECTS OF PH ON IL-1α AND IL-1β BIOACTIVITY 160
FIGURE 6.16 EFFECTS OF TEMPERATURE ON IL-1α AND IL-1β BIOACTIVITY 161

LIST OF TABLES

TABLE 1.1 EFFECTS OF IL-1 IN DIFFERENT CELL TYPES 19

TABLE 1.2 DIFFERENCES IN THE BIOLOGICAL ACTIVITY OF IL-1α AND IL-1β 20

TABLE 3.1 SUMMARY OF BIOINFORMATICS TOOLS USED IN THIS PROJECT 51

TABLE 4.1 AMINO ACID COMPOSITION OF NATIVE IL-1α AND THE CONSTRUCT EXPRESSED HERE USING THE PET-15B/IL-1α PLASMID 73

TABLE 4.2 AMINO ACID COMPOSITION OF NATIVE IL-1β AND THE CONSTRUCT EXPRESSED HERE USING THE PQE-30/IL-1β PLASMID 74

TABLE 4.3 COMPARISON OF THE THEORETICAL PROPERTIES OF IL-1α AND THE CONSTRUCT EXPRESSED HERE USING THE PET-15B/IL-1α PLASMID 75

TABLE 4.4 COMPARISON OF THE THEORETICAL PROPERTIES OF IL-1β AND THE CONSTRUCT EXPRESSED HERE USING THE PQE-30/IL-1β PLASMID 75

TABLE 4.5 SUMMARY OF EXPRESSION TRIALS FOR IL-1α IN *E. COLI* STRAINS 79

TABLE 5.1 AMINO ACID COMPOSITION OF NATIVE EXTRA-CELLULAR DOMAIN OF IL-1RACP AND THE CONSTRUCTS EXPRESSED USING THE PET-15B AND PKLAC2 PLASMIDS 106

TABLE 5.2 AMINO ACID COMPOSITION OF NATIVE EXTRA-CELLULAR DOMAIN OF IL-1RI AND THE CONSTRUCTS EXPRESSED USING THE PET-15B AND PKLAC2 PLASMIDS 107

TABLE 5.3 COMPARISON OF THE THEORETICAL PROPERTIES OF IL-1RACP AND CONSTRUCTS EXPRESSED HERE USING THE PET-15B AND PKLAC2 PLASMIDS 113

TABLE 5.4 COMPARISON OF THE THEORETICAL PROPERTIES OF IL-1RI CONSTRUCTS EXPRESSED HERE USING THE PET-15B AND PKLAC2 PLASMIDS CONSTRUCTS EXPRESSED HERE USING THE PET-15B AND PKLAC2 PLASMIDS 114

TABLE 5.5 SUMMARY OF EXPRESSION TRIALS FOR IL-1RACP IN *E. COLI* STRAINS 117

TABLE 5.6 SUMMARY OF EXPRESSION TRIALS FOR IL-1RI IN *E. COLI* STRAINS 120

TABLE 5.7 IL-1RACP PLASMIDS USED IN K. LACTIS 136

Total number of words: 64,484

Abstract

The University of Manchester

Adriana Barba-Montoya

PhD

MOLECULAR MECHANISMS OF IL-1 RECEPTOR ACTIVATION

2014

Interleukin-1 (IL-1) is a pro-inflammatory cytokine that plays an important role in inflammatory responses to injury and infection, both, systemically and within the central nervous system. There are two IL-1 ligands, IL-1α and IL-1β, which bind to the interleukin 1 receptor type I (IL-1RI) activating multiple pathways that lead to the expression of acute phase and pro-inflammatory proteins. Although IL-1α and IL-1β differ in their amino acid sequence (sharing only 26% homology), they are structurally similar (both protein structures are β-barrel comprised of β-sheets), exert their actions through IL-1RI and are thought to exert similar biological activity. However, in recent years, some differences of action have been observed. Briefly, it has been suggested that IL-1β is more potent when acting in the brain, whereas IL-1α has been proposed to be more potent when acting systemically. Despite considerable research efforts, molecular mechanisms responsible for the observed differential effects remain unclear. The aim of this work is to carry out a comparative study of the effects of temperature and pH on the biophysical properties and bioactivities of IL-1α and IL-1β. The thermal stability of both ligands has been investigated using 1D NMR, circular dichroism and fluorescence and all are consistent in that IL-1α and IL-1β retain their folded conformation at increased temperature. Additionally, we found that pH also has a significant influence in their conformation. In this study, we characterized the biophysical properties and bioactivities of IL-1α and IL-1β under different conditions

Declaration

No portion of the work referred to in the thesis has been submitted in support of an application for another degree or qualification of this or any other university or other institute of learning

Copyright Statement

Abbreviation List

3D	Three dimension
aa	Amino acid
Ab	Antibody
α-MF	α-mating factor
APS	Ammonium persulfate
AUC	Analytical ultracentrifugation
BBB	Blood brain barrier
BCM	Barycentric mean
C	Celsius
CD	Circular Dichroism
cm	Centimetre
CNS	Central nervous system
CV	Column volume
CV	Column volume
deg	Degree
DMEM	Dulbecco's modified eagle medium
dmol	Decimol
DTT	Dithiothreitol
E. coli	*Escherichia coli*
EDTA	Ethylenediaminetetaacetic acid
FCS	Foetal calf serum
HBSS	HEPES-buffered salt solution
i.e.	In example
ICAM	Intracellular adhesion molecule
icv	Intracerebroventricular
IEX	Ion exchange
Ig	Immunoglobulin
IκB	Inhibitor of NFκB
IL-1	Interleukin 1
IL-1ra	Interleukin 1 receptor antagonist
IL-1RAcP	Interleukin 1 receptor accessory protein
IL-1RAcP-His	Interleukin-1 receptor accessory protein with 6 x His tag
IL-1RI	Interleukin 1 receptor type I
IL-1RII	Interleukin 1 receptor type II
IL-1α	Interleukin 1 alpha
IL-1β	Interleukin 1 beta
IMAC	Immobilised metal affinity chromatography
IRAK	Interleukin-1 associated kinase
IRF-3	Interferon regulatory factor-3
JAM	Junctional adhesion molecule
K. lactis	*Kluyveromyces lactis*
kDa	Kilo Daltons
L	Litre
LAF	Lymphocyte activating factor
LB	Luria-Bertani broth medium
LC-MS/MS	Liquid chromatography coupled to tandem mass spectrometry

LP	Lysis pellet
LPS	Lipopolysaccharide
LSN	Lysis supernatant
LTP	Long term potentiation
M	Molar
Mcfp-3	*Mytilus californianus* foot protein three
MES	2-(*N*-morpholino)ethanesulfonic acid
mg	Milligram
mL	Millilitre
MM	Minimal media
mM	Millimolar
MOPS	3-(N-morpholino)propanesulfonic acid
MS	Mass spectrometry
MRW	Mean residue weight
MWCO	Molecular weight cut-off
NBM	Neuro basal media
ng	Nanogram
NLR	NOD-like receptor
nm	Nanometre
NMR	Nuclear magnetic resonance
OD	Optical density
PBMC	Peripherial blood mononuclear cells
PBS	Phosphates Buffered Saline
PDS	Plasma derived serum
PECAM	Platelet/endothelial-cell adhesion molecule
pg	Picogram
PHA	Phytohemagglutinin
ppm	Parts per million
rpm	Revolutions per minute
S	Sedimentation coefficient
SDS	Sodium dodecyl sulphate
SDS-PAGE	Sodium dodecyl sulphate polyacrylamide gel electrophoresis
SEC	Size exclusion chromatography
SEC-MALLS	Size exclusion chromatography-Multiangle laser light scattering
SLS	Static light scattering
T_{agg}	Onset of aggregation
TEMED	Tetramethylethylenediamine
TIR	Toll-like interleukin 1 receptor domain
T_m	Melting temperature
U	Units
VEGF	Vascular endothelial growth factor
WB	Whole blood
wt	Wild type
YCB	Yeast-Carbon-Based
YP	Yeast-peptone
YPGal	Yeast-Peptone-Galactose
YPGlu	Yeast-Peptone-Glucose
μg	Microgram
μL	Microliter

Acknowledgments

I would like to thank:

My supervisors Dr. Alexander Golovanov and Dr. Emmanuel Pinteaux, for giving me the opportunity of getting involved in this project, as well as for their invaluable guidance throughout my project.

To A. Golovanov's group: Richard Tunnicliffe, Uybach Vo, and Stacy Panova for their help and advice with NMR experiments, and Priscilla Kheddo for her help and advice with Optim experiments.

To Emmanuel Pinteaux's group: Catherine Savage, Christine Cowsill and Athina Papaemmanouil for their help on mice handling, isolation of cortical neurons and cell culture advice.

To all people that work in the ground laboratory at the MIB for their invaluable help and advices in all matters lab-related, especially Bella and McKenzie's groups.

To Tim Eyes for his help and advice on protein work and PyMOL use.

To Andrew Currin for his help and advice on lab work, circular dichroism and thesis writing.

Special thanks to Dr. Jordi Bella and Dr. Eddie McKenzie whose wise advise on experiments were too much appreciated

Finally, I would like to thank the Mexican National Council of Science and Technology (CONACYT) and the Bank of Mexico through its program FIDERH for funding my project

This thesis is dedicated first of all to my beloved parents Tere and Toño and to my brother José Antonio whose love and encouragement have always been important in my life.

To my partner Ricardo whose love and support were outstanding throughout my PhD and helped me to keep going even in the hardest moments.

To my family

1 Introduction

1.1 Inflammation

Inflammation can be defined as a complex, nonspecific reaction of vascularised tissues that protects and repairs tissues against injury or infection (Larsen and Henson, 1983, Abbas and Lichtman, 2004). It is characterised by redness, swelling with heat and pain and loss of function caused by the accumulation and activation of leucocytes and plasma proteins (Ryan and Majno, 1977, Larsen and Henson, 1983, Abbas and Lichtman, 2004). This complex reaction is regulated by diverse molecules known as mediators of inflammation, such as enzymes, chemokines, eicosanoids and cytokines. These molecules are capable of enhancing blood flow, increasing vessel permeability and inducing migration of inflammatory cells to the infection/injury site (Larsen and Henson, 1983). Given its pro-inflammatory properties, interleukin-1 (IL-1) is one of the most studied mediators of inflammation. IL-1 was first known as leukocytic pyrogen given its ability to induce fever (Dinarello, 2010). IL-1 also induces leukocyte migration by activating endothelial junctional molecules such as the platelet/endothelial-cell adhesion molecule 1 (PECAM1) (Muller et al., 1993), the junctional adhesion molecule A (JAM-A) (Del Maschio et al., 1999) and the intracellular cell adhesion molecule 2 (ICAM2) (Huang et al., 2006).

1.2 Acidosis and inflammation

Another characteristic of inflammation is acidosis, which is due to either an increase of lactic-acid production by infiltrating neutrophils or to bacterial by-products during infection (Grinstein et al., 1991, Lardner, 2001). Acidosis has been observed in a number of diseases in which IL-1 is also involved, i.e. brain pH has been shown to fall from 7 to 6.2 during ischemia (Nemoto and Frinak, 1981, Yamasaki et al., 1995). Moreover, pH of tumours have been found to be as low as 6.8 whereas pH of normal

tissue is 7.4 (Ashby, 1966, Kasza, 2013, Dinarello, 2014, Wang et al., 2014) and the pH of the lower airway in patients with asthma has been shown to be 5.23 which is two log orders lower than that of healthy patients (7.65) (Hunt et al., 2000, Wei-xu et al., 2014). Despite this, it has been observed that acidosis can negatively affect many cellular responses such as DNA synthesis, cAMP and calcium levels and several enzyme activities (Lardner, 2001) causing serious adverse effects (Arnett, 2010, Close et al., 2013, Gasser et al., 2014, Niu et al., 2014). Several publications suggest that a decrease in local pH does not negatively affect elements of the immune system. For example, Vermeulen and colleagues suggested that extracellular acidosis improves antigen-presenting capacity of murine bone marrow-derived dendritic cells, as their endocytic capacity was up regulated under acidic conditions (Vermeulen et al., 2004). Extracellular acidosis has also been shown to trigger human neutrophil activation (Trevani et al., 1999) through the phosphorylation of Akt, ER1/2 and JNK (Martinez et al., 2006). Furthermore, it has been suggested that in an acidic microenvironment, IL-1β is processed through an alternative pathway independently of NLRP3 and caspase 1 (Edye et al., 2013).

1.3 IL-1 family

The IL-1 family is a group of soluble proteins that are structurally and functionally different (March et al., 1985, Boutin et al., 2003). This group consists of 11 members (Sims and Smith, 2010). The best characterised are the two ligands, IL-1α and IL-1β, and the antagonist IL-1ra (Luheshi et al., 2009b). IL-1 ligands as well as the antagonist are able to bind to 2 different receptors: IL-1 type 1 receptor (IL-1RI) and IL-1 type 2 receptor (IL-1RII), which belong to the IL-1 receptor family. Another member of the IL-1 receptor family is an accessory protein that associates with the

receptors, the IL-1RAcP (Wesche et al., 1997b, Cullinan et al., 1998, Lang et al., 1998, Malinowsky et al., 1998, Sims and Smith, 2003).

Several roles in the innate and adaptative immune response of this family of cytokines have been described; it is well known that they participate in the inflammatory and host-defence responses to injury and infection, both systemically and within the central nervous system (CNS) (O'Neill, 2008, Dinarello, 2009). Although IL-1 has been shown to exert protective effects, it has been observed that its overproduction can lead to pathological symptoms, such as fever, hypotension and modulation of sleep (Schreuder et al., 1995), and for that reason, its involvement in several diseases and disorders has been widely studied. CNS disorders involving IL-1 include stroke, epilepsy, Parkinson's and Alzheimer's diseases (Allan et al., 2005), as well as hepatic acute response, metastases, angiogenesis, rheumatoid arthritis, leukemias and HIV (Schreuder et al., 1995, Auron, 1998).

1.3.1 Biological activity of the IL-1 family

Given that IL-1α and IL-1β exert similar responses when bound to their receptor, IL-1α and IL-1β together are known as IL-1. As it is an important regulator of the immune response, IL-1 biological activity is diverse and involves many different cell types (see Table 1.1). IL-1 exerts its effects through IL-1RI but not IL-1RII, due to the short cytoplasmic domain of IL-1RII (Sims et al., 1993). Thus, IL-1RII is believed to act as a decoy receptor by binding to the excess of IL-1α or IL-1β, and by recruiting IL-1RAcP from the signalling complex (McMahan et al., 1991b).

Despite that IL-1α and IL-1β are believed to exert similar biological actions (Anforth et al., 1998), differences in their activity have been reported (Andre et al., 2005; Horai et al., 1998; Tsakiri et al., 2008) (Table 1.2). For example, although

Table 1.1 Effects of IL-1 in different cell types

Cell type	Effect	Example references
T-lymphocytes	Proliferation Activation	(Dukovich et al., 1986) (Ben-Sasson et al., 2013)
B-lymphocytes	Maturation Proliferation Activation	 (Hoffmann et al., 1984) (Howard et al., 1983)
Monocytes	Activation	
Fibroblasts	Proliferation Induction of IL-6 synthesis, prostaglandins and granulocyte-macrophage colony-stimulating factor	 (Schmidt et al., 1982) (Elias and Lentz, 1990) (Lin et al., 1992)
Neutrophils	Proliferation Recruitment	(Tewari et al., 1990) (Rogers et al., 1994)
Platelets	Proliferation	(Tewari et al., 1990)
Astrocytes	Mitosis Proliferation Astrogliosis RhoA signalling pathway Production of vascular endothelial growth factor (VEGF), secondary inflammatory mediators, interferon regulatory factor-3 (IRF-3) and TNFα	 (Chung and Benveniste, 1990) (John et al., 2004) (Rivieccio et al., 2005) (Pinteaux et al., 2009) (Argaw et al., 2006)
Microglia	Induction of expression of adhesion molecules, chemokines, endothelin-1, NO and granulocyte-macrophage colony-stimulating factor	(Thery and Mallat, 1993) (Pinteaux et al., 2009) (Sieff et al., 1987)
Oligodendrocytes	Differentiation Maturation	(Mason et al., 2001) (Vela et al., 2002)
Neurons	Regulation of sleep, memory, long term potentiation (LTP), fever and sickness behaviour Increment of neuronal susceptibility to hypoxic and axcitotoxic injury	(Pinteaux et al., 2009) (Katsuki et al., 1990) (Allan et al., 2005)

having the same pyrogenic activity when injected intraperitoneally in rats, IL-1β is more effective at inducing fever when injected intracerebroventricularly (icv) (Anforth et al., 1998). This is consistent with the findings that IL-1β also induces fever after local inflammation, as observed with IL-1β deficient (gene deletion) mice injected subcutaneously with turpentine (Horai et al., 1998). These mice did not develop fever and did not secrete glucocorticoids after subcutaneous injection with turpentine, whereas IL-1α deficient mice did. It has also been shown that IL-1β is more potent at inducing IL-6 synthesis in neurones (Tsakiri et al., 2008). On the other hand, IL-1α is more effective at inducing TNFα synthesis in epidermal cells (Andre et al., 2005).

Table 1.2 Differences in the Biological Activity of IL-1α and IL-1β

IL-1α		**IL-1β**	
Effect	**Reference**	**Effect**	**Reference**
More effective at inducing TNFα production for epidermal cells	(Beissert et al., 1998)	Mediates T-cell dependent antibody production	(Nakae et al., 2001a)
		More effective at inducing fever when injected icv	(Anforth et al., 1998)
		Induction of nerve growth factor release form astrocytes	(Juric and Carman-Krzan, 2001)
Mediates contact allergen T-cell activation induced by contact hypersensitivity in mice	(Nakae et al., 2001b)	More potent at inducing IL-6 release from glia at high doses	(Andre et al., 2005)
		More potent at inducing synthesis of IL-6 in neurons	(Tsakiri et al., 2008)
		Induction of fever after local inflammation	(Horai et al., 1998)

1.3.2 IL-1 signalling pathways

IL-1 receptor signal transduction is strongly activated in response to infection, tissue injury or stress (Jensen et al., 2000), occurring within 15 minutes, even when just a few receptors per cell (about 10 receptors) are occupied by their ligands (Sims et al., 1993, Auron, 1998). IL-1RI drives this strong response by activating multiple parallel pathways that synergize to trigger the IL-1 effects (Auron, 1998), leading to the transcription of genes encoding acute phase and pro-inflammatory proteins (Huang et al., 1997, Auron, 1998). The most studied pathways activated by IL-1 are three different mitogen-activated protein (MAP) kinase pathways p38, extracellular signal-regulated kinase 1/2 (ERK1/2) and c-Jun N-terminal kinase (JNK) (Brikos et al., 2007), as well as the activation of the nuclear transcription factor κB (NFkB) (Auron, 1998, Andre et al., 2005). In fact the nature of the activated pathways depends on the tissue or cell system on which IL-1 is acting. Thus, it has been reported that IL-1 is capable of activating ERK1/2 in mixed glia cells (Andre et al., 2005), but not in human glomerular mesangial cells where it activates the JNK pathway (Uciechowski et al., 1996).

The signalling cascade initiates with the binding of IL-1 to IL-1RI in the extracellular space, and the subsequent recruitment of IL-1RAcP, that leads to internalization of IL-1 (Huang et al., 1997, Korherr et al., 1997). IL-1RI and IL-1RAcP are not constitutively associated even though they are in close proximity on the cell surfaces (Greenfeder et al., 1995a). The intra-cytoplasmic portion of IL-1RI as well as that of IL-1RAcP, are domains that belong to the Toll like receptor (TLR) family known as Toll/interleukin-1 (IL-1) receptor (TIR) (O'Neill and Bowie, 2007). The formation of the IL-1/IL-1RI/IL-1RAcP complex leads to the recruitment of the adapter protein MyD88 to the TIR domains of IL-1RI and IL-1RAcP (Wesche et al.,

1997a). Subsequently, the interleukin-1 receptor-associated kinases 1 and 2 (IRAK1 and IRAK2) are recruited (Huang et al., 1997) attracting the tumour necrosis factor receptor-associated factor (TRAF) to the complex and the signalling cascade progresses to the activation of p38, JNK or to the phosphorylation of the inhibitor of NFκB (IκB), which is then degraded permitting the translocation of the activated NFκB to the nucleus where it activates expression and the subsequent secretion of IL-6, IL-8, cell adhesion molecules and other inflammatory mediators (Figure 1.1) (Auron, 1998, Jensen et al., 2000, Boch et al., 2003, Andre et al., 2005, O'Neill and Bowie, 2007).

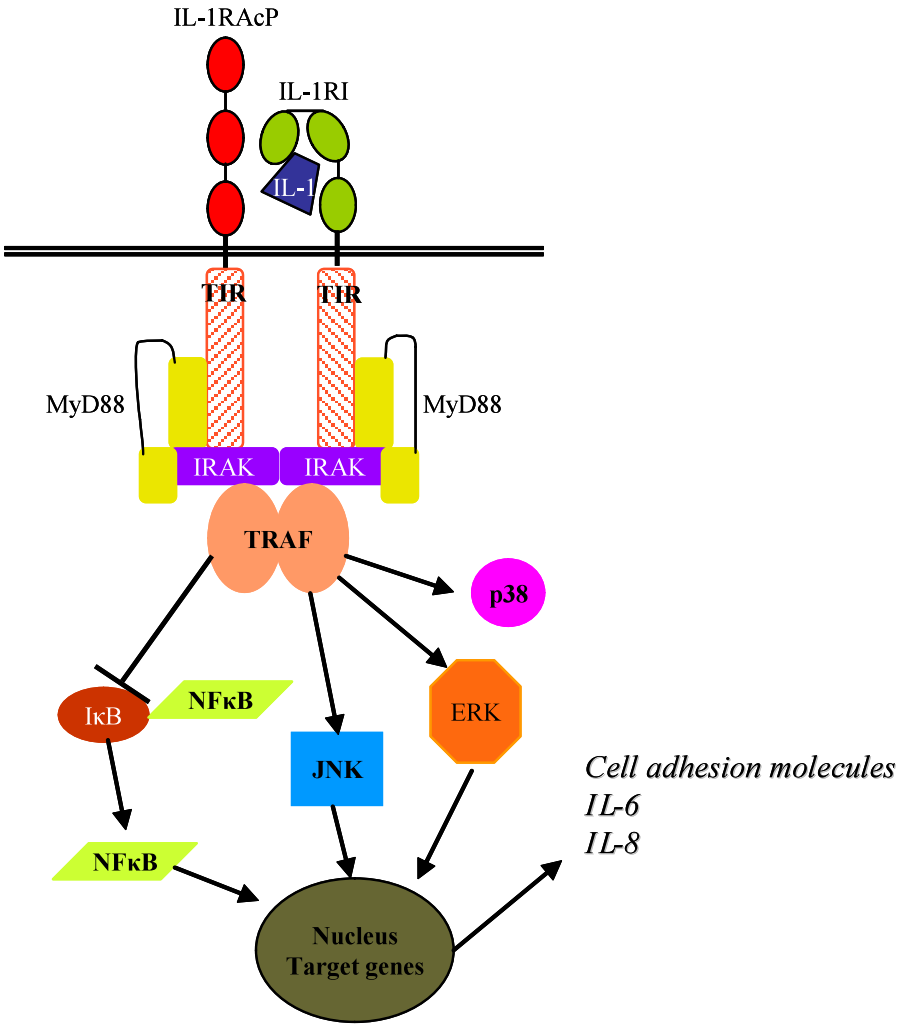

Figure 1.1 Signalling pathways activated by IL-1. Modified from Auron, 1998; Boch et al, 2003 and O'Neill and Bowie, 2007

1.3.3 Early studies of IL-1 ligands

Since its discovery in the middle 40's as a factor that caused fever, IL-1 was first known as "leukocytic pyrogen" (LP), "endogenous pyrogen" (EP), and "lymphocyte activating factor" (LAF) (Dinarello, 2010). Therefore, the attempts to purify and characterise these factors were diverse and it was not before 1974 when Murphy and Wood reported that the rabbit pyrogen had a molecular weight of 14-15 kDa with an isoelectric point (*pI*) of 7 (Murphy et al., 1974). However, in the same year, Dinarello's group found two distinct pyrogenic proteins with a molecular weight between 15-20 kDa and different *pI*: 7, and 5 (Dinarello et al., 1974). Three years later, in 1977, Dinarello and colleagues reported for the first time the purification of the LP, and found that this 17 kDa protein had a *pI* of 7 (Dinarello et al., 1977, Dinarello and Wolff, 1977). By 1979, Aarden et al. proposed the term *Interleukin* to name factors that have the ability to act as communication signals between leukocytes (Aarden, 1979) and named the lymphocyte activating factor (LAF) as interleukin-1 (IL-1); two years later, Dinarello an colleagues demonstrated that LAF and LP were the same molecule (Rosenwasser et al., 1979).

In 1985, March et al., isolated, cloned and sequenced for the first time the cDNA of two different proteins which had the same activity as IL-1, and they called them IL-1α and IL-1β (March et al., 1985). In this study, they discovered that IL-1α and IL-1β are synthesised as larger precursors that are proteolytically cleaved to active forms, and that the precursor form of IL-1α is active, in contrast to the precursor form of IL-1β. Sequences analysis of the ligands demonstrated that, at nucleic acid level IL-1α and IL-1β are 45% homologous, whilst at the protein level they only share 26% homology, having a higher degree of homology in the amino-terminal residues 75-80 (March et

al., 1985). These findings are consistent with the two pyrogenic proteins with different *pI* found by Dinarello and colleagues, as mentioned above.

Even though IL-1α and IL-1β are 17 kDa proteins that seem to exert the same biological activity, they differ in diverse ways: their nucleic acid and amino-acid sequences (March et al., 1985), their *pI* (Dinarello et al., 1974) and their sensitivity to heat (Krakauer, 1985). Nevertheless, it has been stated that they exhibit similar circular dichroism (CD) spectra (Graves et al., 1990).

1.3.4 Molecular structure of IL-1 ligands

IL-1β is synthesized as a 31 kDa (269 residues) inactive precursor and is cleaved by the IL-1β converting enzyme (caspase-1) (Thornberry et al., 1992), generating the 153 carboxyl-terminal active fragment (Figure 1.2-B) (March et al., 1985, Priestle et al., 1988).

IL-1β is composed of 12 β-strands, 6 of these β-strands form a barrel closed in one end by the other 6 strands, thus forming a β-barrel structure (Priestle et al., 1988, Finzel et al., 1989) (Figure 1.3). The crystallographic refinement of IL-1β showed that this molecule looks like a tetrahedron whose triangular faces are formed by three antiparallel β-strands, and its edges are formed by 2 antiparallel β-strands that form hydrogen bonds along their full length. Between strands 4 and 5 there is a β-bulge, comprising residues Gln 48-Asn-53. It can also be seen that one of the tetrahedron's vertices is elongated into a 6 antiparallel β-barrel.

Similar to IL-1β, IL-1α is synthesized as a 31 kDa (270 residues) precursor that is biologically active and cleaved by a calcium-activated neutral protease (CANP) also known as calpain (Kobayashi et al., 1990). The biological activity lies in the 154

carboxy-terminal amino acids from the 270 residues precursor (see figure 1.2-A) (March et al., 1985, Gubler et al., 1986).

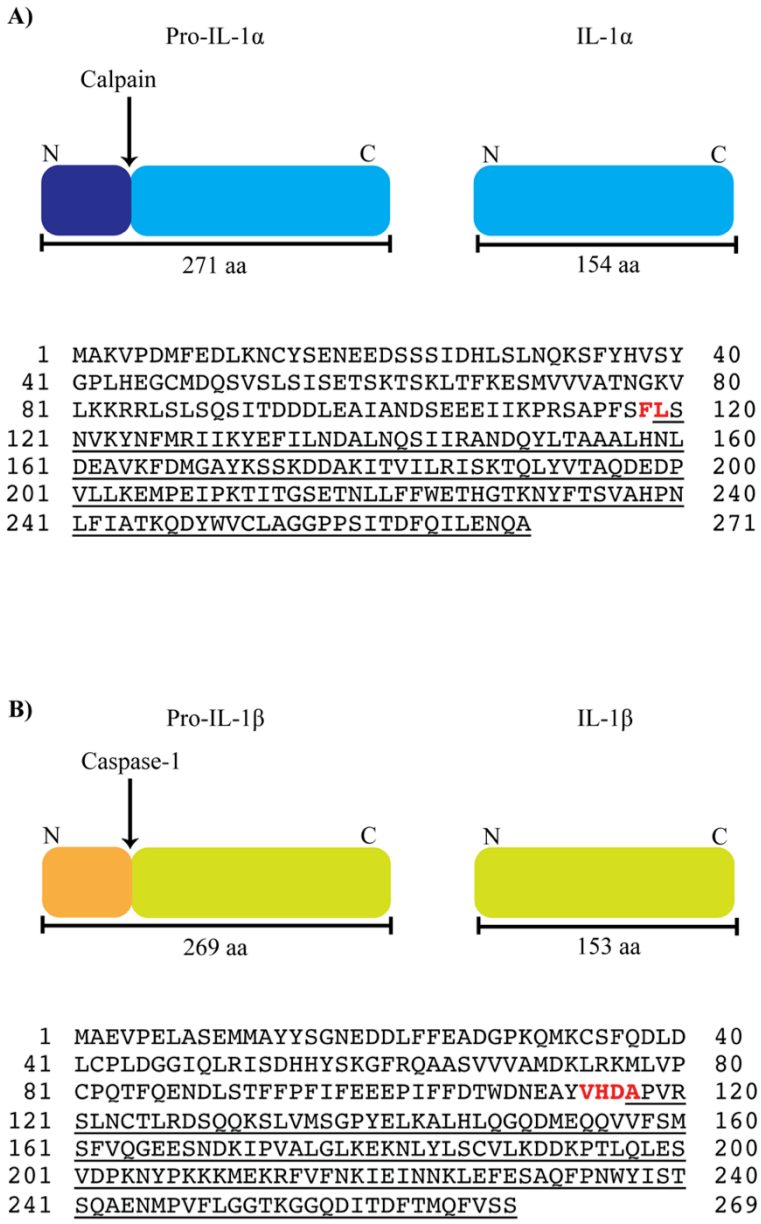

Figure 1.2. Processing of IL-1 precursors. **A)** Calpain cleaves pre-IL-1α at Phe118-Leu119 (Kobayashi et al., 1990) (highlighted in red), realising the carboxy-terminal 154 residues where the activity lies (underlined) (NCBI Reference sequence NP_000566.3). **B)** Caspase-1 cleaves pre-IL-1β at Asp116-Ala117 (Zhang et al., 1998) (highlighted in red), releasing the active 153 aa-peptide (underlined) (NCBI Reference sequence NP_000567.1). Taken and modified from Sims and Smith, 2010

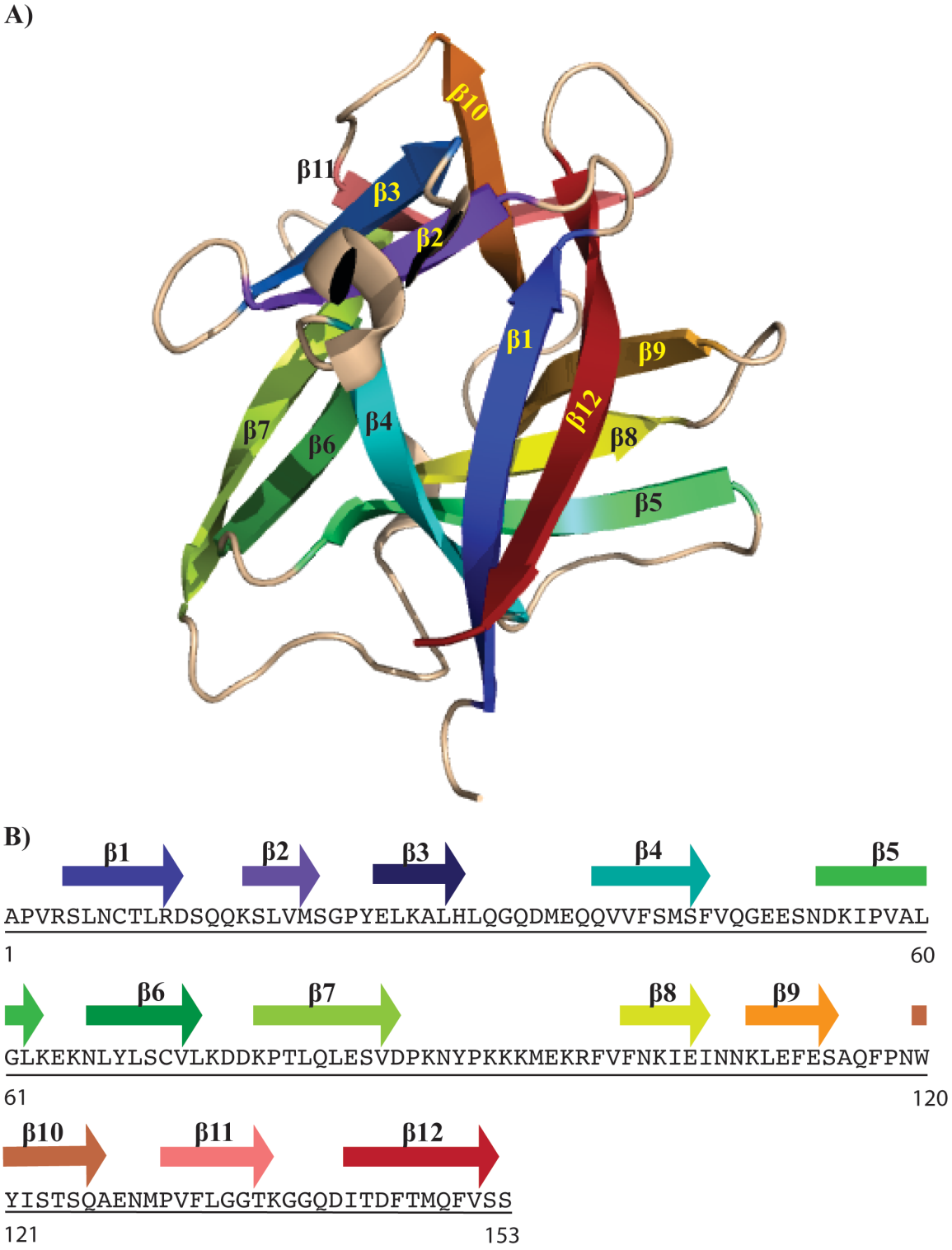

Figure 1.3 Molecular structure of IL-1β. A) Cartoon diagram of IL-1β showing the characteristic β-trefoil structure generated with MacPyMOL. β-sheets are highlighted in different colours. **B)** IL-1β sequence showing β-sheets (arrows). Same colour code as in **A)**. PDB ID: 2I1B from Priestle et al. 1989.

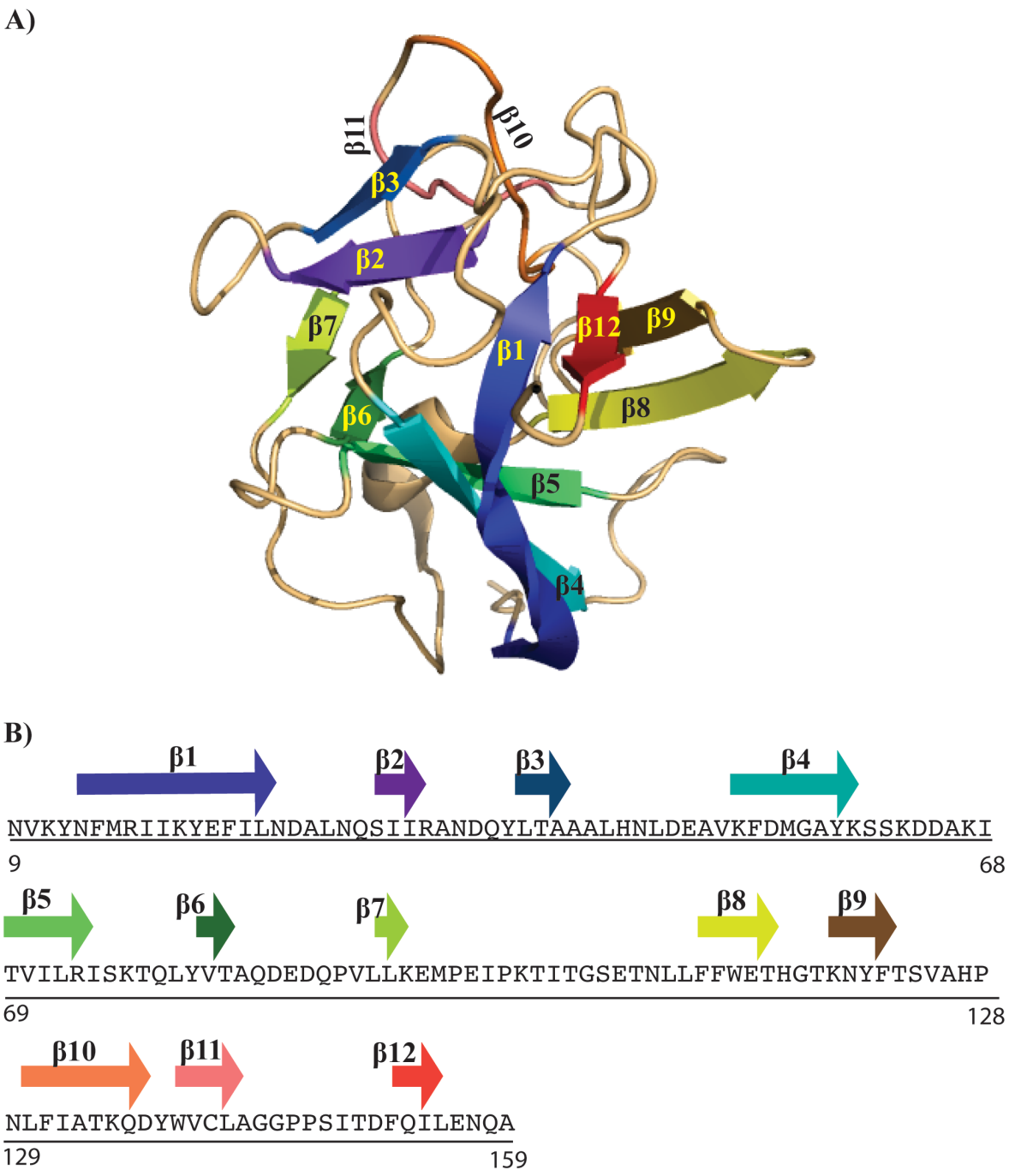

Figure 1.4 Molecular structure of IL-1α. Cartoon diagram of IL-1α showing the characteristic β-trefoil structure. Structure generated with MacPyMOL. β-sheets are highlighted in different colours. **B)** IL-1α sequence showing β-sheets (arrows). Same colour code as in **A)**. PDB ID: 2KKI (Chang et al., 2010),

The overall structure of IL-1α is similar to that of IL-1β. As demonstrated by crystallography studies (Graves et al., 1990) and later confirmed by NMR analysis (Chang et al., 2010), IL-1α showed that its secondary structure is bowl-like, consisting of antiparallel β-sheets, of which the core is a six-stranded β-barrel that is closed at one end by another β-strand (Graves et al., 1990) (Figure 1.4). As IL-1β, there is also a β-bulge between strands 4 and 5. However, contrary to IL-1β structure, the β-barrel core comprises a short β-strand consisting of residues 6-10 near the N-terminus, another β-strand (residues 97-99) and two turns of 3_{10} helix formed by residues 101-105, placing the N-terminus of the structure at a different location (Graves et al., 1990). It is worth mentioning that residues in the N-terminus are important for maintaining structure, since they form one β-barrel. Since deletion of residues 4-10 of N-terminus reduces IL-1β bioactivity, it has been suggested that the N-terminus is important to confer bioactivity by maintaining the overall structure of the molecule (Finzel et al., 1989, Graves et al., 1990, Greenfeder et al., 1995b).

1.3.5 IL-1 binding studies

The IL-1RI/IL-1β binary complex structure was first solved by Vigers and colleagues in 1998 (Figure 1.5), yet, to date, the IL-1RI/IL-1α binary complex has not been solved. Nevertheless, different approaches have been used to identify which residues in IL-1β and IL-1α are implicated on binding to IL-1 receptors as well as which residues are important for activity.

Amino acid position analyses have also been carried out with the purpose of elucidating which residues are important for receptor binding and which residues are important for maintaining the structure. It has been found that of the 80 non-glycine positions that are invariant, 2 Pro, as well as 56 residues are important for structure because of their buried side chains. Of the 20 residues that are invariant across IL-1α

and IL-1β sequences, none of them are surface residues with 10 in the hydrophobic core and 8 buried elsewhere in the structure, implying that both molecules may bind to their receptor in different ways (Finzel et al., 1989, Priestle et al., 1989, Greenfeder et al., 1995b).

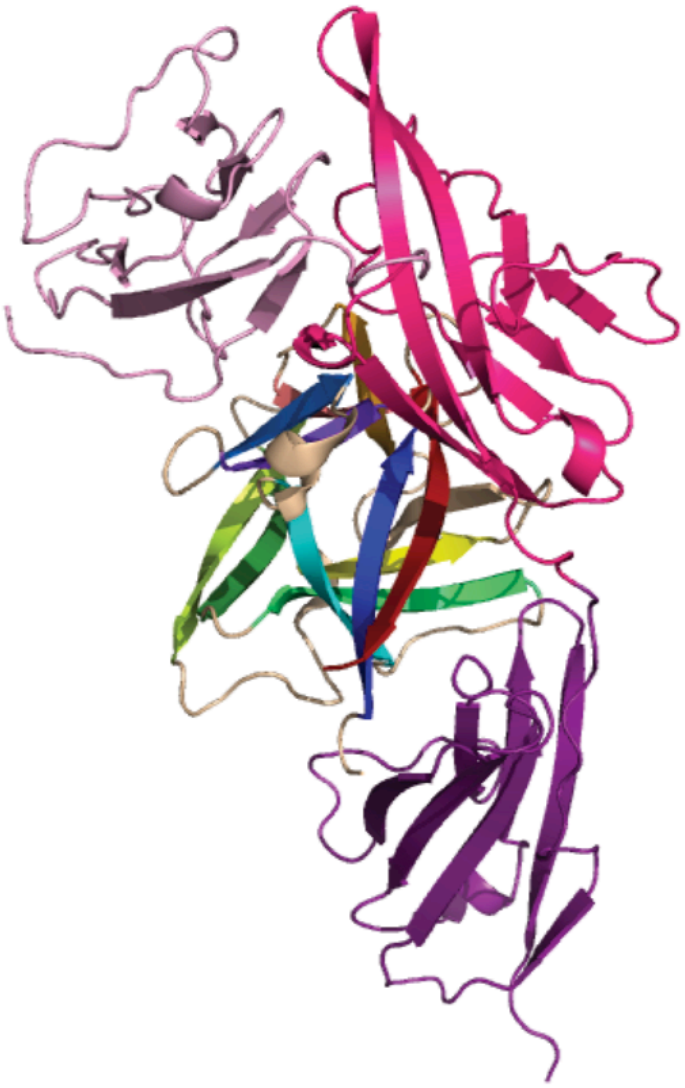

Figure 1.5 Cartoon diagram of IL-1RI/IL-1β complex solved by molecular replacement and multiple isomorphus replacement (MIR) (Vigers et al., 1997). Domain 1 on IL-1RI is highlighted in light pink, domain 2 in pink and domain 3 purple. IL-1β β-sheets are coloured with the same code as in figure 1.3. PDB ID: 1ITB. Figure generated with MacPyMOL

Further crystal studies of IL-1β bound to IL-1 receptor type I have shown that this cytokine has two binding sites: A and B (Figure 1.6-A). Site A consists of 25 residues (11, 13-15, 20-22, 27, 29-36, 38, 126-131, 147 and 149) and lies on one side of the β-barrel. This binding site contacts immunoglobulin-like domains 1 and 2 of IL-1RI (Figure 1.6-B) mainly by residues Arg 11 and Gln 15 that bind to domain 2, and His 30 and Gln 32 that bind to the junction between domain 1 and 2. On the other hand, site B (Figure 1.6-C) consists of 21 residues (4, 6, 46, 48, 51, 53, 54, 56, 92-94, 103, 105, 106, 108, 109, 150 and 152), four of which are hydrophobic (Leu 6, Phe 46, Ile 56 and Phe 150) and are surrounded by hydrophilic residues (Arg 4, Gln 48, Glu 51, Asn 53, Lys 93, Glu 105 and Asn 108) that form a horseshoe like structure around the hydrophobic core. Site B is localized on the top of the β-barrel and only contacts domain 3. Both binding sites have salt bridges (10 and 13), as well as seven hydrogen bonds (Vigers et al., 1997). Residues Arg 4, Leu 6, Phe 46, Ile 56, Lys 93, Lys 103 and Glu 105 in IL-1β were also found to be essential for binding (Labriola-Tompkins et al., 1991).

To identify amino acids involved in IL-1 bioactivity, Greenfeder and co-workers (1995b) substituted certain residues on IL-1ra with their corresponding residues on IL-1β. Thereby, they identified first, that the β-bulge (that is also present in IL-1α, but not in IL-1ra) is involved in biological activity of ligands. The ability of ligands to associate with IL-1RAcP is important for signal transduction and that the lack of biological activity of IL-1ra is due to its failure in recruiting IL-1RAcP. For example, substitution of Lys 145 in IL-1ra with Asp (Asp 145 in IL-1β) confers agonist activity to IL-1ra. Moreover, this agonist activity conferred to IL-1ra was inhibited by the antibody anti-muIL-1RAcP. Thus, it was suggested that Asp 145 is involved in interaction of IL-1β with IL-1RAcP, and hence, with its ability to activate IL-1

signalling pathways. Furthermore, Tyr 147 and Cys 116 are crucial amino acids for IL-1 bioactivity, since substituting them leads to complete loss of activity. However, they are not conserved in IL-1α, so their participation in agonist activity was unclear (Greenfeder et al., 1995b). In a more recent work, Thomas and colleagues (2012) elucidated the ternary complex structure of IL-1RI/IL-1β/IL-1RAcP allowing a more precise mapping of interacting residues. This work will be described further in subsequent sections.

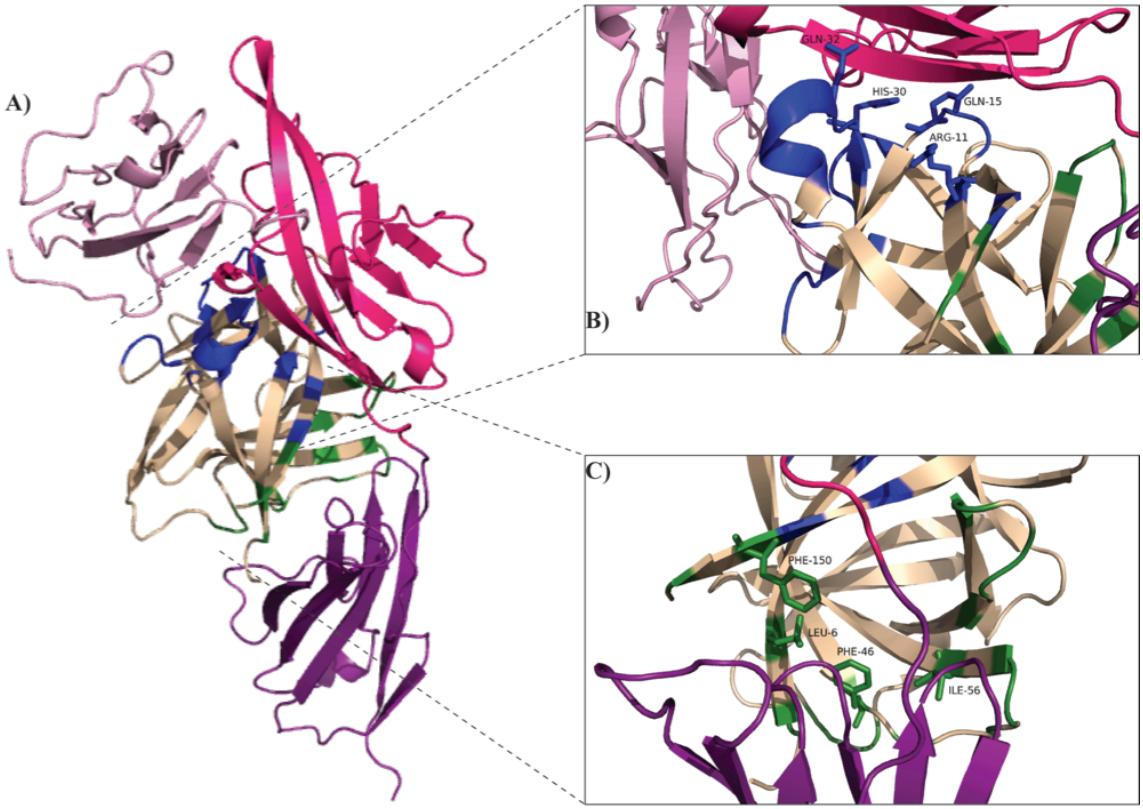

Figure 1.6 Cartoon diagram representing interactions between IL-1RI and IL-1β. A) IL-1RI/IL-1β complex (PDB ID: 1ITB). Domains in IL-1RI are coloured as in Figure 1.5. Binding site A in IL-1β is highlighted in blue; binding site B is highlighted in green.

Through site-directed mutagenesis studies, IL-1α has also been suggested to possess two binding sites (A and B) (Yamayoshi et al., 1990, Labriola-Tompkins et al., 1993, Evans et al., 1995). Seven amino acid residues (Arg 12, Ile 14, Asp 60, Asp 61, Ile 64, Lys 96 and Trp 109) were identified to be crucial for IL-1α binding to IL-1RI, since substitutions of these amino acid residues resulted in loss of binding to IL-1RI (Labriola-Tompkins et al., 1993). Furthermore, based on IL-1α crystallographic studies the side chains of these residues were found to be clustered in one region of IL-1α and exposed on the surface of the protein. Likewise, sequence alignment with IL-1β suggested that IL-1RI recognises homologous regions in both ligands (Labriola-Tompkins et al., 1993). Thus IL-1α binding sites have been suggested to be similar to those of IL-1β: site A is present on one side of the β-barrel and is expected to make contact with IL-1RI domains 1 and 2. Site B is on the top of the β-barrel and is expected to bind only with domain 3 (Evans et al., 1995, Vigers et al., 1997). However, IL-1α conserves only two or three residues that had been shown to be crucial for binding in IL-1β. Mutagenesis studies have shown that a substitution of IL-1β His 30 with Arg considerably decreases its affinity to IL-1R1. However, substitutions of His present in IL-1α do not affect IL-1α binding affinity. These studies suggest that amino acids involved in receptor-binding differ from one molecule to the other (Gronenborn et al., 1988, Labriola-Tompkins et al., 1991), and these differences may be responsible for the differential biological activity observed in IL-1α and IL-1β.

Amino acid residues involved in IL-1α activity have also been identified by mutagenesis studies carried out by Kawashima and co-workers (1992). Leu 24-Asp 26, as well as residues 26 and 151 (which are close together in the 3D structure of IL-1α) were shown to be important for the biological activity of this cytokine. These regions correspond to Leu10-Asp12, and residues 12 and 145 of IL-1β. By substitution of

amino acid residues, they also observed that the charge and size of amino acids, as well as their position are important factors for IL-1α biological activity. For example, the acidic and smaller amino acids are less or not involved in biological activity; uncharged larger amino acids, such as Phe and Tyr are involved in the lymphocytic activation factor (LAF) activity. On the other hand basic amino acids like Lys and Arg are critical for LAF activity (Kawashima et al., 1992).

After succeeding with the purification and characterisation of IL-1, attempts to find its receptor began, and in 1985, Dower and co-workers found and characterised IL-1 from the T-lymphoma cell line LBRM-331A5 an 80 kDa molecule to which IL-1 binds (Dower et al., 1985). The same 80 kDa molecule was cloned from human T cells and fibroblasts (Sims et al., 1989). Kilian and colleagues have shown that IL-1α and IL-1β bind to the same receptor (Kilian et al., 1986). However, a smaller receptor for IL-1 (60 kDa) was found in B- lymphoma and B cells (Matsushima et al., 1986, Horuk et al., 1987), and it was later demonstrated that the receptors expressed in T-cells and B-cells are structurally different molecules produced from different genes (Bomsztyk et al., 1989, Chizzonite et al., 1989). Thus, it was proposed to call IL-1 receptor type I (IL-1RI) the 80 kDa receptor, and IL-1 receptor type II (IL-1RII) the 60 kDa molecule (McMahan et al., 1991b).

Further structural studies of both receptors showed that they resemble each other in their extra-cellular portion that is characterised by 3 immunoglobulin-like domains, despite sharing only 28% homology in the amino acid sequence. However, their cytoplasmic portions are quite different: the IL-1RI cytoplasmic portion is larger (215 residues) than that of the IL-1RII (29 residues) (McMahan et al., 1991b).

1.3.7 Molecular structure of IL-1RI

IL-1RI is a 80 kDa protein (552 residues) expressed in many cells, including T-cells, fibroblasts and endothelial cells (Vigers et al., 1994). Its extracellular portion consists of 319 amino acid residues and has three immunoglobulin-like (Ig-like) domains, which typically have two β-sheets held together by a disulfide bond formed by cysteine residues (Sims et al., 1988). Several N-linked glycosylation sites (X-Asn-X) are found in the extra-cellular portion of IL-1RI that are not involved in IL-1β binding (Wang et al., 2010, Thomas et al., 2012). However, Thomas and co-workers found that the N-acetylglucosamine moiety of Asn 216 is involved in the binding to IL-1RAcP (Thomas et al., 2012). Moreover, the IL-1RI cytoplasmic domain consists of 215 amino acid residues and it has high homology with Toll receptors (Gay and Keith, 1991). The Toll receptors are transmembrane proteins evolutionarily conserved in insects and mammals. These receptors were first found in *Drosophilla* as a protein involved in fly development, as it is required for the establishment of dorso-ventral polarity in the developing fly embryo (Takeda et al., 2003). Subsequently, they were also shown to be involved in immunity, given their antifungal properties (Akira et al., 2001). IL-1RI was the first mammalian molecule found containing these Toll-like domains, thus, these domains are known as Toll/IL-1R domains (TIR domains). Molecules presenting cytoplasmic TIR domains and extra-cellular Ig-like domains now are classified as members of the IL-1 receptor family (Subramaniam et al., 2004).

IL-1RI Ig-like domains are identified as domains 1, 2 and 3 (Figures 1.5-A). Domain 3 is the one that binds to cell membrane and is more rigid. Crystal structure studies of IL-1RI revealed that a disulphide bond between Cys 104 and Cys 147 holds domains 1 and 2 together, whilst domain 3 is more separated and connected to domain 2 by a 5-residue linker. For an easy identification, β-strands forming two β-sheets

present in Ig-like domains were assigned with letters a, b, c, d, e, f and g (Schreuder et al., 1997, Vigers et al., 1997). Strands in domains 1 and 2 are short (3-4 residues), except for strands g and f in domain 2 that are longer and contact domain 1. When making contact with IL-1, the three Ig-like domains of IL-1RI turn to wrap ligands, permitting sites A and B on ligands to make contact with IL-1RI domains 1, 2 and 3, thus forming a binding interface for IL-1RAcP (Figure 1.6 A-C) (Schreuder et al., 1997, Vigers et al., 2000).

1.3.8 Molecular structure of IL-1RAcP

With the purpose of studying IL-1 bioactivity through IL-1R, Lewis et al. (1990) developed two monoclonal antibodies (mAb) that inhibited IL-1 biological activity but not its IL-1R-binding ability. Surprisingly, these mAb were able to co-precipitate more than one molecule, suggesting the existence of an IL-1R multi-molecular complex (Lewis et al., 1990). Later, in 1995, Greenfeder and co-workers isolated for the first time the molecular clone of the second subunit of the IL-1R complex and they called it IL-1 receptor accessory protein (IL-1RAcP). The translated protein consists of 570 (66 kDa) amino acid residues and shows significant homology (25%) to IL-1RI (Greenfeder et al., 1995a). For that reason, IL-1RAcP is considered a member of the IL-1R family (Wesche et al., 1998). Its extracellular domain consists of 340 amino acid residues and is divided into 3 Ig-like domains (similar to IL-1RI); this protein also has a 29 residue transmembrane portion and an intracellular domain of 181 residues (Jensen et al., 2000).

Studies with IL-1RAcP-knockout (KO) cells and mice have shown that the presence of IL-1RAcP is crucial for IL-1 bioactivity, as it is required for IL-1-induced IL-6 synthesis, but is not involved in IL-1 binding to IL-1RI (Cullinan et al., 1998). Given that IL-1RAcP does not recognise IL-1 itself (Greenfeder et al., 1995a, Cullinan

et al., 1998) but that it is essential for IL-1 mediated responses (Wesche et al., 1996, Korherr et al., 1997, Wesche et al., 1997b, Cullinan et al., 1998), two possible functions for IL-1RAcP in the process of IL-1 binding were proposed (Wesche et al., 1998). First, IL-1RAcP was reported to increase the affinity of IL-1 to IL-1RI in CHO cells (Greenfeder et al., 1995a), and Wesche et al. (1998) proposed that IL-1RAcP enhanced the affinity of the receptor complex. However, in the murine cell line EL-4 the same authors did not observe an increase in the affinity of IL-1 to IL-1RI dependent on IL-1RAcP. The second possible function proposed was that IL-1RAcP stabilises the interaction between IL-1 and IL-1RI by covering IL-1 ligated to IL-1RI (Wesche et al., 1998).

At the time when the current project was started there was no experimental structure available for the ternary complex formed by IL-1RII, IL-1β and IL-1RAcP (RII/IL-1/AcP), therefore the precise arrangement of these molecules in the complex remained a matter for debate. Studying such complex structurally was also one of the aims of the current project. *In silico* studies predicted two ways of IL-1RAcP-interaction with the IL-1RI/IL-1 complex: the "Front model" and the "Back model". The Front model suggests that the IL-1AcP covers the "front" of IL-1RI/IL-1 complex making partial contact with the IL-1 residues that are not involved with IL-1 receptor (IL-1R) binding. On the other hand, in the Back model, IL-1RAcP makes contact with the receptor, by placing itself at the "back" of the complex (Casadio et al., 2001). Recently published crystallographic studies of the ternary complexes IL-1RII/IL-1β/IL-1RAcP (Wang et al., 2010) and IL-1RI/ IL-1β/IL-1RAcP (Thomas et al., 2012) finally clarified how the ternary complex is formed and showed that IL-1RAcP and either IL-1RI or IL-1RII (IL-1R) align in a perpendicular manner causing domain 1 to point away from the structure and making contact with neither IL-1R nor IL-1β (Figures 1.7-

1.9). Interestingly, even though the complex RI/IL-1/AcP (Figure 1.8-A) adopts the same structure as RII/IL-1/AcP (Figure 1.9-A), interactions between IL-1RI and IL-1RAcP are distinct from those between IL-1RII and IL-1RAcP (Wang et al., 2010, Thomas et al., 2012). IL-1RAcP binds to the binary complex formed by IL-1R and IL-1β (IL-1R/IL-1), through two binding sites that authors called site III and site IV. Site III refers to the interaction with IL-1β (Figure 1.8-C) and site IV to that one with IL-1R (Figures 1.8-B and D and 1.9-B and C). At site IV domains 3 in both IL-1RI and IL-1RAcP make contact through Tyr 234 and Pro 245 in IL-1RAcP and the N-acetylglucosamine moiety of the Asn 216 in IL-1RI (Figure 1.8-D). On the other hand, Leu 180 in IL-1RAcP domain 2 is involved in binding to Val 160 and Ile 165 of IL-1RI domain 2 (Figure 1.8-B) (Thomas et al., 2012). In contrast, residues involved in domains 3 interactions are His 226, Asn 229, His 231 and Val 232 in IL-1RAcP and Val 225, Ile 226 and Phe 248 in IL-1RII (Figure 1.9-C) (Wang et al., 2010). It is worth mentioning that Leu 180 in IL-1RAcP domain 2 contacts domain 2 of both IL-1RI (Val 160 and Ile 165) (Figure 1.8-B) and IL-1RII (Figure 1.9-B) (at Leu 180) (Wang et al., 2010, Thomas et al., 2012).

At the binding site III, IL-1RAcP domains 2 and 3 contact β9 and residues forming the loops between β4 and β5 (β4-β5) and β11 and β12 (β11-β12) respectively. Arg 286 in domain 3 formed a salt bridge with the Asp 53 in β4-β5, whereas domain 2 contacted β9 through a salt bridge formed between Glu 132 (in domain 2) and Lys 109 (in β9) and a hydrophilic interaction between Glu 111 in β9 and Ser 185 in domain 2 (Figure 1.8-C) (Thomas et al., 2012). It is noteworthy that neither complex of IL-1α and IL-1RI nor IL-1RII have been elucidated yet, so the structural consequences of the difference between biological effects of IL-1α and IL-1β still remain unclear.

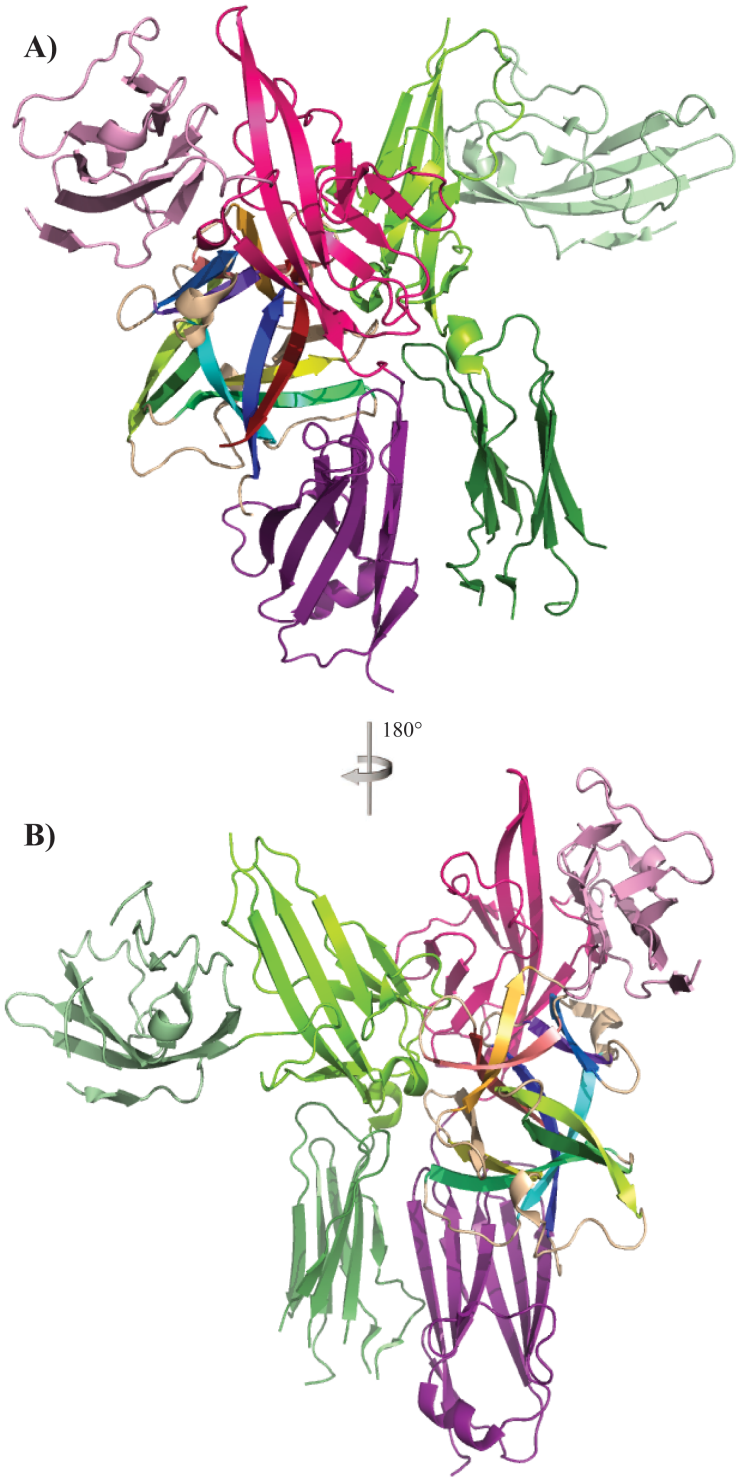

Figure 1.7 Cartoon diagram of the crystal structure of IL-1RI/IL-1β/IL-1RAcP complex in two views. A) Cartoon diagram of the complex structure. Domain 1 on IL-1RI is highlighted in light pink, domain 2 pink and domain 3 purple. Domain 1 on IL-1RAcP is highlighted in light green, domain 2 green and domain 3 dark green. IL-1β β-sheets colour code as in Figure 1.3. **B)** View of the ternary complex rotated 180° over the vertical axis. Figure generated with MacPyMOL. PDB ID: 4DEP (Thomas et al., 2012)

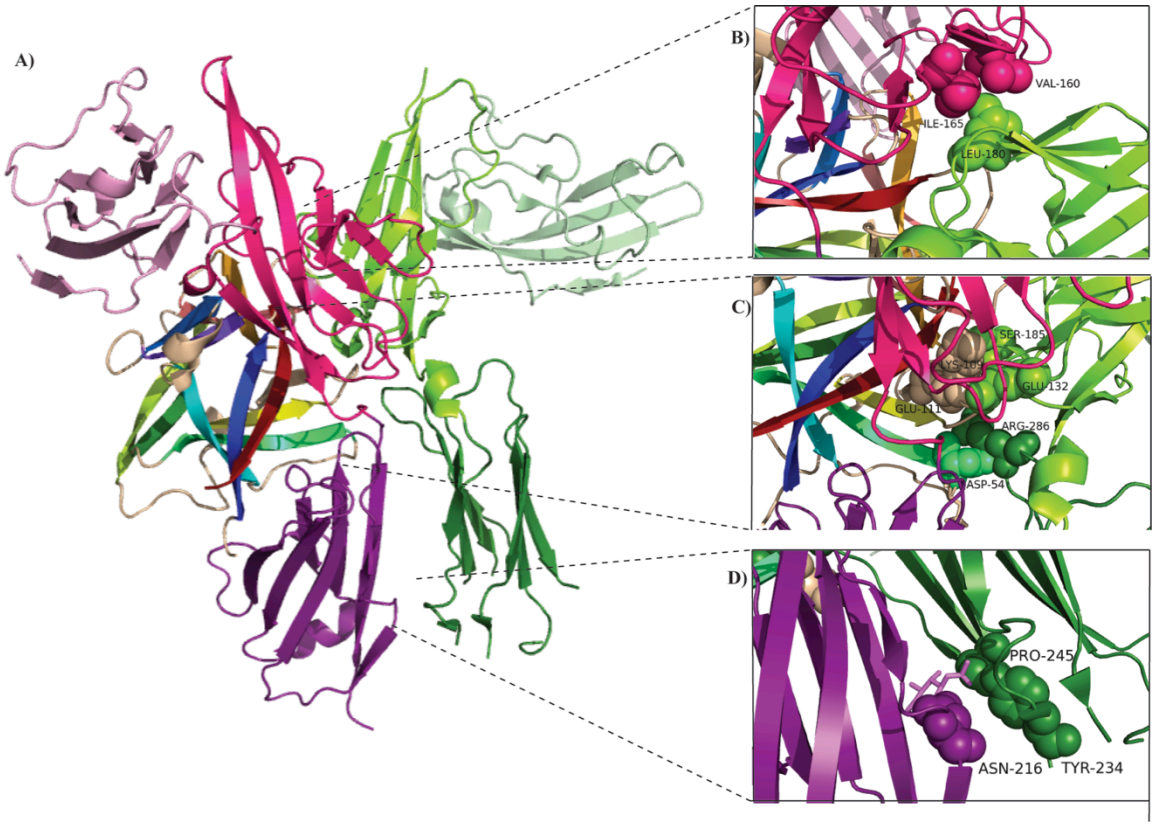

Figure 1.8 Cartoon diagram representing interactions in the IL-1RI/IL-1β/IL-1RAcP ternary complex. A) Cartoon diagram of the overall complex structure. Domain 1 on IL-1RI is highlighted in light pink, domain 2 pink and domain 3 purple. Domain 1 on IL-1RAcP is highlighted in light green, domain 2 green and domain 3 dark green. IL-1β β-sheets colour code as in Figure 1.3. Zoomed-in regions are shown in the panels on the right. **B)** First part of binding site IV, view of the interactions between IL-1RAcP Domain 2 and IL-1RI Domain 2. **C)** Binding site III, view of the interactions between IL-1RAcP and IL-1β. **D)** Second part of binding site IV, view of the interactions between IL-1RAcP Domain 3 and IL-1RI Domain 3. Amino acid residues involved in interactions are represented as spheres and labelled accordingly, and the *N*-acetylglucosamine is represented as sticks. Figure generated with MacPyMOL. PDB ID: 4DEP (Thomas et al., 2012).

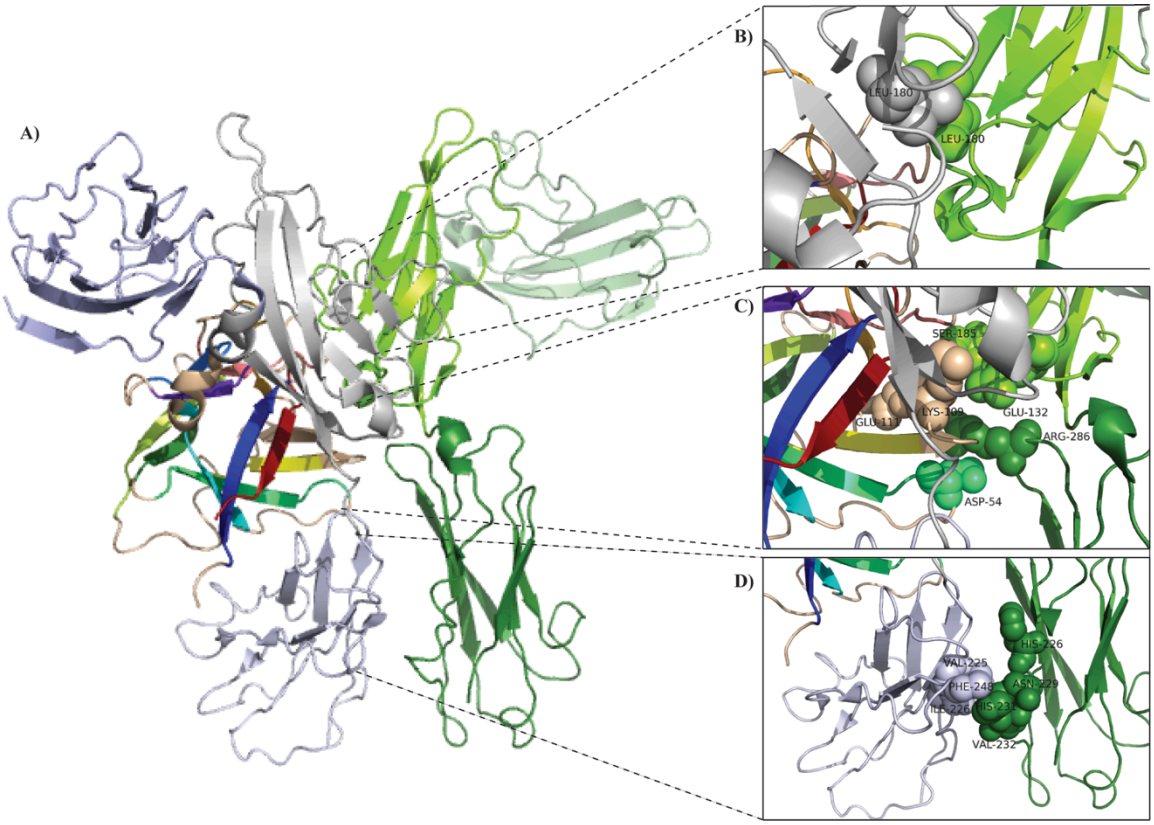

Figure 1.9 Cartoon diagram representing interactions in the IL-1RII/IL-1β/IL-1RAcP ternary complex. A) Cartoon diagram of the overall complex structure. Domain 1 on IL-1RII is highlighted in blue, domain 2 light grey and domain 3 light blue. Domain 1 on IL-1RAcP is highlighted in light green, domain 2 green and domain 3 dark green. IL-1β β-sheets colour code as in Figure 1.3. Zoomed-in regions are shown in the panels on the right. **B)** First part of binding site IV, view of the interactions between IL-1RAcP Domain 2 and IL-1RII Domain 2. **C)** Binding site III, view of the interactions between IL-1RAcP and IL-1β. **D)** Second part of binding site IV, view of the interactions between IL-1RAcP Domain 3 and IL-1RII Domain 3. Figure generated with MacPyMOL. PDB ID: 3O4O (Wang et al., 2010).

1.4 Biophysical approaches to study proteins

It is widely accepted that protein properties such as activity, substrate binding and overall stability are pH- and temperature- dependent (Berisio et al., 2002) and it has been suggested that pH can subtly modify protein conformation or interactions affecting its functionality (Dixon et al., 1991, Gursky et al., 1992, Garlatti et al., 2007, Djoumerska-Alexieva et al., 2010) without affecting the overall structure of the protein.

Protein conformational stability can be defined as the ability of proteins to maintain their native, folded and functional state (Goldberg et al., 2011). For the purpose of studying the conformational stability of proteins under changes in environmental conditions, such as pH, temperature and ionic strength, there are available several biophysical techniques, among many others, that can give information about the conformation of proteins such as circular dichroism (CD), nuclear magnetic resonance (NMR), fluorescence spectroscopy and light scattering (Tsai et al., 1998, Martin and Schilstra, 2008, Goldberg et al., 2011, Chaudhuri et al., 2014). These techniques were used in the current work, and are briefly reviewed below.

1.4.1 Circular dichroism

Circular dichroism (CD) in the far-UV permits the analysis of the secondary structure of proteins, as well as structural alterations resulted from changes in environmental conditions (Martin and Schilstra, 2008). CD refers to the differential absorption of left-handed and right-handed circularly polarized light that is exclusively sensitive to the conformation of certain molecules, which, due to their chirality, are able to interact differently with circularly polarized light (Figure 1.10-A and B) (Woody, 1995, Greenfield, 2006b, Martin and Schilstra, 2008). Thereby, CD spectra of proteins will differ considerably depending on their secondary structure, that is, if it is an α-helix or a β-sheet (Figure 1.10-C) (Woody, 1995). Chromophores contributing to CD spectra of proteins in the far-UV must be either chiral or located in an asymmetric environment, that is to say, chromophores might be achiral but their interaction in the chiral field of the protein leads them to show optical activity (Woody, 1995) and these chomophores are mainly peptide bonds (Kelly et al., 2005). CD spectra are obtained by measuring the difference in absorbance between left-handed (L) and right-handed (R)

circularly polarised components of light and is reported in terms of ellipticity (θ) in degrees (Kelly et al., 2005).

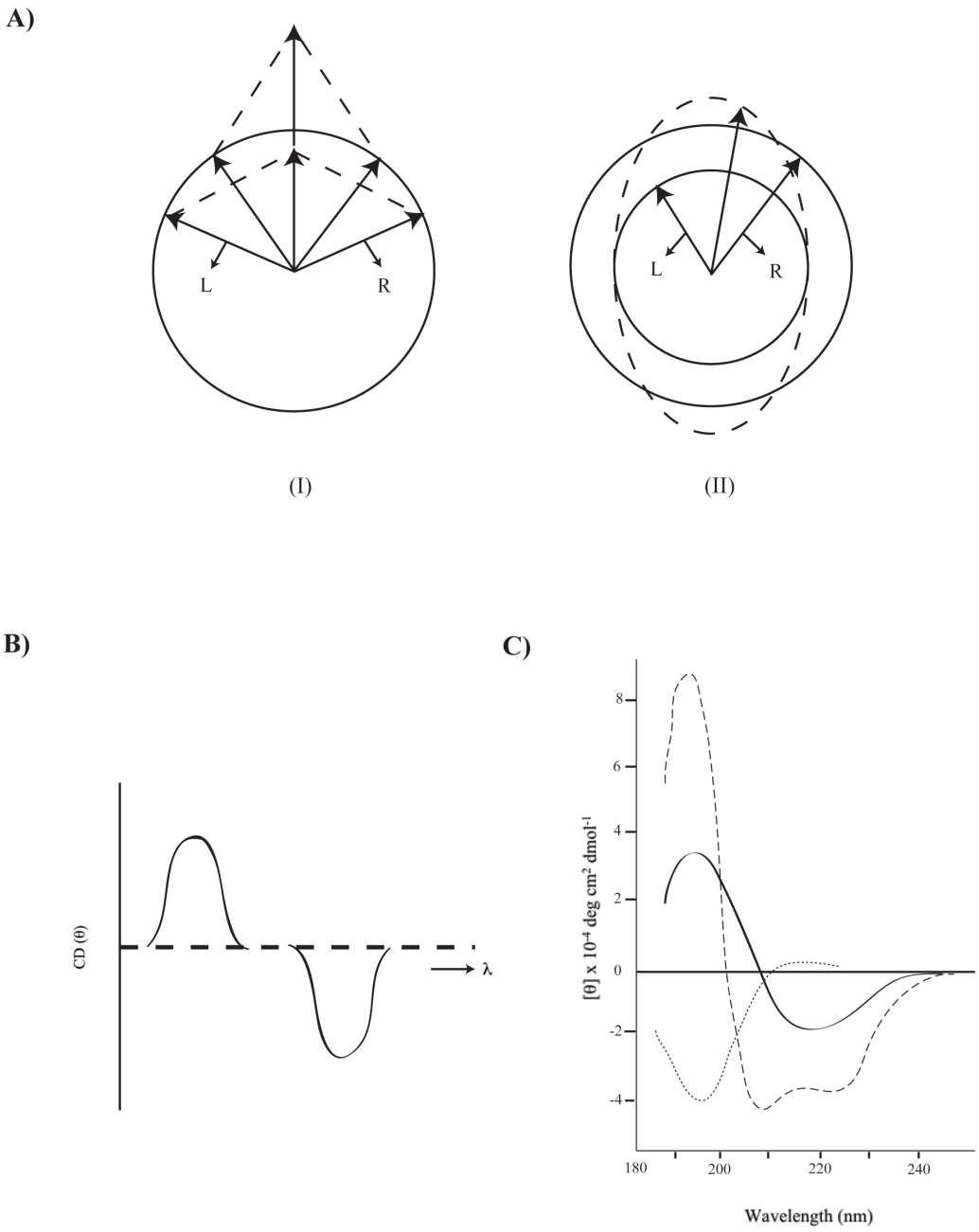

Figure 1.10 Circular Dichroism. A) Origin of the CD effect. (I) The left (L) and right (R) circularly polarised components of plane polarised radiation, when combined, generate plane polarised radiation when both have the same amplitude or (II) generate elliptically polarised radiation when L and R are of different magnitude. **B)** The CD spectrum. A positive CD spectrum is generated when L absorbed more than R. A negative CD spectrum is generated when R absorbed more than L. **C)** CD spectra of representative secondary structures. α-helix, dashed line. β-sheet, solid line. Coil, dotted line. Taken and modified from Kelly et al, 2005.

After CD spectra are acquired they are often analysed with the purpose of estimating the secondary structure composition of proteins. For this, there are several algorithms available most of which utilise data bases comprising the CD spectra of proteins whose structures have been solved by X-ray crystallography (Kelly et al., 2005). Diverse algorithms for protein secondary structure analysis can be found in a website called DICHROWEB (http://dichroweb.cryst.bbk.ac.uk), which is also compatible with formats of different commercial CD instruments as well as with a variety of different units used to report CD data (Lobley et al., 2002). For example, the algorithm K2D, found in DICHROWEB, is an optimised self-organising map algorithm that calculates protein secondary structure composition based on a set of CD spectra of proteins of known structure by responding to similar spectra and corresponding similar values to similar CD spectra (Andrade et al., 1993).

1.4.2 Nuclear magnetic resonance spectroscopy

Nuclear magnetic resonance (NMR) spectroscopy was introduced as a method for protein structural analysis in the 1980's (Wuthrich, 1989). Since then, structures of several molecules have been studied with this technique, including IL-1β (Gronenborn et al., 1988, Clore et al., 1990, Clore and Gronenborn, 1991). NMR is based on the resonance of nuclei (protons) of atoms at their corresponding spinning frequency when exposed to a radio-frequency pulse in a static magnetic field, depending on the chemical shift and spin-spin coupling of each atom (Shin et al., 2008).

Protons have mass, charge and angular momentum (known as spin). Given its charge and spin, protons generate a magnetic field and the strength of a magnetic field is known as magnetic momentum. When an external magnetic field (*H*) is applied to a proton its magnetic moment assumes one of two angles with respect to the direction of *H*, that is to say, the magnetic moment is aligned with or against *H*. When

electromagnetic radiation in the range of radiofrequency is applied, protons absorb this radiation and flip from one orientation to the other and this will depend on the spin number of the nucleus (for ^{1}H, the spin number is ½). Thus, for a given nucleus, there is only a single transition frequency for each value of *H*. In addition, the surrounding environment of protons, i.e. electrons, also affects their resonance frequency. Consequently, the resonance frequency of each nucleus of the same type will depend on the chemical group to which this nucleus belongs and the local environment: this phenomenon is known as chemical shift. Therefore the hydrogen protons in a methyl group will have different chemical shift (resonance frequency) from that of an amino hydrogen proton (Freifelder, 1982), and the groups of a similar type will also have slightly different chemical shifts between each other, giving rise to the signal dispersion. Importantly, positions of signals in the spectra are sensitive to the protein conformation and environment. In this manner, NMR can be used as a powerful tool for the study of structural alterations that result from changes in environmental conditions such as pH and temperature. One dimension (1D) NMR (^{1}H-NMR) is used as a complementary method for the study of protein conformation and aggregation as it provides detailed structural information about the protein. In a ^{1}H-NMR spectrum, the line width of peaks is related to the molecular size, thus, changes in the line width reflect differences in molecular size. During aggregation or denaturation processes proteins enlarge their size causing the line width of a given signal to broaden, loose height and eventually merge with the baseline. On the other hand, protein denaturation can be manifested as the loss of chemical shift dispersion in the methyl or amide regions. Conformational changes can be detected by the characteristic signal shifts. In this manner, monitoring changes in the spectral appearance, namely in the line shape (line width and heights) and chemical shifts of the different signals of a protein,

provides insight of the conformational state of the protein under specific environmental conditions (Tsai et al., 1998).

1.4.3 Fluorescence spectroscopy

Fluorescence spectroscopy is a rapid, robust, precise and economic method for the analysis of protein conformation, stability, binding and solvent interactions (Freifelder, 1982, Garidel et al., 2008). Fluorescence is a property of certain molecules that after absorbing a photon (excitation) emit light of a longer wavelength (emission) (Freifelder, 1982); thus, fluorescence can be measured as a function of excitation or emission wavelength (Eftink, 2000). Protein intrinsic fluorescence refers to the fluorescent emission of fluorescent amino acids, especially Trp, which is the dominant intrinsic fluorophore. Other aromatic amino acids such as Tyr and Phe can also contribute to protein intrinsic fluorescence although to a lesser extent. As the emission spectrum of the indole side chain of Trp is very sensitive to the polarity of its environment it allows native and unfolded states of proteins to be distinguished. Given the aromatic character of Trp side chains, this residue is often buried in the hydrophobic core of proteins, thus, any disruption of protein structure can lead to Trp become exposed to solvent affecting the fluorescence of the protein (Eftink, 1994, Eftink, 2000, Garidel et al., 2008, He et al., 2013, Kranz et al., 2013).

The well-defined three-dimensional structure of proteins, required for their biological activity, is determined by specific environmental conditions (i.e. temperature, pH, ionic strength), when these conditions are altered proteins exhibit structurally unfolded states, which are characterised by different structural and conformational (secondary and tertiary structure) properties (Duy and Fitter, 2006, Garidel et al., 2008, Chaudhuri et al., 2014). When the secondary and tertiary structures of a protein disappear or are altered, proteins tend to form aggregates, and these

phenomena (unfolding, denaturing and aggregation) can alter the microenvironment of Trp affecting the emission spectra. For example, on unfolding, Trp residues that are usually buried among protein structures, become more accessible to the solvent and the emission intensity of the protein decreases (Duy and Fitter, 2006). Additionally, the emission wavelength (emission maximum) can also be shifted as the radiation emitted from an unfolded protein is usually at a longer wavelength; this is due to Trp becoming exposed (Sheehan, 2000). As an example, the emission maximum of a humanised IgG shifted from 330 nm to 337nm when it was thermally denatured, whereas chemically induced denaturation (by addition of GdnHCl) caused the emission maximum to shift to 352 nm. These results suggested that when denaturation of the IgG was thermally induced, Trp were not fully exposed to the solvent, while in chemical denaturation the IgG was more unfolded, hence Trp were more exposed to the solvent, increasing in this manner the maximum emission wavelength (Garidel et al., 2008). Thus, fluorescence spectra can be used for quantitative analyses of unfolding transitions (Duy and Fitter, 2006). Furthermore, fluorescence is widely used to analyse thermal denaturation properties of proteins under specific conditions, disclosing valuable information on the conformational stability of the protein (Garidel et al., 2008). The stability of proteins under particular environmental conditions (i.e. pH, ionic strength) can be analysed using a thermal unfolding experiment, from which the midpoint of unfolding transition or melting temperature (T_m) can be obtained to determine if the protein is stabilised (when T_m is increased) or destabilised (when T_m is decreased) (Goldberg et al., 2011). In this way, a thermal unfolding curve and the Tm of a protein under specific conditions can be obtained by plotting the peak position of the fluorescence emission spectra at determined temperature. Commonly the wavelength of the fluorescence emission maximum is reported as a barycentric mean (BCM) value (centre of mass of the fluorescence peak, in the units of nm) given that it is less sensitive to spectral

anomalies such as noise and shallow shape of the emission peak, which makes the direct determination of the maximum emission wavelength difficult and less precise. This value provides an averaged description of the change in the wavelength of the emission maximum. To calculate the BCM the whole fluorescence spectrum (usually 300-450 nm) of the protein is taken into account, each wavelength and their intensity using the following formula:

$$\lambda_{bcm}^{exp} = \frac{\sum \lambda I_{\lambda}}{\sum I_{\lambda}}$$

Where λ is emission wavelength and $I(\lambda)$ is fluorescence intensity at this wavelength (Avacta, 2014b).

1.4.4 Static light scattering

Light scattering is a method widely used to characterise molecules and to measure the conformational stability of proteins (Freifelder, 1982, Goldberg et al., 2011). Scattering refers to the deflection of an incident beam of light by a molecule and static light scattering (SLS) is a method used for the analysis of the intensity of light scattered from a molecule in solution (Kranz et al., 2013), which is dependent on the size of the molecule. As discussed in previous sections, protein aggregation occurs when partially unfolded proteins exposing their hydrophobic residues come together forming dimers that serve as nucleation sites for further aggregation (Goldberg et al., 2011), and light scattering signals can be used to monitor protein aggregation by measuring changes in the average intensity of scattered light as the intensity of the signals are increased when proteins form aggregates (He et al., 2013, Wang et al., 2013a). The temperature at which light scattering of the protein solution starts to increase from a base level (e.g. by >10%) can be taken as the temperature of the on set

of protein aggregation, T_{agg}, which is a useful measure of the colloidal stability of a protein solution, and ability of protein to maintain its monomeric structure at the higher temperature (Avacta, 2014a). Measurement of such parameter T_{agg} can be done simultaneously with detecting fluorescence, using specialised equipment, such as Optim1000 by Avacta, providing a convenient measures of both colloidal and thermal stability of protein molecules (Avacta, 2014a).

2 Aims

Since the discovery of IL-1α and IL-1β, they were thought to exert the same effects and studies of IL-1 biological activity and signalling corroborated this belief. However, in recent years, some differences in IL-1α and IL-1β have been observed (Horai et al., 1998, Andre et al., 2005, Tsakiri et al., 2008, Trebec-Reynolds et al., 2010). Despite the efforts to elucidate the mechanisms by which these differences are achieved, molecular mechanisms responsible for the differential effects observed remain unclear. As players of the inflammatory response, physiological conditions at which these cytokines exert their effects are far from normal, as changes in temperature and pH under inflammatory conditions have been established. It has been demonstrated that changes in physiological pH can affect protein binding (Borga et al., 1969, Levitt et al., 1986), and this could be reflected in protein bioactivity. Thus the aim of this work is to elucidate differences in the biophysical properties of IL-1α and IL-1β as well as the effects that temperature and pH could have on the conformation and stability of IL-1α and IL-1β.

3 Materials and Methods

3.1 Materials

All reagents were purchased from Fisher Scientific (UK), unless specified. Molecular biology enzymes, *E. coli* and yeast strains were purchased from New England Biolabs (USA), unless specified. Cell culture media and supplements were purchased from Sigma-Aldrich. All flasks and plates used for tissue culture techniques were purchased from Corning (Fisher Scientific, UK).

3.2 Bioinformatics

The bioinformatics tools used throughout the present work, as well as their applications and website addresses are summarised in Table 3.1.

3.3 Molecular biology

3.3.1 Constructs and plasmid vectors

Human mature form of IL-1β DNA sequence was obtained from I.M.A.G.E. (Integrated Molecular Analysis of Genome Expression) and cloned into a pQE-30 vector (Qiagen, UK) in a previous work to this project (Drury BJ, 2009, unpublished data, University of Manchester). Human mature form of IL-1α (as in Graves et al, 1990) as well as the extracellular domains of IL-1RAcP and IL-RI, IL-1RAcP-His, IL-1RAcP-IL-1α synthetic DNA sequences were obtained from GenScript (Piscataway, USA) supplied in pET-15b vector (Novagen, UK) or pKLAC2 vector (NEB, USA). For bacterial plasmids pET-15b the original wt human DNA sequences were adapted for bacterial expression by optimising the codon usage and GC content by GenScript, while maintaining the same amino acid sequence of the wt protein. Vectors, pQE-30 and pET-15b have N-termini 6 x His tag and are ampicillin resistant. Gene sequences,

sequences of protein constructs expressed by the plasmids, and plasmids maps can be found in Appendix 1.

Table 3.1 Summary of Bioinformatics Tools used in this project

Tool	Application	Website
Blastp	Protein sequence alignment	http://blast.ncbi.nlm.nih.gov
Dichroweb	Analysis of CD spectra	http://dichroweb.cryst.bbk.ac.uk
EnCor Biotechnology Inc.	Prediction of protein characteristics from primary sequence	http://encorbio.com/protocols/Prot-MW-Abs.htm
ProtParam	Prediction of protein characteristics from primary sequence	http://web.expasy.org/protparam
PyMol	Protein structure drawing and analysis	http://pymol.org
Translate tool (Expasy)	Translation of DNA into amino acid sequence	http://web.expasy.org/translate/
Uniprot	Gene and protein sequence and available published data	http://www.uniprot.org
GRAVY calculator	Protein hydrophobicity calculation	http://www.gravy-calculator.de/index.php
Protein data bank	Biological macromolecular structures data bank	http://www.rcsb.org/pdb/home/home.do

3.3.2 *E. coli* strains

The *E.coli* strains used for protein expression were T7 Express, T7 Express *LysY* and BL21 DE3 from Novagen (UK). Strains with mutations in the thioredoxin/glutathione pathways that allow the formation of disulfide bonds in bacteria cytoplasm used in this work were Shuffle T7 Express and Shuffle T7 Express *LysY* and Origami, Origami B (DE3) and Rosetta-gami 2, from Novagen (UK). For the maintenance of plasmids, DH5α cells (Invitrogen, UK) were used.

3.3.3 *Kluyveromyces lactis* competent cells

For protein expression in *Kluyveromyces lactis* (*K. lactis*), a *K. lactis* Protein expression kit was purchased from NEB (USA). The strain provided was GG799 and transformation and expression was carried out following the manufacturer's instructions.

3.3.4 Transformation of bacterial competent cells

Vector pET-15b and pQE-30 containing the genes of interest were inserted into DH5α competent cells by the heat shock method. Competent cells were incubated with 1-5µL (20-100 ng) of the plasmid DNA on ice for 30 min. Heat shock was carried out at 42°C for 45 sec followed by incubation on ice for 2 min, and subsequent addition of 600 µL of LB media without antibiotics. Transformed cells were incubated at 37°C for 1 h with shaking at 200 rpm. After incubation, cells were plated in LB-agar with 50 µg/mL of carbenicillin (Melford, UK) and incubated overnight at 37°C. Transformed colonies were picked from the plate and inoculated in 2.5 mL of LB with 50 µg/mL of carbenicillin and incubated overnight with shaking (200 rpm) at 37°C for plasmid preparation and/or glycerol stocks. Glycerol stocks were prepared by adding glycerol to a final concentration of 15%, to overnight cultures. Stocks were then flash frozen with liquid nitrogen and stored at -80°C.

3.4 Recombinant protein expression in bacteria

3.4.1 Isolation of plasmids from bacterial cells

Plasmid DNA was isolated from transformed DH5α cells grown in 10 mL of LB media overnight at 37°C with shaking (200 rpm), with the Qiagen Spin Miniprep Kit (Qiagen), following the manufacturer's protocol. 30 µL of elution buffer were used and DNA was quantified with a NanoDrop 2000 (Thermo Scientific).

3.4.2 Transformation of bacterial expressing cells

Transformation of expressing cells was carried out by the heat shock method previously described in section 3.3.4, with 1-5 µL (20-100ng) of plasmid DNA, and transformed cells were plated in LB-agar with 50 µg/mL of carbenicillin (Melford, UK) plus antibiotics for strain selection (Appendix 1). Following the heat shock, Shuffle T7 Express and Shuffle T7 Express Lys Y cells were incubated at 30°C, as well as LB-agar plates containing these strains. Incubation for any other strain was carried out at 37°C.

3.4.3 Protein expression optimisation

Expression trials were carried out in 50 mL cultures. For this, overnight cultures from either fresh transformations or glycerol stocks were set up in 2.5mL of LB media with antibiotics and incubated overnight at 30°C or 37°C with shaking at 200 rpm. 50 mL cultures were set up in LB media with antibiotics, by inoculating 0.5-1 mL of the overnight culture, with a starting OD_{600} at 0.05-0.1 and incubated at different temperatures. Protein expression was induced for either 4 or 16 h, when cultures reached an OD_{600} at 0.6-0.8, by adding 0.5 or mM of IPTG. 200 µL samples of pre-induction and post-induction sampled every 1 h were taken and centrifuged at 13000 rpm for 10 min. Supernatant and pellet samples were analysed by either SDS-PAGE.

For the soluble and insoluble expression analysis, 200 µL sample pellets were lysed with 50 µL of protein extraction BugBuster reagent (Novagen, UK). A 20 µL aliquot from the lysate was taken and centrifuged along with the whole lysate for 10 min at 13000 rpm. The supernatant was discarded and pellet combined with 20 µL of 2 x sample buffer (LP, insoluble fraction), whereas 20 µL of the supernatant from lysate (LSN, soluble fraction) was combined with 20 µL of 2 x sample buffer for SDS-PAGE analysis.

3.4.4 Recombinant protein expression in large volume cultures

Following protein expression optimisation trials, conditions that yielded the best expression were scaled up proportionately. For this, transformed cells from either colonies grown on LB-agar plates or glycerol stocks were inoculated in 25 mL of LB media plus antibiotics and incubated with shaking (200 rpm) overnight at 37°C. Cultures were inoculated into 0.5 L LB plus antibiotics, at a starting OD_{600} of 0.05-0.1 and grown to log phase (OD_{600} ~ 0.6-0.8). Prior to induction with IPTG, cultures were cooled on ice and after induction with IPTG they were incubated at the optimal temperature (37°C for IL-1α and IL-1β) at 200 rpm, 3 h for IL-1α and 4 h for IL-1β. Then, cells were pelleted at 5 000 rpm for 20 min at 4 °C, using a Beckman Coulter Avanti J-E centrifuge. Supernatant was discarded and pellets were stored at -20°C for future use.

3.4.5 Harvesting protein from bacteria culture

Frozen bacteria pellets were defrosted on ice and resuspended in 20 mL per 5 g of bacterial pellet (1 L culture), of ice-cold lysis buffer: 20 mM phosphate buffered saline (PBS) pH 7 for IL-1β or 8 for IL-1α, 0.5% Triton X-100, 50 mM Arg, 50 mM Glu, 5 mM imidazole, protease inhibitors (EDTA-free inhibitor cocktail, Roche), 10 μg/mL DNAse and RNAse (Sigma-Aldrich) and 5 mM $MgCl_2$ (Appendix 3). Samples were then sonicated on ice using a Vibra-cell sonicator (Sonics and Materials Inc.) for 5 min (15 sec on/15 sec off) at 40% amplitude. The insoluble fraction was removed by centrifugation at 17 000 rpm for 1 h at 4°C, using a Beckman Coulter Avanti J-E centrifuge.

3.5 Recombinant protein expression in yeast

3.5.1 Isolation of plasmids from bacteria cells

pKLAC2 vector constructs were transformed into DH5α cells for propagation by the heat shock method described in section 3.3.4 and isolated as described in section 3.4.1.

3.5.2 Transformation of yeast cells

K. lactis competent cells were transformed by a chemical method following the manufacturer's protocol. Briefly, after isolation of DNA plasmids from DH5α cells, pKLAC2 plasmids containing the genes of interest were linearized by incubating them at 37°C overnight with 20 U SacII per 2 μg of DNA, and further desalting with the QIAquick PCR purification kit (Qiagen), following the instructions of the manufacturer. *K. lactis* competent cells were defrosted on ice and 5-15 μL (1-5 μg) of digested plasmids and 620 μl of transforming reagent (NEB, provided with competent cells) was added. This transformation mixture was incubated at 30 ºC for 30 min, followed by incubation at 37ºC for 1 h in a water bath. Following incubation, cells were pelleted at 7000 rpm for 2 min and resuspended in 1 mL of YPGlu two times and incubated at 30°C with shaking at 250 rpm for 4 h. Cells were diluted 1:2 and 1:10 in deionized water and then spread onto YCB-agar plates containing 5 mM acetamide (both provided with the kit). YCB-agar plates containing transformed cells were incubated at 30°C for 3-4 days until colonies appeared. Individual colonies were then streaked onto fresh YCB-agar plates with 5 mM acetamide and incubated for 1-2 days until patches of >1 cm^2 appeared. An area of approximately 2 mm^2 was scraped from patches and resuspended in 20-50 mL of YPGlu medium and incubated overnight at 30°C with shaking (250 rpm) for further protein expression or glycerol stocks. Glycerol

stocks were prepared by adding glycerol to a final concentration of 20% to overnight cultures. Stocks were then flash frozen with liquid nitrogen and stored at -80°C.

3.5.3 Expression trials in yeast cells

Expression trials in yeast cells were carried out in 500 mL cultures. Transformed *K. lactis* cells from either colonies or overnight cultures from glycerol stocks were patched onto YCB-agar plates with 5 mM acetamide and incubated at 30°C for 1-2 days until patches appeared. An area of approximately 2 mm^2 was scraped from patches and resuspended in 25 mL of YPGlu medium and incubated overnight at 30°C with shaking (250 rpm). Starter cultures were inoculated at a ratio of 1:100 onto fresh YPGlu media. Expression was induced at an OD_{600} ~ 1, by changing YPGlu to YPGal. For this, cultures were cooled on ice and the cells were pelleted at 7 000 rpm for 10 min at 4 °C, using a Beckman Coulter Avanti J-E centrifuge. 1 mL of YPGlu supernatant was kept and stored at -20°C for further Bis-Tris SDS-PAGE analysis. Cells were resuspended in 500 mL of fresh YPGal medium and incubated at 30°C for 72-120 h. 1 mL samples of pre-induction and induction were taken every 24 h and centrifuged at 13 000 rpm for 10 min. Supernatants were then concentrated down 10 x with Vivaspin centrifugal concentrators (Sartorius) following the manufacturer's instructions and analysed by Bis-Tris SDS-PAGE.

3.5.4 Recombinant protein expression in yeast cells

Starter cultures of transformed *K. lactis* cells were set up from either colonies or glycerol stocks as described in section 3.4.3. Starter cultures were inoculated in 500 mL at a ratio of 1:100 into fresh YPGlu media and incubated until cultures reached an OD_{600} ~1. Here, YPGlu medium was changed for YPGal medium as described in section 3.4.3. Cultures were then incubated at 30°C with shaking at 250 rpm for 48 h.

3.5.5 Harvesting protein from yeast culture

YPGal medium containing the heterologous protein of interest was recovered by centrifugation at 7 000 rpm for 20 min at 4°C. Following vacuum-filtration, the medium was diluted 1:100 in 20 mM Tris buffer with proteases inhibitors (EDTA-free inhibitor cocktail, Roche) and concentrated 1000 times with a tangential/cross flow cassette (Sartorious) with a molecular weight cut off (MWCO) of 5 kDa. 50 mL aliquots of concentrated YPGal were made and stored at -20°C for further protein purification.

3.6 Protein Analysis

3.6.1 Analysis by SDS-PAGE

The standard Tris-glycine method was used for sodium dodecyl sulphate-polyacrylamide gel electrophoresis (SDS-PAGE) analysis. IL-1α and IL-1β samples were analysed by 15% SDS-PAGE, whereas IL-1RAcP and IL-1RI samples were analysed by 10% SDS-PAGE. Both 10% and 15% acrylamide gels were typically 1mm thick with either 10 or 15 wells, depending on the number of samples to be analysed and were casted using the BioRad mini-Protean system (BioRad). For the separating gel, a solution containing 2.5 mL of resolving gel buffer (1.5 M Tris-HCl, 0.4% SDS, pH 8.8), 3.3 (10%) or 5 mL (15%) of 30% acrylamide solution (BioRad), 50 µL of 10% ammonium persulfate (APS) and 20 µL of tetramethylethylenediamine (TEMED) was prepared in 10 mL total volume. The stacking gel contained 2.5 mL of stacking gel buffer (0.5 M Tris-HCl, 0.4% SDS, pH 6.8), 1.3 mL of 30% acrylamide solution (BioRad), 50 µL of 10% APS and 20 µL of TEMED in 10 mL total volume. Following addition of APS and TEMED, the separating gel solution was added to the gel plates, water was dropped onto the surface to prevent evaporation and the gel was left to set

for 1 h. Water was then removed and the stacking gel solution along with a 1mm comb was added, again letting it set for 1 h.

For protein samples, 20 µL of sample were diluted with 20 µL 2 x SDS sample buffer containing β-mercaptoethanol (Appendix 3) and boiled at 100°C for 5 min before loading on to the gel alongside the protein molecular weight marker (Page Ruler Prestained Protein Ladder, Fermentas). Gels were then run at 180-200 V in 1 x running buffer (25 mM Tris, 192 mM glycine, 0.1% SDS, pH 8.3) for 45-60 min on a BioRad PowerPac power source (BioRad). After electrophoresis, gels were stained with InstantBlue (Expedeon, UK) for 16 h or ProQ Emerald 300 Glycoprotein Gel Stain (Invitrogen) following the manufacturer's protocol.

To analyse soluble and insoluble proteins, sample pellets were lysed with 50 µL of protein extraction BugBuster reagent (Novagen, UK). Lysate was centrifuged at 13,000 rpm for 10 min. As soluble proteins remained in the lysate supernatant (LSN) and insoluble proteins remained in pellet (LP), 20 µL of LSN and 20 µL of LP were added with sample buffer for SDS-analysis.

3.6.2 Analysis by Bis-Tris SDS-PAGE

IL-1RAcP and IL-1RI samples were analysed in either 1 mm thick Bis-Tris gradient gels (NuPAGE Novex 4-12% Bis-Tris Protein Gels, Invitrogen) or 10% Bis-Tris gels, whereas IL-1α and IL-1β samples were analysed in Bis-Tris gradient gels or 12% Bis-Tris gels. The separating gel was prepared by mixing 30% acrylamide (BioRad) (2.2 mL for 10% gels and 1.2 mL for 12% gels), 2% Bis-acrylamide (1.5 mL for 10% gels and 1.8 mL for 12% gels), 3 mL of 3.5 x gel buffer (1.25 M Bis-Tris, pH 6.5), 50 µL APS, 25 µL TEMED in a total volume of 10 mL. The stacking gel was prepared by mixing 1.3 mL of 30% acrylamide solution, 580 µL of 2% Bis-acrylamide

solution, 3 mL of 3.5 x gel buffer (1.25 M Bis-Tris, pH 6.5), 50 µL APS, 20 µL TEMED and 25 µL of 0.02% bromophenol blue. Gels were cast as described in section 3.5.1, typically 1 mm thick with either 10 or 15 wells, depending on the number of samples to be analysed. Protein samples were diluted with 2 x sample buffer added with β-mercaptoethanol. Following denaturation at 100°C for 5 min, samples were loaded on to the gel alongside the protein molecular weight marker (Page Ruler Prestained Protein Ladder, Fermentas), and electrophoresed at a constant current of 25 mAmp per gel in either 1 x high-molecular-weight (HMW) running buffer (25 mM 3-(N-morpholino)propanesulfonic acid (MOPS) (Melford, UK), 25 mM Tris, 1 mM ethylenediaminetetraacetic acid (EDTA) (Melford, UK), 0.1% SDS and 5 mM sodium bisulphite) or 1 x low-molecular-weight running buffer (25 mM 2-(*N*-morpholino)ethanesulfonic acid (MES) (Melford, UK), 25 mM Tris, 1 mM EDTA, 0.1% SDS and 5 mM sodium bisulphite) for 45-60 min. IL-1RAcP and IL-1RI samples were ran in HMW running buffer and IL-1α and IL-1β in LMW running buffer. After electrophoresis, gels were stained with InstantBlue (Expedeon, UK) or ProQ Emerald 300 Glycoprotein Gel Stain (Invitrogen) following the manufacturer's protocol.

3.6.3 Protein Identification by Mass Spectrometry

Following SDS-PAGE analysis, proteins detected in a band were taken to the Biomolecular Analysis Facility at the University of Manchester for identification by liquid chromatography coupled to tandem mass spectrometry (LC-MS/MS) after complete trypsin digestion.

3.6.4 Recombinant protein quantification using A_{280}

After purification protein concentrations were measured with a Cary 300 Bio Spectrophotometer (Varian Inc.). A spectrum measurement between 200-350 nM was taken and a three-point extrapolation was used to subtract the spectrum absorbance

from the base line (buffer) sample. Concentration was then calculated based on each protein predicted extinction coefficient (*ProtParam*) from the amino acid sequence of the protein under analysis.

3.6.5 SEC- multi-angle laser light scattering (MALLS)

SEC-MALLS analysis was carried out by the Biomolecular Analysis Facility at the University of Manchester. Protein samples of 0.2 mg/mL in 500 µl were loaded into the equilibrated Superdex 75 column (GE Health care) and eluted at 1 mL/min flow rate. MALLS data was collected using a DAWN HELEOS-II instrument (Wyatt Technology) using a laser wavelength of 658 nm. Refraction index and light scattering were measured with an Optilab rEX refractometer and QELS dynamic light scattering detector, respectively (both form Wyatt Technology).

3.7 Protein purification

3.7.1 Immobilised metal affinity chromatography

Protein constructs containing 6 x His tag were purified by immobilised metal affinity chromatography (IMAC) with cobalt resin (Talon Superflow Metal Affinity Resin, Clontech) using gravity flow columns (BioRad).

Following protein harvest from either bacteria or yeast cultures, the protein solution (bacteria lysate or yeast supernatant) was filtered with a 0.2 µm acrodisc (Millipore) and loaded on to a gravity flow column containing 2 mL of Talon resin previously equilibrated with equilibration buffer (Appendix 3) added with 5-20 mM imidazole and proteases inhibitors (EDTA-free inhibitor cocktail, Roche). Given that purification buffers were different for each protein, the detailed content of each buffer is shown in Appendix 3. The flow-through was recovered and a 20 µL sample was kept

at -20°C for further SDS-PAGE analysis. After recovering the flow-through, resin was washed with 20 column volumes (CV) of wash buffer. After washing, 20 µL sample of the resin was taken to confirm binding and stored at -20°C for further SDS-PAGE analysis. Proteins were then eluted by adding 2 mL of elution buffer containing 300 mM imidazole. This was repeated for a total of 5 elution cycles. A 20 µL sample of the final resin was taken and stored at -20°C for further SDS-PAGE analysis. Protein concentration in elution samples was quantified based on extinction coefficient of each protein at $A_{280.}$ Samples were further analysed in SDS-PAGE or Bis-Tris SDS-PAGE.

3.7.2 Ion exchange chromatography

In order to find the best ion exchange column for protein purification, a HiTrap IEX selction kit was used (GE Healthcare). The kit contains three HiTrap cation exchange columns (SP, SP-XL and CM) and four anion exchange columns (DEAE FF, Q, Q-XL and ANX-FF). For cation exchange columns, buffers with acidic *pKa* were used and for anion exchange columns buffers with basic *pKa* were chosen. To allow proteins to bind to the columns they must be held in buffers of low ionic strength (i.e 0 M NaCl) (Buffer A) and in order to elute the protein an ionic strength gradient was carried out by combining Buffer A with a high ionic strength buffer (i.e. 1 M NaCl) (Buffer B).

After harvesting and concentrating proteins produced in *K. lactis*, 10 mL samples were buffer-exchanged in Buffer A, at a pH appropriate for each IEX column (Appendix 3) using Vivaspin 20 centrifugal concentrators with a MWCO 5 kDa (Sartorious). After this, samples were applied to IEX column, previously equilibrated in Buffer A on an AKTA FPLC system (GE Healthcare Life Sciences). Unbound proteins were removed using 10 CV (10 mL) of buffer A and bound proteins were eluted with a slow stepwise increase in ionic strength using Buffer B. Increments of

100 mM NaCl were done every 4 CV.

After trying all columns provided in the HiTrap IEX selection kit, columns DEAE FF and Q-XL showed to be able to bind proteins, thus, these columns were chosen for protein purification from larger batches. For this, 5 mL Hitrap DEAE FF and 5 mL HiTrap Q-XL, both from GE Healthcare, were used as described above.

3.7.3 Size-exclusion chromatography

Protein samples for size-exclusion chromatography (SEC) were first concentrated to 0.5-5 mL volume using either an Amicon stirred cell (Millipore) with a 5 kDa MWCO membrane (Millipore), and/or a centrifugal concentrator Vivaspin 500 (Sartorious) before loading into the column. To remove debris, protein solutions were centrifuged at high-speed (13 000 rpm for 10 min at 4°C) immediately prior to loading. A HiLoad 26/600 Superdex 200 prep grade column (GE Healthcare) was used for IL-1α and IL-1β second stage purification and Superdex 200 10/300 GL column was used for IL-1RAcP second stage purification (GE Healthcare), with an AKTA FPLC system. IL-1α was eluted with 20 mM PBS, 300 mM NaCl, 50 mM Arg + Glu, 10 mM Met 5 mM β-mercaptoethanol, pH 8. IL-1β was eluted with 20 mM PBS, 150 mM NaCl, 50 mM Arg + Glu, 10 mM Met pH 7.5. IL-1RAcP was eluted with 20 mM Tris, 150 mM NaCl, 50 mM Arg + Glu, pH 8.

For IL-1α and IL-1β second stage purification with HiLoad Superdex 200 column, 5 mL of the concentrated IMAC samples were loaded into a 10 mL loop attached to the AKTA FPLC system, previously equilibrated with the corresponding buffer. Separation was carried out at 2 mL/min flow rate, collecting 1 mL elution fractions in a 96 well plate.

For IL-1RAcP, 0.5-1 mL of the concentrated IEX sample was loaded into a 2 mL loop attached to the AKTA FPLC, previously equilibrated with 20 mM Tris, 150 mM NaCl, 50 mM Arg, 50 mM Glu buffer at pH 8. Separation was carried out at 0.5 mL/min flow rate, collecting 0.5 mL elution fractions in a 96 well plate.

A calibration curve was done in both Superdex columns to determine the expected retention volume of proteins based on their molecular weight. For this, a Gel Filtration Calibration kit (GE Healthcare) containing HMW and LMW standards was used. The protocols and buffers used for protein purification (described above) were used for calibrations curves.

3.7.4 Concentration of protein samples

Amicon stirred cell (Millipore) with 5 kDa MWCO membrane (Millipore) was used to concentrate IL-1α and IL-1β IMAC and SEC samples. For IL1RAcP and IL-1RAcP-His YPGal media concentration and buffer exchange a tangential/cross flow cassette (Sartorious) with a 5 kDa MWCO was used following the manufacturer's instructions. Vivaspin centrifugal concentrators (Sartorius) with a MWCO 5 kDa were used to concentrate small volumes (1-10 mL) of protein solution.

3.7.5 Dialysis

For effects of pH on IL-1 experiments, dialysis was performed for buffer exchange in PBS buffer at pH 5.5, 6.2 or 7.5 for further biophysical and bioactivity characterization. 50-1000 μL aliquots of IL-1α or IL-1β purified samples were added to either Gabaflex-Mini Dialysis Tubes 800 μL, 3.5 kDa MWCO or Gabaflex-Mini Dialysis Tubes 3 mL, 3.5 kDa MWCO (Generon, UK) and the dialysis volume was 1000 times the volume of the sample. Samples were incubated with stirring overnight at 4°C. For larger volumes (> 10 mL), Snakeskin Pleated Dialysis Tubing 3.5 kDa

MWCO (Thermo Scientific) was used. For this, a piece 10-25 cm was cut and carefully washed with deionised water. Tubing clips were used to close both ends of the Snakeskin tubing and the tubing containing the sample was placed in a beaker with the appropriate buffer. Dialysis volume was 100-200 times the volume of the sample and was carried out with stirring at 4°C, overnight.

3.8 Cell culture

3.8.1 Maintenance of bEND5 cells

The mouse endothelial cell line bEND5 was grown in 75 cm^2 cell culture flasks at a density of 1-1.5 x 10^6 cells/mL with Dulbecco's Modified Eagle Medium (DMEM) supplemented with 10% heat-inactivated foetal bovine serum (FBS), 1% penicillin/streptomycin, 1% non-essential amino acids and 4 mmol/l L-Glutamine (Invitrogen). Cells were incubated at 37°C in a humidified incubator (5% CO_2/95% humidity). Media changes were done every 48 h. bEND5 cells between passages 10 and 20 were used for all experiments. DMEM media used for bEND5 cells was always prepared as it has been described in this section and in subsequent sections "supplemented DMEM" will refer to this composition.

3.8.2 Passaging bEND5 cells

bEND5 cells were subcultured every 4-5 days with an initial concentration of 1.5 x 10^6 cells/mL. For this, a confluent (95-100%) 75 cm^2 dish was washed in sterile PBS and 1 mL of 1 x trypsin (Invitrogen) was added, followed by incubation at 37°C for 3 min. After this, trypsin activity was stopped with the addition of supplemented DMEM and cell sheet was broken by gently pipetting. Cell solution was transferred to a 50 mL conical tube and centrifuged at 1 500 rpm for 5 min. Supernatant was discarded and the cell pellet was gently resuspended in fresh DMEM media and

replated as needed. To determine the viability and number of cells, a cell suspension was diluted 1:5 with a 0.4% trypan blue solution and viable cells (excluded by the dye) were counted on a haemocytometer under a light microscope.

3.8.3 Isolation of primary murine cortical neurons

Primary murine cortical neurons were obtained from wild type embryonic mice C57BL/6J at developmental stages of E14-17. Embryos were removed from their mothers after the latter were killed by cervical dissociation. The cortex was removed from embryos and incubated at 37°C with shaking at 50 rpm for 30 min in DMEM media supplemented with 1% penicillin/streptomycin, 1 x trypsin and 750 U of DNAse (Invitrogen). Trypsin was neutralised with 2 mL of foetal calf serum (FCS). A series of 3 washes with DMEM media supplemented with 10% FCS and 1% penicillin/streptomycin were conducted. Tissue was then transferred to 5 mL of Neuro Basal Media (NBM) without glutamine (Invitrogen) supplemented with 5% plasma derived serum (PDS), 1% L-Glutamine, 2% B27 with antioxidants (Invitrogen) and 1% penicillin/streptomycin and filtered through a sterile 80 μm gauze/mesh. Another 5 mL of supplemented NBM as well as fluorodeoxyuridine in a 1:1000 proportion were added and cells were seeded at a density of 0.4-0.6 x 10^6 cells/mL on 48 well plates previously coated with 20 μg/mL poly-D-Lysine. Primary neurons were incubated at 37°C in a humidified incubator (5% CO_2/95% humidity).

The animals were maintained and handled according to the Animal Scientific Procedures Act 1986 (as amended 2012) by licensed colleagues.

3.8.4 Maintenance of primary neurons

At day 5 after isolation from embryos, media was fully changed to NBM supplemented with 5% PDS, 1% L-Glutamine, 2% B27 without antioxidants

(Invitrogen) and 1% penicillin/streptomycin. At day 7 only half media was changed (with the above mentioned NBM media), to avoid cells get in contact with oxygen. Neurons were used for experiments at day 12.

3.9 Biophysical studies

3.9.1 ^{1}H- Nuclear Magnetic Resonance

For IL-1α and IL-1β folding state characterisation by ^{1}H-Nuclear magnetic resonance spectroscopy (^{1}H-NMR), samples purified by SEC were buffer exchanged to a lower salt buffer (20 mM phosphates, 50 mM Arg, 50 mM Glu, 50 mM β-mercaptoethanol, 10 mM EDTA, 10 mM DTT and 50 mM NaCl, pH 6.2), using a Snakeskin tubing as described in section 3.7.5. Samples were then concentrated to 0.5 mg/mL in 0.5 mL volume with a Vivaspin 500 centrifugal concentrator. ^{1}H-NMR spectra were acquired at 25°C on a Bruker 600 MHz spectrometer equipped with a cryoprobe. A 1D proton spectra with water presaturation were acquired using 32k data points and 9615.4 Hz spectral width, and processed in Topspin 1.3 (Bruker).

For pH effects on IL-1α and IL-1β studies, IL-1 samples purified by SEC were concentrated to 0.7-1 mg/mL with Vivaspin concentrators (depending on the sample volume). Samples were then dialysed against 20 mM phosphate, 50 mM NaCl buffer at the desired pH (5.5 or 7.5) with Gabaflex-mini dialysis tubes (depending on the sample volume) as described in section 3.7.5. ^{1}H-NMR spectra were acquired at 25°C on a Bruker 800 MHz spectrometer equipped with a cryoprobe. A 1D proton spectra with water presaturation were acquired as described above.

3.9.2 Circular Dichroism

Circular dichroism (CD) analyses were carried out using a J-810 spectropolarimeter (Jasco) equipped with a Peltier temperature controller and a Forma

Scientific water bath accessory. Data were collected and analysed using the Spectra Manager J-800 control driver software (Jasco). Both protein and buffer control samples were added to a CD quartz glass cell (path length 1 mm, Starna Scientific) and the far-UV spectrum was measured between 200 nm and 260 nm. The following instrumental parameters were adopted for consistent high quality signal: measurement ranges 260-200 nm, data pitch 0.2 nm, band width 1 nm, response 16 sec, scan speed 20 nm/min, 8 accumulations. To investigate the temperature dependence of the CD spectra, data were collected at 20°C and up to 85°C in 5°C increments with the following instrumental parameters: measurement ranges 260-200 nm, data pitch 0.2 nm, band width 1 nm, response 8 sec, scan speed 10 nm/min, 4 accumulations.

For each spectrum the signal was subtracted from a buffer base line control to generate a protein-derived spectrum. The mean residue elipticity [θ] was then be calculated to normalise the absorbance for path length and protein concentration using the equation:

$$\mathbf{[\theta]} = (\text{Millidegrees} \times \text{MRW}) / (\text{Path length} \times \text{concentration})$$

Resulting units for [θ] are deg cm^2 $dmol^{-1}$. The mean residue weight (MRW) units are g mol^{-1}, path length units are in mm and concentration units are in mg mL^1.

Protein samples for analysis by CD were first buffer exchanged into a compatible buffer (20 mM sodium phosphate, 100 mM NaCl at pH 5.5, 6.2 or 7.5) by dialysis, as described in section 3.7.5. Samples were adjusted to a concentration of 0.2 mg/mL with the corresponding buffer, in a volume of at least 200 µl, and loaded into the CD quartz 1 mm path length spectrophotometer cell. For full spectra, the chamber temperature was set to 25°C. To investigate the temperature dependence of the CD spectra, data were collected at 20° and up to 85°C in 5°C increments with the following instrumental

parameters: measurement ranges 260-200 nm, data pitch 0.2 nm, band width 1 nm, response 8 sec, scan speed 10 nm/min, 4 accumulations.

3.9.3 Intrinsic Fluorescence and Static Light Scattering

The melting temperature (T_m) and onset of aggregation (T_{agg}) of IL-1α and IL-1β were determined simultaneously with the instrument Optim 1000 (Avacta, Thorp Arch Estate, Wetherby). The T_m was obtained by measuring the intrinsic fluorescence of the proteins. The T_{agg} was obtained by measuring the static light scattering of the proteins at 266 nm (SLS_{266}) or 473 nm (SLS_{473}). The Optim protocol used was "Determine Melting and Aggregation Onset Temperatures" using a "Stepped Ramp" mode. 9 µL of samples at different pH were loaded in triplicate onto Micro-Cuvette Array sample holders. Temperature profile was set with 1°C increment from 20°C to 90°C. Raw data of intrinsic fluorescence and SLS were extracted using the Optim Analyser software (Avacta). T_m and T_{agg} were determined by visual examination of the traces of each sample transition derivative.

3.9.4 Analytical Ultracentrifugation

IL-1α and IL-1β were first buffer exchanged into 20 mM PBS buffer at pH 5.5, 6.2 or 7.5 by dialysis, as described in section 3.7.5. Samples were adjusted to a concentration of 0.2 mg/mL with the corresponding buffer, in a volume of at least 1 mL and were taken to the Biomolecular Analysis Facility at the University of Manchester (University of Manchester) for AUC analysis.

3.10 IL-1 bioactivity

3.10.1 IL-1 bioactivity in bEND5 cells

In order to determine if IL-1α and IL-1β were biologically active, effects of the heterologous IL-1α and IL-1β on IL-6 expression in bEND5 cells were tested. For this,

cells were plated on 96 well plates at a density of 1.5 x 10^5 cells/mL in supplemented DMEM and were treated with IL-1α and IL-1β when they reached ~ 95-100% confluence. Supplemented DMEM media was added with either IL-1α or IL-1β at an initial concentration of 1000 ng/mL and serial dilutions up to 0.5 ng/mL were done in supplemented DMEM. For controls, small aliquots of IL-1α or IL-1β were denatured at 100°C for 30 min and added to a final concentration of 500 ng/mL in supplemented DMEM media, with the purpose of proving that possible effects seen on IL-6 expression levels were due to IL-1α and/or IL-1β and not to possible bacterial contamination of purified samples. 100 ng/mL of bacterial lipopolysaccharide (LPS) (Sigma) was used as a positive control. Cells were treated in triplicates with the different concentrations of IL-1α and IL-1β, as well as controls, for 24 h. Media was then recovered and stored at -20°C for further mouse-specific IL-6 enzyme-linked immunosorbent assay (ELISA).

3.10.2 IL-1 bioactivity in primary cortical neurons

To test IL-1α and IL-1β biological activity in mice primary cortical neurons, treatments were prepared as described in section 3.10.1, using LPS as a positive control as well as heat-denatured IL-1α and IL-1β. As contact with oxygen needs to be avoided, only half media changes were done, thus, starting concentrations were 2 times more concentrated, i.e. to get a final concentration of 100 ng/mL DMEM media prepared at 200 ng/mL of IL-1. Neurons were treated at day 12 with IL-1α, IL-1β and controls for 24 h. Media was recovered and stored at -20°C for further mouse-specific IL-6 ELISA.

3.10.3 Effects of pH on IL-1 bioactivity in bEND5 cells

With the purpose of determining the effects of acidic pH on IL-1α and IL-1β bioactivity, IL-6 expression in bEND5 after treatment with IL-1α and IL-1β under acidic conditions was tested. Acidic conditions were simulated with HEPES-buffered salt solution (HBSS, 20 mM HEPES, 145 mM NaCl, 2.5 mM KCl, 1 mM $MgCl_2$, 1.8 mM $CaCl_2$, 10 mM Glu, 0.01% BSA) at pH 6.2. For this, bEND5 cells were plated on 96 well plates at a density of 1.5 x 10^5 cells/mL in supplemented DMEM, until they reached ~ 95-100% confluence. 50 ng/mL of IL-1α or IL-1β were added to either supplemented DMEM or HBSS and cells were treated with these solutions for 8 h, incubated at 37°C. Cell supernatants was recovered after 8 h of treatment or, for time course experiments, cell supernatant was recovered at 2, 4, 6 or 8 h, and stored at -20°C for further mouse-specific IL-6 ELISA.

3.10.4 Effects of temperature on IL-1 bioactivity in bEND5 cells

In order to determine the effects of temperature on IL-1 bioactivity, bEND5 cells were treated with IL-1α or IL-1β and incubated at 37°C or 40°C in a humidified incubator (5% CO_2/95% air) for 24 h. For this, bEND5 cells were plated in 96 well plates at a density of 1.5 x 10^5 cells in supplemented DMEM and incubated at 37°C until they reached ~95-100% confluence, when they were treated with 50 ng/mL of either IL-1α or IL-1β. A set of control cells was incubated at 37°C and another set at 40°C for 24 h. Cell supernatants were recovered and stored at -20°C for further mouse specific IL-6 ELISA.

3.10.5 ELISA

Immunoreactive IL-6 in cell culture supernatants was assayed with a validated mouse-specific ELISA DuoSet kit (R&D Systems, UK). bEND5 supernatants were

diluted 1:3 in PBS whereas cortical neurons supernatants were diluted 1:2 in PBS. Standards were assayed in triplicate and samples in duplicate. Absorbance was measured using a plate reader and results were calculated from the standard curve taking into account dilutions.

3.11 Graphs plot and statistical analyses

The software GraphPad Prism version 6 was used to plot SEC-MALLS, CD, SLS, Intrinsic fluorescence, AUC and Bioactivity assays. One-way ANOVA with Bonferroni's multiple comparison tests were carried out with the same software.

4 Results: Biophysical and functional characterisation of IL-1α and IL-1β

As was already discussed in the introduction, IL-1α and IL-1β are key players in the innate and adaptive immune response. Even though both IL-1α and IL-1β are 17 kDa proteins that seem to exert the same biological activity, they differ in several ways, including their *pI* (Dinarello et al., 1974, March et al., 1985). They are products of different genes (March et al., 1985), and given their high sequence homology it has been suggested that they resulted from gene duplication (Steinkasserer et al., 1992). At the amino acid level they are 26% homologous (March et al., 1985).

The aim of this part of work was to characterise the biophysical properties of the human mature form of both IL-1α and IL-1β, and the first step was to produce them with high purity in a heterologous system.

4.1 Sequence analysis of IL-1α and IL-1β

Analysis of protein sequences is an important tool when working with proteins, as it allows prediction of their properties, such as, among others, molecular weight, extinction coefficient and isoelectric point (*pI*). Such properties are of importance when designing experiments, as they have to be considered when preparing sample solutions, choosing best gels for PAGE analysis, etc. Thus, for the purpose of knowing the predicted properties of the constructs expressed in this work (native human mature form with additional tag residues such as 6 x His and cleavage sites), amino acid sequences of constructs as well as the native IL-1α and IL-1β (human mature form) (Figure 4.1, Appendix 1), were analysed using different bioinformatics approaches (Table 4.1-4.4).

Table 4.1 Amino acid composition of native IL-1α and the construct expressed here using the pET-15b/IL-1α plasmid.

Amino acid	Quantity		Percentage	
	IL-1α	pET-15b/IL-1α	IL-1α	pET-15b/IL-1α
Ala	13	13	8.4%	7.4%
Arg	3	4	1.9%	2.3%
Asn	10	10	6.5%	5.7%
Asp	10	10	6.5%	5.7%
Cys	1	1	0.6%	0.6%
Gln	8	8	5.2%	4.5%
Glu	8	8	5.2%	4.5%
Gly	5	8	3.2%	4.5%
His	3	10	1.9%	5.7%
Ile	13	13	8.4%	7.4%
Leu	15	16	9.7%	9.1%
Lys	11	11	7.1%	6.2%
Met	3	5	1.9%	2.8%
Phe	9	9	5.8%	5.1%
Pro	6	7	3.9%	4.0%
Ser	9	14	5.8%	8.0%
Thr	12	12	7.7%	6.8%
Trp	2	2	1.3%	1.1%
Tyr	7	7	4.5%	4.0%
Val	7	8	4.5%	4.5%
Total number of amino acids	155	176		

The molecular weight of IL-1α and IL-1β is reported to be 17 kDa, and this is consistent with the predicted molecular weight of both proteins expressed in this study, which are 17.64 kDa for IL-1α, and 17.38 kDa for IL-1β (Table 4.3 and 4.4). The protein construct obtained using pET-15b/IL-1α plasmid contains extra 6x His tag at the N-terminus, along with a protease recognition site that allows the cleavage of the 6x His tag with thrombin (Figure 4.1). It also has three extra linker residues between these 6x His tag and the thrombin cleavage site, and additional residues due to the presence of restriction sites. These additional amino acids increased molecular weight of IL-1α protein construct to 19.39 kDa. This protein contains only one cysteine, thus there is no disulfide bridge in its structure (see Table 4.1 for total amino acid

composition of IL-1α). The predicted *pI* of IL-1α is 5.3, and the additional residues changed this pH to 6.34 (Table 4.3). On the other hand, the protein construct obtained using the pQE-30/IL-1β plasmid (previously available and used in this research group) does not have a cleavage site between the 6x His tag and IL-1β, and only has four additional residues resulted from the presence of DNA restriction sites used during cloning process, thus, the additional residues only increased its molecular weight to 20.08 kDa, and the predicted *pI* is increased from 5.91 to 7.8 (Table 4.4). Therefore, although the expressed protein constructs had additional tag sequences, the impact of these sequences on the total molecular mass and pI was fairly minimal.

Table 4.2 Amino acid composition of native IL-1β and the construct expressed here using the pQE-30/IL-1β plasmid.

Amino acid	Quantity		Percentage	
	IL-1β	pQE-30/IL-1β	IL-1β	pQE-30/IL-1β
Ala	5	7	3.3%	3.9%
Arg	3	5	2.0%	2.8%
Asn	9	10	5.9%	5.6%
Asp	8	8	5.2%	4.5%
Cys	2	2	1.3%	1.1%
Gln	12	12	7.8%	6.7%
Glu	11	12	7.2%	6.7%
Gly	8	12	5.2%	6.7%
His	1	7	0.7%	3.9%
Ile	5	5	3.3%	2.8%
Leu	15	17	9.8%	9.6%
Lys	15	16	9.8%	9.0%
Met	6	7	3.9%	3.9%
Phe	9	9	5.9%	5.1%
Pro	8	10	5.2%	5.6%
Ser	14	16	9.2%	9.0%
Thr	6	7	3.9%	3.9%
Trp	1	1	0.7%	0.6%
Tyr	4	4	2.6%	2.2%
Val	11	11	7.2%	6.2%
Total number of amino acids	153	178		

Table 4.3 Comparison of the theoretical properties of IL-1α and the construct expressed here using the pET-15b/IL-1α plasmid.

	IL-1α	pET-15b/IL-1α
Molecular Weight (kDa)	17.64 kDa	19.39 kDa
Total number of amino acids	155	176
Molar extinction coefficient[1]	21430 M^{-1} cm-1	21430 M^{-1} cm^{-1}
Absorbance of 1 mg/mL solution[1]	1.215	1.075
Theoretical isoelectric point	5.30	6.34

[1] Molar extinction coefficient and absorbance of 1 mg/mL were calculated at 280nm

Table 4.4 Comparison of the theoretical properties of IL-1β and the construct expressed here using the pQE-30/IL-1β plasmid

	IL-1β	pQE-30/IL-1β
Molecular Weight (kDa)	17.38	20.08
Total number of amino acids	153	178
Molar extinction coefficient[1]	11585 $M^{-1}cm^{-1}$	11585
Absorbance of 1 mg/mL solution[1]	0.667	0.577
Theoretical Isoelectric point	5.91	7.8

[1] Molar extinction coefficient and absorbance of 1 mg/mL were calculated at 280nm

A)

```
   1  atgggcagcagccatcatcatcatcatcacagcagcggcctggtgccgcg  50
  51  cggcagccatatgagctttctgtccaatgtcaaatacaactttatgcgca  100
 101  tcatcaaatacgaatttatcctgaacgacgctctgaaccagtccatcatc  150
 151  cgtgccaacgatcagtatctgaccgcggccgcactgcataatctggatga  200
 201  agctgttaaatttgacatgggcgcgtacaaaagctctaaagatgacgcta  250
 251  aaattacggtcatcctgcgcattagcaaaacccaactgtatgtgacggca  300
 301  caggatgaagaccaaccggttctgctgaaagaaatgccggaaatcccgaa  350
 351  aaccattacgggcagtgaaaccaacctgctgtttttctgggaaacccatg  400
 401  gtacgaaaaactattttacctccgtcgcccacccgaacctgtttatcgca  450
 451  acgaaacaggattactgggtgtgcctggcaggtggtccgccgtcaatcac  500
 501  cgactttcaaattctggaaaatcaagcgtaataaggatcc            540
```

B)

```
   1  MGSSHHHHHHSSGLVPRGSHMSFLSNVKYNFMRIIKYEFILNDALNQSII     50
  51  RANDQYLTAAALHNLDEAVKFDMGAYKSSKDDAKITVILRISKTQLYVTA     100
 101  QDEDQPVLLKEMPEIPKTITGSETNLLFFWETHGTKNYFTSVAHPNLFIA     150
 151  TKQDYWVCLAGGPPSITDFQILENQA*                           176
```

Figure 4.1 Vector and construct sequences of human mature IL-1α. A) pET-15b/IL-1α vector DNA sequence. The DNA section coding for 6 x His is highlighted in red. DNA section coding for thrombin cleavage site is highlighted in green. Human mature IL-1α DNA sequence is in black. *NdeI* restriction site is highlighted in purple. *BamHI* restriction site is highlighted in blue**.** Additional codons from pET15-b vector are highlighted in orange. **B)** Human mature IL-1α protein sequence of the construct expressed in pET-15b vector. The 6 x His tag is highlighted in red. The cleavage site for thrombin is highlighted in green. The native sequence of human mature IL-1α is highlighted in black. Residues added due to the presence of *NdeI* restriction site are highlighted in purple. Additional amino acid residues from pET-15b are highlighted in orange. * represents stop codons.

A)

```
   1  atgagaggatcgcatcaccatcaccatcacggatccgcgccggtgcgcag  50
  51  cctgaactgcaccctgcgcgatagccagcagaaaagcctggtgatgagcg 100
 101  gcccgtatgaactgaaagcgctgcatctgcagggccaggatatggaacag 150
 151  caggtggtgtttagcatgagctttgtgcagggcgaagaaagcaacgataa 200
 201  aattccggtggcgctgggcctgaaagaaaaaaacctgtatctgagctgcg 250
 251  tgctgaaagatgataaaccgaccctgcagctggaaagcgtggatccgaaa 300
 301  aactatccgaaaaaaaaaatggaaaaacgctttgtgtttaacaaaattga 350
 351  aattaacaacaaactggaattgaaagcgcgcagtttccgaactggtatat 400
 401  tagcaccagccaggcggaaaacatgccggtgtttctgggcggcaccaaag 450
 451  gcggccaggatattaccgattttaccatgcagtttgtgagcagcgagctc 500
 501  ggtaccccgggtcgacctgcagccaagcttaattaggagctc          542
```

B)

```
   1  MRGSHHHHHHGSAPVRSLNCTLRDSQQKSLVMSGPYELKALHLQGQDMEQ  50
  51  QVVFSMSFVQGEESNDKIPVALGLKEKNLYLSCVLKDDKPTLQLESVDPK 100
 101  NYPKKKMEKRFVFNKIEINNKLEFESAQFPNWYISTSQAENMPVFLGGTK 150
 151  GGQDITDFTMQFVSSELGTPGRPAAKLN*                       178
```

Figure 4.2 Vector and construct sequences of human mature IL-1β. A) pQE-30/IL-1β vector DNA sequence. The DNA section coding for 6 x His is highlighted in red. Human mature IL-1β DNA sequence is in black. *BamHI* restriction site is highlighted in cyan**.** *SacI* restriction site is highlighted in blue. Additional codons from the pQE-30 vector are highlighted in orange. **B)** Human mature IL-1β protein sequence of the construct expressed in pQE-30 vector. 6 x His tag at the N-terminus is highlighted in red. The native sequence of human mature IL-1β is highlighted in black. Residues added due to the presence of *BamHI* restriction site are highlighted in cyan. Additional amino acid residues from pQE-30 are highlighted in orange. * represents stop codons.

4.2 IL-1 Expression

4.2.1 IL-1α expression in *E. coli*

In order to find the optimal expression of IL-1α, the pET-15b/IL-1α plasmid was transformed into T7 Express LysY *E.coli* strain. Expression trials were carried out in 50 mL cultures, incubated at 25°C, 30°C or 37°C, and induced with either 0.5 mM or 1 mM IPTG for 16 h. Samples of pre-induction (PI) state and induction state every 1 h for 6 h, as well as 16 h, were analysed in 12% Bis-Tris-PAGE, along with the soluble (LS) and insoluble (LP) fractions of 16 h expression (Figure 4.3). After induction with IPTG a band at ~20 kDa (indicated by black arrows) became stronger with time in all conditions tried (Figure 4.3 A-F), and it was more evident when expression was induced at 37°C with either 0.5 mM IPTG (Figure 4.3-E) or 1 mM IPTG (Figure 4.3-F). As mentioned in section 4.1, the molecular weight of the expressed IL-1α construct resulting from the pET-15b/IL-1α plasmid is 19.39 kDa and this MW is consistent with the ~ 20 kDa band that was later confirmed by liquid chromatography coupled to mass spectrometry (LC-MS/MS) to be human mature IL-1α. Generally, IL-1α expression was low, and after 16 h of expression the majority of the expressed protein was found in the insoluble fraction. Nevertheless, the total expression yield seemed to be slightly higher when induced at 37°C. With the purpose of finding the expression time for optimal soluble expression at 37°, the soluble and insoluble fractions at every 1 h up to 6 h, as well as at 16 h, were analysed by 4-12% Bis-Tris gradient-PAGE (Figure 4.4). Despite insoluble expression showed the same level as the soluble, the maximum soluble expression was reached after 3 h of induction with either 0.5 mM or 1 mM IPTG (Figure 4.4 A and B), and was higher with 1 mM compared to 0.5 mM These results showed that the optimal conditions for soluble IL-1α expression are 37°C and 1 mM IPTG.

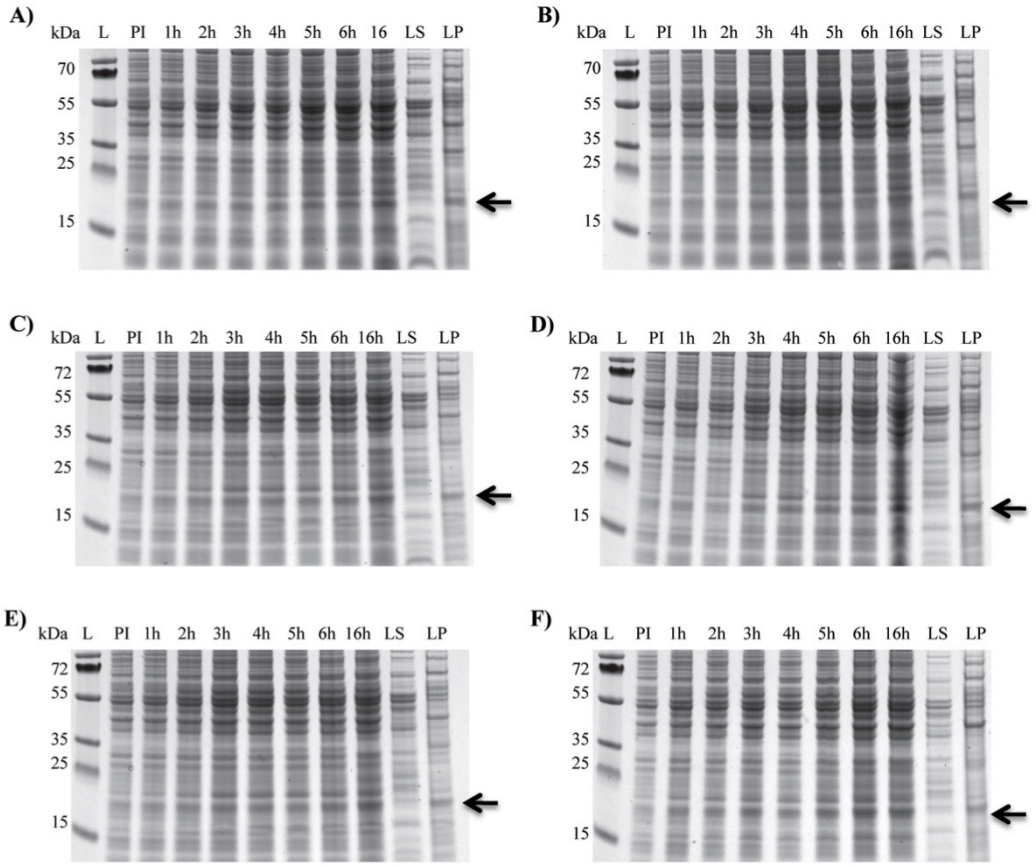

Figure 4.3 IL-1α expression trials in T7 Express *LysY* cells. T7 Express LysYcells were transformed with the pET-15b/IL-1α construct. Expression trials were carried out in 50 mL cultures, and induced at an $OD_{600} \approx 800$ for 16 h. Conditions used were: **A)** 25°C, 0.5 mM IPTG. **B)** 25°C, 1 mM IPTG. **C)** 30°C, 0.5 mM IPTG. **D)** 30°C, 1 mM IPTG. **E)** 37°C, 0.5 mM IPTG. **F)** 37°C, 1 mM IPTG The molecular weight marker is labelled **L**. Pre-induction sample is labelled **PI** and the soluble and insoluble fractions at 16 h are labelled **LS** and **LP** respectively. IL-1α presence is indicated with a black arrow.

Table 4.5 Summary of expression trials for IL-1α in *E. coli* strains

***E. coli* strain**	**Expression**	**Solubility**	**Purification**
Origami B DE3	Low	Low	Aggregation
BL21 DE3	Medium	Medium	Aggregation
Shuffle T7 Express	Low	Not detected	Not tried
Shuffle T7 Express *LysY*	Not detected	Not tried	Not tried
NiCo	Medium	Not detected	Not tried
T7 Express *LysY*	Medium	Low	Acceptable

E. coli strains were transformed with the plasmid pET-15b/IL-1α. Expression trials were carried out as described in section 3.3.4

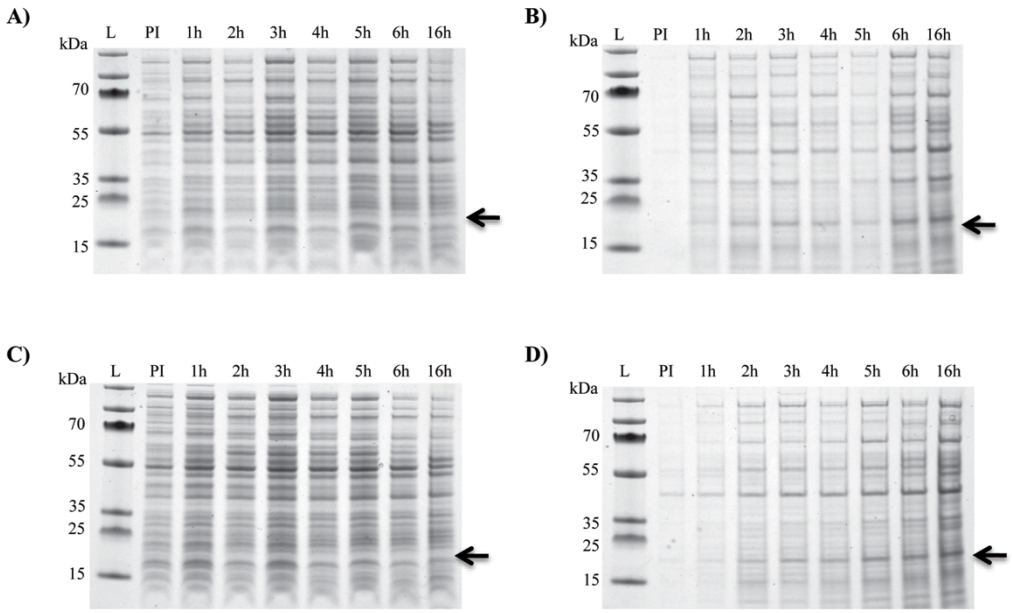

Figure 4.4 Soluble and insoluble expression of IL-1α in T7 Express LysY cells. T7 Express LysYcells were transformed with the pET-15b/IL-1α construct. Expression trials were carried out in 50 mL cultures at 37°C, and induced with 0.5 mM or 1 mM IPTG, at an $OD_{600} \approx 800$ for 16 h. **A)** Soluble expression induced with 0.5 mM IPTG. **B)** Insoluble expression induced with 0.5 mM IPTG. **C)** Soluble expression induced with 1 mM IPTG. **D)** Insoluble expression induced with 1 mM IPTG. The molecular weight marker is labelled **L**., and pre-induction sample is labelled **PI.**

In summary, IL-1α soluble expression was challenging. Several *E. coli* strains, not presented in this chapter, were also tested in order to optimise IL-1α soluble expression and purification, although without success. A summary of the strains used is shown in Table 4.5. The best soluble expression of IL-1α was obtained using *E. coli* strain T7 Express *LysY*, providing sufficient quantities of purified protein for this work.

4.2.2 IL-1β expression in *E. coli*

With the purpose of finding the best conditions for IL-1β expression in *E. coli,* the pQE-3/IL-1β plasmid was successfully transformed into Origami BDE3 cells. Expression trials were carried out in 50 mL cultures, incubated at 30°C or 37°C, and

induced with either 0.5 mM or 1 mM IPTG for 4 h. Samples of pre-induction (PI) state and induction state every 1 h were analysed by 12% Bis-Tris-PAGE, along with the soluble (LS) and insoluble (LP) fractions of 4 h expression (Figure 4.5). As mentioned in section 4.1, the protein expressed from the pQE-30/IL-1β construct has predicted molecular weight of 20.08 kDa, and after 1 h of induction with IPTG a band at ~20 kDa (indicated by black arrow) was evident and became stronger with time. LC-MS/MS analysis of the aforementioned ~ 20 kDa band confirmed it was IL-1β. Total expression was higher at 37°C when induced with 0.5 mM IPTG (Figure 4.5-C). Despite that a large portion of the total IL-1β expression was found in the insoluble fraction, the yield of soluble protein remained high.

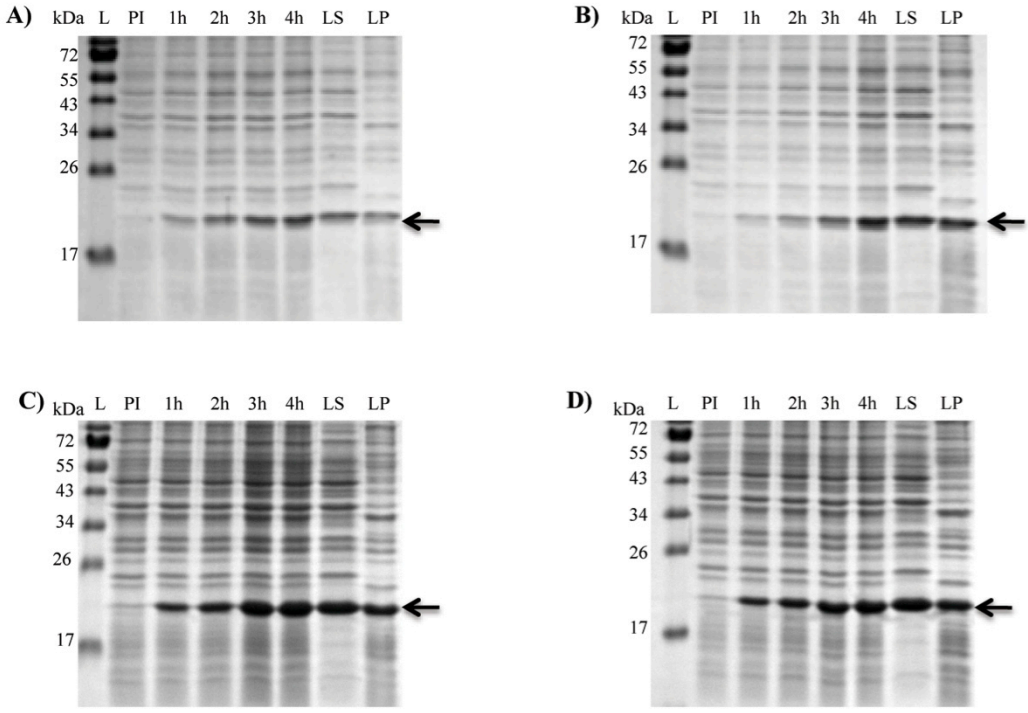

Figure 4.5 IL-1β expression trials in Origami B DE3 cells. Origami B DE3 cells were transformed with the pQE-30/IL-1β construct. Expression trials were carried out in 50 mL cultures, and induced at an $OD_{600} \approx 800$ for 4 h. Conditions used were: **A)** 30°C, 0.5 mM IPTG. **B)** 30°C, 1 mM IPTG. **C)** 37°C, 0.5 mM IPTG. **D)** 37°C, 1 mM IPTG. The molecular weight marker is labelled **L**. Pre-induction sample is labelled **PI** and the soluble and insoluble fractions are labelled **LS** and **LP** respectively. IL-1β presence is indicated with a black arrow.

4.3 IL-1 purification

Purification of IL-1α and IL-1β was carried out under native conditions in two steps, starting with immobilised-metal affinity chromatography (IMAC), and followed by size exclusion chromatography (SEC). With this purpose, the optimised conditions for soluble protein expression were used to scale up cultures.

4.3.1 IL-1α purification

Despite efforts to obtain high yield of soluble expression of IL-1α, total and soluble expression remained low, reaching its maximum level when induced at 37°C with 1 mM IPTG, for 3 h in T7 Express *LysY* cells. Therefore, in order to obtain enough soluble protein for further characterisation and bioactivity studies, IL-1α cultures were scaled up to 3 L. After cell lysis and centrifugation at 17,000 rpm, the soluble fraction was removed to be used for IMAC purification. For this, 2 mL of equilibrated Talon superflow metal affinity resin (Clontech Laboratories Inc., USA) were used in a 20 mL gravity column. The flow-through was loaded in a second column with 2 mL of equilibrated Talon resin. After this, both columns were washed with wash buffer containing 20 mM imidazole, to remove unspecific bound proteins, and IL-1α was eluted with 300 mM imidazole from both columns. Samples at each IMAC purification step were analysed by 12% Bis-Tris-PAGE (Figure 4.6 A and B). As seen in Figure 4.6, there was a high level of unspecific binding to the Talon resin beads (RB and Elution lanes). The manufacturer recommends washing the resin bound with 10-20 bed volumes of wash buffer and we increased it up to 30 bed-volumes. 20 mM imidazole was also added to equilibration and wash buffers with the purpose of reducing unspecific binding. However, IL-1α-His binding to the cobalt resin was weak, as seen in FT1 fraction (Figure 4.6 A and B), thus, imidazole concentration in washes could not be further increased.

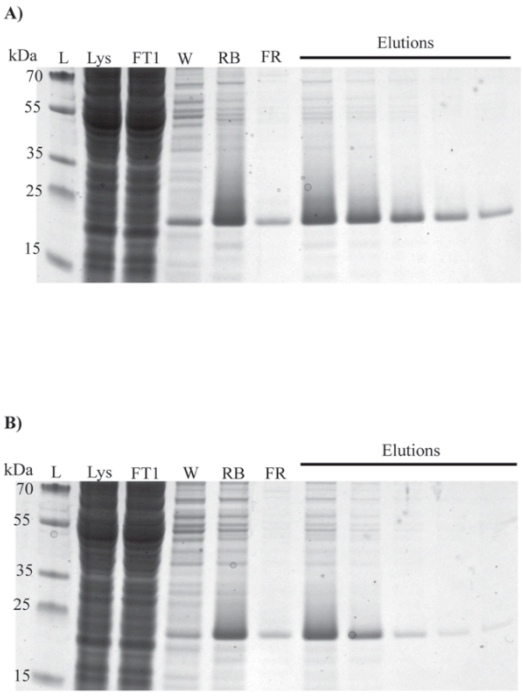

Sample	Concentration (mg/ml)	Quantity (mg)
Elution 1	0.95	1.9
Elution 2	0.77	1.54
Elution 3	0.53	1.06
Elution 4	0.29	0.58
Elution 5	0.22	0.44
Total protein (mg)		5.52

Sample	Concentration (mg/ml)	Quantity (mg)
Elution 1	1.41	2.82
Elution 2	0.80	1.60
Elution 3	0.31	0.62
Elution 4	0.20	0.40
Elution 5	0.18	0.36
Total protein (mg)		5.55

Figure 4.6 IMAC purification of IL-1α. 12% Bis-Tris-PAGE showing each step of purification. Gel **A)**, shows purification from *E.coli* cleared lysate (**Lys**), flow-through (**FT1**), wash (**W**), resin bound after washes (**RB**), final resin after elutions (**FR**), and elutions (**E1**, **E2**, **E3**). The flow-through FT1 was loaded in a second IMAC column and purified as the first one, samples of this second purification are showed in gel **B)**. IL-1α could be recovered from flow-through and its yield was increased satisfactorily. The molecular weight ladder is labelled as **L**. Concentration calculations were made based on A_{280} and quantity was calculated by multiplying concentration and volume.

Following IMAC purification, all elutions resulting from purification from cleared lysate and flow-through, were pooled together and concentrated to 5 mL, using an Amicon pressure concentrator with a MWCO 5 kDa membrane. After concentration, IL-1α IMAC samples were purified by SEC with a Hiload 26/600 Superdex 200 prep grade column (GE Helathcare). Interestingly, after concentration, the majority of unspecific bands shown in elutions disappeared, and the expected band at ~ 20 kDa became more abundant (Figure 4.7 B, IMAC conc lane). Nevertheless, an

upper band of more than 25 kDa, can be seen in the protein solution. The SEC purification of concentrated IMAC samples showed two peaks (Figure 4.7 A).

A)

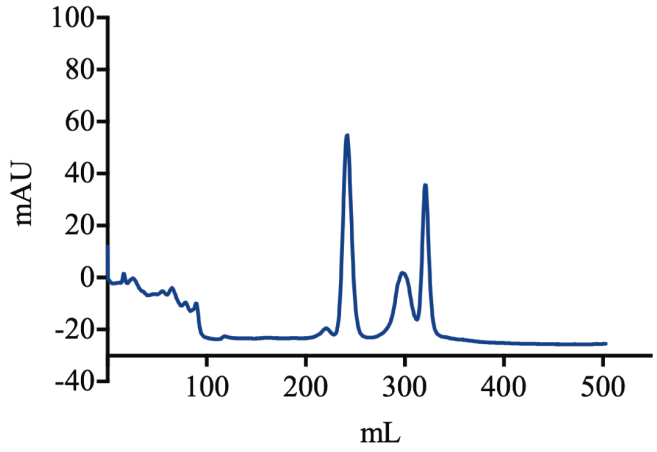

B)

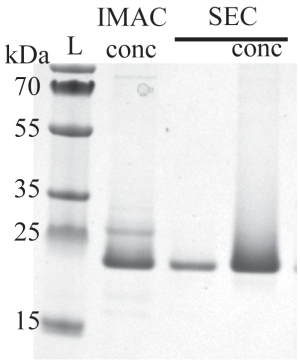

Sample	Concentration (mg/mL)	Quantity (mg)
IMAC conc	1.7	6.8
SEC	0.8	2.3
SEC conc	1.2	1.2

Figure 4.7 SEC purification of IL-1α. Elutions resulting from IMAC purification were pooled together and concentrated for further size exclusion purification. **A)** SEC trace of IL-1α shows 3 peaks. The main peak corresponds to IL-1α and the second and third to lower molecular weight peptides, possibly resulting from degradation. **B)** The main peak shown in SEC trace was analysed by 12% Bis-Tris-PAGE before and after concentration (conc). **L**, ladder. Concentration calculations were made based on A_{280} and quantity was calculated by multiplying concentration and volume.

The main peak corresponded to IL-1α, and the second peak corresponded to lower molecular weight molecules, possibly due to degradation of the sample. A small "shoulder" can be seen at the bottom of the main peak (Figure 4.7 A) and this "shoulder" corresponded to the protein of more than 25 kDa band seen in IMAC purification. Bis-Tris-PAGE analysis of SEC purification (Figure 4.7 B) showed that the band at ~ 25 kDa was separated from IL-1α, remaining in the aforementioned "shoulder", and IL-1α was obtained with an acceptable purity.

In summary, IL-1α was purified under native conditions with an acceptable yield. Regardless of the low soluble expression seen in expression trials, scaling up cultures to 3 L allowed increasing soluble expression and the yield of IMAC-purified protein obtained from 3 L culture growth was 11 mg in total.

4.3.2 IL-1β purification

IL-1β was expressed in a soluble form with a high yield in Origami B DE3 cells after 4 h induction with 0.5 mM IPTG. Thus, with the purpose of purifying it for further characterisation and bioactivity analysis, its production was scaled up to 1 L using these conditions. After cell lysis and centrifugation, the resulting supernatant containing the soluble fraction was loaded in 2 mL of Talon superflow resin (Clontech, USA) pre-equilibrated in Tris buffer. After washing steps to remove any unspecific binding, IL-1β was eluted with 300 mM imidazole. Figure 4.8 shows Bis-Tris-PAGE analysis of the IMAC purification process. Although IL-1β was not fully removed from the cobalt resin, as seen in the final resin (FR) lane, IL-1β was purified with high yield, as it can be seen in elution lanes (E1, E2, E3).

After IMAC purification, elutions were pooled together and concentrated using an Amicon pressure concentrator with a MWCO 5 kDa membrane, to 5 mL. SEC

purification was carried out with a Hiload 26/600 Superdex 200 prep grade column. (GE Healthcare). SEC purification shows a single peak (Figure 4.9 A) and the analysis by 12% Bis-Tris gel (Figure 4.9 B) shows that this peak corresponds to IL-1β. This two-step protocol of IMAC purification followed by SEC was successfully optimised to produce IL-1β samples of high purity and with a high yield.

A)

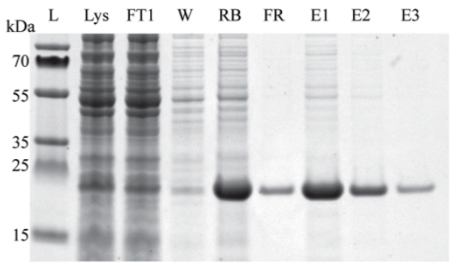

B)

Sample	Concentration (mg/mL)	Quantity (mg)
Elution 1	6.05	30.25
Elution 2	2.72	13.6
Elution 3	1.10	5.5
Total protein (mg)		49.5

Figure 4.8 IMAC purification of IL-1β. 12% Bis-Tris-PAGE showing each step of purification. IL-1β was purified from Origami B (DE3), under native conditions with a high yield, as seen in elution (**E1, E2, and E3**). **L**, ladder; **Lys**, cleared lysate; **FT** flow-through, **W** wash; **RB** resin bound after washes; **FR** final resin after elutions. Concentration calculations were made based on A_{280} and quantity was calculated by multiplying concentration and volume.

A)

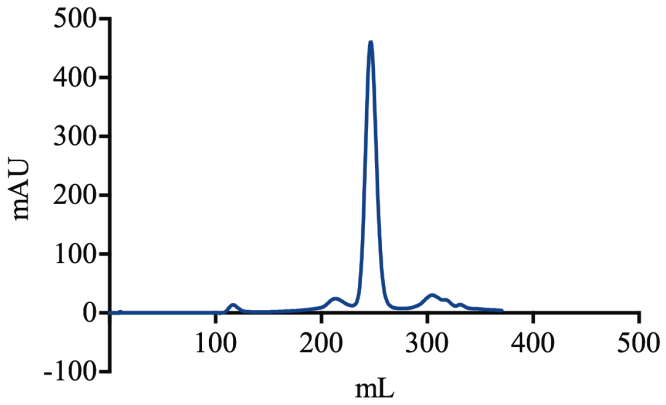

B)

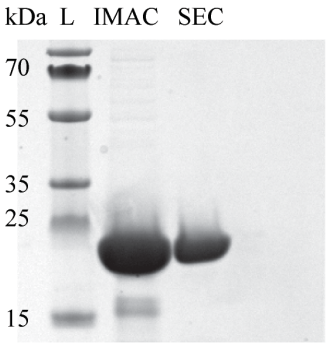

Sample	Concentration (mg/mL)	Quantity (mg)
IMAC conc	14	70
SEC	1.7	34

Figure 4.9 SEC purification of IL-1β. Elutions resulting from IMAC purification were pooled together and concentrated for further size exclusion purification. **A)** SEC trace of IL-1β shows a single peak. **B)** The original sample from IMAC purification and the peak shown in SEC trace were analysed by 12% Bis-Tris-PAGE. **L**, ladder. Concentration calculations were made based on A_{280} and quantity was calculated by multiplying concentration and volume.

4.4 IL-1 characterization

After successfully producing IL-1α and IL-1β with high purity, with sample identity confirmed by LC-MS/MS, the next step was to characterise these IL-1 ligands using a range of techniques. For this purpose, IL-1 produced in *E. coli* was analysed by multi-angle laser light scattering coupled to size exclusion chromatography (SEC-MALLS), circular dichroism (CD), fluorescence and one dimension nuclear magnetic resonance spectroscopy (1D NMR)

4.4.1 IL-1 SEC-MALLS analysis

Following 2-steps purification, IL-1 was analysed by SEC-MALLS. SEC-MALLS allows determination of the molecular weight and size distribution of proteins in solution, which is important to understand their oligomerisation state and function (Oliva et al., 2001).

IL-1α SEC-MALLS analysis (Figure 4.10) showed a uniform mass distribution. Light scattering gave a molecular mass of 19.25 kDa, which is consistent with the predicted molecular weight (Table 4.3, pET-15b/IL-1α construct), confirming that 100% of IL-1α is monomeric and highly pure. IL-1β SEC-MALLS analysis also showed that the protein has a uniform mass distribution (Figure 4.11-A) and 100% of the protein mass analysed is monomeric and highly pure. Light scattering of the elution gave a molar mass of 17.15 kDa, which is not consistent with the predicted molecular weight for the construct pQE-30/IL-1β (Table 4.4), but is consistent with the predicted and reported molecular weight for IL-1β. Nevertheless, as this construct does not have any cleavage site between the His-tag and the protein sequence, the molecular weight added by the tag is very low thus, this difference between the predicted molecular weight (20.08 kDa) and the molecular mass given by light scattering (17.15 kDa) is not significant.

A)

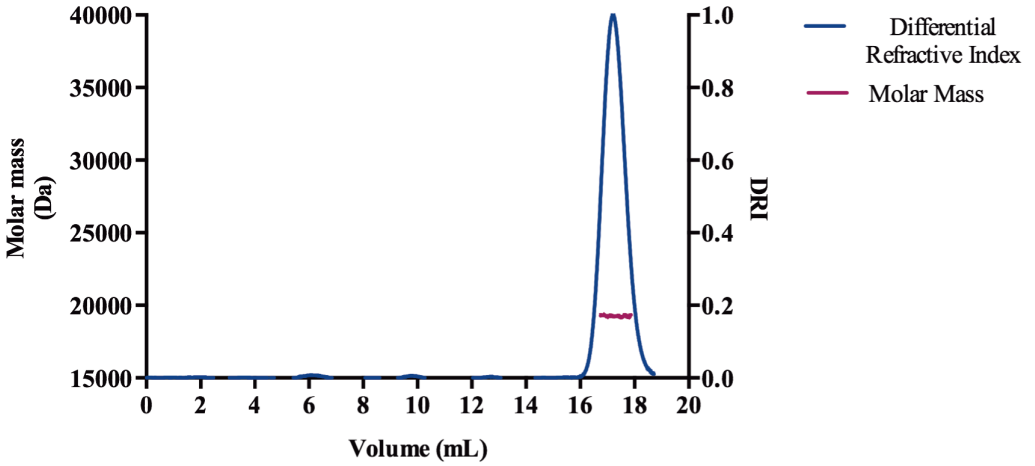

B)

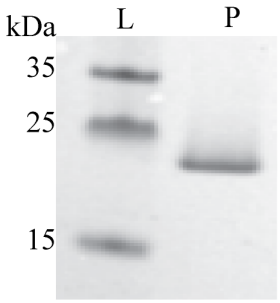

C)

Molar mass (Da)	19250
Mass fraction (%)	100

Figure 4.10 SEC-MALLS analysis of IL-1α. After 2-step purification IL-1α was analysed by SEC-MALLS. **A)** Protein mass detected by MALLS alongside the SEC trace. Only one protein population was detected with a molar mass of 19.25 kDa. **B)** 12% Bis-Tris-PAGE analysis of sample recovered after SEC-MALLS shows a band at ~ 20 kDa. **L**, ladder; **P**, peak (SEC-MALLS sample). **C)** SEC-MALLS data on detected protein. The peak represents 100% of the total protein with a molar mass of 19.25 kDa.

A)

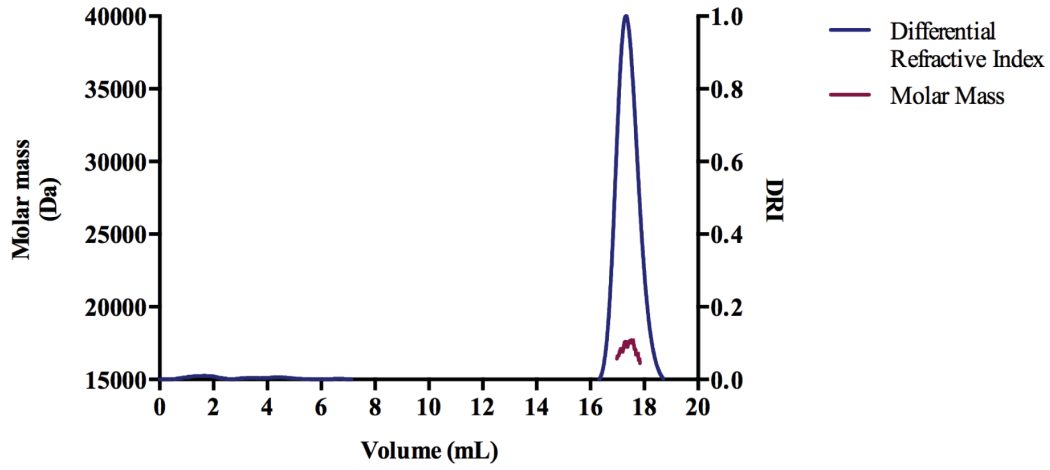

B)

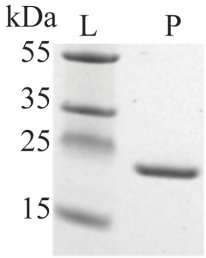

C)

Molar mass (Da)	17150
Mass fraction (%)	100

Figure 4.11 SEC-MALLS analysis of IL-1β. After 2-step purification IL-1β was analysed by SEC-MALLS. **A)** Protein mass detected by MALLS alongside the SEC trace. Only one protein population was detected with a molar mass of 17.15 kDa. **B)** 12% Bis-Tris-PAGE analysis of sample recovered after SEC-MALLS shows a band at ~ 20 kDa. **L**, ladder; **P**, peak (SEC-MALLS sample). **C)** SEC-MALLS data on detected protein. The peak represents 100% of the total protein with a molar mass of 17.15 kDa.

4.4.2 Circular Dichroism

Analysis of proteins by circular dichroism (CD) in the far UV region allows assessment of their secondary structure. IL-1 is known for its β-barrel structure that consists of anti-parallel β-sheets (Finzel et al., 1989). In order to characterise IL-1 secondary structure, purified samples were buffer-exchanged to PBS, without addition of amino acids (Arg + Glu), which were otherwise used during protein purification, given that these amino acids have elipticity and can interfere with the protein CD spectrum. Samples were diluted to 0.2 mg/mL in PBS buffer, prior to collection of CD spectrum at 25°C, between 200 and 260 nm.

As expected, CD spectra in the far UV region of both proteins, IL-1α and IL-1β, showed the characteristic β-sheet that consists of a major negative peak at 215-220 nm (Figures 4.12-A and 4.13-A). Interestingly, IL-1α CD spectrum showed a positive peak between 224-240 nm (Figure 4.12-A), which is not present in IL-1β spectrum (Figure 4.13-A). Woody (Woody, 1994) demonstrated that the interactions between side chains of aromatic amino acids such as Trp, Tyr and Phe can contribute to CD spectra of proteins in the far UV, being responsible of the positive peak at 220-230 nm that some proteins show. Proximity of aromatic amino acids within IL-1α and IL-1β structures are shown in Figure 4.14. IL-1α contains a higher level of Trp (2) and Tyr (7) than IL-1β (1 Trp and 4 Tyr) (Tables 4.1 and 4.2). Furthermore, these aromatic residues are in close proximity within IL-1α structure (Figure 4.14-A), whereas Trp, Tyr and Phe are less clustered together within IL-1β structure (Figure 4.14-B). Thus, differences in CD spectra of IL-1α and IL-1β are consistent with the level of Tyr and Trp content and their clustering within the structures.

A)

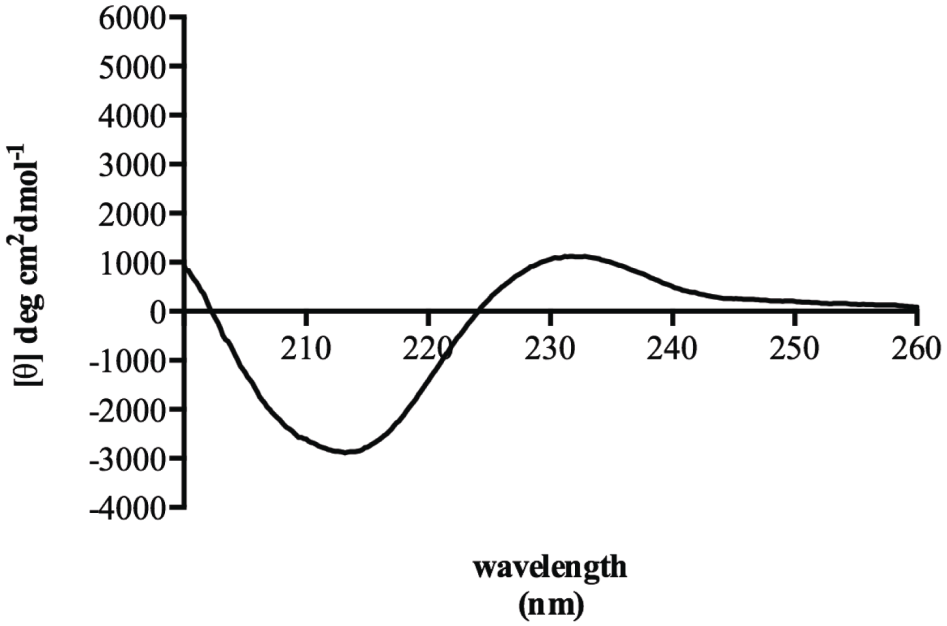

B)

α-helix	β-sheet	Coil
0.09	0.43	0.47

Figure 4.12 Circular dichroism analysis of IL-1α purified from *E.coli*. IL-1α was analysed in the far UV region at 25°C. The CD spectrum (**A**) shows evidence that IL-1α has β-sheet conformation. An unusual peak at 230 nm is also shown. Dichroweb prediction with K2D algorithm (**B**), estimates IL-1α β-sheet content to be 43%.

Dichroweb analysis was carried out using the algorithm K2D, which is a program that determines α-helix, total β-structure and coils, by finding correlations in data (Greenfield, 2006b). IL-1α Dichroweb analysis suggests that the protein structure is mainly β-sheet (43%) and turns (47%), with a very low level of α-helix (9%) (Figure 4.12-B). IL-1β Dichroweb analysis was very similar to IL-1α, being mainly β-structure (44%), and turns (48%), and only has 8% of α-helix (Figure 4.13-B). This is consistent with previous structural analysis of IL-1, which demonstrated that these proteins

structure consist of anti-parallel β-sheets that form a β-barrel. The predicted α-helix level was low as expected.

A)

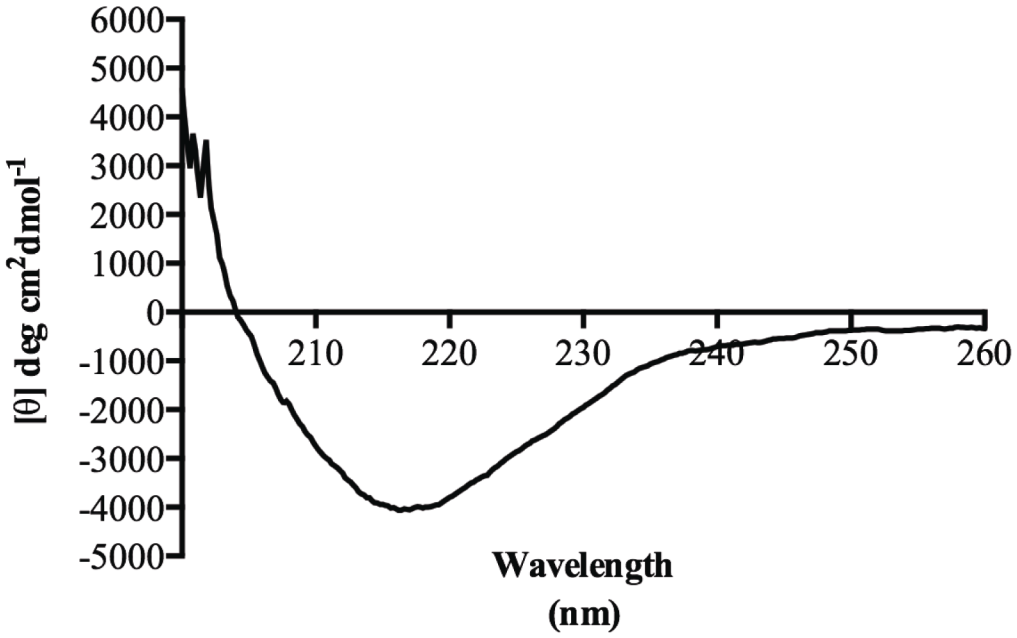

B)

α-helix	β-sheet	Coil
0.08	0.44	0.48

Figure 4.13 Circular dichroism analysis of IL-1β purified from *E.coli*. IL-1β was analysed in the far UV region at 25°C. The CD spectrum (**A**) shows evidence that IL-1β has β-sheet conformation. Dichroweb prediction with K2D algorithm (**B**), estimates IL-1β β-sheet content to be 44%.

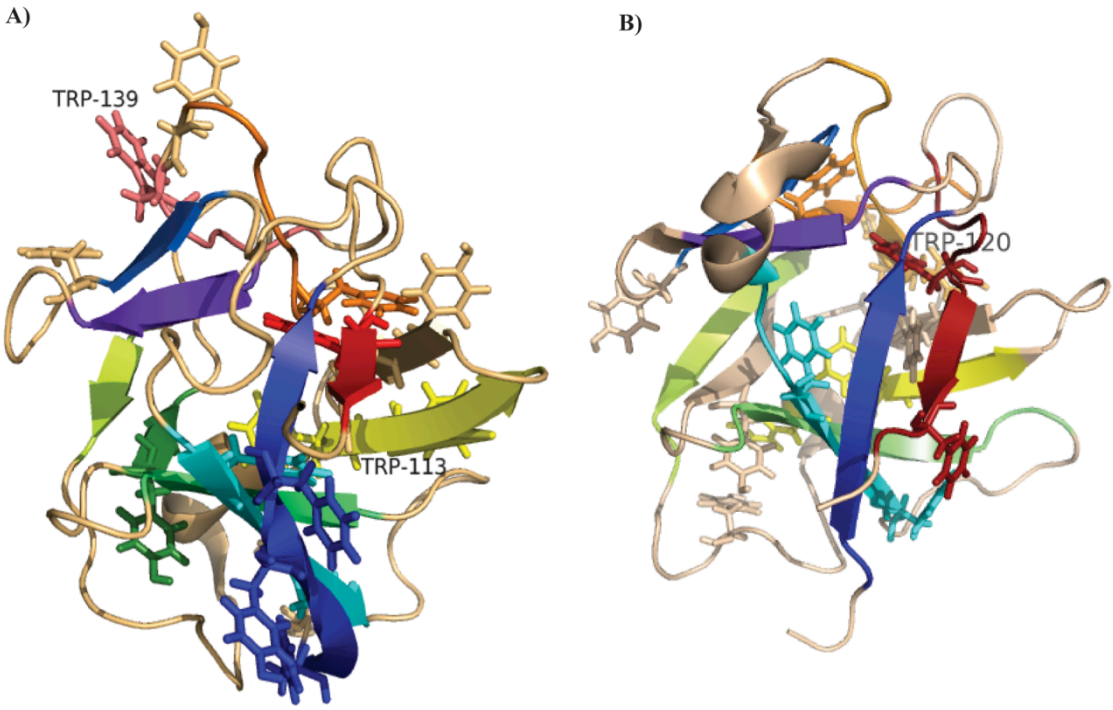

Figure 4.14 IL-1α and IL-1β models showing position of aromatic amino acids. Aromatic amino acids are shown as sticks. **A)** IL-1α contains two Trp (labeled), seven Tyr and 9 Phe which are close together within the structure. The proximity of aromatic amino acid side chains could contribute to the positive peak in the 230 nm region. **B)** IL-1β aromatic amino acids content is lower than that of IL-1α, as it contains 1 Trp (labeled), 4 Tyr and 9 Phe. IL-1α PDB ID: 2KKI (Chang et al., 2010); IL-1β PDB ID: 6I1B (Clore et al., 1991)

In summary, IL-1α and IL-1β produced in *E. coli*, have the correct secondary structure, previously reported as β-barrel.

4.4.4 IL-1 ^{1}H-NMR

Nuclear magnetic resonance spectroscopy (NMR) is a powerful tool for the study of the structure of organic compounds as well as protein structure, dynamics and interactions. For this, several NMR methods have been developed. The earliest applications of NMR mainly utilised proton NMR (^{1}H-NMR), also sometimes referred to as 1D NMR (Marion, 2013). ^{1}H-NMR is widely used to study the structure of

organic compounds and was the first NMR method used to study proteins with unknown structures. This method utilises a magnetic field to allow the measurement of the resonance frequency of the proton nuclei within a compound. These signals, that depend on the environment surrounding the proton (i.e. shielding by electrons), are characterised by their chemical shifts, as they are measured as the resonating frequency difference in parts per million (ppm) from a reference compound. Thus, depending of their molecular composition and 3D structure, molecules will show a particular NMR spectrum.

Given the complexity of proteins and spectra, ^{1}H-NMR only gives an overall indication for the presence of the tertiary structure of a protein, but this method is quick and does not require isotopic labelling. Therefore, for the purposes of this work, IL-1α and IL-1β were analysed by ^{1}H-NMR, in order to confirm that they were folded. Figures 4.15 and 4.16 show NMR spectra of IL-1α and IL-1β, respectively. The presence of upfield-shifted methyl signals near 0 ppm (Figures 4.15-A and 4.16-A) indicates that both proteins are folded. The chemical shift of these is characteristic of methyl groups located within close proximity to the side chain of aromatic amino acids such as Tyr, Phe and tryptophan Trp. This arrangement of amino acid side chains is typical of that found within the hydrophobic core of a globular protein. The electrons within the aromatic ring can provide a significant shielding effect from the magnetic field to nearby methyl groups therefore lowering their chemical shift relative to methyls within unstructured regions.

The well-dispersed amide signals observed from 8 to 9.8 ppm (Figures 4.15-B and 4.16-B), are also typically present in a folded protein, they are characteristic of amide groups situated within a β-sheet secondary structure; signals closer to 10-10.5 ppm originate from tryptophan side chain indoles.

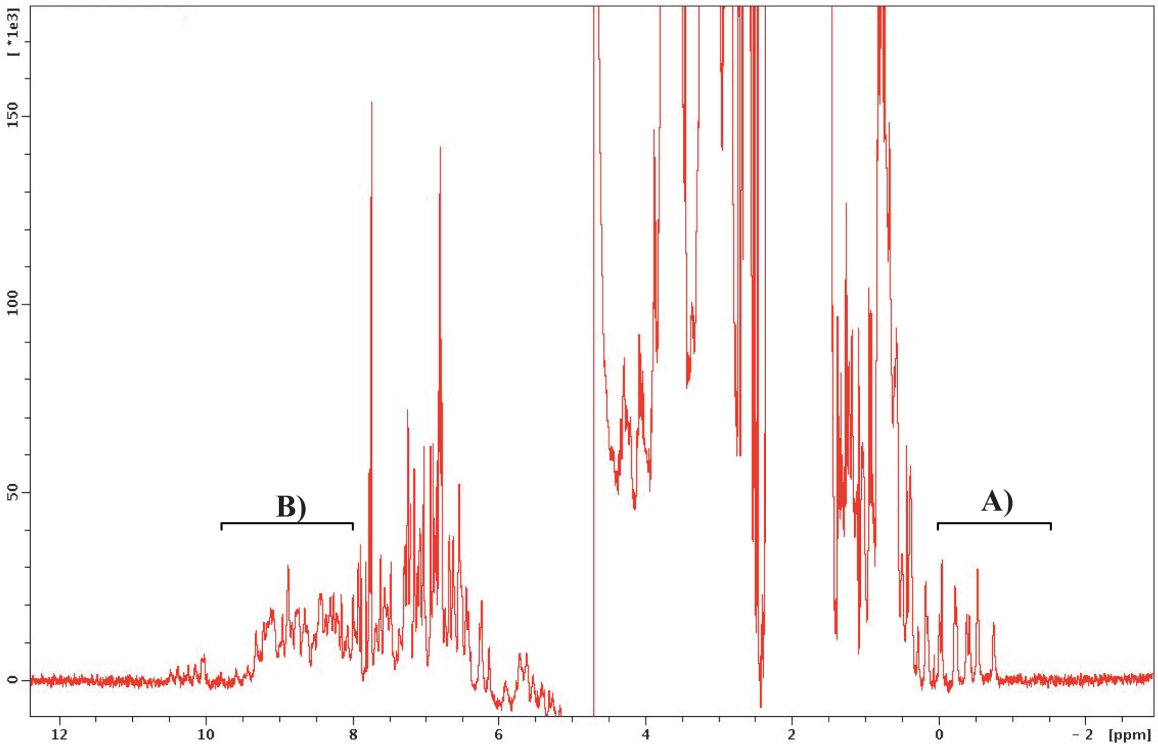

Figure 4.15 ^{1}H-NMR spectrum of IL-1α. IL-1α purified from *E. coli* was analysed by ^{1}H-NMR with the purpose of confirming it was properly folded. The presence of multiple upfield shifted methyl signals near 0 ppm (**A**) indicates that the protein is folded. The well-dispersed amide signals observed in the range 8-9.8 ppm (**B**) are typically observed in folded proteins with β-sheet secondary structure. The horizontal axis shows proton chemical shift and the vertical axis the signals intensity (arbitrary units)

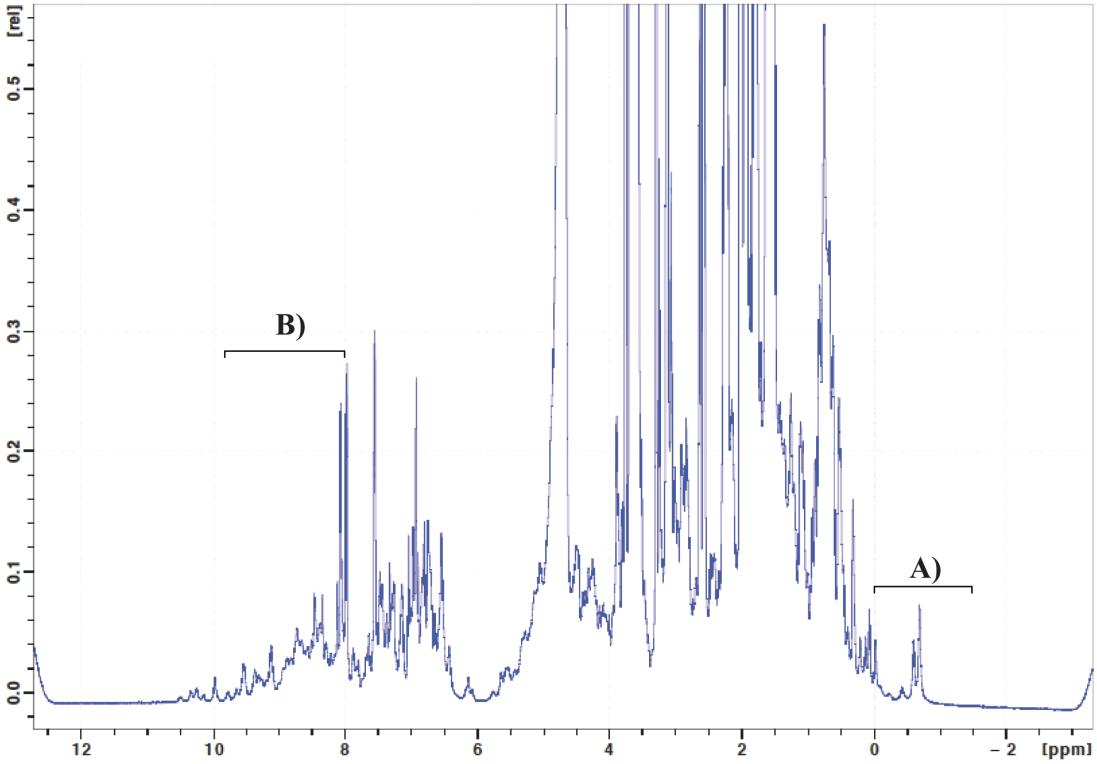

Figure 4.16 ^{1}H-NMR spectrum of IL-1β. IL-1β purified from *E. coli* was analysed by ^{1}H-NMR with the purpose of confirming it was properly folded. The presence of multiple upfield shifted methyl signals near 0 ppm (**A**) indicates that the protein is folded. The well-dispersed amide signals observed in the range 8-9.8 ppm (**B**) are typically observed in folded proteins with β-sheet secondary structure. The horizontal axis shows proton chemical shift and the vertical axis the signals intensity (arbitrary units)

4.5 Background on IL-1 Bioactivity

To assess the biological activity of the purified cytokines, a number of experiments have been conducted. To assist the reader to follow these more easily, below the brief background on IL-1 bioactivity is included.

In response to infection, tissue injury or stress, IL-1 binds to IL-1RI and subsequently recruits IL-1RAcP, activating multiple parallel pathways that synergistically lead to the transcription of genes encoding acute phase and pro-inflammatory proteins. The formation of the IL-1/IL-1RI/IL-1RAcP complex leads to

the recruitment of the adapter protein MyD88 to the TIR domains of IL-1 receptors, leading to the recruitment of IRAK1 and IRAK2, which in turn attract TRAF. As a consequence, the inhibitor of NFκB (IκB) is phosphorylated and then degraded permitting the translocation of NFκB to the nucleus and the subsequent secretion of IL-6 and other cytokines and inflammatory mediators.

Lipopolysaccharide (LPS), a key component of the Gram-negative bacteria cell wall, is known for its proinflammatory properties. LPS can also induce IL-6 expression in endothelial cells through its binding to the Toll-like receptor 4 (TLR4), which cytoplasmic domain shares homology to the TIR domain.

4.5.1 IL-1 bioactivity in endothelial cells

The mouse endothelial cell line bEnd5, is a well-established *in vitro* model of blood-brain barrier that can be exposed under normal and hypoxic conditions (Yang et al., 2007). It is worth pointing out that, given their high level of identity with murine IL-1 (Gray et al., 1986), human IL-1α and IL-1β have been proved to be able to exert their biological activity through IL-1RI in murine systems (Dinarello et al., 1986, Akeson et al., 1996). Thus, in order to test the bioactivity of purified IL-1α and IL-1β produced in *E.coli*, here bEnd5 cells were treated with increasing concentrations of either IL-1α or IL-1β. LPS was used as a positive control and untreated cells as negative control. Given that IL-1α and IL-1β were produced and purified from bacteria, a third control using denatured (DN) IL-1 was also used with the purpose of eliminating that the observed effects were due to bacterial contamination of the sample. For this, IL-1 was heated at 95°C for 30 min, and cells were treated with 100 ng/mL of DN. bEnd5 cells were plated in 96 well plates at a density of 150,000 cells/mL. IL-1 treatments were prepared as serial dilutions of the highest concentration (500 ng/mL),

and cells were treated at a confluence of about 95%, with IL-1, 100 ng/mL of LPS and 100 ng/mL of DN. After 24 h, supernatants were recovered and assayed with mouse specific IL-6 ELISA.

IL-1α induced strong increase in IL-6 levels, even with the lowest concentration (0.5 ng/mL) (Figure 4.17-A). There was a significant difference between IL-1α treatments and control, but not between the concentrations. As expected, denatured IL-1α did not increase IL-6 levels compared to control levels.

Response elicited by treatments with IL-1β was lower than that induced by IL-1α (Figure 4.17-B), as its effects on IL-6 were observed only with higher concentrations of 100 ng/mL and 500 ng/mL. Concentrations ranging 0.5-50 ng/mL did not induce significant response compared to untreated control cultures. Denatured IL-1β did not induce IL-6 release, meaning that the observed effect was due to IL-1β and not due to endotoxin contamination from *E. coli*.

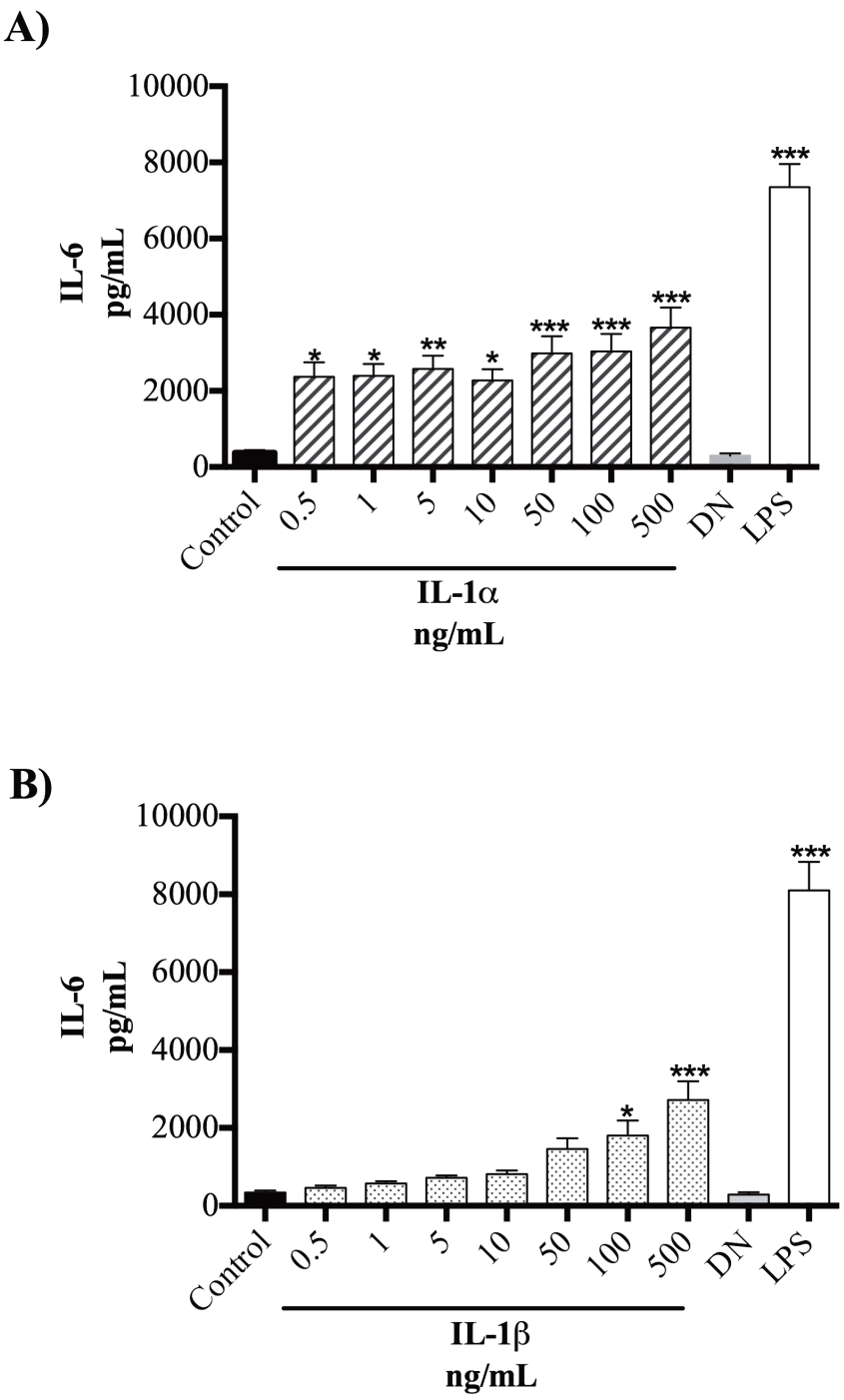

Figure 4.17 IL-1α and IL-1β bioactivity in bEND5 cells. bEND5 cells were treated with different concentrations of IL-1α or IL-1β (from 0.5 to 500 ng/mL), 100 ng/mL of LPS for positive control, and 100 ng/mL of heat-inactivated (DN) IL-1α or IL-1β, for 24 h. Cell supernatants were collected and assayed with mouse specific IL-6 ELISA. Data are presented as mean ± SEM of three independent experiments. * $p < 0.01$; ** $p < 0.001$*** $p < 0.001$, significant differences between control and treated cells. Non significant differences between control and DN, using one-way ANOVA with Bonferroni's multiple comparison post-hoc tests.

4.5.2 IL-1 bioactivity in neurones

IL-1 is a key mediator of immunity in the brain. It has recently emerged that the central nervous system (CNS) not only is target of some systemic cytokines, but it can also synthesize IL-1, IL-6, TNFα and TGFβ, mainly by microglia cells and astrocytes. Along with glia cells, some types of neurones express receptors for cytokines, like IL-1RI (Nestler et al., 2009). Thus, with the purpose of testing IL-1 bioactivity in neurones, primary neuronal cell cultures from embryonic mice were treated with increasing concentrations of IL-1α and IL-1β. As explained in previous section, untreated-, LPS- or DN-treated cells were used as controls. Following isolation from mice embryos, neurones were seeded at a density of 400,000-600,000 cells/mL, and treated after 12 days of growth for 24 h. Supernatants were then collected and assayed with mouse specific IL-6 ELISA.

IL-1α induced a strong increase on IL-6 levels in neurones in a dose-response manner, even with 0.5 ng/mL, and inducing highest response with 500 ng/mL (Figure 4.18-A). On the other hand, IL-1β increased IL-6 levels, also in a concentration-dependent manner, but starting from 5 ng/mL, whilst response with 0.5 or 1 ng/mL IL-1β was not significant (Figure 4.18-B). IL-6 level was increased with increasing concentrations of IL-1α (from 50-500 ng/mL), significant differences between these treatment and control were significant, but not between treatments (Figure 4.18-A).

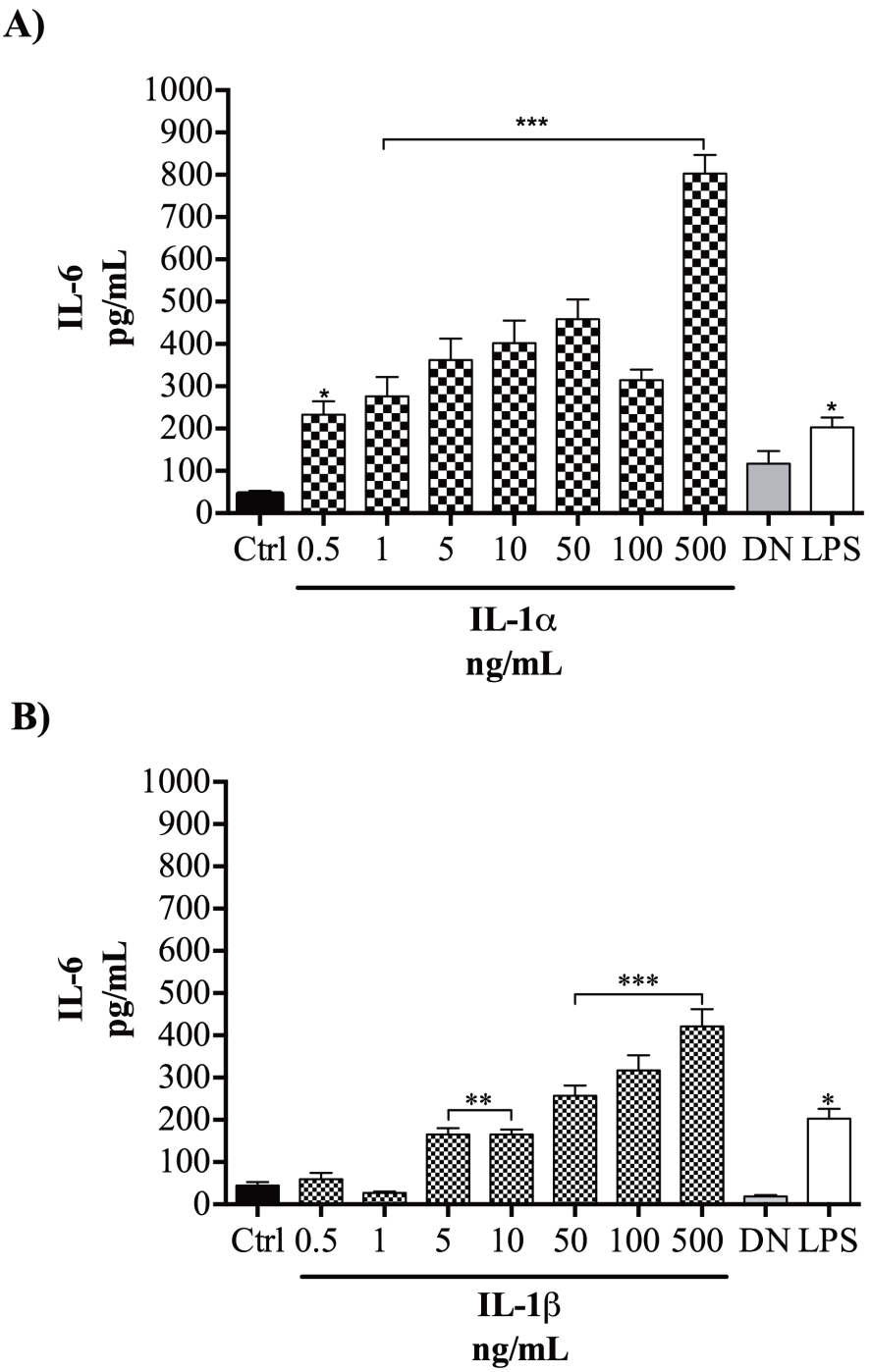

Figure 4.18 IL-1α and IL-1β bioactivity in neurones. Primary mouse neuronal cultures were treated with different concentrations of IL-1α or IL-1β (from 0.5 to 500 ng/mL), 100 ng/mL of LPS for positive control, and 100 ng/mL of heat-inactivated (DN) IL1α or IL-1β, for 24 h. Cell supernatants were collected and assayed with mouse specific IL-6 ELISA. Data are presented as mean ± SEM of three independent experiments. * $p < 0.01$; ** $p < 0.001$ *** $p < 0.001$, significant differences between control and treated cells; no significant difference between control and DN using one-way ANOVA with Bonferroni's multiple comparison post-hoc tests.

Summary of biophysical and functional characterisation of IL-1α and IL-1β

IL-1α and IL-1β were successfully produced and purified from E. *coli*. Both proteins were correctly folded as shown by CD and ^{1}H-NMR spectra, have the expected molecular weight and were mono-disperse as shown by SEC-MALLS analysis. Mass spec along with SEC-MALLS analysis confirmed that both proteins were highly pure. Both IL-1α and IL-1β were bioactive in endothelial cells as well as in neurones, and IL-1α showed a stronger response, compared to IL-1β. Interestingly, despite sharing high homology at nucleic acid and protein level, some of their biophysical properties are different. IL-1β soluble expression in bacteria was high, whereas IL-1α soluble expression was rather challenging. Analysis of their secondary structure by CD in the far UV region showed that, contrary to IL-1β, IL-1α has aromatic amino acid side chains clustered together.

5 Results: Expression and characterisation of IL-1RAcP and IL-1RI

5.1 Background

IL-1α and IL-1β exert their biological activity by forming the IL-1RI complex with the interleukin-1 receptor type I (IL-1RI), and the interleukin-1 receptor accessory protein (IL-1RAcP) (Fitzgerald and O'Neill, 2000). Both IL-1RI and IL-1RAcP belong to the IL-1R subfamily, which also belongs to the IL-1/Toll-like receptor superfamily (TIR family). Members of the TIR family are transmembrane proteins that share functional and structural properties, since all of them contain a Toll like receptor motif (Martin and Wesche, 2002, O'Neill, 2008). Proteins of the IL-1R subfamily are characterised by an intra-cytoplasmic TIR domain and extra-cellular immunoglobulin-like (Ig-like) domains. IL-1RI and IL-1RAcP share 25% homology at the amino acid level, and are structurally very similar. In addition to the aforementioned TIR domain, both IL-1RAcP and IL-1RI have three Ig-like domains. Ig-like domains are comprised by 70-100 amino acid residues, forming two β-sheets held together by a disulfide bond, and a Trp located near the C-terminal (Bodelon et al., 2013).

IL-1RI and IL-1RAcP are key players in IL-1 biological activity given that, when forming the IL-1RI complex, IL-1 signalling pathways, including MAP kinase pathways p38, JNK and ERK1/2, are activated (reviewed in previous sections). IL-1 binds to IL-1RI, but not IL-1RAcP, the latter is recruited to the complex after IL-1 is bound to IL-1RI. Here, in order to characterise the molecular interactions between IL-1α and IL-1β with the IL-1RI complex, expression and purification trials in *E. coli* and yeast, of the extra-cellular portion of both IL-1RI and IL-1RAcP, were carried out with the further aim to characterise structurally the complex using X-ray crystallography and/or NMR spectroscopy.

5.2 Analysis of IL-1RAcP and IL-1RI sequences cloned into pET-15b and pKLAC2

As stated in section 4.1, protein sequence analysis allows prediction of protein properties that are important to consider when designing experiments to characterise a particular protein. Thus, with the purpose of expressing and purifying IL-1RI and IL-1RAcP, sequences of native IL-1RI and native IL-1RAcP, as well as of the protein constructs used in this work to express both receptors in *E. coli* and yeast, were analysed. At the time when this work was started, no published protocol existed describing how to produce (express and purify) large amounts of IL-1RAcP in natively-folded form. As for IL-1RI, there were available four crystal structures of the aforementioned protein. Three of these works expressed and purified IL-1RI from insect cells (Schreuder et al., 1995, Schreuder et al., 1997, Vigers et al., 1997, Vigers et al., 2000) and only one (Vigers et al., 1997) expressed and purified it from *E. coli* followed by refolding. Nonetheless, this publication does not give detail of the protocol they followed and referred to a manuscript in preparation that, to date, has not been published. It was therefore decided to attempt the expression in both systems to maximize the chances of success. The expression in *E. coli* with 6 x His tag may be the easiest in principle and more conventional (but may suffer from incorrect folding, disulfide bond formation, or lack of glycosylation and lack of other post-translational modifications), while expression in yeast (*K. lactis*) may be more technically challenging to get working in this relatively new expression system, but could potentially yield glycosylated and correctly folded proteins.

Table 5.1 Amino acid composition of native extra-cellular domain of IL-1RAcP and the constructs expressed using the pET-15b and pKLAC2 plasmids

Amino acid	IL-1RAcP		pET-15b/ IL-1RAcP		pKLAC2/ IL-1RAcP		pKLAC2/ IL-1RAcP-His	
	Q	%	Q	%	Q	%	Q	%
Ala	12	3.6	12	3.3	13	3.8	13	3.5
Arg	18	5.3	19	5.3	19	5.6	20	5.4
Asn	20	5.9	20	5.6	20	5.8	21	5.6
Asp	18	5.3	18	5.0	18	5.3	18	4.8
Cys	10	3.0	10	2.8	10	2.9	10	2.7
Gln	8	2.4	8	2.2	8	2.3	9	2.4
Glu	22	6.5	22	6.1	22	6.4	25	6.7
Gly	13	3.8	16	4.5	13	3.8	18	4.8
His	8	2.4	15	4.2	9	2.6	14	3.8
Ile	22	6.5	22	6.2	22	6.4	22	5.9
Leu	24	7.1	25	7.0	24	7.0	27	7.3
Lys	23	6.8	23	6.5	23	6.7	23	6.2
Met	6	1.8	8	2.0	7	2.0	6	1.6
Phe	14	4.1	14	3.9	14	4.1	16	4.3
Pro	22	6.5	23	6.5	22	6.4	25	6.7
Ser	22	6.5	27	7.0	22	6.4	27	7.3
Thr	27	8.0	27	7.6	27	7.9	27	7.3
Trp	7	2.1	7	2.0	7	2.0	7	1.9
Tyr	15	4.4	15	4.2	15	4.4	15	4.0
Val	27	8.0	28	7.9	27	7.9	29	7.8
Total number of amino acids	338		359		342		372	

Q = quantity

Human IL-1RAcP consists of 570 amino acid residues (66 kDa) (Appendix 1), of which 340 comprise the three Ig-like domains of the extracellular portion (Jensen et al., 2000). Figures 5.1-5.3 and Table 5.1 show the amino acid content of native extracellular portion of IL-1RAcP, as well as the constructs expressed in *E. coli*, pET-15b/IL-1RAcP, and yeast, pKLAC2/ IL-1RAcP and pKLAC2/ IL-1RAcP-His. As expected, given the conserved pair of Cys that characterise Ig-like domains, IL-1RAcP Cys content is rather high (10 Cys residues). Interestingly, Trp content was also high (seven Trp residues), representing 2.1% of the protein, in contrast to the average

protein which Trp content usually represents about 1.2% (Nakashima et al., 1986). On the other hand, IL-1RI consists of 552 amino acid residues (80 kDa) and its extra-cellular portion is made up of 319 amino acid residues (Vigers et al., 1997). As expected, its amino acid content (Table 5.2) is similar to IL-1RAcP, containing a high level of Cys (10 residues) and five Trp.

Table 5.2 Amino acid composition of native extra-cellular domain of IL-1RI and the constructs expressed using the pET-15b and pKLAC2 plasmids

Amino acid	IL-1RI		pET-15b/IL-1RI		pKLAC2/IL-1RI	
	Q	%	Q	%	Q	%
Ala	16	5.1	16	4.8	17	5.3
Arg	12	3.8	13	3.9	13	4.1
Asn	21	6.7	21	6.3	21	6.6
Asp	16	5.1	16	4.8	16	5.0
Cys	10	3.2	10	3.0	10	3.1
Gln	10	3.2	10	3.0	10	3.1
Glu	25	7.9	25	7.5	25	7.9
Gly	13	4.1	15	4.5	13	4.1
His	9	2.9	16	4.8	10	3.1
Ile	24	7.6	24	7.2	24	7.5
Leu	23	7.3	24	7.2	23	7.2
Lys	25	7.9	25	7.5	25	7.9
Met	3	1.0	4	1.2	4	1.3
Phe	10	3.2	10	3.0	10	3.1
Pro	18	5.7	19	5.7	18	5.7
Ser	19	6.0	22	6.6	18	5.7
Thr	16	5.1	16	4.8	16	5.0
Trp	5	1.6	5	1.5	5	1.6
Tyr	17	5.4	17	5.1	17	5.3
Val	23	7.3	24	7.2	23	7.2
Total number of amino acids	315		332		318	

Q = quantity

A)

```
   1  atgggcagcagccatcatcatcatcacagcagcggcctggtgccgcgcggcagccat  60
  61  atgtcggaacgttgcgacgactggggcctggataccatgcgtcagattcaagttttcgaa  120
 121  gacgaaccggcacgcatcaaatgtccgctgttcgaacatttcctgaaattcaactacagc  180
 181  accgcccacagcgcgggtctgaccctgatttggtactggacccgtcaggatcgcgacctg  240
 241  gaagaaccgattaacttccgtctgccggaaaatcgcatctccaaagaaaaagacgtgctg  300
 301  tggtttcgtccgaccctgctgaacgatacgggtaattatacctgcatgctgcgcaacacc  360
 361  acgtactgtagcaaagttgcgttcccgctggaagtggttcagaaagactcttgctttaat  420
 421  agtccgatgaaactgccggtccataaactgtatattgaatacggcattcaacgtatcacc  480
 481  tgcccgaatgttgatggttatttcccgagctctgtcaaaccgaccatcacgtggtatatg  540
 541  ggctgttacaaaatccaaaacttcaacaacgtgatcccggagggtatgaatctgagtttt  600
 601  ctgattgcgctgatctccaacaatggcaactatacgtgcgtcgtgacctacccggaaaat  660
 661  ggtcgtacctttcacctgacccgcacgctgaccgttaaagttgtcggctcaccgaaaaac  720
 721  gccgtcccgccggtgattcattcgccgaatgatcacgtggtttatgaaaaagaaccgggt  780
 781  gaagaactgctgatcccgtgtacggtctacttttccttcctgatggattcacgcaacgaa  840
 841  gtgtggtggaccattgacggcaaaaaaccggatgacattacgatcgatgttaccattaat  900
 901  gaaagtatctcccattcacgtacggaagacgaaacgcgcacccagattctgtcgatcaaa  960
 961  aaagtgaccagcgaagatctgaaacgttcttatgtttgtcacgcacgcagcgctaaaggt  1020
1021  gaagttgcgaaagctgcgaaagtcaaacagaaagtcccggccccgcgctacaccgtctaa  1080
1081  taa                                                          1083
```

B)

```
   1  MGSSHHHHHHSSGLVPRGSHMSERCDDWGLDTMRQIQVFEDEPARIKCPL  50
  51  FEHFLKFNYSTAHSAGLTLIWYWTRQDRDLEEPINFRLPENRISKEKDVL  100
 101  WFRPTLLNDTGYTCMLRNTTYCSKVAFPLEVVQKDSCFNSPMKLPVHKLY  150
 151  IEYGIQRITCPNVDGYFPSSVKPTITWYMGCYKIQNFNNVIPEGMNLSFL  200
 201  IALISNNGNYTCVVTYPENGRTFHLTRTLTVKVVGSPKNAVPPVIHSPND  250
 251  HVVYEKEPGEELLIPCTVYFSFLMDSRNEVWWTIDGKKPDDITIDVTINE  300
 301  SISHSRTEDETRTQILSIKKVTSEDLKRSYVCHARSAKGEVAKAAKVKQK  350
 351  VPAPRYTV*                                            360
```

Figure 5.1 Construct sequences of the extracellular domain of human IL-1RAcP cloned into pET-15b vector. A) pET-15b/IL-1RAcP vector DNA sequence. The DNA section coding for 6 x His is highlighted in red. DNA section coding for thrombin cleavage site is highlighted in green. Human extracellular domain of IL-1RAcP is in black. *NdeI* restriction site is highlighted in purple. *BamHI* restriction site is highlighted in blue. Additional codons from pET-15b vector are highlighted in orange. **B)** Human IL-1RAcP extracellular domain protein sequence of the construct expressed in pET-15b vector. The 6 x His tag is highlighted in red. The cleavage site for thrombin is highlighted in green. The native sequence of human IL-1RAcP extracellular domain is in black. Residues added due to the presence of *NdeI* restriction site are highlighted in purple. Additional amino acid residues from pET-15b vector are highlighted in orange. * represents the stop codon.

A)

```
   1  atgaaattctctactatattagccgcatctactgctttaatttccgttgttatggctgct  60
  61  ccagtttctaccgaaactgacatcgacgatcttccaatatcggttccagaagaagccttg  120
 121  attggattcattgacttaaccggggatgaagtttccttgttgcctgttaataacggaacc  180
 181  cacactggtattctattcttaaacaccaccatcgctgaagctgctttcgctgacaaggat  240
 241  gatctcgagaaaagagaggctgaagctagaagagctcatatgtcggaacgttgcgacgac  300
 301  tggggcctggataccatgcgtcagattcaagttttcgaagacgaaccggcacgcatcaaa  360
 361  tgtccgctgttcgaacatttcctgaaattcaactacagcaccgcccacagcgcgggtctg  420
 421  accctgatttggtactggacccgtcaggatcgcgacctggaagaaccgattaacttccgt  480
 481  ctgccggaaaatcgcatctccaaagaaaaagacgtgctgtggtttcgtccgaccctgctg  540
 541  aacgatacgggtaattatacctgcatgctgcgcaacaccacgtactgtagcaaagttgcg  600
 601  ttcccgctggaagtggttcagaaagactcttgctttaatagtccgatgaaactgccggtc  660
 661  cataaactgtatattgaatacggcattcaacgtatcacctgcccgaatgttgatggttat  720
 721  ttcccgagctctgtcaaaccgaccatcacgtggtatatgggctgttacaaaatccaaaac  780
 781  ttcaacaacgtgatcccggagggtatgaatctgagttttctgattgcgctgatctccaac  840
 841  aatggcaactatacgtgcgtcgtgacctacccggaaaatggtcgtacctttcacctgacc  900
 901  cgcacgctgaccgttaaagttgtcggctcaccgaaaaacgccgtcccgccggtgattcat  960
 961  tcgccgaatgatcacgtggtttatgaaaaagaaccgggtgaagaactgctgatcccgtgt  1020
1021  acggtctacttttccttcctgatggattcacgcaacgaagtgtggtggaccattgacggc  1080
1081  aaaaaaccggatgacattacgatcgatgttaccattaatgaaagtatctcccattcacgt  1140
1141  acggaagacgaaacgcgcacccagattctgtcgatcaaaaaagtgaccagcgaagatctg  1200
1201  aaacgttcttatgtttgtcacgcacgcagcgctaaaggtgaagttgcgaaagctgcgaaa  1260
1261  gtcaaacagaaagtcccggccccgcgctacaccgtctaataaggatcc              1308
```

B)

```
   1  MKFSTILAASTALISVVMAAPVSTETDIDDLPISVPEEALIGFIDLTGDE      50
  51  VSLLPVNNGTHTGILFLNTTIAEAAFADKDDLEKREAEARRAHMSERCDD      100
 101  WGLDTMRQIQVFEDEPARIKCPLFEHFLKFNYSTAHSAGLTLIWYWTRQD      150
 151  RDLEEPINFRLPENRISKEKDVLWFRPTLLNDTGNYTCMLRNTTYCSKVA      200
 201  FPLEVVQKDSCFNSPMKLPVHKLYIEYGIQRITCPNVDGYFPSSVKPTIT      250
 251  WYMGCYKIQNFNNVIPEGMNLSFLIALISNNGNYTCVVTYPENGRTFHLT      300
 301  RTLTVKVVGSPKNAVPPVIHSPNDHVVYEKEPGEELLIPCTVYFSFLMDS      350
 351  RNEVWWTIDGKKPDDITIDVTINESISHSRTEDETRTQILSIKKVTSEDL      400
 401  KRSYVCHARSAKGEVAKAAKVKQKVPAPRYTV*                       432
```

Figure 5.2 Construct sequences of the extracellular domain of human IL-1RAcP cloned into pKLAC2 vector. A) pKLAC2/IL-1RAcP vector DNA sequence. Human extracellular domain of IL-1RAcP is in black. Section coding for the *K. lactis* α-mating factor secretion domain is highlighted in pink. Section coding for Kex protease cleavage sites are highlighted in yellow. *NdeI* restriction site is highlighted in purple. *BamHI* restriction site is highlighted in blue. Additional codons from pKLAC2 vector are highlighted in orange. **B)** Human IL-1RAcP extracellular domain protein sequence of the construct expressed in pKLAC2 vector. The native sequence of human IL-1RAcP extracellular domain is in black. The *K. lactis* α-mating factor secretion domain is highlighted in pink. Kex protease cleavage site is highlighted in yellow. Residues added due to the presence of *NdeI* restriction site are highlighted in purple. Additional amino acid residues from pKLAC2 vector are highlighted in orange. * represents stop codon.

A)

```
   1  atgaaattctctactatattagccgcatctactgctttaatttccgttgttatggctgct  60
  61  ccagtttctaccgaaactgacatcgacgatcttccaatatcggttccagaagaagccttg  120
 121  attggattcattgacttaaccggggatgaagtttccttgttgcctgttaataacggaacc  180
 181  cacactggtattctattcttaaacaccaccatcgctgaagctgctttcgctgacaaggat  240
 241  gatctcgagaaaagatcggaacgttgcgacgactggggcctggataccatgcgtcagatt  300
 301  caagttttcgaagacgaaccggcacgcatcaaatgtccgctgttcgaacatttcctgaaa  360
 361  ttcaactacagcaccgcccacagcgcgggtctgaccctgatttggtactggacccgtcag  420
 421  gatcgcgacctggaagaaccgattaacttccgtctgccggaaaatcgcatctccaaagaa  480
 481  aaagacgtgctgtggtttcgtccgaccctgctgaacgatacgggtaattatacctgcatg  540
 541  ctgcgcaacaccacgtactgtagcaaagttgcgttcccgctggaagtggttcagaaagac  600
 601  tcttgctttaatagtccgatgaaactgccggtccataaactgtatattgaatacggcatt  660
 661  caacgtatcacctgcccgaatgttgatggttatttcccgagctctgtcaaaccgaccatc  720
 721  acgtggtatatgggctgttacaaaatccaaaacttcaacaacgtgatcccggagggtatg  780
 781  aatctgagttttctgattgcgctgatctccaacaatggcaactatacgtgcgtcgtgacc  840
 841  tacccggaaaatggtcgtacctttcacctgacccgcacgctgaccgttaaagttgtcggc  900
 901  tcaccgaaaaacgccgtcccgccggtgattcattcgccgaatgatcacgtggtttatgaa  960
 961  aaagaaccgggtgaagaactgctgatcccgtgtacggtctacttttccttcctgatggat 1020
1021  tcacgcaacgaagtgtggtggaccattgacggcaaaaaaccggatgacattacgatcgat 1080
1081  gttaccattaatgaaagtatctcccattcacgtacggaagacgaaacgcgcacccagatt 1140
1141  ctgtcgatcaaaaaagtgaccagcgaagatctgaaacgttcttatgtttgtcacgcacgc 1200
1201  agcgctaaaggtgaagttgcgaaagctgcgaaagtcaaacagaaagtcccggccccgcgc 1260
1261  tacaccgtcgaactggaagttctgttccaggggcccggcagcagccatcatcatcatcat 1320
1321  cacagcagcggcctggtgccgcgcggatccgaattcctgcaggtaatta             1370
```

B)

```
   1  MKFSTILAASTALISVVMAAPVSTETDIDDLPISVPEEALIGFIDLTGDE   50
  51  VSLLPVNNGTHTGILFLNTTIAEAAFADKDDLEKRSERCDDWGLDTMRQI   100
 101  QVFEDEPARIKCPLFEHFLKFNYSTAHSAGLTLIWYWTRQDRDLEEPINF   150
 151  RLPENRISKEKDVLWFRPTLLNDTGNYTCMLRNTTYCSKVAFPLEVVQKD   200
 201  SCFNSPMKLPVHKLYIEYGIQRITCPNVDGYFPSSVKPTITWYMGCYKIQ   250
 251  NFNNVIPEGMNLSFLIALISNNGNYTCVVTYPENGRTFHLTRTLTVKVVG   300
 301  SPKNAVPPVIHSPNDHVVYEKEPGEELLIPCTVYFSFLMDSRNEVWWTID   350
 351  GKKPDDITIDVTINESISHSRTEDETRTQILSIKKVTSEDLKRSYVCHAR   400
 401  SAKGEVAKAAKVKQKVPAPRYTVELEVLFQGPGSSHHHHHHSSGLVPRGS   450
 451  EFPAGN*                                              456
```

Figure 5.3 Construct sequences of the extracellular domain of human IL-1RAcP cloned into pKLAC2 vector with 6 x His tag. A) pKLAC2/IL-1RAcP-His vector DNA sequence. Human extracellular domain of IL-1RAcP is in black. Section coding for the *K. lactis* α-mating factor secretion domain is highlighted in pink. Section coding for 6 x His is highlighted in red. Section coding for thrombin cleavage site is highlighted in green Section coding for Kex protease cleavage site is highlighted in yellow. *XhoI* restriction site is highlighted in cyan. *SbfI* restriction site is highlighted in blue. Additional codons from pKLAC2 vector are highlighted in orange. **B)** Human IL-1RAcP extracellular domain protein sequence of the construct expressed in pKLAC2 vector with a 6 x His tag. The native sequence of human IL-1RAcP extracellular domain is in black. The *K. lactis* α-mating factor secretion domain is highlighted in pink. The 6 x His tag is highlighted in red. Kex protease cleavage site is highlighted in yellow. Residues added due to the presence of *XhoI* restriction site are highlighted in cyan. Residues added due to the presence of *SbfI* restriction site are highlighted in blue. Additional amino acid residues from pKLAC2 vector are highlighted in orange.

A)

```
   1  atgggcagcagccatcatcatcatcacagcagcggcctggtgccgcgcggcagccat  60
  61  atgctggaagcagataaatgcaaagaacgtgaagaaaaaatcatcctggtgtcatcggcc  120
 121  aacgaaatcgacgtgcgtccgtgtccgctgaacccgaatgaacataaaggcaccattacg  180
 181  tggtataaagatgactcaaaaaccccggtgtcgacggaacaggcgagccgtatccatcaa  240
 241  cacaaagaaaaactgtggtttgtgccggccaaagttgaagattctggtcactattactgc  300
 301  gtggttcgtaacagctcttattgtctgcgcatcaaaatctcagcaaaattcgtggaaaac  360
 361  gaaccgaatctgtgctacaatgcgcaggccattttcaaacaaaaactgccggttgctggt  420
 421  gatggcggtctggtgtgtccgtacatggaatttttcaaaaacgaaaacaacgaactgccg  480
 481  aaactgcagtggtacaaagattgcaaaccgctgctgctggacaatattcatttttccggt  540
 541  gtgaaagatcgtctgatcgttatgaacgtcgcagaaaaacatcgcggcaattatacctgt  600
 601  cacgctagctatacgtacctgggtaaacaatacccgattacccgtgttattgaatttatc  660
 661  acgctggaagaaaacaaaccgacccgcccggtcattgtgagcccggccaatgaaacgatg  720
 721  gaagtggatctgggcagccagattcaactgatctgcaacgttaccggtcagctgtctgac  780
 781  attgcctattggaaatggaatggcagtgttatcgatgaagatgacccggtcctgggtgaa  840
 841  gactattactccgtcgaaaacccggcaaataaacgtcgctcaaccctgattacggttctg  900
 901  aacattagtgaaatcgaatcccgcttctacaaacacccgtttacctgtttcgcgaaaaat  960
 961  acgcacggcatcgacgctgcatacattcaactgatttacccggtcacctaataaggatcc  1020
```

B)

```
   1  MGSSHHHHHHSSGLVPRGSHMLEADKCKEREEKIILVSSANEIDVRPCPL   50
  51  NPNEHKGTITWYKDDSKTPVSTEQASRIHQHKEKLWFVPAKVEDSGHYYC   100
 101  VVRNSSYCLRIKISAKFVENEPNLCYNAQAIFKQKLPVAGDGGLVCPYME   150
 151  FFKNENNELPKLQWYKDCKPLLLDNIHFSGVKDRLIVMNVAEKHRGNYTC   200
 201  HASYTYLGKQYPITRVIEFITLEENKPTRPVIVSPANETMEVDLGSQIQL   250
 251  ICNVTGQLSDIAYWKWNGSVIDEDDPVLGEDYYSVENPANKRRSTLITVL   300
 301  NISEIESRFYKHPFTCFAKNTHGIDAAYIQLIYPVT*                335
```

Figure 5.4 Construct sequences of the extracellular domain of human IL-1RI cloned into pET-15b vector. A) pET-15b/IL-1RI vector DNA sequence. The DNA section coding for 6 x His is highlighted in red. DNA section coding for thrombin cleavage site is highlighted in green. Human extracellular domain of IL-1RI is in black. *NdeI* restriction site is highlighted in purple. *BamHI* restriction site is highlighted in blue. Additional codons from pET-15b vector are highlighted in orange. **B)** Human IL-1RI extracellular domain protein sequence of the construct expressed in pET-15b vector. The 6 x His tag is highlighted in red. The cleavage site fro thrombin is highlighted in green. The native sequence of human IL-1RI extracellular domain is in black. Residues added due to the presence of *NdeI* restriction site are highlighted in purple. Additional amino acid residues from pET-15b vector are highlighted in orange. * represents stop codon.

A)

```
   1  atgaaattctctactatattagccgcatctactgctttaatttccgttgttatggctgct  60
  61  ccagtttctaccgaaactgacatcgacgatcttccaatatcggttccagaagaagccttg  120
 121  attggattcattgacttaaccggggatgaagtttccttgttgcctgttaataacggaacc  180
 181  cacactggtattctattcttaaacaccaccatcgctgaagctgctttcgctgacaaggat  240
 241  gatctcgagaaaagaggctgaagctagaagagctcatatgctggaagcagataaatgc  300
 301  aaagaacgtgaagaaaaaatcatcctggtgtcatcggccaacgaaatcgacgtgcgtccg  360
 361  tgtccgctgaacccgaatgaacataaaggcaccattacgtggtataaagatgactcaaaa  420
 421  accccggtgtcgacggaacaggcgagccgtatccatcaacacaaagaaaaactgtggttt  480
 481  gtgccggccaaagttgaagattctggtcactattactgcgtggttcgtaacagctcttat  540
 541  tgtctgcgcatcaaaatctcagcaaaattcgtggaaaacgaaccgaatctgtgctacaat  600
 601  gcgcaggccattttcaaacaaaaactgccggttgctggtgatggcggtctggtgtgtccg  660
 661  tacatggaatttttcaaaaacgaaaacaacgaactgccgaaactgcagtggtacaaagat  720
 721  tgcaaaccgctgctgctggacaatattcatttttccggtgtgaaagatcgtctgatcgtt  780
 781  atgaacgtcgcagaaaaacatcgcggcaattatacctgtcacgctagctatacgtacctg  840
 841  ggtaaacaatacccgattacccgtgttattgaatttatcacgctggaagaaaacaaaccg  900
 901  acccgcccggtcattgtgagcccggccaatgaaacgatggaagtggatctgggcagccag  960
 961  attcaactgatctgcaacgttaccggtcagctgtctgacattgcctattggaaatggaat  1020
1021  ggcagtgttatcgatgaagatgacccggtcctgggtgaagactattactccgtcgaaaac  1080
1081  ccggcaaataaacgtcgctcaaccctgattacggttctgaacattagtgaaatcgaatcc  1140
1141  cgcttctacaaacacccgtttacctgtttcgcgaaaaatacgcacggcatcgacgctgca  1200
1201  tacattcaactgatttacccggtcacctaataaggatcc                       1239
```

B)

```
   1  MKFSTILAASTALISVVMAAPVSTETDIDDLPISVPEEALIGFIDLTGDE  50
  51  VSLLPVNNGTHTGILFLNTTIAEAAFADKDDLEKREAEARRAHMLEADKC  100
 101  KEREEKIILVSANEIDVRPCPLNPNEHKGTITWYKDDSKTPVSTEQASRI  150
 151  HQHKEKLWFVPAKVEDSGHYYCVVRNSSYCLRIKISAKFVENEPNLCYNA  200
 201  QAIFKQKLPVAGDGGLVCPYMEFFKNENNELPKLQWYKDCKPLLLDNIHF  250
 251  SGVKDRLIVMNVAEKHRGNYTCHASYTYLGKQYPITRVIEFITLEENKPT  300
 301  RPVIVSPANETMEVDLGSQIQLICNVTGQLSDIAYWKWNGSVIDEDDPVL  350
 351  GEDYYSVENPANKRRSTLITVLNISEIESRFYKHPFTCFAKNTHGIDAAY  400
 401  IQLIYPVT*                                           408
```

Figure 5.5 Construct sequences of the extracellular domain of human IL-1RI cloned into pKLAC2 vector. A) pKLAC2/IL-1RI vector DNA sequence. Human extracellular domain of IL-1RI is in black. Section coding for the *K. lactis* α-mating factor secretion domain is highlighted in pink. Section coding for Kex protease cleavage sites are highlighted in yellow. *NdeI* restriction site is highlighted in purple. *BamHI* restriction site is highlighted in blue. Additional codons from pKLAC2 vector are highlighted in orange. **B)** Human IL-1RI extracellular domain protein sequence of the construct expressed in pKLAC2 vector. The native sequence of human IL-1RI extracellular domain is in black. The *K. lactis* α-mating factor secretion domain is highlighted in pink. Kex protease cleavage site is highlighted in yellow. Residues added due to the presence of *NdeI* restriction site are highlighted in purple.. Additional amino acid residues from pKLAC2 vector are highlighted in orange. * represents stop codon.

Table 5.3 Comparison of the theoretical properties of IL-1RAcP and constructs expressed here using the pET-15b and pKLAC2 plasmids

	IL-1RAcP	pET-15b/IL-1RAcP	pKLAC2/IL-1RAcP	pKLAC2/IL-1RAcP-HIS
Molecular Weight (kDa)	38.99	41.27	39.48	42.66
Total number of amino acids	338	359	342	372
Molar extinction coefficient [1] (M^{-1} cm^{-1})	60850	60850	61475	61475
Absorbance of 1 mg/mL solution[1]	1.56	1.47	1.55	1.447
Theoretical *pI*	7.52	7.99	8.01	7.31

[1] Molar extinction coefficient and absorbance of 1 mg/mL were calculated at 280nm

Table 5.4 Comparison of the theoretical properties of IL-1RI and constructs expressed here using the pET-15b and pKLAC2 plasmids

	IL-1RI	pET-15b/IL-1RI	pKLAC2/IL-1RI
Molecular Weight (kDa)	36.18	38.11	36.73
Total number of amino acids	315	332	320
Molar extinction coefficient [1] (M^{-1} cm^{-1})	52830	52830	53455
Absorbance of 1 mg/mL solution[1]	1.46	1.39	1.45
Theoretical *pI*	6.18	6.62	6.40

[1] Molar extinction coefficient and absorbance of 1 mg/mL were calculated at 280nm

The pET-15b/IL-1RAcP and pET-15b/IL-1RI plasmids were designed to express receptors in *E. coli*. The protein constructs coded by these plasmids contained an additional 6 x His tag (His-tag) at the N-terminal to facilitate purification. They also have a cleavage site for thrombin, which was added with the purpose of cleaving out the His-tag after purification (Figures 5.1 and 5.4). On the other hand, in order to express IL-1RI and IL-1RAcP in yeast, specifically in the yeast *K. lactis*, IL-1RI and IL-1RAcP were re-cloned into the pKLAC2 vector. This plasmid codes for a fusion protein, the α-mating factor domain (α-MF), at the N-terminal that allows secretion of the expressed protein, through the yeast secretory pathway (Figures 5.2, 5.3 and 5.5). The α-MF is cleaved by the Kex protease at Arg/Arg or Lys/Arg. In addition to the α-MF domain at the N-terminal, the pKLAC2/IL-1RAcP-His plasmid contains a His-tag in the C-terminal along with a thrombin cleavage site between the His-tag and the protein (Figure 5.3).

The predicted molecular weight of the native IL-1RAcP extra-cellular portion is 38.99 kDa (Table 5.3). His-tag and restriction sites do not increase dramatically the molecular weight of the protein, being all around 40 kDa. The additional amino acid residues did not affect the molar extinction coefficient at 280 nm, but the *pI* was increased from 7.52 to 7.99 in the pET-15b/IL-1RAcP and to 8.01 in pKLAC2/IL-1RAcP construct, and decreased to 7.31 in the pKLAC2/IL-1RAcP-His (Table 5.3). Nevertheless, these changes are not remarkable. Table 5.4 shows the theoretical properties of the IL-1RI constructs. The predicted molecular weight of the native IL-1RI extracellular portion is 36.18 kDa. Additional amino acid residues in construct pET-15b/IL-1RAcP increased the molecular weight to 38.11 kDa, and they did not dramatically affect molar extinction coefficient and *pI*. As for the pKLAC2/IL-1RI

construct, additional residues did not notably affect the molecular weight nor the *pI*. Thus, additional amino acid residues in constructs expressed in this work, had a minimal impact in IL-1RAcP and IL-1RI *pI* and did not increased much their molecular weight.

5.3 IL-1 receptors expression in *E.coli*

As mentioned in previous sections, *E coli* properties, along with the vast knowledge about its genome, makes this system the first choice for heterologous protein expression. At present, several genetically modified strains are commercially available.

5.3.1 IL-1RAcP expression in *E. coli*

IL-1RAcP extracellular domain consists of 3 Ig-like domains formed by β-sheets. It contains 10 Cys (Table 5.1), of which six form the disulfide bonds characteristic of the Ig-like domains and two form a disulphide bond that link together domains 1 and 2. For this reason, strains used to find the optimal soluble expression of this protein contained the genotype *trxB*$^{-}$ and *gor*$^{-}$. These mutations allow the formation of disulfide bonds in bacterial cytoplasm, which otherwise is not a proper environment for the formation of such bonds. With the purpose of finding the best conditions for soluble expression of IL-1RAcP, the construct pET-15b/IL-1RAcP was successfully transformed in several *E. coli* strains with the aforementioned genotype; Table 5.5 shows a summary of these strains. The construct pET-15-b/IL-1RAcP was successfully transformed into different *E.coli* strains (summarised in Table 5.5), and expression trials were carried out in 50 mL cultures grown at 25°C or 30°C and expression was induced with either 0.5 or 1 mM IPTG for 4 h. Figure 5.6 shows the analysis of expression trials in Shuffle T7 Express *LysY*, which is the strain that expressed IL-1RAcP with the highest yield of total expression. Samples of pre-induction state (PI)

and induced state every one h were analysed by 10% SDS-PAGE, as well as the soluble (LS) and insoluble (LP) fractions of 4 h expression. The 41 kDa expected band is absent in pre-induction sample and present in induced samples of all conditions (Figure 5.6 A-D). Expression in all conditions was gradual, starting at about 2 h after induction at 25°C (Figure 5.6 A and B) and after 1 h of induction at 30°C (Figure 5.2 C and D), reaching the maximum level of expression at 4 h. However, as shown in lanes LS and LP, most of the protein remained insoluble.

Thus, in order to determine the optimal time of induction for soluble protein expression, soluble and insoluble fractions of pre-induction and post-induction samples of all conditions, were analysed by 10% SDS-PAGE (figure 5.7). As shown in this analysis, IL-1RAcP was expressed in an insoluble form, as the 41 kDa band was found only in the insoluble fractions so here we concluded that *E.coli* was not a suitable host for IL-1RAcP soluble expression.

Table 5.5 Summary of expression trials for IL-1RAcP in *E. coli* strains *E. coli* strains were transformed with the construct pET-15b/IL-1RAcP. Expression trials were carried out as described in section 3.2

***E. coli* strain**	**Expression**	**Solubility**
Origami B DE3	Medium	Not detected
Rosetta-gami 2	High	Not detected
Shuffle T7 Express	High	Not detected
Shuffle T7 Express *LysY*	High	Not detected

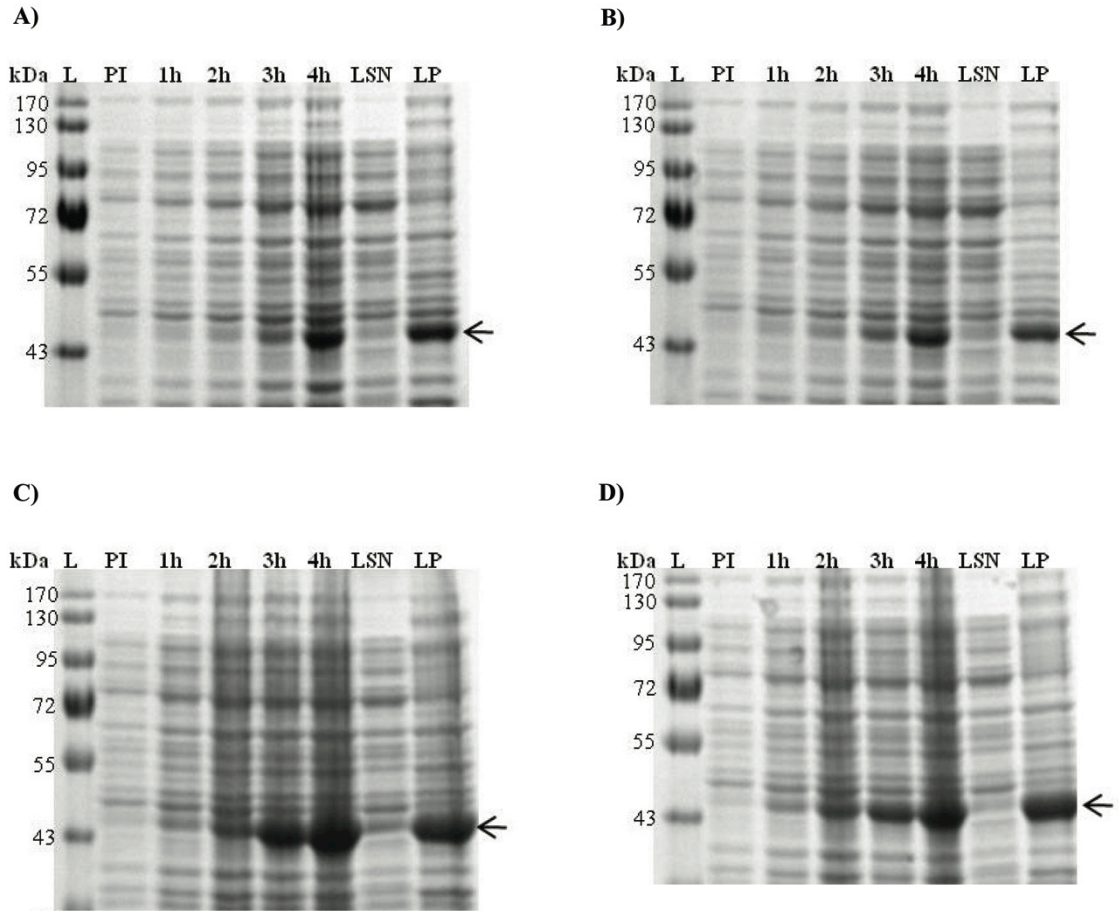

Figure 5.6 10% SDS-PAGE analysis of IL-1RAcP Expression trials in Shuffle T7 Express *LysY* cells. Shuffle T7 Express Lys Y cells were transformed with the pET15b/IL-1RAcP construct. Expression trials were carried out in 50mL cultures and were induced when an $OD_{600} \approx 0.8$ was reached. Conditions used were **A)** 25°C, 0.5mM IPTG; **B)** 25°C, 1mM IPTG; **C)** 30°C, 0.5mM and **D)** 30°C, 1mM IPTG. The molecular weight marker is labelled **L**, Pre-induction samples are labelled **PI** and the soluble and non soluble fractions after 4 h of induction are labelled as **LSN** and **LP** respectively. IL-1RAcP presence is indicated with a black arrow.

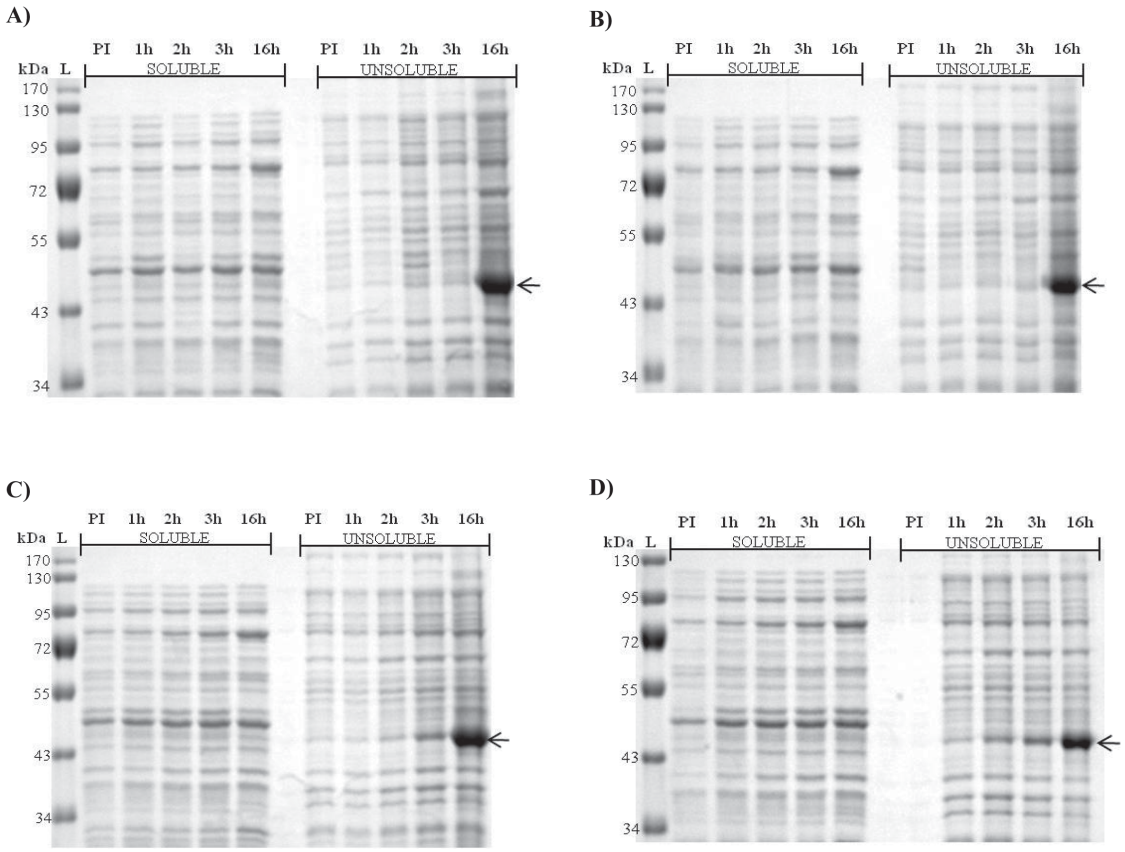

Figure 5.7 10% SDS-PAGE analysis of IL-1RAcP soluble and insoluble expression in Shuffle T7 Express *LysY*. Shuffle T7 Express cells were transformed with the pET15b/IL-1RAcP construct. Expression trials were carried out in 50 mL cultures and were induced when an $OD_{600} \approx 0.8$ was reached. Conditions used were **A)** 25°C, 0.5 mM IPTG; **B)** 25°C, 1 mM IPTG; **C)** 30°C, 0.5 mM and **D)** 30°C, 1 mM IPTG. The molecular weight marker is labelled **L**, and pre-induction samples are labelled **PI.**

5.3.2 IL-1RI expression in *E.coli*

IL-1RI extracellular portion consists of 319 amino acid residues. As seen in table 5.2, IL-1RI contains 10 Cys, eight of which form the disulphide bonds characteristic of Ig-like domains and that held together domains 1 and 2. Thus, similar to that with IL-1RAcP, *E. coli* strains that were used to find the optimal soluble expression of this protein contained the genotype *trxB*$^-$ and *gor*$^-$. For these purposes, the

construct pET-15b/IL-1RI was successfully transformed into Shuffle T7 Express. Expression trials were carried out in 50 mL cultures growth at 25°C or 30°C and induced with either 0.5 mM or 1 mM IPTG for 4 h. Samples of pre-induction state every 1 h were analysed by 10% SDS-PAGE, as well as the soluble (LS) and insoluble (LP) fractions of 4 h expression. As shown in Table 5.4, the expected molecular weight of IL-1RI with its N-terminal His-tag is 38 kDa. Figure 5.8 shows IL-1RI expression trials in Shuffle T7 Express cells. IL-1RI started being expressed after 1 h of induction in all conditions (Figure 5.8 A-D), and total expression was higher at 25° C when induced with 0.5 mM IPTG (figure 5.8-A). Nevertheless, analysis of the soluble and insoluble fractions of 4 h of induction shows that the protein is expressed in an insoluble form.

Despite been expressed in *E. coli* systems that allow disulfide bond formation (summarised in Table 5.6), IL-1RI was totally insoluble. This could be due to formation of disulfide bonds between incorrect Cys, or because of the absence of post-translational modifications that might be essential for the correct folding of IL-1RI. It also may be that bacteria lack necessary chaperones to assist the correct folding of this protein.

Table 5.6 Summary of expression trials for IL-1RI in *E. coli* strains

E. coli strains were transformed with the construct pET-15b/IL-1RI. Expression trials were carried out as described in section 3.2

***E. coli* strain**	**Expression**	**Solubility**
Origami B DE3	Medium	Not detected
Shuffle T7 Express	Medium	Not detected
Shuffle T7 Express *LysY*	High	Not detected

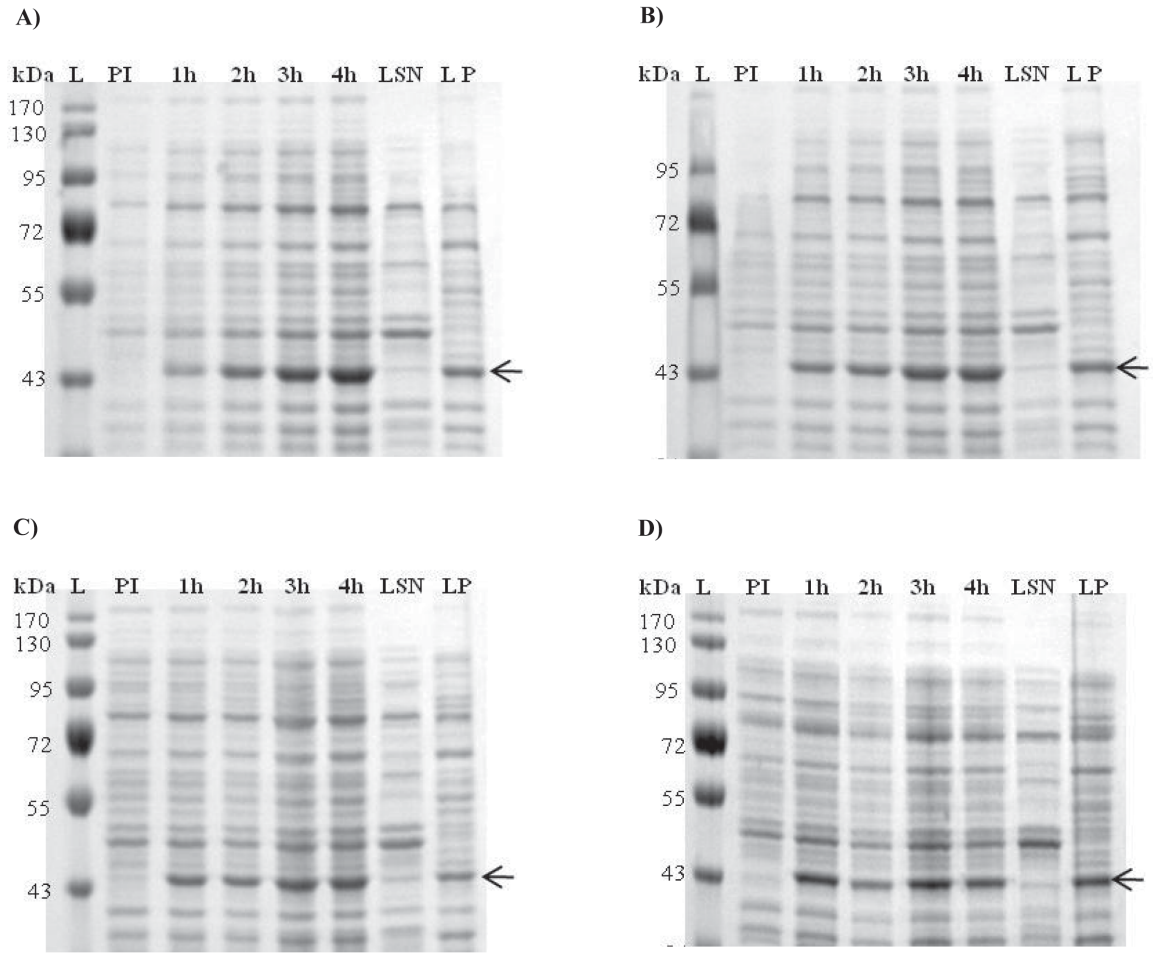

Figure 5.8 10% SDS-PAGE analysis of IL-1RI Expression trials in Shuffle T7 Express. Shuffle T7 Express cells were transformed with the pET15b/IL-1RI construct. Expression trials were carried out in 50mL cultures and were induced when an $OD_{600} \approx 0.8$ was reached, conditions used were **A)** 25°C, 0.5mM IPTG; **B)** 25°C, 1mM IPTG; **C)** 30°C, 0.5mM and **D)** 30°C, 1mM IPTG. The molecular weight marker is labelled **L**, Pre-induction samples are labelled **PI** and the soluble and non soluble fractions after 4 h of induction are labelled as **LSN** and **LP** respectively. IL-1RAcP presence is indicated with a black arrow.

5.3.3 Summary of IL-1 RI and IL-1RAcP expression in *E. coli*

Expression and purification of IL-1RI and IL-1RAcP in *E. coli* in soluble and natively-folded form was ineffective. With the purpose of obtaining soluble protein, other diverse approaches, not shown here, were carried out. At first, optimisation of soluble protein expression by changing induction conditions was tried using

temperatures form 16°C to 37°C, as well as different IPTG concentrations, ranging from 0.1 mM to 1 mM. However, even if in some cases total expression of both receptors was improved, the expressed proteins remained insoluble. Using the optimal conditions for total expression, IMAC purification from soluble and insoluble fractions was carried out (results not included in this work). IMAC purification from soluble fractions was fruitless, meaning that the total expressed protein was insoluble. On the other hand, IMAC purification under denaturing conditions allowed both IL-1RAcP and IL-1RI purification in unfolded form with an acceptable yield (15 mg/mL out of 1 L culture), however, for the purposes of this work, both receptors were needed to be properly folded in order to bind to IL-1. Thus, refolding trials for IL-1RAcP under redox conditions were carried out (results not included in this work). For this, denatured IL-1RAcP was dialysed against a series of buffers with decreasing concentrations of urea, and reduced l-glutathione + oxidised l-glutathione; these last additives were added with the purpose of providing a redox environment. Still, this last approach to obtain soluble IL-1RAcP was not effective, as protein precipitated when decreasing urea concentration during dialysis process. Thus the attempts to refold these proteins in vitro were not successful.

Even though bacterial strains used allowed in principle disulfide bond formation, both expressed proteins were completely insoluble. On the other hand, IL-1RAcP precipitation during refolding trials might be due to disulfide bond formation between incorrect Cys. Given the high level of disulfide bonds and consequently of Cys (Tables 5.1 and 5.2) in both IL-1RAcP and IL-1RI constructs, refolding trials were rather challenging as the probability of disulfide bond formation between incorrect Cys is high. Additionally, the high number of predicted glycosylation sites (five in IL-1RAcP and four in IL-1RI) made us suspect that for these proteins, glycosylation might

be important for their structure. As yet, the role of protein glycosylation is not well understood and it has been suggested that glycosylation may be important for correct protein structure and protein stability (Drickamer and Taylor, 1998). Results presented in this section suggested that *E. coli* is not suitable for IL-1RAcP and IL-1RI expression. Thus, we decided to try a different expression system capable to perform both glycosylation and allow disulfide bond formation.

5.4 IL-1RAcP and IL-1RI expression in yeast

As mentioned in previous sections, Ig-like domains are characterised by a disulfide bond that holds together the two β-sheets. Analysis of IL-1RAcP and IL-RI construct sequences predicted at least five N-glycosylation sites in IL-1RAcP and four in IL-1RI. Crystallographic studies of the IL-1 ternary complex carried out by Thomas and colleagues (2012) later confirmed four glycosylation sites in both IL-1RI and IL-1RAcP. Disulfide bonds, as well as N-glycosylation, are commonly found in eukaryote proteins, and can be a bottleneck when expressing eukaryote proteins in *E. coli*. Whenever there is difficulty when producing heterologous proteins in bacteria because of incorrect folding or glycosylation, it is suggested to use eukaryote systems such as yeast. As eukaryote system, yeast presents many advantages to produce heterologous proteins. These advantages include, among others, high density growth, disulfide bond formation, ability to glycosylate, ability of using episomal and integrative vectors, as well as the possibility of exporting the protein to the medium, when using proper sequences. (Demain and Vaishnav, 2009). The yeast *Kluyveromyces lactis* (*K. lactis*) potentially has many advantages over other yeast systems such as not needing to be grown in fermenters, as well as the commercial availability of vectors that allow secretion of the protein, such as the plasmid pKLAC2. Additionally, *K. lactis* wild type strain GG799 is known for its outstanding ability to synthesize and

secret heterologous proteins (van Ooyen et al., 2006). For purposes of this work, plasmids pKLAC2/IL-1RAcP, pKLAC2/IL-1RI and pKLAC-2/IL-1RAcP-His were used to transform *K. lactis* GG799.

5.4.1 IL-1RAcP expression in *K. lactis*

The plasmid pKLAC2/IL-1RAcP was successfully transformed into *K. lactis* GG799 cells. Expression trials for the IL-1RAcP construct were carried out in 500 mL of cultures, incubated in YPGlu medium at 30°C, expression was induced at an OD_{600} of 1, by changing YPGlu to YPGal, and incubating at 30°C for further 72 h. LC-MS/MS analysis of YPGal medium after 72 h expression, identified the presence of IL-1RAcP with a 45% of peptide coverage. Samples at each 24 h were analysed by 10% SDS-PAGE (Figure 5.9). After 12 h of expression, two bands at around 58 kDa became evident, and became more intense after 48 h. Even though the predicted molecular weight for the pKLAC2/IL-1RAcP construct was 39.62 kDa (Table 5.4), it has been shown that carbohydrate moieties added during glycosylation process can increase the molecular weight of a protein in up to 40% of that of the predicted or not glycosylated isoform (Fountoulakis and Gentz, 1992). IL-1RAcP construct was predicted to have a high level of possible glycosylation sites, thus, the increase of its molecular weight to close to 60 kDa is not a surprise.

The plasmid pKLAC2/IL-1RAcP-His was also successfully transformed into *K. lactis* GG799 cells. Expression trials were carried out in 500 mL of culture and expression was induced as described above for 48 h. Samples of pre-induction and expression at each 24 h were concentrated 10x and analysed by gradient Bis-Tris-PAGE (Figure 5.10). An increment on molecular weight from 42 kDa to nearly 60 was expected and a band corresponding to this MW is indicated by a black arrow.

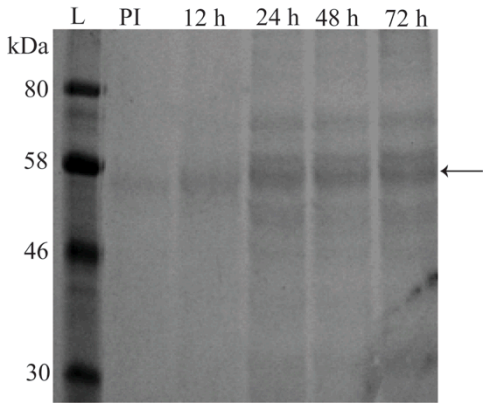

Figure 5.9 IL-1RAcP expression in *K. lactis*. *K. lactis* cells were transformed with the pKLAC2/IL-1RAcP plasmid and grown in 500 mL of YPGlu media. Induction was carried out at an OD_{600} 1 by changing to YPGal medium, and incubating for 72 h. A ~ 58 kDa protein was detected at 24 h of induction, reaching its maximum level at 48 h. Samples at each 24 h were analysed by 10% SDS-PAGE stained with Coomassie blue. The molecular marker is labelled as **L**, and pre-induction sample as **PI**.

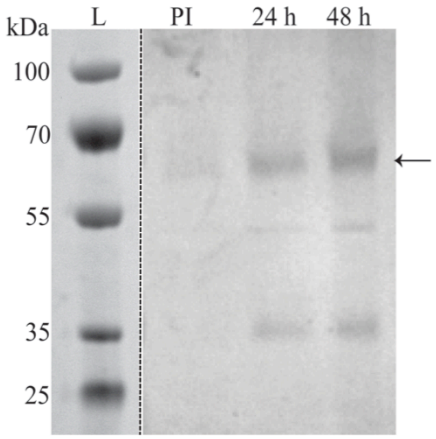

Figure 5.10 IL-1RAcP-His expression in *K. lactis*. *K. lactis* GG799 cells were transformed with the pKLAC2/IL-1RAcP-His plasmid and grown in 500 mL of YPGlu medium. Induction was carried out at an OD_{600} ~ 1 by changing to YPGal media, and incubating for 48 h. A ~ 60 kDa protein was detected at 24 h of induction, reaching its maximum level at 48 h. Samples at each 24 h were analysed by 10% SDS-PAGE stained with Coomassie blue. The molecular marker is labelled as **L**, and pre-induction sample as **PI**.

Both constructs, IL-1RAcP and IL-1RAcP-His, were expressed as proteins close to the expected MW of ~60 kDa, with an optimal time of expression at 48 h. LC-MS/MS analysis of both IL-1RAcP and IL-1RAcP-His bands identified IL-1RAcP among other proteins. However, level of expression was difficult to estimate with SDS-PAGE stained with Coomassie brilliant blue. Previously, it has been demonstrated that N-linked glycosylation interferes with Coomassie brilliant blue binding to protein, making Coomassie blue-based methods underestimating protein concentration up to 30-40% (Fountoulakis et al., 1992). Thus, in order to characterise the glycosylated isoforms of IL-1RAcP and IL-1RAcP-His, YPGal samples of 48 h of expression of both constructs, were analysed by 10% Bis-Tris-PAGE stained with ProQ Emerald (Invitrogen) to detect glycosylated proteins. Pro-Q Emerald stain reacts with carbohydrates attached to protein allowing visualisation at 300 nm in a UV transilluminator. Following analysis with Pro-Q emerald, the gel was stained with Coomassie Blue. The 60 kDa proteins detected in IL-1RAcP and IL-1RAcP-His expression show strong intensity when stained with Pro-Q Emerald (Figure 5.11-A). However, when stained with Coomassie blue, both samples look rather faint. This could be possibly to high levels of glycosylation, rather than to high yield of expression.

After successful transformation of GG799 cells with the plasmid pKLAC2/IL-1RI, expression trials were carried out as described above, in 500 mL of cultures for 72 h. Samples of cell culture media collected every 24 h were concentrated 10x and analysed by 10% SDS-PAGE (Figure 5.12). Similar to IL-1RAcP, IL-1RI N-glycosylation level is high; at least four N-glycosylation sites were predicted to IL-1RI construct used in this work. Thus, IL-1RI molecular weight could be increased up to 58 kDa, just as IL-1RAcP. Expression of a 58 kDa band is evident after 24 h induction,

and the maximum level of expression was reached at 48 h. In order to confirm IL-1RI presence in YPGal medium, bands at 48 h and 72 h were analysed by LC-MS/MS, and, apart from *K.lactis* proteins, IL-1RI was not detected. At that point, it was not clear whether the IL-1RI expression in *K. lactis* cells was unsuccessful, or the quantity of expressed protein was just too low, and was obscured by other proteins present in the mixture.

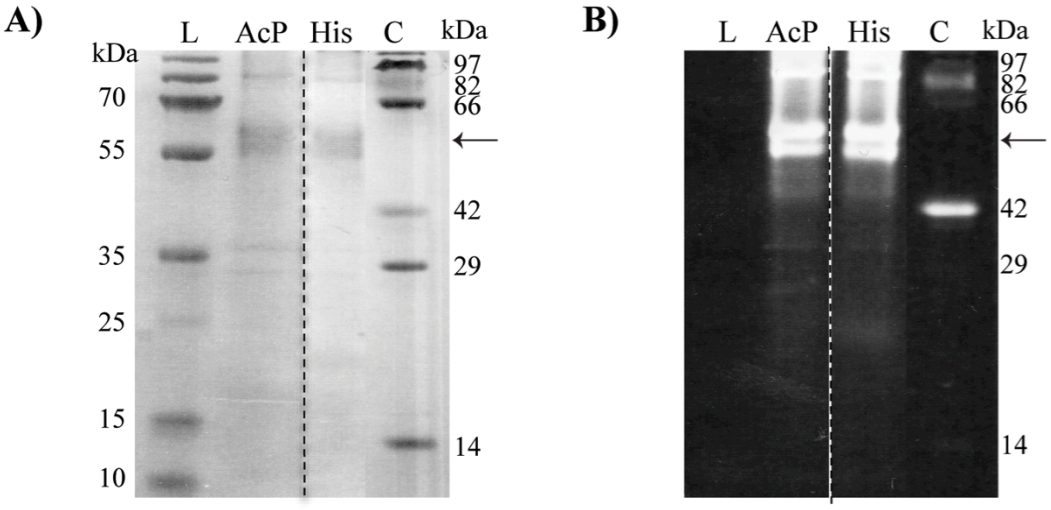

Figure 5.11 Glycosylated protein staining of IL-1RAcP and IL-1RAcP-His constructs expression. Samples of 48 h expression in YPGal of IL-1RAcP and IL-1RAcP –His constructs were analysed in 10% Bis-Tris PAGE stained with ProQ Emerald Glycoprotein stain (**B**) followed by Coomassie blue stain (**A**). Bands at ~ 60 kDa are highly glycosylated as it can be seen in gel **B**).

5.5 IL-1RAcP purification

Following expression trials, IL-1RAcP and IL-1RAcP-His constructs were grown in 500 mL cultures of YPGlu at 30°C, and changed to 500 mL of YPGal to induce expression. After 48 h of induction, cultures were centrifuged and the supernatant was recovered for further purification. Two or three-steps purification were

attempted for all constructs. Given that the IL-1RAcP construct did not have a tag to facilitate their purification, a first attempt to purify them by ion exchange chromatography (IEX) was carried out, followed by size exclusion chromatography (SEC). IL-1RAcP-His was purified by immobilised-metal affinity chromatography (IMAC) followed by SEC.

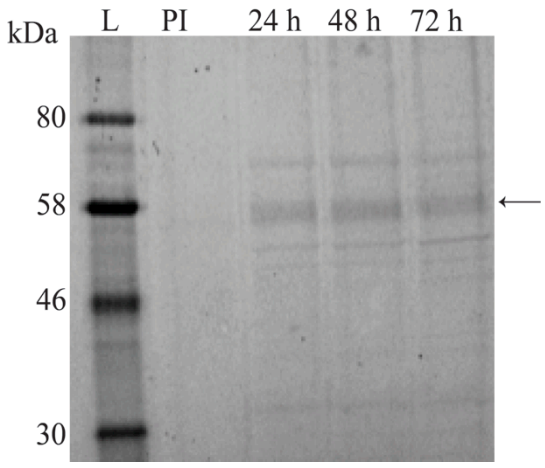

Figure 5.12 IL-1RI expression in *K. lactis*. *K. lactis* GG799 cells were transformed with the pKLAC2/IL-1RI plasmid and grown in 500 mL of YPGlu medium. Induction was carried out at an OD_{600} ~ 1 by changing to YPGal media, and incubating for 72 h. Samples at each 24 h were analysed by 10% SDS-PAGE. The molecular marker is labelled as **L**, and pre-induction sample as **PI**.

5.4.1 Anion exchange purification

In order to find out the best conditions for IEX purification, a set of four IEX columns for anion and cation exchange were tried, with a range of buffers at different pH. IL-1RAcP bound only to anion exchange columns at pH 8.5. Thus, for the purposes of this work, weak anion exchange column HiTrap DEAE FF was used to purify IL-1RAcP from YPGal.

After 48 h of IL-1RAcP expression in YPGal, medium was recovered by centrifugation and concentrated 10 times with a tangential/crossflow cassette (Sartorious) After concentration the sample was washed 1:100 volumes of 20 mM Tris buffer and then applied to a weak anion exchange column (HiTrap DEAE FF, GE). Elution was carried out by increasing NaCl concentration up to 1 M, in a stepwise manner. Three different peaks were eluted (Figure 5.13-A), and fractions from the three peaks were analysed by gradient 4-12% Bis-Tris-PAGE (Figure 5.13-B). Peak one eluted at about 50-250 mM NaCl (Figure 5.13-A), and gradient Bis-Tris-PAGE showed four different isoforms inside this peak, with different molecular weights, ranging from 35 to 72 kDa (Figure 5.13-B, black arrows). IL-1RAcP was identified, among other proteins in the four bands, by LC-MS/MS.

A protocol for IL-1RAcP purification from YPGal media was optimised, allowing purification of four isoforms of IL-1RAcP with different molecular weight. In order to further characterise such IL-1RAcP isoforms, a second step purification needed to be added.

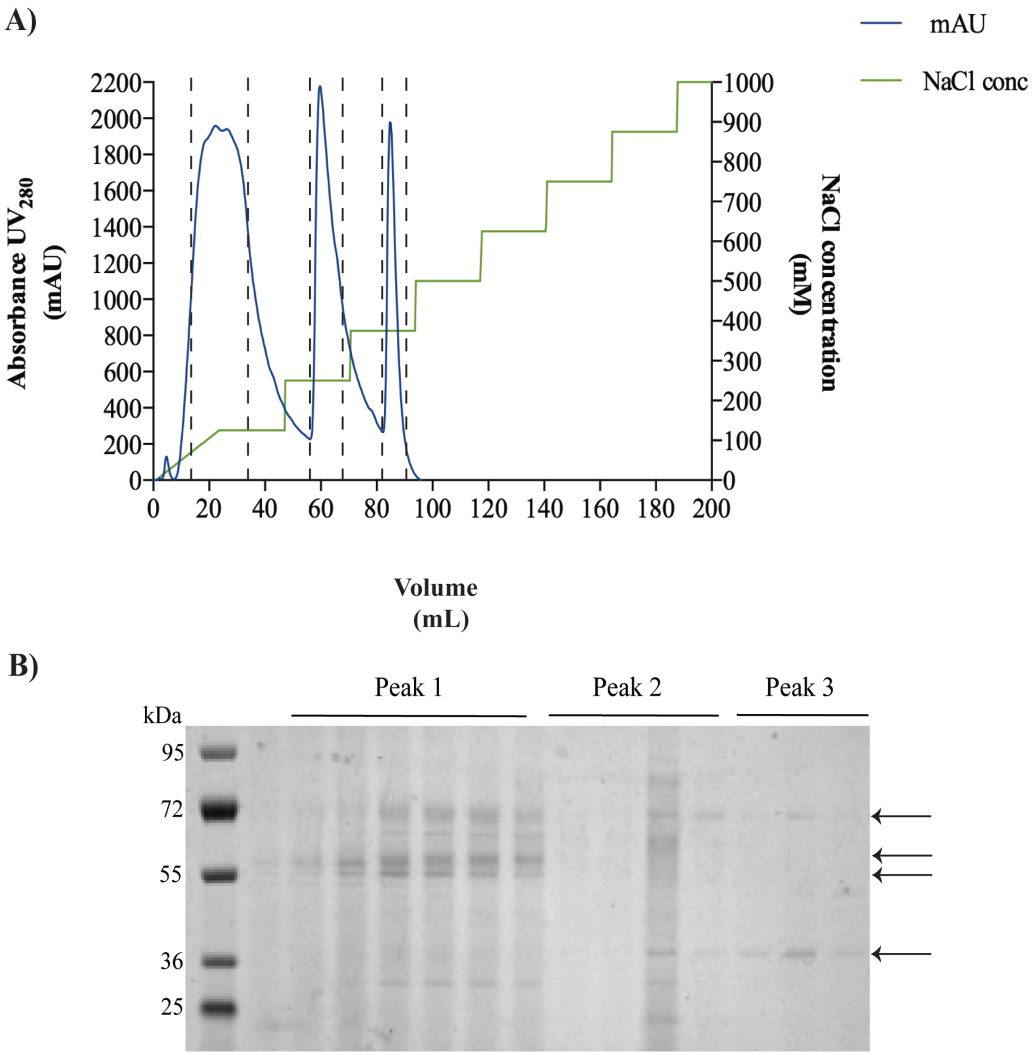

Figure 5.13 Anion exchange chromatography of IL-1RAcP. A) After washing with Tris buffer at pH 8 and concentrated 10x, YPGal media after 48 h expression was applied to a HiTrap DEAE FF anion exchange column and eluted with gradual increase in NaCl concentration up to 1M (100%). IL-1RAcP is eluted at 220-550 mM NaCl. **B)** 10% SDS-PAGE analysis of IL-1RAcP anion exchange chromatography shows four IL-1RAcP isoforms at 72, 36 kDa and two isoforms at 55-60 kDa.

5.5.2 SEC purification

Four IL-1RAcP isoforms with different molecular weights could be purified from YPGal media, after 48 h expression, by weak anion exchange. In order to separate the aforementioned IL-1RAcP isoforms, IEX samples eluted at 220-550 mM NaCl were pooled together and concentrated 10 times for further SEC purification with Superdex 200 column (GE). A single peak eluted at 16 mL (Figure 5.14-A). However,

as IEX sample contained four IL-1RAcP isoforms with different molecular weights, more than one peak was expected. Nevertheless, a shoulder in the peak at about 19 mL could be seen, indicating that the eluted sample was not totally homogenous. Thus, SEC elutions were concentrated 10 times and analysed by SDS-PAGE (Figure 5.14-B). According to the calibration curve carried out for the Superdex column, samples eluting at 16 mL have a molecular weight close to 44 kDa (Ovalbumin was used as a 44 kDa standard), so, it was expected that samples eluted in SEC purification have a molecular weight at about 44 kDa, yet, SDS-PAGE analysis showed no protein in any of eluted samples, in spite of samples been concentrated 10 times.

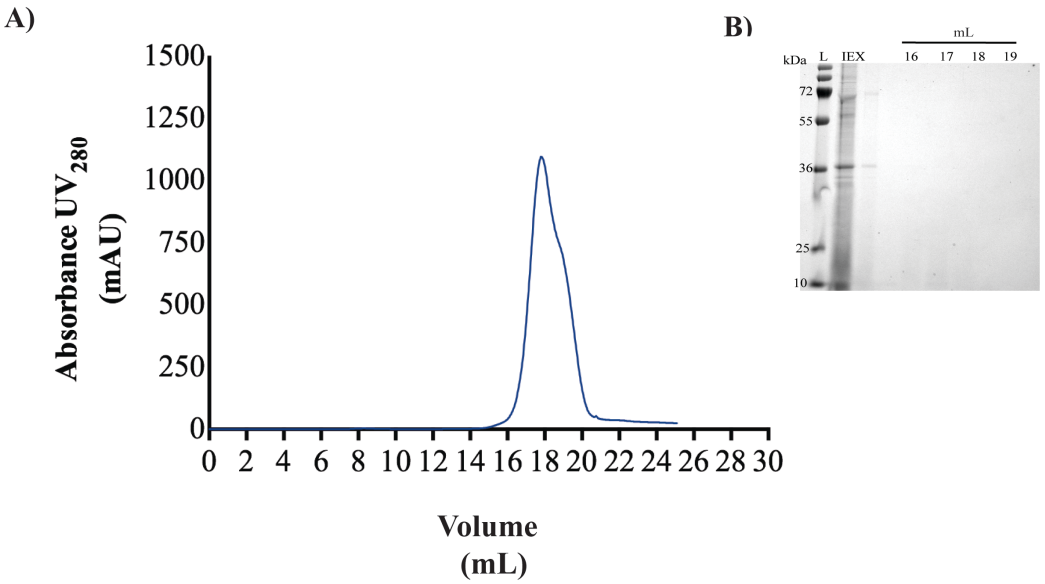

Figure 5.14 SEC purification of IL-1RAcP. Elutions resulting for IEX purification were pooled together and concentrated for further SEC purification. **A)** SEC trace of IL-1RAcP shows a single peak with a shoulder. **B)** The original sample from IEX purification and samples at different points of the peak were analysed by 10% SDS-PAGE. The three IL-1RAcP bands from anion exchange purification can be seen in IEX lane, however, nothing can be seen in elutions.

5.5.3 IMAC purification

An IL-1RAcP plasmid with a 6 x His tag was designed in order to facilitate IL-1RAcP purification. For this, after 48 h of IL-1RAcP expression in YPGal, medium was recovered by centrifugation and concentrated 10 times. After concentration, it was washed 1:100 volumes of 20 mM Tris buffer and then applied to a cobalt resin for IMAC purification. From the beginning, IMAC purification was ineffective, despite several attempts to improve IL-1RAcP-His binding to cobalt resin. An anion exchange pre-step purification before IMAC was also tried without success. Figure 5.15 shows 10% Bis-Tris PAGE analysis of IMAC purification process, stained with Pro-Q Emerald glycosylated protein staining (Figure 5.15-A) and Coomassie blue staining (Figure 5.15-B). A 55 kDa band can be seen in 48 h expression YPGal sample (Figure 5.15 A and B, YP) as well as in the flow through (Figure 5.15 A and B, FT). However, given that the resin bound sample is empty (Figure 5.15 A and B, RB), it is clear that IL-1RAcP-His did not bind the cobalt resin. $MgCl_2$, is commonly used during protein purification processes as a protein-structure stabiliser and molecular interactions enhancer. Thus, 5-10 mM $MgCl_2$ were also added to buffers. Nevertheless, no improvement was seen with $MgCl_2$ addition. In order to find explanation for the lack of binding, a meticulous sequence analysis of IL-1RAcP-His construct identified a site Lys392-Arg393 (as in pKLAC2/IL-1RAcP-His construct numbering; Figure 5.3) near the C-terminal, which potentially may resemble a restriction site for Kex protease, the enzyme responsible of cleaving the α-MF (Figure 5.12). Consequently, the His tag, which is at the C-terminal, may be cleaved out of IL-1RAcP, which may explain the unsuccessful attempt to bind this protein to the cobalt resin. This possible C-terminal cleavage may also potentially interfere with the total level of protein yield and could destabilize expressed protein structurally, and lead to further protein degradation during the purification process.

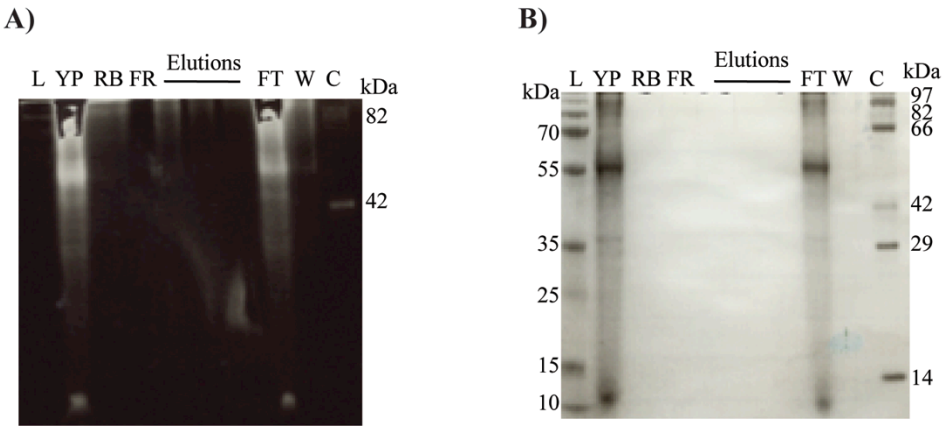

Figure 5.15 IMAC Purification of IL-1RAcP-His. 10% Bis-Tris PAGE showing each step of IL-1RAcP IMAC purification from *K. lactis*. Gel was stained with Pro-Q Emerald glycosylated protein staining (**A**) followed by Coomassie blue staining (**B**). 48 h expression YPGal (**YP**) was applied to cobalt resin for IMAC purification. IL-1RAcP did not bind to the cobalt resin (**RB**) and all protein remained in the flow through (**FT**). **L**, ladder. **FR**, final resin. **W**, wash. **C**, Candy cane, glycoprotein molecular weight standard.

5.6 IL-1RAcP characterisation by SEC-MALLS

In an attempt to characterise IL-1RAcP isoforms purified by IEX, IEX purification samples were analysed by SEC-MALLS. Three different peaks were identified (Figure 5.16-A) and the molar mass distribution of IL-1RAcP IEX sample was not uniform, ranging from 2 kDa to approximately 80 kDa. Fractions of less than 12 mL retention volume had the largest molecular weight of about 70 kDa, which is consistent with the largest IL-1RAcP isoform found in IEX samples (Figure 5.13-B). However, this fraction only represents 0.61% of the total mass. The most abundant protein (86.53%) was found in a longer retention volume (>14.6 mL) and light scattering of this fraction gave a molecular mass of 3.06 kDa, which is very low compared to IL-1RAcP predicted molecular weight. Samples resulting from SEC-MALLS analysis were concentrated 10x and analysed by 10% Bis-Tris PAGE (Figure 5.16-B). As expected, given the low molecular weight of fractions found in peaks 2 and 3, nothing can be seen in these lanes. However, fraction in peak 1 showed three bands at different molecular weights, ranging from 55 kDa to 70 kDa. The large proportion of

A)

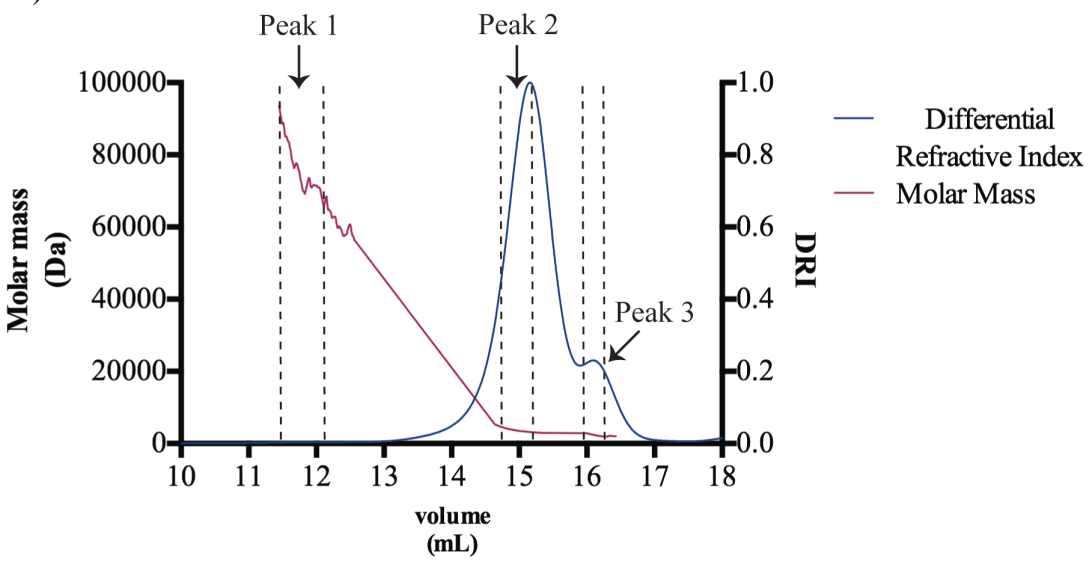

B)

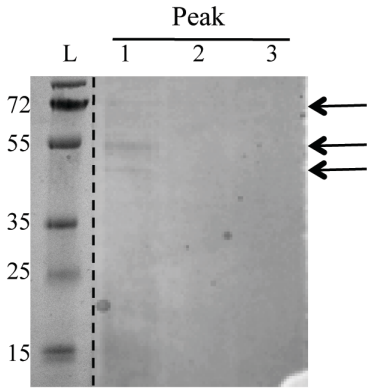

C)

	Molar mass (Da)	Mass fraction (%)
Peak 1	6999.0	0.61
Peak 2	3064	86.53
Peak 3	2111	12.85

Figure 5.16 SEC-MALS analysis of IL-1RAcP. After IEX purification IL-1RAcP was analysed by SEC-MALS. **A)** Proteins mass detected by MALS alongside the SEC trace. Proteins with different molecular mass were detected, with early protein of > 70 kDa down to 2 kDa. **B)** 10% Bis-Tris PAGE analysis of concentrated protein fractions found in SEC-MALS. The lowest MW population in peaks 2 and 3 could not be seen given that their MW is too low. A 70 kDa band can be seen in peak 1, along with 2 more bands at ~55 kDa. **C)** SEC-MALS data of the three populations detected. Peak 1 had a molecular mass of 69.99 kDa and represented only 0.61% of the total protein. Peak 2, the most abundant protein, represented 86.5% of the total mass and had a molecular weight of 3.06 kDa. Peak 3, with a molecular mass of 2.11 kDa, represents 12.85% of the total protein.

2-3 kDa proteins suggested that IL-1RAcP purified by IEX might be degraded. In addition, the variability of molecular masses found in IL-1RAcP IEX samples (2-80

kDa), suggested that the resulting peptides from degradation might be aggregating, being responsible of the larger molecular masses identified by light scattering, as well as of the peak observed in SEC purification (Figure 5.14-A), which retention volume is comparable to retention volume of ovalbumin, a 44 kDa protein.

5.7 Summary of the results of IL-1RI and IL-1RAcP expression, purification and characterisation

IL-1RI and IL-1RAcP expression and purification was highly problematic. Despite the attempts to optimise soluble expression in *E. coli*, IL-1RAcP and IL-1RI remained totally insoluble. Attempts to refold these proteins *in vitro* were not successful. A high level of glycosylation sites in both proteins, as well as multiple disulphide bonds, likely make *E. coli* an unsuitable host for their production. Thus, given the capacity of yeast to carry out post-translational modifications and assist correct disulphide bond formation, expression and purification of IL-1RI and IL-1RaCP in *K. lactis* was also tried. Nevertheless, protein expression was not easy to achieve. IL-1RI could not been expressed in *K. lactis*, and of all the IL-1RAcP constructs tried in this work (Table 5.7) only 2 could be expressed. However, characterisation of proteins produced in *K. lactis* was also difficult. At first, given the high level of glycosylation of IL-1RAcP, expression estimation was difficult, as N-linked glycosylation interferes with Coomassie blue-protein binding. Thus, a glycosylated protein stain (ProQ Emerald, Invitrogen) was used and 10% Bis-Tris PAGE analysis of IL-1RAcP 48 h expression YPGal stained with ProQ Emerald showed a considerable level of expression of IL-1RAcP and IL-1RAcP-His constructs. Yet, purification was also difficult. In order to identify IL-1RAcP, samples at each state, from expression to purification were analysed by LC-MS/MS, given that this method has been shown to be a powerful tool for protein identification from complex mixtures (Delahunty and Yates, 2005, Stults and Arnott, 2005) A high level of IL-

1RAcP peptides, corresponding to 45% of the native sequence used in this work (338 residues), were found in YPGal media after 48 h expression. However, the number of peptides identified in purification samples decreased at each purification step. The construct IL-1RAcP-His could not be purified by IMAC, likely due to a restriction site for the Kex protease found at the C-terminal of the protein just before the His-tag, thus, the His-tag was cleaved out of the protein just before it was secreted to the medium. SEC-MALLS analysis of IL-1RAcP purified by IEX, showed that this sample contained a high proportion of low molecular weight proteins (2-3 kDa), making us suspect that IL-1RAcP was degraded. Samples were always kept on ice during purification process, and protease inhibitors were added to purification buffers. However, in order to analyse IL-1RAcP samples by Bis-Tris-PAGE, samples were always concentrated up to 100 x, hence, concentration process might have contributed to degradation of the sample.

Table 5.7 IL-1RAcP plasmids used in *K. lactis*

Construct	Expression	Purification
pKLAC2/IL-1RAcP	High	Degradation
pKLAC2/IL-1RAcP-His	High	His-tag loss
pKLAC2/IL-1RAcP-IL-1α	Not detected	Not tried
pKLAC2/IL-1RAcP-Peptides	Not detected	Not tried

6 Results: Effects of pH and temperature on IL-1

As it has been discussed throughout this work, the molecular mechanisms involved in the differences observed between IL-1α and IL-1β bioactivity remain unclear. In addition, although it has been suggested that IL-1α and IL-1β share similar binding sites to IL-1RI, the amino acids involved in binding and bioactivity are not conserved between IL-1α and IL-1β (Gronenborn et al., 1988, Labriola-Tompkins et al., 1991, Kawashima et al., 1992, Evans et al., 1995, Vigers et al., 1997). Yet, the structure of IL-1α bound to IL-1RI has not been elucidated. Due to their ability to induce fever, IL-1α and IL-1β were first known, together, as the "pyrogenic factor". To date, it is well known that both cytokines are key players in inflammation processes, and have been found to be involved in several chronic diseases such as diabetes type 2, autoimmune diseases and stroke. Moreover, it has been established that under inflammatory conditions there can be a drop in pH either systemically (Arnett, 2010) or locally (Nemoto and Frinak, 1981) as well as an increase in tissue temperature. Furthermore, it is well established that, for most proteins, temperature and pH are key factors in the maintenance of structure and stability; hence protein functional properties can be affected by changes in temperature and pH (Berisio et al., 2002). We therefore hypothesised that the slightly different biological activity of IL-1α and IL-1β can be related to different sensitivity of these cytokines to temperature and/or pH. If the latter is true, small near-physiological variations of temperature and/or pH should have different effects on structure and/or stability of these proteins, therefore providing an "environmentally-driven" regulatory mechanism, i.e. in a response to local inflammation. Thus, with the purpose of characterising biophysical differences between IL-1α and IL-1β as well as the effects that pH and temperature have on them,

IL-1α and IL-1β were analysed by CD, static light scattering (SLS), ^{1}H-NMR, fluorescence and analytical ultracentrifugation (AUC).

6.1 Effects of pH in thermal stability

6.1.1 Acidic pH influences thermal stability of IL-1β secondary structure but not IL-1α.

As it has been disclosed in Chapter 1, during the inflammation processes, tissue pH has been shown to become acidic, i.e. brain pH can drop to 6.2 during ischemia and the lower airway pH has been shown to be 5.2 in patients with asthma (Nemoto and Frinak, 1981, Hunt et al., 2000). Furthermore, it has been demonstrated that IL-1 plays a key role in inflammation in both asthma and stroke (Rothwell, 2003, Wei-xu et al., 2014). With the purpose of analysing the effects that acidic pH has on IL-1 thermal stability (as a function of their secondary structure composition), IL-1α and IL-1β solutions in PBS at pH 5.5, 6.2 and 7.5 were prepared and analysed by CD at increasing temperatures from 20°C to 85°C. A Dichroweb analysis with the algorithm K2D (explained in Section 1.4.1) of CD spectra was carried out in order to estimate the secondary structure composition of IL-1α and IL-1β in all conditions. It has been demonstrated that both IL-1α and IL-1β secondary structures consist mainly of β-sheets (Priestle et al., 1988, Finzel et al., 1989, Graves et al., 1990). Figure 6.1 shows the predicted β-sheet content of both IL-1α and IL-1β. IL-1α predicted β-sheet content was highly similar (~ 48%) at all pH tested, suggesting that IL-1α secondary structure is not affected significantly by pH. Interestingly, even though small changes can be seen at higher temperatures (from 60°C), the secondary structure appears to be unaffected by temperature in the range up to 85°C. However, IL-1α CD spectra at pH 5.5 (shown in Appendix 4, Figure A4-2) showed a gradual change in the protein

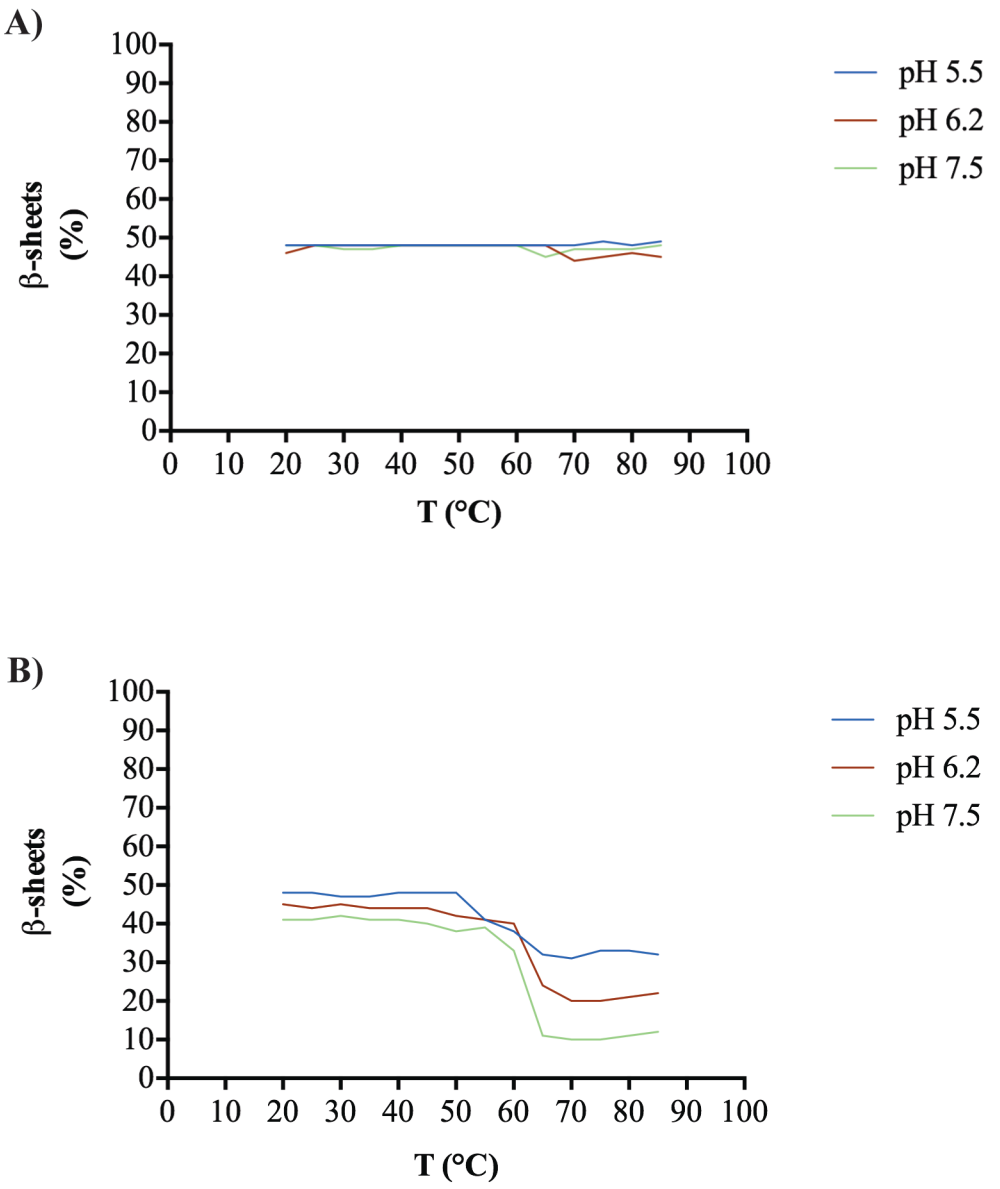

Figure 6.1 β-sheet content prediction of IL-1α and IL-1β at increasing temperatures under different pH conditions. IL-1α and IL-1β purified from *E. coli* were analysed by CD in the far UV region at increasing temperatures under different pH conditions. CD spectra were analysed with Dichroweb using the algorithm K2D. **A)** IL-1α predicted β-sheet content indicates similarity between IL-1α secondary structure at pH 5.5 (blue line), 6.2 (red line) and 7.5 (green line) at all temperatures tested (20-85°C), suggesting that IL-1α has thermal stability at different pH. **B)** IL-1β predicted β-sheet content indicates similarity between IL-1β secondary structure at pH 5.5, 6.2 and 7.5 (same colour code as above) at temperatures from 20-60°C. After 60°C the β-sheet content starts to decrease, indicating IL-1β is thermally stable up to 60°C.

secondary structure that is not consistent with the β-sheet prediction content. For example, the CD spectrum at 20°C is greatly different from that at 85°C. As for IL-1α CD spectra at pH 6.2 and 7.5 (Figure A4-2), changes in the CD spectra with respect to temperature are not very obvious. It is worth to point out that β-sheet characteristic CD spectra have a negative band at 215-220 nm (Greenfield, 2006b), thus, in order to estimate changes in β-sheet structures, this region needs to be monitored. Additionally, this thermal "stability" above 60-65°C in all pH analysed is not consistent with biophysical analysis carried out along with CD; this is discussed in the following sections in this chapter. Figure 6.1-B shows the predicted β-sheet content of IL-1β at increasing temperatures at pH 5.5, 6.2 and 7.5. Contrary to IL-1α, IL-1β secondary structure content is reduced above 60°C at all the three pH tested. The reduction in β-sheets is more drastic at pH 7.5 (~ 75%) compared to pH 6.2 (~ 50%) and pH 5.5 (~20%) (For more detailed information on β-sheet content at all temperatures tested see Figure A4-2 in Appendix 4). These predictions suggested that at acidic pH IL-1β secondary structure is more resistant to thermal denaturation.

As mentioned above, β-sheet structure has a characteristic negative band at 215-220 nm. A different approach to study the thermal stability of proteins by CD is monitoring protein ellipticity at a single wavelength. With this purpose, IL-1α and IL-1β solutions in PBS at pH 5.5, 6.2 and 7.5 were analysed by CD at a single wavelength (217 nm) at increasing temperatures from 20°C to 85°C, with increments of 5°C. Changes in IL-1α ellipticity at pH 5.5, 6.2 and 7.5, can be observed above 60°C; however, these changes are only small even at 85°C (Figure 6.2-A). This is consistent with Dichroweb prediction of IL-1α secondary structure (Figure 6.1-A), which shows that the percentage of β-sheets remains the same at 85°C in acidic and neutral pH. IL-

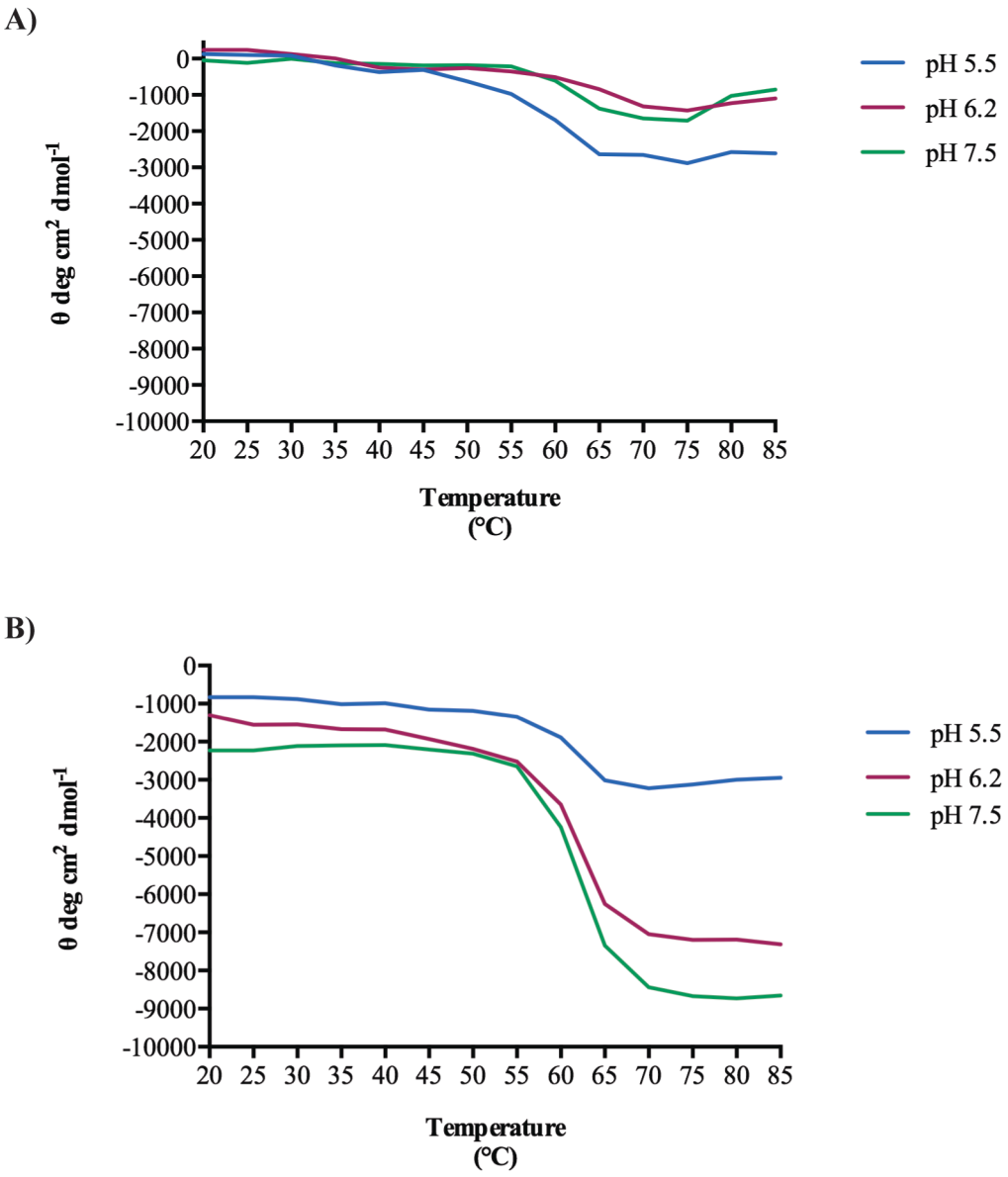

Figure 6.2 Effects of pH in thermal stability of IL-1α and IL-1β. A) Changes in IL-1α ellipticity at 217 nm as temperature increased, at pH 5.5 (blue line), 6.2 (red line) and 7.5 (green line). Similar small changes in IL-1α ellipticity are observed around 60°C at all pH. **B)** Changes in IL-1β ellipticity at 217 nm as temperature increased, at pH 5.5 (blue line), 6.2 (red line) and 7.5 (green line). Ellipticity changes can be observed at the three different pH above 60°C, but at pH 5.5 this change is small. At pH 6.2 and 7.5, ellipticity change at >60° is more prominent and pH 7.5 has the more dramatic change in ellipticity.

1β changes in ellipticity can also been observed above 60°C at pH 5.5, 6.2 and 7.5 (Figure 6.3-B). However, at pH 5.5, these changes are smaller than at pH 6.2 and 7.5, and the most drastic change can be observed at pH 7.5. These findings are consistent

with Dichroweb prediction shown in Figure 6.1, where it can be seen that the β-sheet content of IL-1β is more affected in pH 7.5 at 85°C.

These findings suggest that pH does have an effect on IL-1β secondary structure thermal stability, and IL-1β β-sheet conformation appears to be more stable at acidic pH. On the other hand, secondary structure stability of IL-1α at high temperatures is not affected much by the pH, and generally appears to be higher than that of IL-1β.

6.1.2 IL-1β intrinsic fluorescence differs at acidic pH

The tertiary structure of proteins can be studied by measuring their intrinsic fluorescence, which is given by the aromatic amino acids Trp and Tyr. Due to the hydrophobic nature of Trp and Tyr, these residues are commonly hidden within the structures of proteins. When a protein is partially or totally unfolded, hydrophobic amino acids become exposed resulting in a rise in intrinsic fluorescence. With the aim of studying the effects of pH on IL-1α and IL-1β conformation, their intrinsic fluorescence was measured at increasing temperature and at pH 5.5, 6.2 and 7.5 with Optim 1000. IL-1α intrinsic fluorescence is very similar in all pH, and the melting temperature (T_m) is observed above 70°C, suggesting that pH has no effects on IL-1α conformation (Figure 6.3-A). Conversely, IL-1β intrinsic fluorescence is lower at pH 7.5 than at pH 5.5 and 6.2 (Figure 6.3-B). In addition, T_m at pH 7.5 is also lower, and at pH 7.5 a change in IL-1β conformation can be seen at about 55°C whereas at pH 6.2 IL-1β T_m is about 65°C and at pH 5.5 is about 75°C. These findings suggest that IL-1β conformation is more stable at lower pH. Additionally, pH also has an effect on IL-1β conformation, as intrinsic fluorescence is different at pH 7.5 compared to acidic pH.

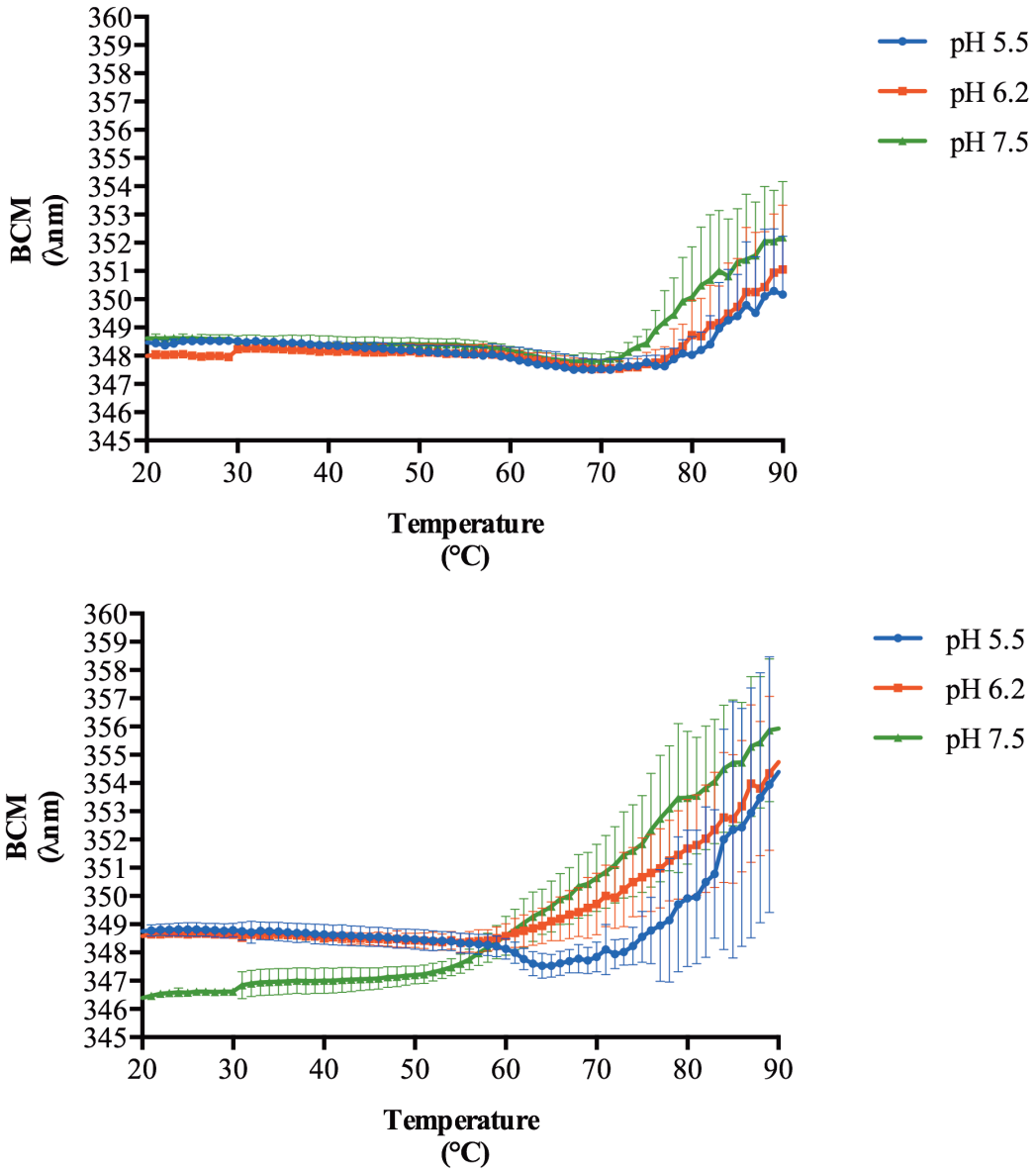

Figure 6.3 Effects of temperature and pH on IL-1α and IL-1β conformation. Changes on IL-1α and IL-1β fluorescence at increasing temperatures and at different pH were measured with Optim 1000. **A)** Fluorescence changes on IL-1α at increasing temperatures at pH 5.5 (blue line), 6.2 (red line) and 7.5 (green line). Fluorescence of IL-1α is considerably similar between the three pH used. An increase in IL-1α fluorescence can be observed above 70°C. **B)** Fluorescence changes on IL-1β at increasing temperatures at pH 5.5 (blue line), 6.2 (red line) and 7.5 (green line). IL-1β fluorescence is very similar among acidic pH (5.5 and 6.2) but not pH 7.5. IL-1β fluorescence is increased above 70°C. Data are presented as mean + SD of three independent experiments.

6.1.3 Colloidal stability of IL-1

An alternative approach to studying protein stability is the analysis of protein aggregation. As aforementioned, hydrophobic residues tend to be hidden within protein structure, and become exposed as the protein starts to unfold, thus making protein more hydrophobic. This change in protein hydrophobicity can lead to unspecific self-association of the protein, namely aggregation. The temperature at which a protein starts to aggregate is known as onset of aggregation (T_{agg}). Static light scattering (SLS) is a powerful tool for the study of protein aggregation and the T_{agg} can be obtained from the temperature at which light scattering of the protein solution starts to increase from a base level for more than 10%. T_{agg} can be used as an additional, indirect measure of protein stability in solution, namely colloidal stability. Thus, with the purpose of studying the effects of pH on IL-1α and IL-1β on thermal stability, IL-1α and IL-1β were analysed by SLS at 266 and 473 nm, in order to measure IL-1α and IL-1β T_{agg} at pH 5.5, 6.2 and 7.5. Figures 6.4 and 6.5 show IL-1α SLS and T_{agg} at 266 and 473 nm, respectively. IL-1α SLS_{266} is similar at pH 5.5, 6.2 and 7.5 (Figure 6.4-A). Likewise, IL-1α SLS_{473} is similar at all pH (Figure 6.5-A), although it seems to be more homogenous at 473 nm. IL-1α T_{agg} at 266 nm at pH 5.5 is 51°C, in contrast to T_{agg} at pH 6.2 and 7.5, which are about 59°C (Figure 6.4-B). At 473 nm (Figure 6.5-B) however, IL-1α T_{agg} at pH 6.2 is about 63°C, which is higher than at pH 5.5 and 7.5, both 60°C, nevertheless, this increase in T_{agg} is minimal and therefore the differences were found to be non-significant between the three pH. These data suggests that pH does not affect colloidal stability of IL-1α, as there is not difference in IL-1α T_{agg} between pH 6.2 and 7.5.

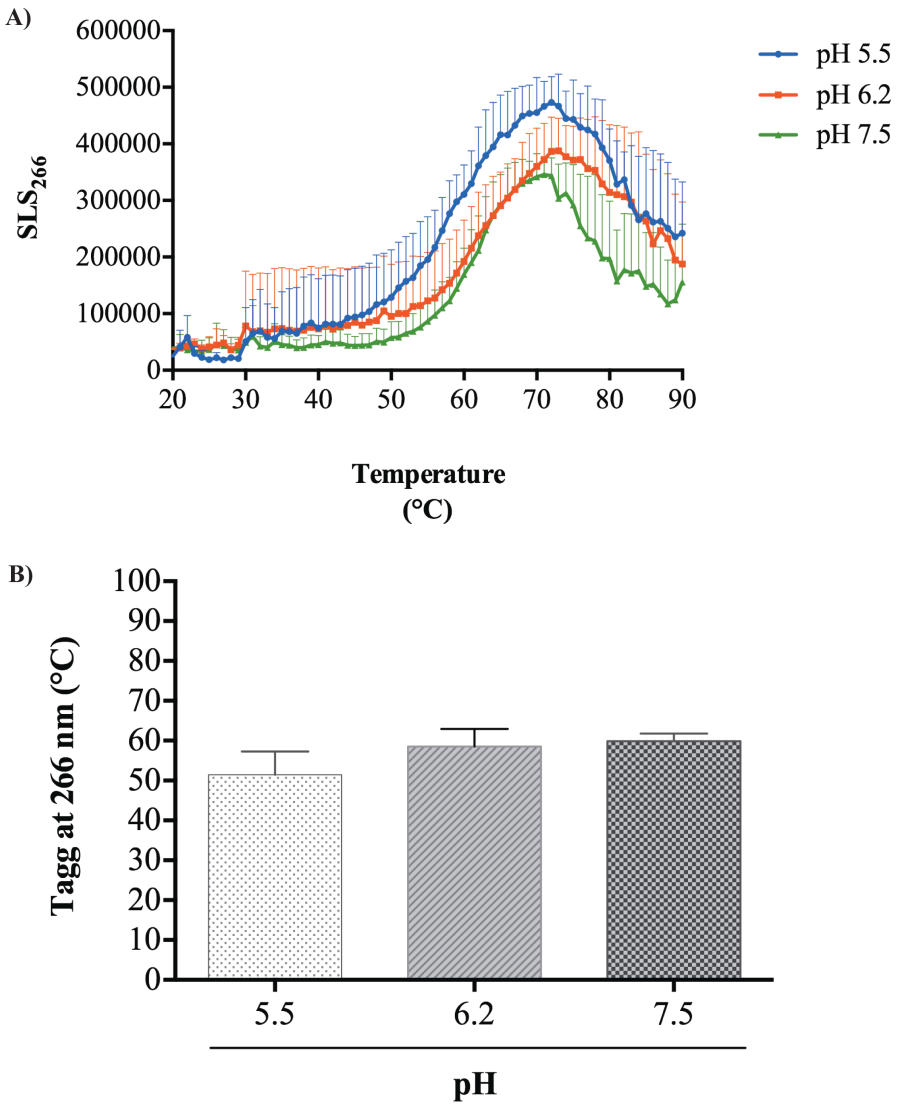

Figure 6.4 Effects of pH on IL-1α SLS and T_{agg} at 266 nm. A) IL-1α SLS_{266} at pH 5.5 (blue line), 6.2 (red line) and 7.5 (green line) are highly similar; changes in SLS can be seen above 50°C in all pH. **B)** IL-1α T_{agg} at pH 5.5, 6.2 and 7.5. No difference can be observed between IL-1α T_{agg} on pH 5.5, 6.2 and 7.5. T_{agg} was obtained from SLS_{266} raw data and plotted as a mean + SD of three independent experiments. Non significant differences between treatments using one-way ANOVA with Bonferroni's multiple comparison post-hoc tests.

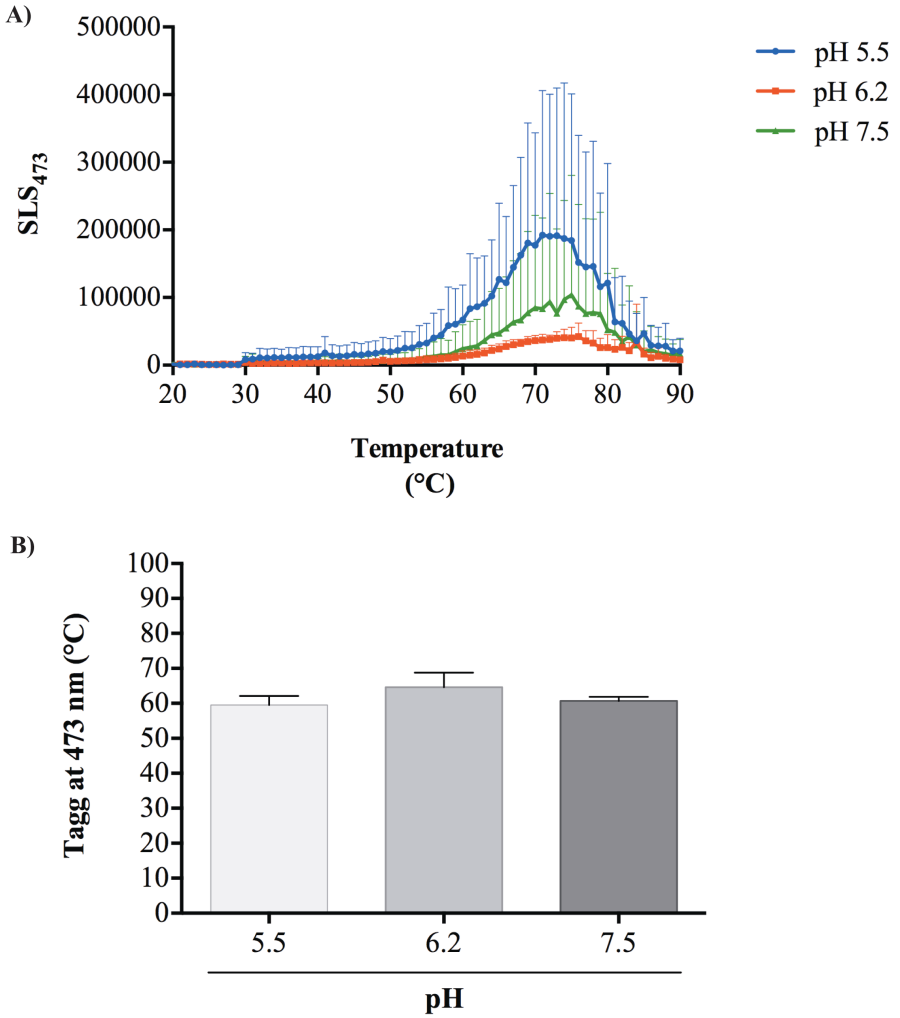

Figure 6.5 Effects of pH on IL-1α SLS and T_{agg} at 473 nm. A) IL-1α SLS_{473} at pH 5.5 (blue line), 6.2 (red line) and 7.5 (green line) are highly similar; changes in SLS can be seen above 60°C in all pH. **B)** IL-1α T_{agg} at pH 5.5, 6.2 and 7.5. No difference can be observed between IL-1α T_{agg} on pH 5.5, 6.2 and 7.5. T_{agg} was obtained from SLS_{473} raw data and plotted as a mean + SD of three independent experiments. Non significant differences between treatments using one-way ANOVA with Bonferroni's multiple comparison post-hoc tests.

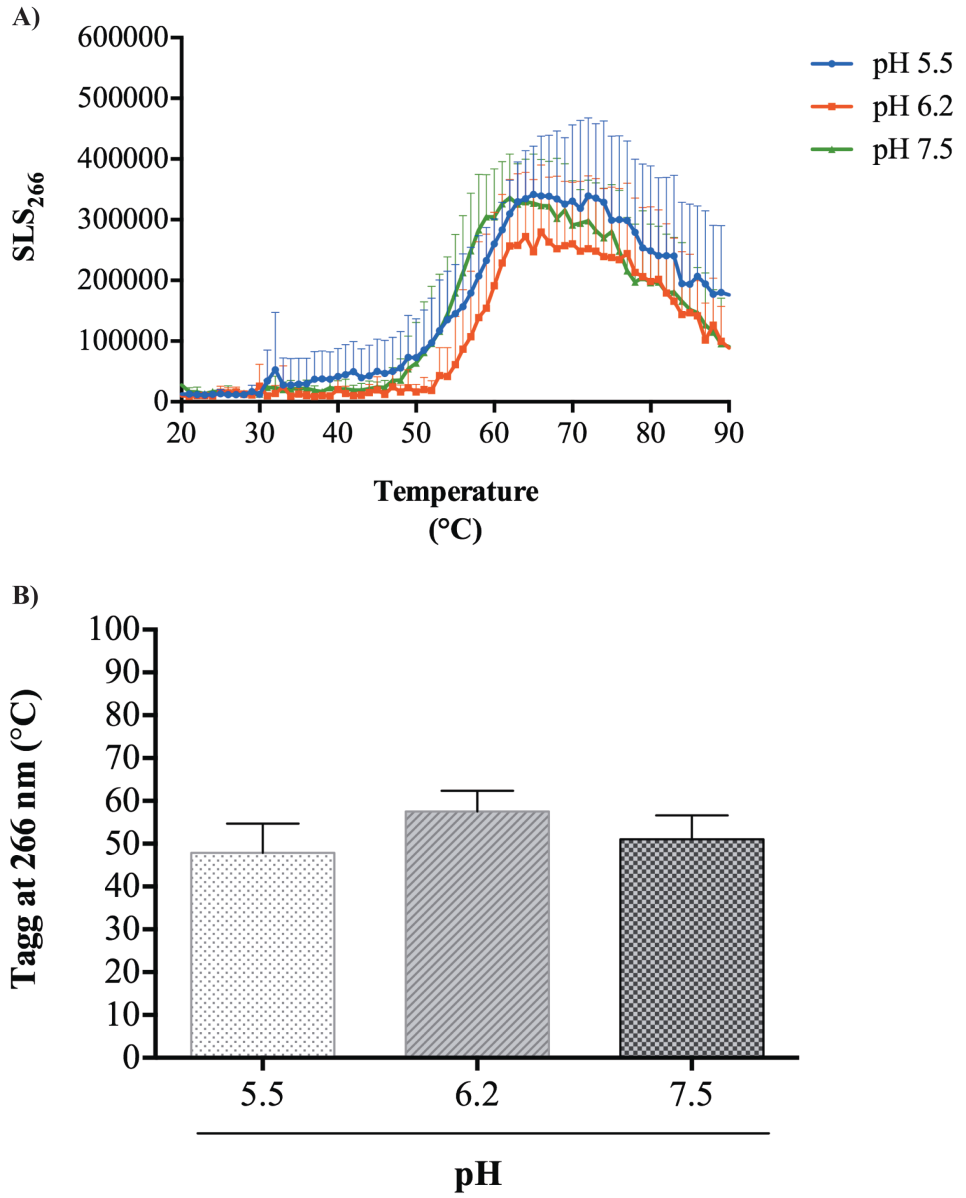

Figure 6.6 Effects of pH on IL-1β SLS and T_{agg} at 266 nm. A) IL-1β SLS_{266} at pH 5.5 (blue line), 6.2 (red line) and 7.5 (green line) are highly similar; changes in SLS can be seen above 50°C in all pH. **B)** IL-1β T_{agg} at pH 5.5, 6.2 and 7.5. No difference can be observed between IL-1α T_{agg} on pH 5.5, 6.2 and 7.5. T_{agg} was obtained from SLS_{266} raw data and plotted as a mean + SD of three independent experiments. Non significant differences between treatments using one-way ANOVA with Bonferroni's multiple comparison post-hoc tests.

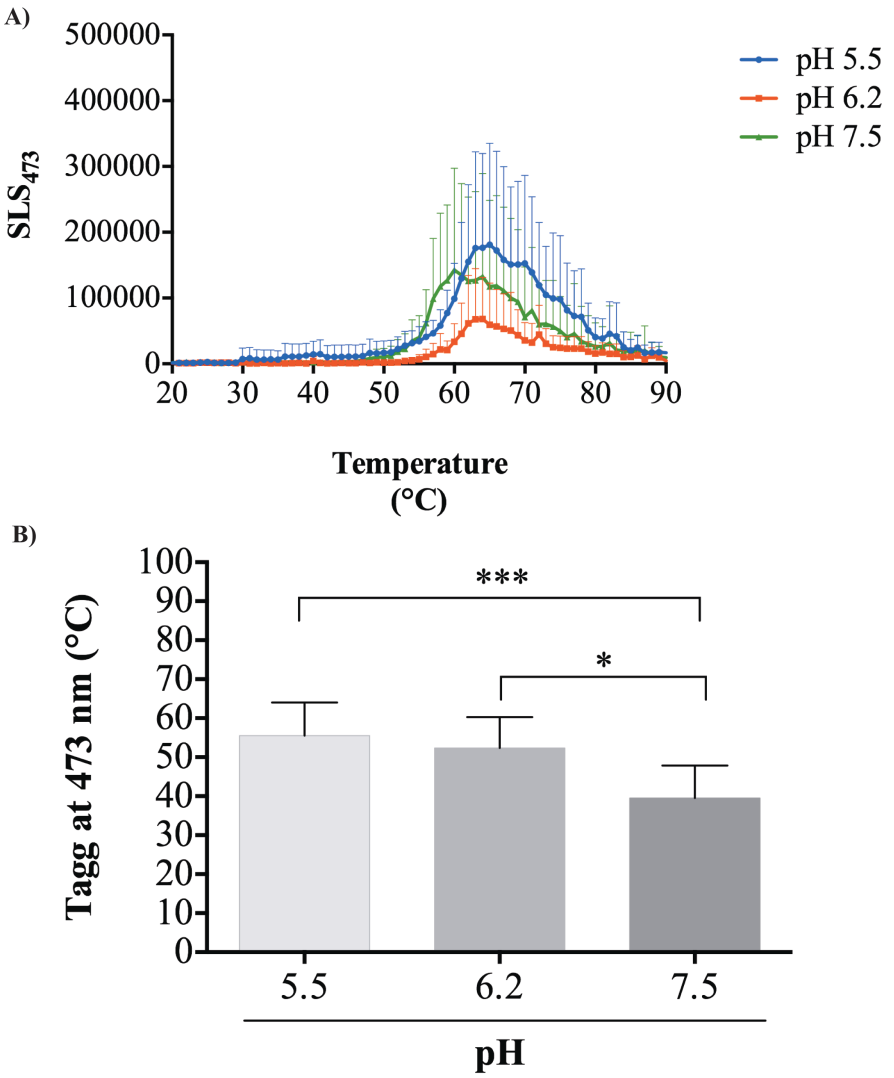

Figure 6.7 Effects of pH on IL-1β SLS and T_{agg} at 473 nm. A) IL-1β SLS_{473} at pH 5.5 (blue line), 6.2 (red line) and 7.5 (green line) are highly similar; changes in SLS can be seen above 50°C in all pH. **B)** IL-1β T_{agg} at pH 5.5, 6.2 and 7.5. A small decrease on IL-1β T_{agg} can be observed at pH 7.5. T_{agg} was obtained from SLS_{473} raw data and plotted as a mean + SD of three independent experiments. *p<0.01; ***p<0.001, significant differences between pH 5.5 and 7.5 and between pH 6.2 and 7.5, non significant differences between pH 5.5 and 6.2, using one-way ANOVA with Bonferroni's multiple comparison post-hoc tests.

Similarly, IL-1β SLS_{266} is not affected by pH (Figure 6.6-A) in the same way as IL-1β SLS_{473} (Figure 6.7-A). However, T_{agg} resulting from SLS_{266} (Figure 6.6-B) seems to be to some extent higher at pH 6.2 (58°C) than at pH 5.5 (50°C) or 7.5 (51°C), nonetheless, statistical analysis reflects non-significant differences on T_{agg} resulting from SLS_{266} between the three pH tested. On the other hand, the tendency to decrease as pH increases is more obvious in T_{agg} obtained from SLS_{473} (Figure 6.7-B), where IL-1β T_{agg} at pH 5.5 is 56°C, at pH 6.2 is 54°C and at 7.5 it is 40°C. Significant differences between acidic pH and neutral pH were found thus, from this analysis it was concluded that IL-1β is more stable at acidic pH, as it becomes less prone to aggregation.

6.1.4 pH 6.2 has an effect on IL-1β hydrodynamic properties

Protein hydrodynamics can be defined as the study of mass, conformation and interaction properties of a protein in solution conditions. Analytical ultracentrifugation (AUC) is a method commonly used for protein characterization as it provides information about size and shape of proteins (Laue, 2001). In order to analyse the effects of pH on IL-1α and IL-1β hydrodynamics, IL-1α and IL-1β were analysed by analytical centrifugation at 48,000 rpm. Figure 6.8 shows the velocity analytical ultracentrifugation sedimentation profiles of IL-1α (Figure 6.8-A) and IL-1β (Figure 6.8-B) at pH 5.5, 6.2 and 7.5. IL-1α sedimentation coefficient remains the same (1.85) at all the three pH, whereas IL-1β sedimentation coefficient is lowered at pH 6.2, indicating that at this pH IL-1β is elongated.

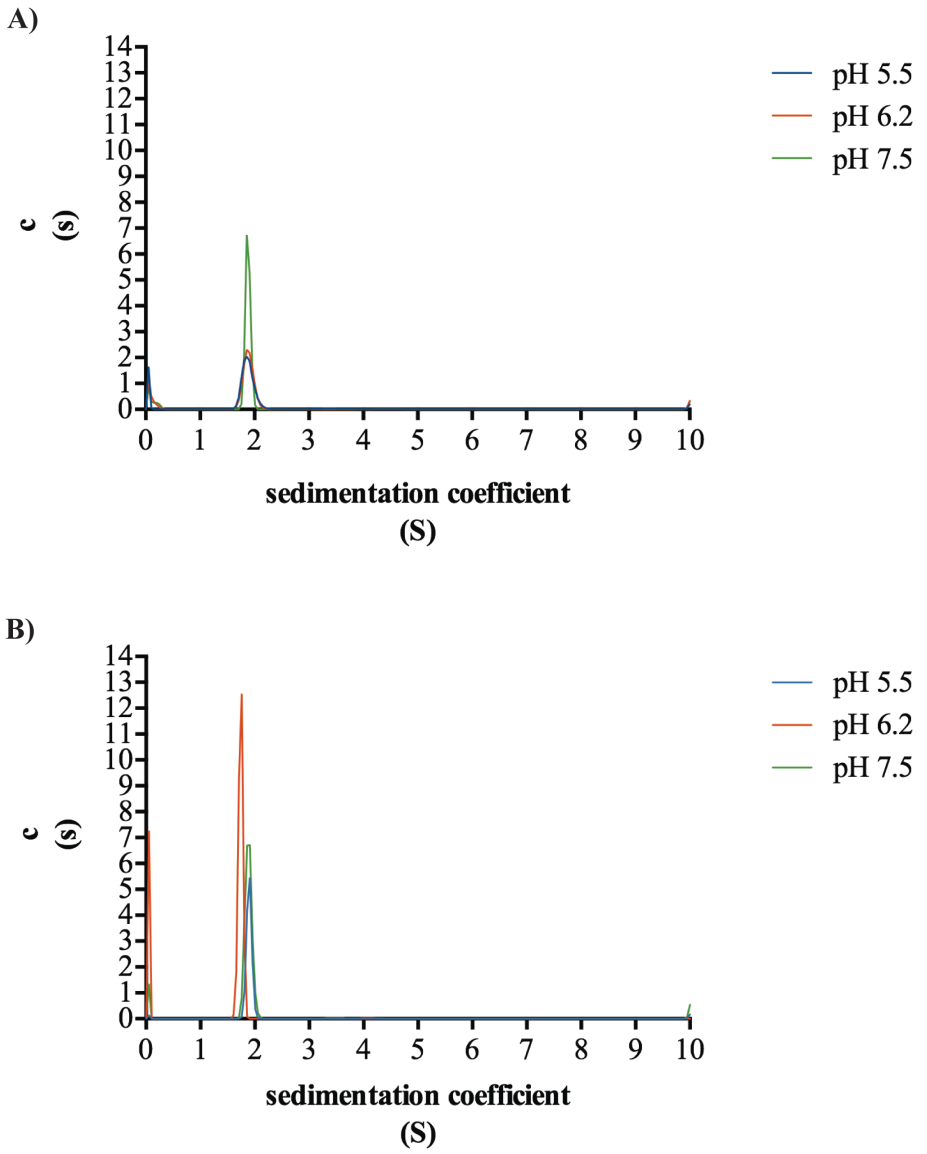

Figure 6.8 Effects of pH on IL-1α and IL-1β sedimentation. A) Velocity analytical ultracentrifugation sedimentation profiles of IL-1α at pH 5.5 (blue line), 6.2 (red line) and 7.5 (green line). Sedimentation coefficient of IL-1α is 1.85 at all the three pH used in this analysis. **B)** Velocity analytical ultracentrifugation sedimentation profiles of IL-1β at pH 5.5 (blue line), 6.2 (red line) and 7.5 (green line). Sedimentation coefficient of IL-1β at pH 5.5 and 7.5 is 1.90, and at pH 6.2 is 1.75.

6.1.5 Effects of pH on IL-1α and IL-1β thermal stability characterised by ^{1}H-NMR

Previous analyses of IL-1α and IL-1β conformation were based on aromatic amino acids Trp and Tyr biophysical properties. These amino acids are responsible for the intrinsic fluorescence of proteins. On the other hand, due to their hydrophobic nature, their position within the protein structure also affects protein hydrophobicity. pH-dependent changes on intrinsic fluorescence as well as onset of aggregation of IL-1β, but not IL-1α, were observed (Figures 6.3-A and 6.7). As mentioned in Chapter 4, the NMR signals less than 0 ppm are characteristic of methyl groups of aliphatic amino acids Val, Ile and Leu, located within close proximity to the side chain of aromatic amino acids such as Tyr, Phe and Trp. Therefore observing the effects of pH and temperature on the chemical shifts of these methyl signals can provide valuable information on protein stability, which can be complementary to the data obtained using intrinsic fluorescence measurements. Consequently, here the chemical shifts of methyl signals of IL-1α and IL-1β were analysed by ^{1}H-NMR at pH 5.5 and 7.5. Figures 6.9 and 6.10 show the methyl signals of IL-1α at increasing temperatures at pH 5.5 and 7.5 respectively. As disclosed in section 1.4.2, the chemical shift of a chosen group, i.e. methyl group, will have slightly different chemical shifts depending on the environment that surrounds them giving rise to the signal dispersion. IL-1α signal dispersion varies with temperature at both pH 5.5 and 7.5 (Figures 6.9 and 6.10, respectively). IL-1β does not have as many signals from methyls in the range 0.5 to -0.8 ppm (Figures 6.11 and 6.12) as IL-1α due possibly to its lower content of hydrophobic amino acids, namely Tyr, Trp and Ile (Tables 4.1 and 4.2). Dispersion of IL-1β also varies when temperature is increased (Figures 6.11 and 6.12). Importantly, unlike IL-1α, this protein is totally denatured and becomes aggregated, with the signals

decreasing and disappearing, at 65°C in pH 5.5 (Figure 6.11) and at 60°C in pH 7.5 (Figure 6.12).

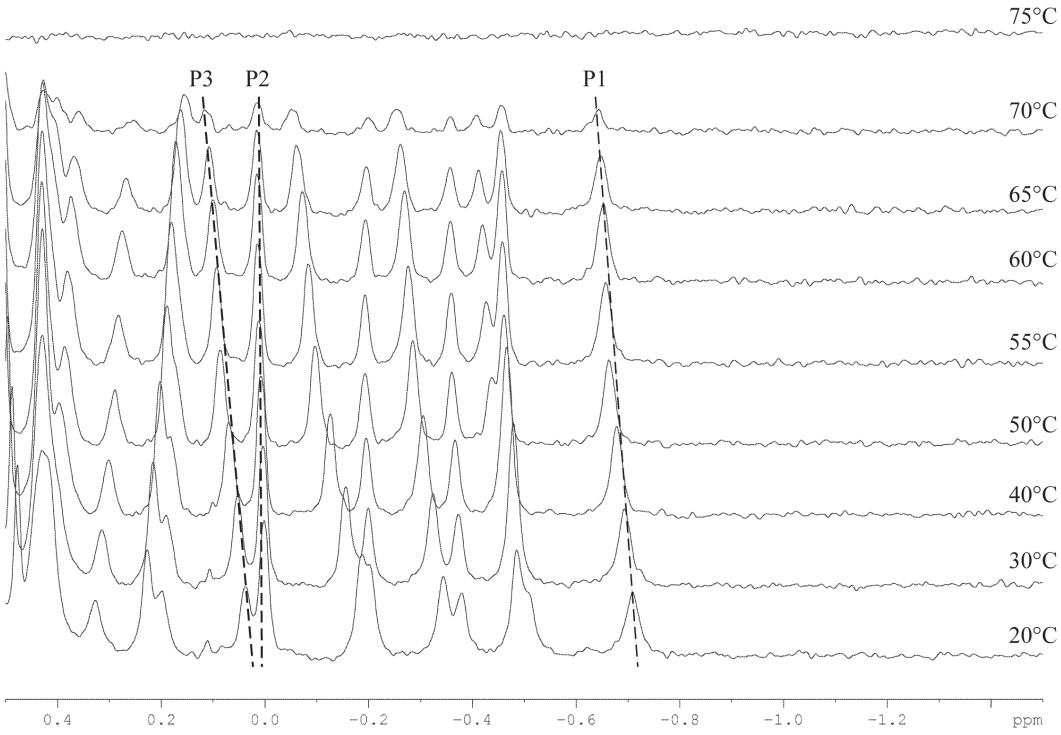

Figure 6.9 IL-1α temperature-dependent ^{1}H-NMR of methyl region at pH 5.5. IL-1α at pH 5.5 at increasing temperatures was analysed by ^{1}H-NMR. Methyl signals (0.5 to -1.5 ppm) at temperatures 20-75°C. Minor changes in methyl signals occur during temperature increments up to 65°C suggesting that IL-1α is thermally stable up to this temperature at pH 5.5. The broadened and short peaks at 70°C and the loss of signals at 75°C are indicative of protein denaturation and aggregation due to high temperature. **P1**, **P2** and **P3** are arbitrary chosen example peaks to illustrate the typical temperature response of chemical shifts of methyl signals.

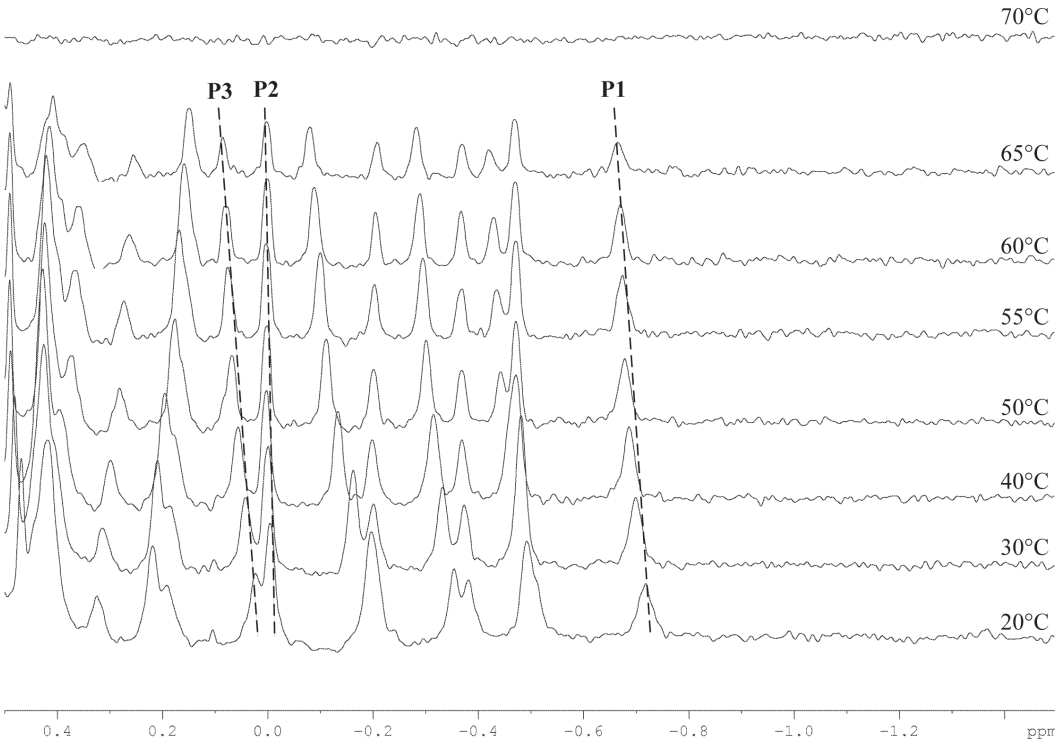

Figure 6.10 IL-1α temperature-dependent ^{1}H-NMR of methyl region at pH 7.5. IL-1α at pH 7.5 at increasing temperatures was analysed by ^{1}H-NMR. Methyl signals (0.5 to -1.5 ppm) at temperatures 20-70°C. Minor changes in methyl signals occur during temperature increments up to 60°C suggesting that IL-1α is thermally stable up to this temperature at pH 7.5. The loss of signals at 75°C is indicative of protein denaturation and aggregation due to high temperature. **P1**, **P2** and **P3** are arbitrary chosen example peaks to illustrate the typical temperature response of chemical shifts of methyl signals.

The signals of a protein undergoing denaturation are broadened and loose height, that is to say, their intensities are decreased. IL-1α methyl signals at 70°C in Figure 6.9-A are a clear example of a denaturation process. Thus, with the purpose of illustrating the thermal denaturation of IL-1α and IL-1β, the intensities at increasing temperatures of six arbitrary chosen signals of both proteins were analysed (Figure 6.13). For this, intensities for each signal were normalised relative to the first point, i.e., intensity at 20°C. The intensities of IL-1α at pH 5.5 remain similar while temperature is increased up to 60°. (Variations of signal intensities observed were due to variations in the baseline). After this temperature, the intensities decreased drastically until at 75°C they drop to the level of the baseline noise. Conversely, at pH 7.5 intensities decreased gradually until they drop to the baseline noise level at 70°C. These observations suggest that IL-1α is resistant to denaturation at very high temperatures and may be more thermally stable at pH 5.5. On the other hand, intensities of IL-1β signals decrease gradually and they drop to the baseline noise level at 65°C at pH 5.5 and 60°C at pH 7.5.

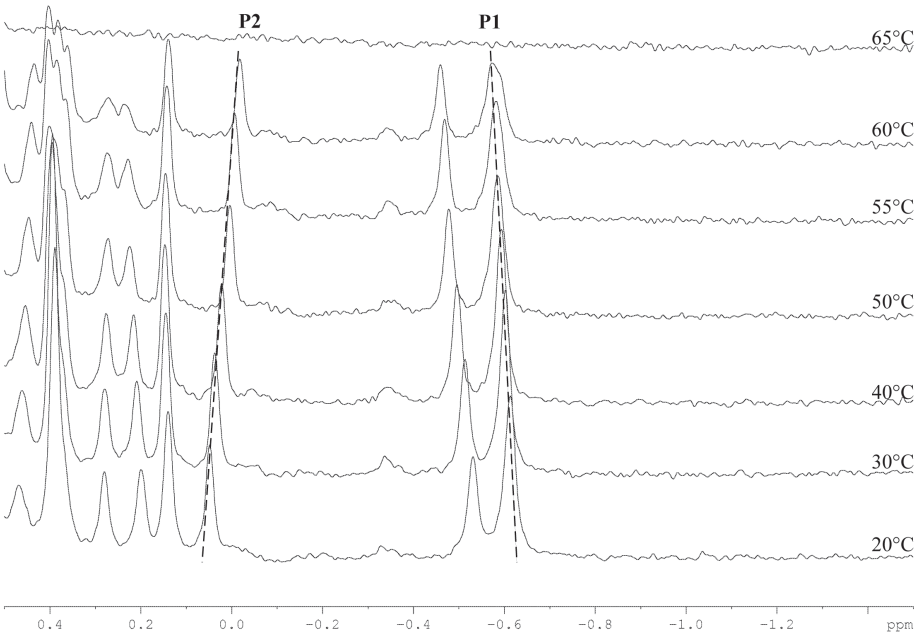

Figure 6.11 IL-1β temperature-dependent ^{1}H-NMR of methyl region at pH 5.5. IL-1β at pH 5.5 at increasing temperatures was analysed by ^{1}H-NMR. Methyl signals (0.5 to -1.5 ppm) at temperatures 20-65°C. Minor changes in methyl signals occur during temperature increments up to 60°C suggesting that IL-1β is thermally stable up to this temperature at pH 5.5. The loss of signals at 65°C is indicative of protein denaturation due to high temperature. **P1** and **P2** are arbitrary chosen example peaks to illustrate the typical temperature response of chemical shifts of methyl signals.

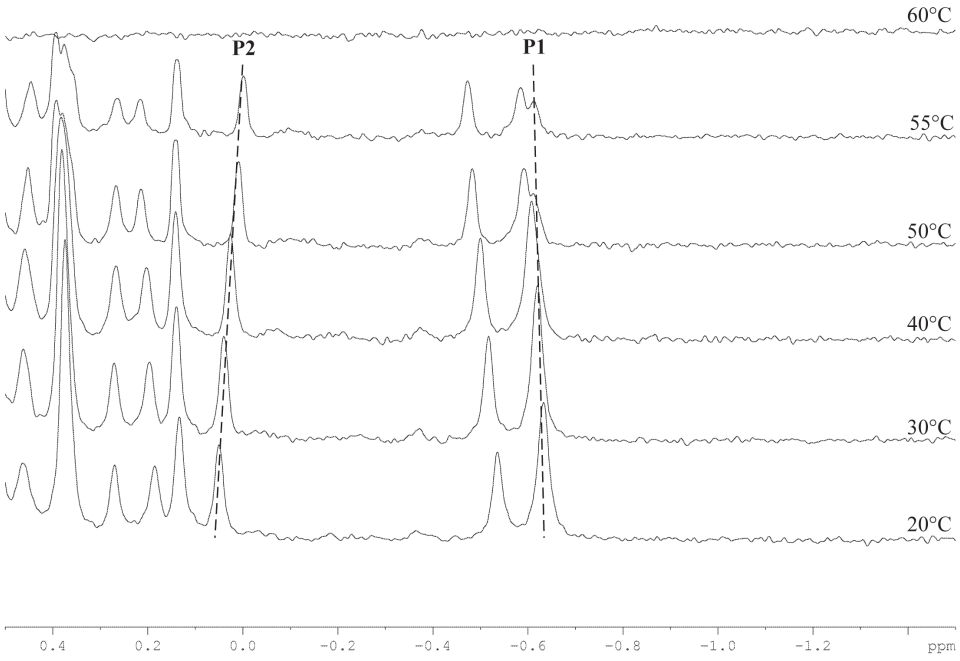

Figure 6.12 IL-1β temperature-dependent ^{1}H-NMR of methyl region at pH 7.5. IL-1β at pH 7.5 at increasing temperatures was analysed by ^{1}H-NMR. Methyl signals (0.5 to -1.5 ppm) at temperatures 20-60°C. Minor changes in methyl signals occur during temperature increments up to 55°C suggesting that IL-1β is thermally stable up to this temperature at pH 7.5. The loss of signals at 60°C is indicative of protein denaturation due to high temperature. **P1** and **P2** are arbitrary chosen example peaks to illustrate the typical temperature response of chemical shifts of methyl signals.

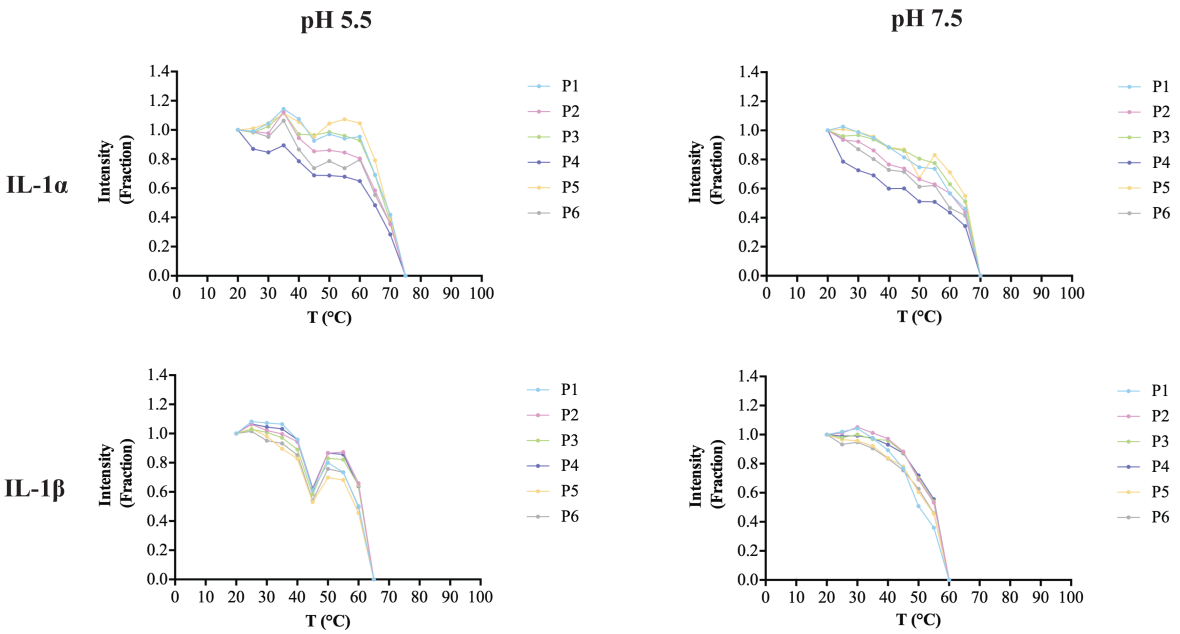

Figure 6.13 Temperature-dependence of intensity of six arbitrary chosen example signals at different pH. Effects of pH on thermal stability of IL-1α and IL-1β were analysed by ^{1}H-NMR. Six example signals were arbitrary chosen and data was normalised by defining the first point intensity (20°C) for each signal as 1. At pH 5.5, IL-1α intensities remain close to one up to 60°C and signals completely disappear at 75°C. At pH 7.5, IL-1α intensities decrease gradually and are totally lost at 70°C. IL-1β intensities at pH 5.5 are close to one up to 55°C, with the signals completely lost at 65°C. At pH 7.5 IL-1β intensities decrease gradually and are lost at 60°C.

In summary, these results suggest that IL-1α is thermally more stable than IL-1β, and that both proteins are more thermally stable at acidic pH than a neutral pH.

6.2 IL-1 bioactivity at pH 6.2

With the aim of determining whether the observed effects of pH on IL-1β biophysical properties were translated to change in bioactivity, bEND5 cells were treated with 50 ng/mL of either IL-1α or IL-1β at pH 6.2. Given that DMEM media used to incubate cells is buffered to pH 7.5 and that it is not possible to maintain a lower pH in this medium, cells were incubated in HEPES-buffered salt solution

(HBSS) at pH 6.2. Nevertheless, after 24 h incubation in HBSS, all cells died. Thus, a time course of IL-1 bioactivity under acidosis conditions was carried out. For this, 50 ng/mL solutions of either IL-1α or IL-1β in DMEM or HBSS pH 6.2 were prepared to treat bEND5 cells for 8 h. Supernatants were recovered and assayed with mouse specific IL-6 ELISA.

IL-1α did not exert bioactivity after 8 h either in DMEM or in HBSS at pH 6.2 (Figure 6.14). Conversely, IL-1β gradually increased IL-6 levels from 2 h, and after 8 h, IL-6 levels were highly increased in both DMEM and HBSS at pH 6.2 (Figure 6.14). Consequently, in order to compare IL-1β bioactivity in DMEM and HBSS, bEND5 cells were treated with 50 ng/mL of IL-1α or IL-1β in DMEM, or HBSS at pH 6.2 or HBSS at pH 7.5, for 8 h. IL-1α did not increase IL-6 levels, neither in DMEM nor HBSS at pH 6.2 or 7.5 (Figure 6.15), nonetheless, as expected, IL-1β did increase IL-6 levels at those conditions. However, even though the level of IL-6 was higher in DMEM compared to HBSS at both pH 6.2 and 7.5, IL-6 levels were comparable between HBSS at pH 6.2 and pH 7.5. Despite the fact that no differences in IL-1β bioactivity at acidic pH were found, these results are not conclusive as HBSS is not a proper environment for bEND5 cells to grow. A time course survival assay with MTT (data not included) showed that a considerable percentage of cells died when incubated in HBSS. As cell death is difficult to control under these conditions, testing IL-1 bioactivity using HBSS is not recommendable, so further experiments need to be done to test the effects of pH on IL-1 bioactivity.

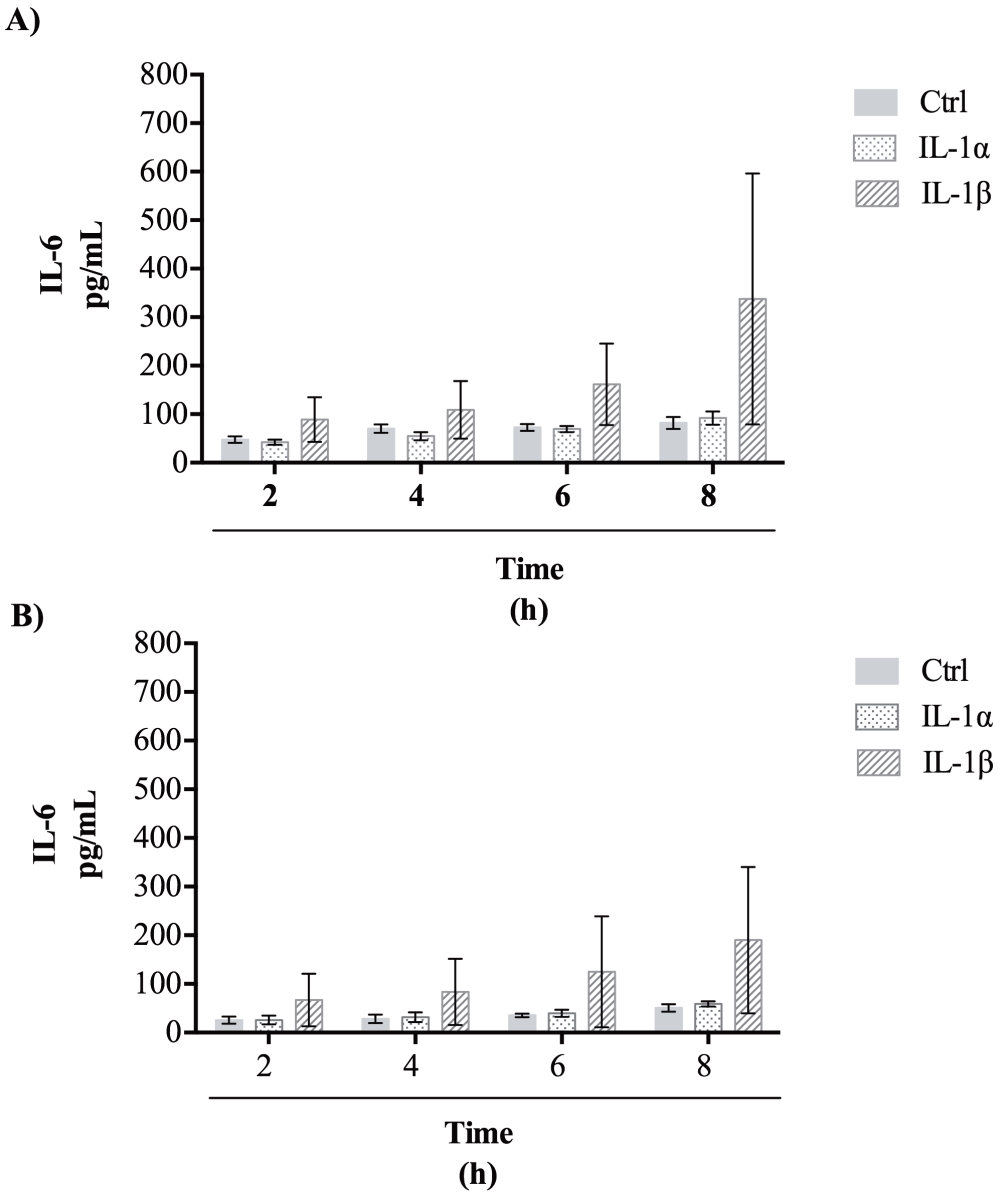

Figure 6.14 Effects of pH on IL-1α and IL-1β bioactivity. bEND5 cells were treated with 50 ng/mL of IL-1α or IL-1β, in DMEM (**A**) or HSSB pH 6.2 (**B**) for 8 h. Cell supernatants were collected every 2 h and assayed with mouse specific IL-6 ELISA. Data are presented as mean and range of two independent experiments.

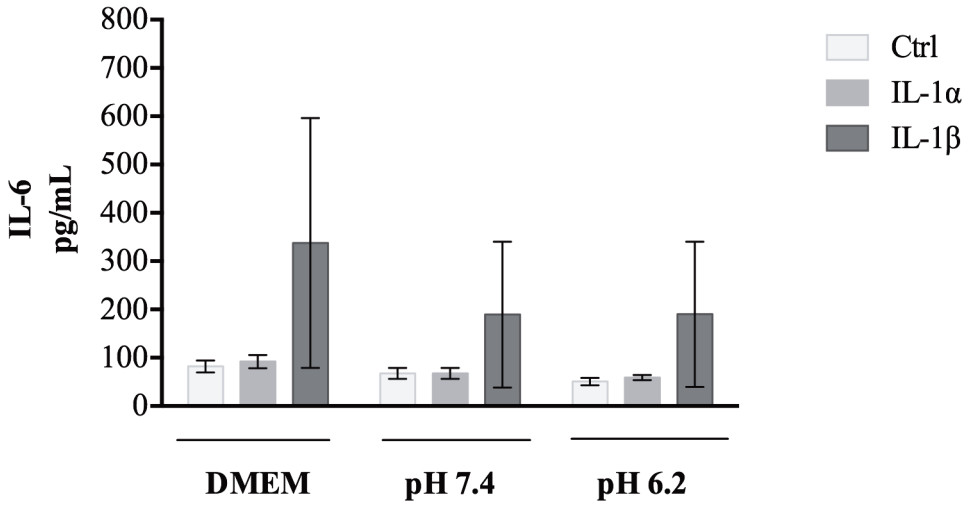

Figure 6.15 Effects of pH on IL-1α and IL-1β bioactivity. bEND5 cells were treated with 50 ng/mL of IL-1α or IL-1β, in DMEM, HBSS pH 6.2 or HBSS pH 7.5 for 8 h. Cell supernatants were collected at 8 h and assayed with mouse specific IL-6 ELISA. Data are presented as mean and range of two independent experiments.

6.3 IL-1 bioactivity at 40°C

As aforementioned, during inflammation conditions tissue temperature is increased. With the purpose of testing temperature effects of IL-1α and IL-1β bioactivity, bEND5 cells were treated with 50 ng/mL of either IL-1α or IL-1β and incubated at 37°C or 40°C. Supernatants were recovered after 24 h of incubation and assayed with mouse specific IL-6 ELISA.

IL-6 levels induced by IL-1α did not differ between 37°C and 40°C (Figure 6.16). However, response elicited by IL-1β was highly potentiated at 40°C, as IL-6 levels were increased by 3 fold at the latter temperature. Interestingly, at lower temperature (37°C) the response elicited by IL-1β was much weaker than the response triggered by IL-1α. The data suggest that the differential biological effects of IL-1α

and IL-1β may be modulated by temperature, however to be conclusive the *n* of experiments needs to be increased, and more experiments have to be conducted.

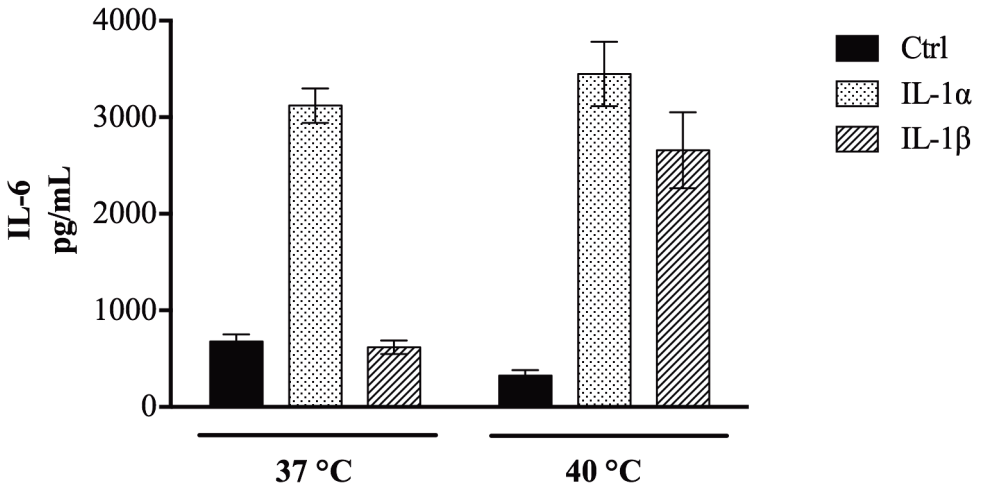

Figure 6.16 Effects of temperature on IL-1α and IL-1β bioactivity. bEND5 cells were treated with 50 ng/mL of IL-1α or IL-1β for 24 h. Cell supernatants were collected and assayed with mouse specific IL-6 ELISA. Data are presented as mean and range of two independent experiments.

Summary

The effects of temperature and pH on IL-1α and IL-1β biophysical properties and bioactivity were tested. The results of the present work suggest that IL-1α is more thermally stable than IL-1β and that IL-1β stability may be affected by pH, whereas IL-1α might be equally stable at acidic or neutral pH. Some differences between results obtained with the different approaches can be observed, but all are consistent in that IL-1α is more resistant to thermal denaturation than IL-1β. CD data analysis was rather hard to interpret, possibly due to the low quality of the CD spectra. It has to be noted that settings chosen for CD in the far UV at increasing temperatures had the purpose of optimising time and being able to analyse the CD spectra at increasing temperatures of the same sample. These resulted in low quality CD spectra that were difficult to

interpret. However, it should also be pointed out that Dichroweb predictions at lower temperatures (when the protein is expected to be folded) were as expected based on the available high-resolution protein structures. Additionally, it was demonstrated that pH had effects on IL-1β but not IL-1α fluorescence. IL-1β intrinsic fluorescence was lower at pH 7.5, suggesting that Trp and Tyr might be less exposed at pH 7.5 than at pH 5.5 or 6.2. These findings were consistent with ^{1}H-NMR analysis, where a shift in methyl signals could be detected. Moreover, IL-1β T_m and T_{agg} were also lower at pH 7.5 than at pH 6.2, implying that at an acidic pH IL-1β may be more stable. Furthermore, sedimentation analysis by AUC, suggested that at pH 6.2, IL-1β is more elongated than at pH 7.5. It is worth mentioning that in all the aforementioned experiments, IL-1α was not affected by pH showing considerable stability in all pH used in this work. Finally, effects of pH on IL-1 bioactivity were also tested. Unfortunately, keeping the cell culture media at pH 6.2 and keeping the cells viable at this pH for the duration of experiments was technically difficult, thus results obtained were inconclusive, and experiments need to be repeated in the future, possibly using different cell lines and different media. Interestingly, we observed an important increase in IL-1β bioactivity at 40°C (compared with its bioactivity at 37°C), suggesting that temperature may be an important factor in regulating IL-1 bioactivity.

7 Discussion

7.1 A comparative study of IL-1α and IL-1β

The main aim of this work was to elucidate the molecular mechanisms responsible of the differential effects observed between IL-1α and IL-1β bioactivity. Since their discovery, studies of their biological activity and signalling confirmed their similarity, as it has been established that both bind to same receptor activating the same signalling pathways. It should be emphasized that the differences observed in IL-1α and IL-1β bioactivity are in terms of "potency" rather than in terms of effects (Henderson and Pettipher, 1988). Nevertheless, it is worth pointing out that despite their high similarity in terms of structure and bioactivity, both proteins exhibit differences at other levels that will be discussed below in this section.

7.1.1 Recombinant expression of IL-1α and IL-1β

As an attempt to discern IL-1α and IL-1β differences at the molecular level, here a comparative study of IL-1α and IL-1β biophysical and bioactivity properties was carried out. For this, the first step was to produce both human mature forms of IL-1α and IL-1β in a heterologous system. Given that *E. coli* has the advantages of being an economic and rapid heterologous expression system, it was our first choice.

IL-1α and IL-1β sequence analysis showed that IL-1α has only one Cys (Table 4.1), whereas IL-1β contains two Cys (Table 4.2). At the time this work was initiated, IL-1β Cys content made us hypothesise the presence of a disulfide bond, thus, Origami cells were initially chosen for IL-1β heterologous expression. Nonetheless, by the time we found out later that these Cys did not form disulfide bonds (Teodorescu et al., 1991) the protocols for IL-1β soluble expression in Origami cells and purification were

already optimised giving a good yield of soluble protein: this satisfactory yield did not justify switching to a different cell line later.

Despite the difficulties faced during the first attempts to transform Origami cells with the pQE-30/IL-1β, expression was rather straightforward and with a high level of soluble expression. Due to genotype of Origami cells, transformation efficiency was low and slow, as it took up to 48 h to obtain colonies. Once the initial transformation problem was overcome, IL-1β was expressed with a high yield in all conditions tested, and the optimum condition for soluble expression was at 37°C and 0.5 mM IPTG. Even though IL-1β yield from 1 L culture was about 50 mg, about half of the totally expressed protein remained insoluble. The possible formation of disulfide bonds between the two Cys of IL-1β, favoured by the oxidising cytoplasm of Origami cells, might be responsible for this incorrect folding of IL-1β, thus, inducing the formation of inclusion bodies. Nevertheless, further characterisation studies of IL-1β purified from the soluble fraction demonstrated that the protein was folded, with the correct molecular size and was bioactive.

On the other hand, IL-1α expression was not as straightforward compared to that of IL-1β. Several *E. coli* strains and conditions were tested and, even though in some of them soluble expression was achieved, i.e. BL21 DE3, purification attempts were unsuccessful. Factors that may affect soluble protein expression in *E. coli* are well characterised and approaches to improve, in principle, heterologous protein expression in this system have been developed in the past decades. Bacterial cytoplasmic environment may not be suitable for correct protein folding (i.e. disulfide bond formation) and post-translational modifications (i.e. glycosylation) of eukaryote proteins (Sorensen and Mortensen, 2005a). However, IL-1α does not require the

formation of disulfide bridges (as it only contains one Cys) and it is unknown whether *N*-acetylglycosylation is required for maintaining its structure. Furthermore, human IL-1α has been previously successfully expressed and purified from *E. coli* (Graves et al., 1990, Kawashima et al., 1992, Rajalingam et al., 2007, Chang et al., 2010). In order to optimise protein expression several aspects must be considered such as, among many others, growth and induction conditions, i.e. cell density, temperature and duration of induction (Donovan et al., 1996, Weickert et al., 1996, Jana and Deb, 2005). Stress situations such as heat shock or high levels of expression may provoke formation of recombinant protein aggregates, also known as inclusion bodies (Sorensen and Mortensen, 2005a, b). Bacteria tend to express proteins with a high rate and when recombinant proteins are expressed in large amounts they tend to misfold and the accumulation of protein folding intermediates favours the formation of inclusion bodies (de Marco et al., 2005, Sorensen and Mortensen, 2005a). This can be overcome by decreasing the temperature of induction of expression or IPTG concentration (Donovan et al., 1996, Jana and Deb, 2005). It has been proposed that the best temperature for correct folding is about 16-20°C, given that at those temperatures the transcription and translation rates decrease, providing enough time for proper protein folding (Jana and Deb, 2005). For an optimal expression of soluble protein, IPTG concentrations in the range of 0.005-1mM have been recommended (Donovan et al., 1996). Here, IL-1α expression at 25°C, and induction of expression with IPTG concentration as low as 0.25 mM were tested, but neither improvement in protein expression nor in protein solubility was achieved. Moreover, the aforementioned publications regarding recombinant human IL-1α recommended induction of expression at 30°C or 37°C. After our numerous expression trials, IL-1α was successfully expressed at 37°C inducing with 1 mM IPTG with an acceptable yield.

During IMAC purification, IL-1α tended to aggregate on the cobalt resin. For this reason, several purification trials were carried out until the best buffer conditions that reduced IL-1α aggregation on the column were found. For instance, addition of 5 mM β-mercaptoethanol and 20 mM imidazole helped to reduce IL-1α aggregation on the column. Increasing culture volumes to 3 L also helped in increasing IL-1α purification yield, and the quantity of highly pure IL-1α obtained from T7 Express *LysY* cells was sufficient for the purposes of this work.

The differences observed during expression and purification attempts of IL-1α and IL-1β, suggest that IL-1β is more stable than IL-1α, as attempts to express it and purify it from an heterologous system were not as problematic as those of IL-1α.

7.1.2 Biophysical and biological characterisation of IL-1α and IL-1β

After successfully purifying IL-1α and IL-1β from *E. coli*, the next objective was to carry out a biophysical characterisation of the recombinant proteins. SEC-MALL analysis confirmed the molecular weight of the purified proteins, as well as their monodispersity and level of purity. After two-step purification, IL-1α as well as IL-1β were monodisperse, as it could be seen by the molar mass trace in Figures 4.10 and 4.11. Only one protein population with a molar mass of 19.25 kDa was detected in IL-1α samples and one with a molar mass of 17.5 kDa for IL-1β. These results mean that IL-1α and IL-1β purified from *E.coli* had a homogenous mass, thus there were not products of degradation or aggregation. These findings were confirmed by the ^{1}H-NMR spectra of IL-1α and IL-1β, which, besides confirming proteins were well folded, also suggested that both proteins were monomeric.

In order to confirm that heterologous IL-1α and IL-1β had the β-sheet structure that characterise them, a CD analysis in the far UV region was carried out. At the

structural level, IL-1α and IL-1β have been shown to be similar, both consisting of β-sheets that form a β-barrel (Priestle et al., 1988, Graves et al., 1990). It has also been suggested that the CD spectra of IL-1α is similar to that of IL-1β and IL-1ra (Latypov et al., 2007). An interesting finding of this work is that, in spite of having β-sheet structure, CD spectra in the far UV region of IL-α and IL-1β are different (Figures 4.12 and 4.13). Both IL-1α and IL-1β showed a negative band at about 215 nm, which is characteristic of β-sheet structures. However, IL-1α had strong signal at 230 nm that resulted in a positive peak that is not present in IL-1β CD spectra. It has been shown that the interactions among side chains of Trp and other residues with aromatic side chains such as Tyr or Phe, are responsible of such signals in the 220-230 region. IL-1α content of such residues is rather high, as it has two Trp, seven Tyr and nine Phe. In contrast, IL-1β only has one Trp and four Tyr, and similarly to IL-1α, nine Phe. Furthermore, Trp, Tyr and Phe are in close proximity within IL-1α (Figure 4.14-A), whereas in IL-1β they are not as close as in IL-1α (Figure 4.14-B). This findings are of interest, as the biochemical properties of amino acids confer to proteins their biochemical and biophysical characteristics. Thus, these results on IL-1α and IL-1β characterisation suggest that their biophysical characteristics might be different. For example, protein-protein interactions depend, among others, on the hydrophobicity of the proteins (Jones and Thornton, 1996). Protein hydrophobicity is conferred by the level and position of hydrophobic residues. Amino acids such as Trp, Phe and Tyr are hydrophobic due to their aromatic side chains. The proximity of the side chains of the aforementioned amino acids in IL-1α, but not in IL-1β, suggests that IL-1α may have a more hydrophobic core. Moreover, Trp 109 of IL-1α has been identified to be critical for binding to IL-1RI (Labriola-Tompkins et al., 1993). These differences in

hydrophobicity of IL-1α and IL-1β, could affect their affinity to IL-1RI, and thus, the potency of their biological effects.

7.1.3 Differential effects of IL-1α and IL-1β on different cell types

IL-1α and IL-1β are involved in numerous inflammatory, metabolic, physiologic, haematopoietic and immunologic events (Dinarello, 1991). It is generally recognised that IL-1β is not constitutively expressed in healthy cells, with the exception of neurons that constitutively express IL-1β (Torres et al., 2011). Conversely, pro-IL-1α is constitutively present in a wide range of healthy cells throughout the body, such as epidermal cells, epithelial cells of mucosal membranes, platelets, cells of organs such as liver, lung and kidney and endothelial cells (Hauser et al., 1986, Thornton et al., 2010, Dinarello et al., 2012, Kasza, 2013). Furthermore, most cells express high levels of IL-1 receptors (Braddock and Quinn, 2004) hence almost every tissue can respond to IL-1 stimulation (Dinarello, 1991). It has been observed that following injury or infection IL-1β (mRNA and protein) is the predominant form in human pathological fluids (Dinarello et al., 1986). In addition, IL-1β mRNA levels were shown to be higher and more stable than those of IL-1α in human peripherial blood mononuclear cells (PBMC) stimulated with LPS or TNF, as well as in the monocytic cell line U937, suggesting that IL-1β rate of transcription is greater than IL-1α (Demczuk et al., 1988, Turner et al., 1989). Conversely, IL-1α mRNA levels were shown to be higher than IL-1β in T cells stimulated with OKT3 antibody (Ab) (Acres et al., 1987). OKT3 Ab (Janssen-Cilag) is an anti-CD3 used as immunosuppressant, as by blocking CD3 it inhibits T cell activation. Based on these observations, it has been suggested that IL-1α and IL-1β genes are regulated independently and in a tissue specific manner. Furthermore, it has been demonstrated that IL-1β mRNA levels, but

not IL-1α, are modulated by cAMP in murine peritoneal macrophages (Ohmori et al., 1990)

The bioactivity of the recombinant mature forms of human IL-1α and IL-1β produced in this work was tested in two different cell systems: an *in vitro* model of the blood-brain barrier (BBB), the mouse endothelial cell line bEND5, and primary cultures of mouse neurons. It should be pointed out that despite being human, recombinant IL-1α and IL-1β were expected to exert their effects in these mouse cells, as it has been demonstrated that human IL-1 is able to bind mouse IL-1RI (Greenfeder et al., 1995b). Moreover, human IL-1RI has 63% identity with its homologue in mouse, whereas human and mouse IL-1α and IL-1β have 60% and 67% identity respectively (Gray et al., 1986, Dinarello, 1991, Liu et al., 1996). Furthermore, it is well accepted that brain endothelial cells as well as neurons express IL-1RI (Ban et al., 1991, Ban et al., 1993, Parnet et al., 1994, Liu et al., 1996, Banks, 1999). Additionally, bEND5 cells, a commercially available cell line derived from brain endothelial cells of Balb/c mice and immortalized with the murine polyoma virus middle T antigen, have been shown to react to pro-inflammatory cytokines by expressing proteins such as CAM1 and VCAM-1 so it is considered to be a reliable BBB model for the study of brain hypoxia exposure (Yang et al., 2007).

IL-1α was shown to be more potent than IL-1β in bEND5 cells as it was able to induce IL-6 synthesis even with the lowest concentration tested (0.5 ng/mL) (Figure 4.17). Interestingly, there was not significant difference between the different concentrations used to treat bEND5 cells (0.5-500 ng/mL), suggesting that IL-1α had a potent effect on this system. Conversely, IL-1β effects on IL-6 synthesis were seen at a concentration of 100 ng/mL, and the levels of IL-6 induced by IL-1β were about two-fold lower than those observed with IL-1α at the same concentration (Figure 4.17). It

has been previously reported that IL-1β potency to stimulate bEND5 cells is low (Tacheny et al., 2002), but there has been not report of IL-1α activity on this cell type. Similarly as in bEND5 cells, IL-1α was more potent at inducing IL-6 than IL-1β in neuron culture. These results are in contrast with previous observations that IL-1α had no effects on IL-6 synthesis in primary neurons (Tsakiri et al., 2008) but supports the hypothesis that IL-1β is more potent when acting centrally than systemically.

It is worth discussing the time course experiments carried out in our study (Figure 6.14). Given that bEND5 cells were not viable in HBSS used to study pH effects on IL-1 bioactivity, time course experiments with 50 ng/mL of IL-1α or IL-1β were carried out with the purpose of finding the optimal time for IL-1 effects on IL-6 synthesis in bEND5 cells incubated in HBSS at pH 6.2. As a control, a set of bEND5 cultures in DMEM was used, and results obtained with this control will be used to discus IL-1 bioactivity in this section. Surprisingly, IL-1β, but not IL-1α induced IL-6 significantly after 6 h incubation, implying that IL-1β was more potent than IL-1α at inducing IL-6 in bEND5 cells. Further time course experiments carried out by a Master student (Olivera Rajkovic, MSc student, University of Manchester, 2013), showed that the optimal time to see effects of IL-1α and IL-1β on IL-6 synthesis in bEND5 cells was 24 h. IL-6 could be detected at 16 h of induction with IL-1α, in contrast to IL-1β which effect on IL-6 induction could be detected from 6 h. In this experiment IL-1α was also shown to be more potent than IL-1β, as IL-6 levels after 16 h treatment were higher with IL-1α than with IL-1β. These findings are of interest, as IL-1α and IL-1β effects on IL-6 production seem to be not only concentration-dependent, but also time-dependent. It has been observed that after stimulating cells present in whole blood (WB) and PBMC with LPS or phytohemagglutinin (PHA), IL-6 protein levels were increased during the first 4-8 h when they stabilized into a plateau (DeForge and

Remick, 1991, De Groote et al., 1992), Accordingly, our results showed that IL-1β but not IL-1α was capable of inducing IL-6 expression in brain endothelial cells as fast as LPS or PHA induced it in PBMC and WB. The time-course of action seems to be another difference between IL-1α and IL-1β biology. For example, after oral infection with *Yersinia enterocolitica 08,* IL-1β mRNA levels increased more rapidly than those of IL-1α (Rausch et al., 1994). Moreover, following a lethal infection with the neurotropic JHM strain of mouse hepatitis virus, IL-1β mRNA levels were shown to increase from day 3 after infection in mouse brains, in contrast to IL-1α and IL-6 levels which were delayed until day 5 (Parra et al., 1997). Additionally, in stimulated synoviocytes from a mouse arthritic model overexpressing IL-1α, the mature IL-1α could be detected after 24 h and reached a plateau between 72-96 h, whereas the pro-IL-1α bound to cells membrane reached a plateau by 24 h after stimulation and remained stable for 96 h (Niki et al., 2004). These results suggest that IL-1α processing and activation *in vivo* is also belated process. On the other hand, as it was discussed in Chapter 1, in contrast to pro-IL-1β, pro-IL-1α is biological active and is capable of exerting its effects through IL-1RI (Mosley et al., 1987). Pro-IL-1α is soluble in the cytosol and following a stress stimulus can either move to the cell surface membrane to activate adjacent cells (Kurt-Jones et al., 1985, Kaplanski et al., 1994) or be transported to the nucleus (Luheshi et al., 2009a, Luheshi et al., 2009c) where it activates transcriptional machinery through an IL-1R-independent activation of NFκB and AP-1 (Kimura et al., 1998, Werman et al., 2004). Pro-IL-1α has also been suggested to be released from the cells only after cell death as IL-1α is only found in the circulation or body fluids during severe disease conditions and it has been suggested that it is cleaved by calpain or other proteases after it is released from necrotic cells (Dinarello, 1996, Dinarello et al., 2012). Conversely, it is known that IL-1β is released immediately after

cleavage by Caspase-1, which in turn is activated when it is recruited to the inflammasome (Brough et al., 2011). The inflammasome is a molecular platform composed by adaptor molecules and cytosolic pattern recognition receptor of the NOD family (NLR family) (Luheshi et al., 2012). Nonetheless, there is to date no real consensus on the mechanism of IL-1 secretion, and it is unknown whether multiple tissue-specific secretion mechanisms exist (Brough et al., 2011). It is interesting to note from all these studies the differential timing of IL-1α and IL-1β biology as it appears that IL-1β is transcribed, processed, released and exerts its activity more rapidly than IL-1α. However, given that pro-IL-1α is constitutively expressed in many healthy cells it has been shown to act more rapidly after tissue injury, i.e. during ischemia where it is released from necrotic cells, without requiring time for synthesis (Chen et al., 2007, Rider et al., 2011). The observations that pro-IL-1α is active, constitutively expressed in many healthy cells and it is auto-regulated could explain the higher level of potency of IL-1α compared to IL-1β. Nonetheless, it would be interesting to investigate the affinity of pro-IL-1α to IL-1RI as well as the kinetics of pro-IL-1α actions. Furthermore, as yet the ternary complex of IL-1RI/IL1α/IL-1RAcP is not available, nor those of the binary complex with IL-1RI or IL-1RII. These structures would help understanding differences IL-1α and IL-1β bioactivity.

Another interesting observation is that, despite the fact that IL-1β has been shown to exert a faster effect than IL-1α on IL-6 synthesis in bEND5 cells, after 24 h incubation, IL-6 levels induced by IL-1α were about 2-fold higher than those induced by IL-1β, suggesting different regulation mechanisms for IL-1α and IL-1β. It is well accepted that IL-1RII regulates IL-1 bioactivity given its ability to bind IL-1α and IL-1β without activating signalling pathways (Sims, 2002). IL-1RII has been shown to

bind to IL-1β with higher affinity than to IL-1α, as the dissociation rate of the IL-1RII/IL-1β complex is considerably slower (2 h) than that of the IL-1RII/IL-1α complex (3 min) (Arend et al., 1994). These differences on the dissociation rate might be responsible of the differential effects on IL-6 induction by IL-1α and IL-1β at 8 h, 16 h and 24 h.

As aforementioned, our findings of IL-1α bioactivity in primary neurons, contradicted the observations made by Tsakiri et al, as we found that IL-1α bioactivity in this system is comparable to that of IL-1β, whereas they did not observed any effect of IL-1α on IL-6 induction in the same system. The main difference between our and their experimental design is the time of incubation of neurons with IL-1α and IL-1β: we incubated primary neurons with IL-1α and IL-1β for 24 h, whereas they did it for 7 h. Thus, differences observed in IL-1α bioactivity in neurons by Tsakiri et al and us, might be due to the time of incubation with IL-1α, rather than because of lack of activity. Nevertheless, time course experiments on IL-1 bioactivity in neurons should be carried out in future work, with the purpose of confirming this hypothesis. Yet, the differential effects that IL-1α and IL-1β bioactivity have on the two cell systems used in this work cannot be explained in this way. That is to say, the observation that IL-1α was shown to be more potent that IL-1β at inducing IL-6 synthesis in bEND5 cells, but not in primary neurons, where IL-6 synthesis induced by IL-1α and IL-1β was shown to be similar. This suggests that the mechanisms involved in IL-1 bioactivity and/or down-regulation may differ between the two systems. It has been shown that both IL-1RI and IL-1RII are expressed in many cell types including neurons (Mcmahan et al., 1991a), thus, if IL-1RII is involved in the differential effects observed in IL-1 bioactivity in bEND5 cells, it is not the case in neurons. Previously, it has been

proposed the existence of alternative signalling pathways triggered by IL-1 in neurons (Tsakiri et al., 2008), and this hypothesis is strongly supported by the results of the present work. Nevertheless, a broad study needs to be done in this matter.

In conclusion, the findings done in this work confirm differences in bioactivity of IL-1α and IL-1β. This was demonstrated with the observation that response elicited by IL-1α in IL-6 levels in endothelial cells was higher that that of IL-1β. In contrast, both IL-1α and IL-1β were shown to be equally bioactive in neurons. These findings support the hypothesis that IL-1α and IL-1β trigger alternative signalling pathways in different cell systems. Additionally, IL-1α had effect on IL-6 bioactivity with low concentrations in both neurons and endothelial cells, whereas concentrations needed to induce IL-6 synthesis by IL-1β differ from one system to the other. Neurons required less IL-1β concentration to express IL-6 than endothelial cells, suggesting that the first system is more sensitive to IL-1β action while both, endothelial and neurons seem to be equally sensitive to IL-1α. Finally, time course experiments in endothelial cells also shown differences in IL-1α and IL-1β bioactivity, suggesting that time plays a key role in the differential effects of IL-1α and IL-1β biology. Albeit IL-1β was shown to elicit an earlier induction on IL-16 synthesis, as levels of this last cytokine were detected from 6 h, in contrast to IL-1α which effects were seen until 16 h, levels of IL-6 induced by IL-1α were about 2-fold higher than those induced by IL-1β.

For future work it would be interesting to look at IL-1 bioactivity in IL-1RII/KO neurons and endothelial cells to elucidate the participation of this decoy receptor in IL-1α and IL-1β differences in potency at inducing IL-6. It would be interesting as well to observe pro-IL-1α expression following induction with IL-1α in order to elucidate if induction of this pro-form would also account for IL-1α potent

effects. A time course experiment of IL-1α and IL-1β bioactivity could also bring more information about the mechanisms involved in IL-1 bioactivity in neurons. In addition, measuring expression levels with respect to time and IL-1 concentration of other molecules induced by IL-1 would bring insights into the differential molecular mechanisms involved in IL-1 bioactivity in different cell systems.

7.2 Recombinant expression of IL-1RI and IL-1RAcP

It is well established that IL-1α and IL-1β are capable of binding to two different receptors: IL-1RI and IL-1RII, and that their biological activity is exerted exclusively through binding to IL-1RI but not IL-1RII (Sims et al., 1993, Slack et al., 1993, Dinarello, 1998). IL-1RI expression is broad, as it is present in a broad range of cell types (Table 1.1). In order to trigger signalling pathways, IL-1RAcP needs to be recruited to the IL-1RI/IL-1 complex (Huang et al., 1997, Korherr et al., 1997). To date, it is widely accepted that IL-1α and IL-1β exert their bioactivity only through IL-1RI, given that, besides IL-1RII, it is not known any other receptor capable of binding to IL-1α and/or IL-1β with a consequent activation of signalling cascades. Thus, IL-1RI along with IL-1RAcP are key players in IL-1α and IL-1β bioactivity. With the purpose of studying the molecular mechanism responsible of the differences observed on IL-1α and IL-1β bioactivity, one of our main objectives was to express and purify IL-1RI and IL-1RAcP for further characterisation of the complexes formed with IL-1RI, IL-1RAcP and IL-1α or IL-1β (at the time when this study was initiated, none of the experimental ternary complex structures have been described). Consequently, a large portion of this study was dedicated to expression and purification of IL-1RI and IL-1RAcP in two different heterologous expression systems.

7.2.1 Heterologous expression of IL-1RI and IL-1RAcP in *E. coli*

The soluble portions of both IL-1RI and IL-1RAcP consist of three Ig-like domains. Each Ig-like domain consists of β-sheets held together by disulfide bonds (Sims et al., 1988), and the 10 Cys in both IL-1RI and IL-1RAcP are paired (Thomas et al., 2012). For this reason, *E. coli* strains chosen for IL-1RI and IL-1RAcP expression had a phenotype that allowed disulfide bond formation. IL-1RAcP total expression in most of the strains tried (Table 5.5) was high, but the soluble expression was absolutely null. IL-1RI total expression was not as high as that of IL-1RAcP, but the soluble expression was ineffective as well. As previously discussed in section 7.1.1, there are many factors that may affect the solubility of proteins expressed in heterologous systems. As with IL-1α, several approaches were carried out to improve receptors soluble expression, although without success. The lowest temperature tried for IL-1RI and IL-1RAcP expression was 16°C (induced overnight) and the lowest IPTG concentration was 0.1 mM. Remarkably, with these conditions IL-1RAcP expression was still high, but no traces of soluble protein were found. As for IL-1RI lowering temperature and IPTG reduced total protein expression without improving solubility, suggesting that the optimal temperature for total expression of IL-1RI is above 30°C. Solubilisation and refolding attempts were also carried out without success. The only previous work that produced IL-1RI in bacteria (Vigers et al., 1997) purified it from inclusion bodies and subsequently refolded it. However, this publication does not give any detail of the protocol and referred to a manuscript in preparation that, to our knowledge has not yet been published. Furthermore, Vigers and colleagues group later published a second Crystallographic structure of IL-1RI (Vigers et al., 2000) and for this work they produced IL-1RI in insect cells. As bacteria is considered the workhorse system for heterologous protein production (Glick and Pasternak, 2003) given that is rapid and economical (Donovan et al., 1996, Glick and Pasternak, 2003, Jana and Deb,

2005) we suspected that the protocol they used for making IL-1RI may not be reproducible. Moreover, *in vitro* refolding is time consuming and difficult and the yield of soluble protein is low (de Marco et al., 2005) and it is even more laborious if proteins require disulfide bonds to be properly folded, as a redox system is need. Nevertheless, here a protocol involving sequential dialysis in a redox system and decreasing concentrations of urea was designed and tried to refold IL-1RI and IL-1RAcP, but as soon as urea was eliminated from the buffer proteins precipitated and no trace of soluble protein could be found. The presence of several *N*-glycosylation sites in both proteins made us believe that this post-translational modification may be relevant for both receptors solubility. There is a controversy as to whether *N*-glycosylation is of importance for protein structure, stability, function or none of these. It has been demonstrated to be important for some proteins structure, but not for others, and for a large number of proteins *N*-glycosylation has been demonstrated to play a key role in protein-protein binding (Drickamer and Taylor, 1998). Subsequent crystallographic studies showed four glycosylated Asn on IL-1RAcP and four in IL-1RI. None of these glycosylation sites in IL-1RAcP were involved in receptor-ligand or receptor-receptor interactions (Wang et al., 2010, Thomas et al., 2012). On the other hand, *N*-glycosylation of IL-1RI Asn216 was found to be involved in receptor-receptor interactions as it made contact with a Pro and Tyr on IL-1RAcP (Thomas et al., 2012). This publication confirmed the importance of *N*-glycosylation in IL-1RI, as IL-1RI-IL-1RAcP interaction is required for IL-1 signal transduction (Wesche et al., 1997b, Wesche et al., 1998)

In summary, based on the unsuccessful soluble expression and purification of IL-1RI and IL-1RAcP in *E. coli*, and subsequently published structural studies of IL-1

receptor complexes, it was decided to carry out expression of both receptors in an eukaryote system that allowed protein *N*-glycosylation.

7.2.2 Heterologous expression of IL-1RI and IL-1RAcP

In order to produce correctly folded IL-1RI and IL-1RAcP, we decided to use the yeast *K. lactis*. *K. lactis* has been claimed to have many advantages over other yeast systems. For instance, *K. lactis* cultures are easy to scale-up as large-scale protein production does not require explosion-proof fermentation, expression can be induced with a carbon source such as galactose, and recombinant protein expression can be done with a low cost. In addition, heterologous proteins can be secreted to the growth media and vectors that allow heterologous protein secretion are commercially available (Gellissen et al., 1992, van Ooyen et al., 2006). Recombinant protein secretion in principle has the advantage of facilitating protein purification as fewer contaminants are found in the medium, resulting in production of proteins that are significantly pure (van Ooyen et al., 2006, New-England-Biolabs, 2007, Sugiki et al., 2008). Despite been a relatively new system for recombinant protein production, several proteins have been produced in *K.lactis*, including, among others, IL-1β (Fleer et al., 1991, Blondeau et al., 1994a), the sweet-tasting protein brazzein (Jo et al., 2013), the *Mytilus californianus* (California mussel) foot protein three (Mcfp-3) (Platko et al., 2008), the mouse α-amylase (Tokunaga et al., 1997) and the *Arxula adeninivorans* (dimorphic yeast) glucoamylase (Merico et al., 2004). Additionally, *K. lactis* has also been proposed as a low-cost protein expression system for ^{15}N-labeled proteins for further NMR studies (Sugiki et al., 2008). Thus, as NMR studies of the IL-1 complexes were among our main objectives, expression and purification trials of IL-1RI and IL-1RAcP were carried out.

Despite all the advantages of using *K. lactis* as a recombinant system described in the literature, IL-1RI and IL-1RAcP expression and purification was challenging, and characterisation of proteins produced in the system was rather problematic. Expression of IL-1RI could not been achieved, and of all the IL-1RAcP constructs used in this study, only two were found to be expressed. For expression in *K. lactis* IL-1RI and IL-1RAcP were cloned into the pKLAC2 vector. pKLAC2 is an integrative vector that is linearized prior to introducing it into yeast cells. Linearization of the vector produces an expression cassette that is then integrated into the *K. lactis* genome (New-England-Biolabs, 2007). It has been noted that despite providing higher stability than episomal vectors, integrative vectors are usually maintained at lower copy numbers (van Ooyen et al., 2006). This observation could account for the low expression achieved for both IL-1RI and IL-1RAcP. Additionally, the lack of protein bands in SDS-PAGE analysis of pre-induction samples drew attention, as there was very little protein in these samples. Nonetheless, when comparing SDS-PAGE analysis of other members of the lab working with the same system but different constructs, we noticed that this is reproducible. Moreover, Platko and colleagues (2013) showed the SDS-PAGE analysis of Mcfp-3 expression and the protein pattern of pre-induction sample was highly similar to ours, and so was the SDS-PAGE analysis showing maltose binding protein expression in *K. lactis* of the *K. lactis* kit user's manual ((New-England-Biolabs, 2007). The low quantity of non-induced samples is reasoning, as MS analysis of *K. lactis* medium found 81 secreted proteins out of 178 that *in sillico* analysis of *K. lactis* proteome predicted to be secreted via the general secretory pathway (Swaim et al., 2008). Interestingly, the strain Swaim and co-workers used for this analysis was GG799, the same we used for this work. Furthermore, an additional attempt to improve expression in *K. lactis* was carried out along this work by the Erasmus student Claire Gabe (Gabe C, 2012, unpublished data, University of

Manchester). For this, two different media, Yeast-Peptone (YP) media (rich media) and minimal media (MM) were used to express the IL-1RAcP-His protein construct. It has previously been suggested that pH may affect *K. lactis* growth and hence, protein expression (Blondeau et al., 1994b, Merico et al., 2004), and that the optimal pH for *K. lactis* growth was 6 in either rich media (Blondeau et al., 1994b) or MM (Merico et al., 2004). In contrast, Gabe found that the optimal pH to grow *K. lactis* GG799 in MM was 7, as OD_{600} values at pH 7 where greater that those at pH 6.5 or 6. The differences in the observations made by Merico and colleagues and Gabe may be due to the strains used in each work, Gabe used *K. lactis* GG799 and Merico used the strain JA6. Furthermore, as a control, Gabe monitored the pH in YPGal media and observed that after 24 h it was gradually increased from 7 until it reached 8 at 50 h, when it was stabilised (Gabe C, 2012, unpublished data, University of Manchester). In a later publication it was found that the optimal pH for protein expression in YPGal was 5.5 (Jo et al., 2013). It is noteworthy that Jo and colleagues used the strain GG799, the vector pKLAC2 and YPGal media, that is, the same strain, vector and media we used. Given that we expressed IL-1RAcP and IL-1RI in YP media for 48 h, it is very likely that pH could account for the low expression of both receptors.

Furthermore, given the high level of glycosylation of IL-1RAcP, expression estimation was difficult, as N-linked glycosylation has been shown to interfere with Coomassie blue-protein binding (Fountoulakis et al., 1992). Furthermore, even though it was claimed that secretion of the protein to the media would facilitate purification, we found that it was rather difficult. *K. lactis* cultures were grown in rich media (YP) that is rather thick and dark and we found it to interfere with chromatography-based purification methods. Thus, before attempting purification, a buffer-exchange was needed in order to get rid of any component of the YP media composition that could

interfere with purification. This process was time-consuming as to perform the buffer exchange media was concentrated 10 times, for further being submitted to a series of dilution-concentration process. Moreover, despite the buffer-exchange, A_{280} of protein samples remained high, suggesting that protein concentration was high. Nevertheless, Coomassie-blue stained gel of IL-1RAcP samples showed faint bands and an alternative staining method had to be used. The glycosylated protein stain ProQ Emerald was used and strong bands corresponding to IL-1RAcP were seen on Bis-Tris gels, suggesting that the protein was highly glycosylated.

With the purpose of confirming IL-1RAcP identity, samples at each state, from expression to purification were analysed by LC-MS/MS. Protein identification by mass spectrometry (MS) offers advantages such as specificity, sensitivity and resolving power (Yoon et al., 2012). MS is a powerful tool for protein analysis that allows measuring the mass of molecules with very high sensitivity (Mann et al., 2001) without the need of antibodies, commercial availability of which to some proteins can be very limited (Boehmer et al., 2010). There are wide range of MS methods used in numerous applications, such as LC-MS/MS. This method allows identification from complex mixtures of large numbers of proteins all at once, as it combines efficient separations of biological materials and sensitive identification of individual proteins (Mann et al., 2001). In this manner, a high level of IL-1RAcP peptides, corresponding to ~ 45% of the sequence, were found in YPGal media after 48 h expression. However, the number of peptides identified in purification samples decreased at each purification step. Moreover, SEC-MALLS analysis of IL-1RAcP purified by IEX showed that this sample contained a high proportion of low molecular weight peptides (2-3 kDa). Degradation by endogenous proteases of recombinant proteins in yeast is a well-known factor that affects the yield and in *K. lactis* at least five secretory pathway aspartyl-

proteases have been identified (Ganatra et al., 2011). IL-1RAcP contains 18 Asp (Table 5.1), thus it is very likely that the low molecular weight peptides identified by SEC-MALLS were products of IL-1RAcP degradation by these proteases. In addition, recombinant protein secretion in *K. lactis* is achieved with the presence of a signal sequence up-stream the cloning site on pKLAC2 vector called α-mating factor domain (α-MF). Once the α-MF drives the recombinant protein to the secretory pathway, it is cleaved by the Kex protease at Lys-Arg or Arg-Arg. An Arg-Arg site was found within IL-1RAcP sequence near the C-terminal, and the resulting peptide was predicted to have a molecular weight of 3 kDa. As the hexahistidine tag on the IL-1RAcP-His construct was added at the C-terminal, it was also cleaved preventing the IL-1RAcP construct to be purified by IMAC.

In summary, given the complexity of IL-1RI and IL-1RAcP, that is to say, their high content of disulfide bonds and N-glycosylation sites, IL-1RI and IL-1RAcP recombinant expression was challenging. *E.coli* was shown to be an unsuitable system for the expression of these proteins. Furthermore, expression and purification from *K. lactis* was extremely problematic. IL-1RAcP was susceptible to degradation, likely by the Kex protease as well as by aspartyl-proteases. A site directed mutagenesis of the Kex cleavage site within IL-1RAcP, could help avoid degradation by this protease. In addition, protease-deficient *K. lactis* strains are commercially available and later were purchased by our lab. Transformations were carried out, but there was not enough time to continue with expression trials. Moreover, expression seemed to be also affected by the pH of the media, thus, further expression trials controlling pH in YP media should be done.

It is noteworthy that IL-1RAcP was discovered in the earlier nineties and its structure took almost 20 years to be solved despite its general importance, suggesting

the inherent difficulties obtaining this protein in large amounts. The recombinant systems used by the authors to express IL-1RAcP and IL-1RI were Hi5 insect cells (Wang et al., 2010) and the mammalian cell line HEK293 GnTI$^-$ (Thomas et al., 2012), suggesting that posttranslational modifications are of importance for IL-1RAcP correct folding and structure stability. As for IL-1RI, expression was low in *E. coli* and null in *K. lactis*, thus, vectors with stronger promoters or *K. lactis* episomal vectors should be tried.

7.3 Effects of temperature and pH on IL-1 stability and bioactivity

The main aim of the present work was to elucidate the molecular mechanisms responsible of the observed differential effects of IL-1α and IL-1β. It was previously suggested that the effectiveness of IL-1α and IL-1β in recruiting IL-1RAcP to the receptor might be involved in this observation; thus, our first aim was to carry out structural studies of the ternary complexes of IL-1α and IL-1β. Nevertheless, as it was discussed in Section 7.2, given the complexity of receptors structure, recombinant expression and purification turned out highly problematic. Moreover, the crystal structure of the ternary complex formed by IL-1β with receptors was published in 2012 (Thomas et al., 2012), when our study was under way.

When they were first discovered, IL-1α and IL-1β were known together as "pyrogenic factor" due to their ability to induce fever. The fact that such pyrogenic factor were actually two different proteins was observed when they where isolated for the first time based on their *pI* (March et al., 1985). It has been established that temperature and pH are key factors for the maintenance of the structure and, thus, the stability of most proteins, hence, protein functional properties can be affected by changes in pH and temperature (Berisio et al., 2002). As a matter of fact, many proteins have been shown to be temperature and/or pH-regulated (Carroll et al., 1999).

Moreover, it has been shown that under inflammatory conditions there can be a systemic or local drop of pH and an increase in tissue temperature (Nemoto and Frinak, 1981, Lardner, 2001, Arnett, 2010). It is well accepted that an acid-base equilibrium is important in the maintenance of cellular and physiological homeostasis, as many cellular responses tend to be dampened at low pH (Lardner, 2001). As it was previously discussed in Chapter 1, acidosis has been observed in a number of diseases where IL-1 has been shown to be involved, and following inflammation process the tissue pH has been found to drop up to 5.2 (i.e. in the lower airway of patients with asthma) (Hunt et al., 2000). Moreover, following ischemia, brain pH has been observed to drop to 6.2 (Nemoto and Frinak, 1981). Based on these observations, we proposed that the differences observed in IL-1α and IL-1β bioactivity may be regulated by temperature and pH. Thus, with the aim of investigating the effects of pH on IL-1α and IL-1β thermal stability a biophysical and bioactivity analysis of IL-1α and IL-1β at physiological pH (7.5) and two different acidic pH (5.5 and 6.2) was carried out. As aforementioned, the physical stability of proteins can be compromised by factors such as pH and temperature. The thermal stability of proteins refers to their capacity to resist irreversible changes in their structure at high temperatures (Vogt et al., 1997, Bischof and He, 2005, Frokjaer and Otzen, 2005). The most drastic and important structural change of a protein during its loss of stability is denaturation (Bischof and He, 2005). Thus, evaluating protein thermal denaturation processes under defined environments, i.e. pH, could therefore grant insight in their overall stability at that particular environment. In this manner, the effects of acidic pH (observed in inflammatory conditions) on IL-1 thermal denaturation were analysed using different biophysical approaches. For this purpose, IL-1 ligands solutions at three different pH were submitted to thermal denaturation by increasing temperature from 20°C-85°C.

7.3.1 IL-1β but not IL-1α stability is pH-dependent

As a consequence of organisms adaptation to their environment, proteins have a limited temperature range at which their structure integrity is maintained and their function is efficient (Argos et al., 1979). Thus protein stability can be estimated as function of temperature, and CD is a powerful tool to measure protein conformational changes in a wide range of temperatures (Greenfield, 2006a). The thermal denaturation of IL-1 ligands at the three different pH was analysed by CD in the far UV region. However, as discussed in section 6.1.1, given the settings chosen for these analyses, CD spectra were difficult to interpret, and the secondary structure prediction (based on CD data) of IL-1α at higher temperatures (< 60-65°C) was inconsistent with all the biophysical analysis carried out, as it suggested that IL-1α was thermally stable even at the higher temperatures. Nonetheless, the overall conclusion of these experiments was in accord with the observations that pH does have an effect on IL-1β thermal stability but not on IL-1α. In order to get good quality CD spectra that may account for reliability of the secondary structure predictions there are at least three settings that can be adjusted, these are the data pitch, the scan speed and the accumulations. The data pitch determines the number of data points taken during the scan in nm (i.e. 0.2nm); the scan speed determines the speed at which the scan will be acquired in nm/min and the accumulations determine the number of scans that will be averaged by the software and exported as a single scan (Sullivan and Magliery, 2010). With the purpose of optimising time for these analyses, the scan speed chosen was 10 nm/min and four accumulations (for the high quality CD spectra of Figures 4.12 and 4.13 scan speed was 20 nm/min and 8 accumulations). Moreover, CD-based predictions of secondary structure with algorithms others than K2D, i.e. SELCON3, CONTIN and CDSSTR, were attempted. Although these algorithms utilise reference sets of proteins (provided in DICHROWEB settings) that allow a more accurate secondary structure prediction

(Sreerama and Woody, 2000), nevertheless, none of the reference sets provided fit our spectra, mainly because of the measurement range employed (200-260 nm).

As it has been discussed in previous sections, protein aggregation occurs when partially unfolded proteins expose their hydrophobic residues leading to unspecific protein self-association. The colloidal stability (stability in solution) of proteins can be measured by SLS, as a function of the T_{agg} (previously defined in Section 6.1.3). This method is widely used in the pharmaceutical industry to monitor the colloidal stability of proteins of therapeutic interest such as Ab (Wang et al., 2013b, Kheddo et al., 2014), with the aim of finding the best solution conditions (i.e. pH, ionic strength) for their storage and distribution (Avacta, 2014a)

With the purpose of studying the effects of acidic pH on IL-1α and IL-1β stability as a function of colloidal stability, the T_{agg} was measured by SLS_{266} and SLS_{473}. According to SLS_{473} analysis, T_{agg} of IL-1β was lower at pH 7.5 than at pH 6.2 or 5.5, implying that at an acidic pH IL-1β is more stable that at a neutral. However, no significant differences were found between T_{agg} with SLS_{266}. The SLS_{473} and SLS_{266} values are sensitive to different sizes of aggregates, therefore they report on the onset of the same aggregation process, but measuring different types of aggregates appearing at the higher temperature. Chrunyk and colleagues (1993) found that at pH 6.8 IL-1β T_{agg} was 58.6°C, this T_{agg} is higher than the observed in this work, however, the method they used (fluorescence light scattering) as well as the pH (6.8) and ionic strength were different (Chrunyk et al., 1993).

Furthermore, the colloidal stability of IL-1α was not affected by pH, supporting our hypothesis that IL-1α is more stable than IL-1β. Accordingly, ^{1}H-NMR analyses of IL-1 ligands thermal stability supported the observation that IL-1α is more thermostable

than IL-1β as the temperatures at which IL-1α was totally denatured and aggregated were 10°C higher than those observed in IL-1β. The differential behaviour of IL-1β at different pH can be explained by its *pI*. The predicted *pI* of IL-1β was 5.9 and it was increased to 6.7 with the additional sequences of the IL-1β construct. This last one was closer to the reported *pI* for IL-1β (7) (Dinarello, 2010). In order to find out the real *pI* for the IL-1β construct used in this work, a preliminary analysis by 2D gel electrophoresis (see Appendix A4-3) was carried out. In this analysis 3 different ~20 kDa bands were found at pH 6.9 and 7 Further LC-MS/MS analysis of these bands confirmed them to be IL-1β isoforms. This finding was consistent with the reported *pI* for IL-1β. The same attempt was tried for IL-1α but, given technical difficulties, it was unsuccessful. It is well accepted that when the *pI* of a protein is closer to the pH in its surrounding environment, the protein is less colloidally-stable and it becomes more prone to aggregation (Chi et al., 2003). This is because the *pI* can be defined as the pH at which a protein has a zero net electric charge (Daintith, 2008), thus, because of the lack of charge there is no nonspecific repulsion driven by protein charges, hence proteins aggregate. On the other hand, changes in pH are reflected in changes on protein charge, and increased charge repulsion within the protein can lead to destabilisation of the protein conformation (Chi et al., 2003). However, it is very interesting that, despite the predicted and reported *pI* for IL-1α was 5.3, and it was increased to 6.3 by additional sequences on the IL-1α protein construct, results obtained in this work showed IL-1α was highly stable at pH 5.5 and 6.2. Given that the pH used for the analysis done in this work was very close to the predicted *pI* of IL-1α, it would have been expected that the IL-1α protein construct used in this work would be colloidally unstable at any of both pH. Thus, in order to find the current *pI* of the IL-

1α protein construct used in this study, repeating the 2D gel electrophoresis analysis could help explain IL-1α stability at different pH.

Intrinsic fluorescence analysis of IL-1α and IL-1β were very interesting. Protein fluorescence is widely used for protein tertiary structure and unfolding studies. It is well known that protein fluorescence is due to Trp and Tyr residues, which given their hydrophobic characteristics, are usually found hidden within the structure of soluble proteins (Burstein et al., 1973). In this manner, when protein is partially or totally unfolded a change in protein fluorescence can be observed given that Trp and Tyr get more exposed. For the purposes of this work, effects of pH on IL-1α and IL-1β fluorescence were studied. IL-1α fluorescence was not affected at all at different pH, implying that IL-1α is highly stable in all pH used. IL-1β fluorescence at acidic pH was similar to that of IL-1α, and a decrease in fluorescence intensity could be seen at pH 7.5. These findings were supported by AUC studies were IL-1β seemed to be more elongated at pH 6.2. Our results of IL-1β fluorescence are consistent with previous studies on IL-1β conformation and stability. IL-1β fluorescence has been attributed to its Trp and four Tyr and has been shown to be affected by acidic pH as at pH 7.5 its Trp is quenched and at pH 6.5 is dequenched (Craig et al., 1987, Epps et al., 1989) Moreover, ionic strength has been shown to affect IL-1β fluorescence and hence its Trp environment, but not that of IL-1α (Epps et al., 1997). These observations are in accordance with our results that suggested that IL-1α is more stable than IL-1β. It is noteworthy that IL-1β Trp (Trp 120) is found close to site B, although it is not involved with binding to IL-1RI. Despite it has not been shown to interact with IL-1RI, its side chains do interact with adjacent residues as it has been suggested that it is quenched by neighbouring charged residues and its fluorescence has been attributed to a local conformational change that removes quenching group from the proximity of Trp 120

(Craig et al., 1987, Epps et al., 1989). Interestingly, IL-1β is not the only cytokine that has been probed to undergo pH-dependent conformational changes. IL-6, another cytokine regulated by IL-1, has been shown to be prone to form folding intermediates in a pH-dependent manner (Ward et al., 1995). IL-6 conformation and stability are affected by lower pH as its fluorescence has been observed to be decreased at lower pH (4) given that its Trp was quenched. These changes in conformation were not caused by unfolding, as CD spectroscopy was proven to be stable in a pH range of 2-10 (Ward et al., 1993). As a pro-inflammatory cytokine, IL-6 has been implicated in a wide range of diseases including rheumatoid arthritis, renal disease and stroke among others (Calabrese and Rose-John, 2014). Moreover, as it has been discussed along this work IL-6 expression is induced by IL-1, thus the suggestion that low pH confers to this proteins more stability and drives conformational changes without affecting their folding is not surprising. Moreover, this pH-dependent stability of IL-6 has also been suggested to be responsible of the differential affinity to its cell-surface receptor (low affinity) and to the converter and signal transducing subunit gp30 (Ward et al., 1995).

Based on SLS, CD, ^{1}H-NMR and fluorescence studies of the effects of pH on IL-1 thermal stability, the overall conclusion is that IL-1β, but not IL-1α, stability and conformation are affected by acidic pH. Low pH influences IL-1β fluorescence and confers more thermal stability.

These preliminary results suggest that pH may have a subtle influence on IL-1β conformation without affecting its folding state, and that, we propose, could affect its affinity to IL-1RI binding and hence, its bioactivity. Nevertheless, more studies on this matter need to be done. For example, better quality CD spectra at increasing temperatures should be acquired in order to determine the effects of pH on IL-1 ligands thermal stability as function of secondary structure. More NMR analysis should be

done with the aim of identifying which amino acid residues are more susceptible to pH. Importantly, native protein constructs with all unnatural tags removed should be used for these experiments, to rule out their potential effect on protein structure and stability. With the aim of studying the kinetics of aggregation, SLS analysis at a single temperature over a period of time should be carried out.

In summary, all together, the presented results support the hypothesis that IL-1β and IL-1α biophysical properties are different as demonstrated by the biophysical analysis discussed in this section. Moreover, they strongly support the hypothesis that pH could be responsible of the difference observed on IL-1α and IL-1β bioactivity, as influence of pH on IL-1β stability were discerned.

7.3 Preliminary studies of effects of temperature and pH on IL-1α and IL-1β bioactivity

IL-1α and IL-1β were first discovered "as a factor that caused fever" (Dinarello, 2010). To date, their participation on inflammatory process is well established (Pinteaux et al., 2009, Arnett, 2010, Denes et al., 2012), and it is well known that under inflammatory conditions there is an increment in local or systemic temperature (Romanovsky et al., 2005), and pH can also been drop both systemically and locally (Nemoto and Frinak, 1981, Arnett, 2010). As it has been discussed in previous sections, acidosis has been observed in numerous diseases where IL-1 has been shown to be involved, including diabetes asthma, stroke and cancer among many others, and pH as low as 5.2, 6.2 and 6.8 have been found in tissues where inflammation has been triggered (Ashby, 1966, Nemoto and Frinak, 1981, Hunt et al., 2000, Kasza, 2013). Moreover pH has been suggested to be beneficial for the activity of diverse elements of the immune system (Trevani et al., 1999, Vermeulen et al., 2004, Edye et al., 2013). Furthermore, it has been suggested that hyperthermia may augment the immune

response (Dinarello, 2012) as it has been observed that in mouse models of neutrophil recovery from radiation, fever enhances IL-1-induced haematopoiesis (Capitano et al., 2012) In addition, IL-2 has been shown to elicit a greater response at 39°C compared to 37°C and elevated temperature has been proposed of being responsible of increasing passage of IL-1β into the brains of old rats (Buchanan et al., 2008) possibly due to melting transition of lipids (below 40°C) that have been suggested to be important in inducing hypermeability of membranes at elevated temperatures (Bischof and He, 2005).

In the present work insights into the effects of pH and temperature on IL-1 stability and conformation were raised. Thus, with the aim of determining whether the observed effects of pH on IL-1β biophysical properties were translated to change in bioactivity, as well as effects that an increment of temperature could have on IL-1α and IL-1β bioactivity, experiments under acidosis conditions and high temperature were carried out on endothelial cells (bEND5).

Preliminary results of the effects of high temperature on IL-1α and IL-1β bioactivity suggested an increase of the potency of IL-1β at inducing IL-6 synthesis. It has previously been observed that temperature could induce conformational transitions in proteins without affecting their overall structure, and temperature can also influence protein-protein binding (Palleros et al., 1991). However, IL-1α bioactivity seemed not to be affected by high temperature, as the levels of IL-6 induced by IL-1α at 40°C were not significant different to those seen at 37°C. These result suggest that IL-1β, but not IL-1α, can also been affected by slight changes of temperature. Nevertheless, further studies on this area need to be done to confirm these observations.

Effects of pH on IL-1α and IL-1β bioactivity experiments were technically challenging to study. Due to the components of the media used to keep cells (DMEM), as well as the CO_2 concentration in incubators, keeping pH at 6.2 was impossible. As an alternative, a HBSS solution at pH 6.2 previously used in acidosis studies (Edye et al., 2013) was tried, however, as the optimal time to see IL-1α and IL-1β effects was 24 h, these experiments were unsuccessful, as cells were not viable in HBSS for long periods of time. These results are not conclusive and it would be interesting to carry out further studies of the effects of pH on IL-1α and IL-1β bioactivity. It has been demonstrated that changes in physiological pH can affect protein binding, and thus, bioactivities (Borga et al., 1969, Levitt et al., 1986).

7.4 Concluding remarks

This work was aimed to elucidate the molecular mechanisms responsible of the differential effects on IL-1α and IL-1β bioactivities. As players of the inflammatory response, physiological conditions at which these cytokines exert their effects are far from normal, as changes in temperature and pH under inflammatory conditions have been established. In this work we have observed that biophysical properties of IL-1α are different that those of IL-1β. For instance, IL-1α was shown to be more stable than IL-1β even under acidic conditions, whereas IL-1β conformation and stability is strongly influenced by pH. Based on these findings, we suggest that the acidic pH and high temperature found under inflammatory conditions may be involved in the differences observed between IL-1α and IL-1β bioactivity. Moreover, time was shown to play a key role in IL-1 biology, and this hypothesis was supported by previous studies on time of expression and regulation of IL-1α and IL-1β. Nonetheless, these findings are preliminary and more experiments need to be design to verify our hypotheses.

References

Blastp. p Protein sequence alignment. http://blast.ncbi.nlm.nih.gov

Dichroweb. p Analysis of CD spectra. http://dichroweb.cryst.bbk.ac.uk

EnCor Biotechnology Inc., p Predicition of protein characteristics from primary sequence. http://encorbio.com/protocols/Prot-MW-Abs.htm

GRAVY calculator. p Protein hydrophobicity calculation. http://www.gravy-calculator.de/index.php

Protein Data Bank pBiological macromolecular strucutres data bank. http://www.rcsb.org/pdb/home/home.do

ProtParam. p Prediction of protein characteristics from primary sequence. http://web.expasy.org/protparam

PyMOL. p Protein structure drawing and analysis. http://pymol.org

Translate tool (Expasy). p Translation of DNA into amino acid sequence. http://web.expasy.org/translate/

Uniprot. p Gene and protein sequence and available published data. http://www.uniprot.org

Aarden L (1979) Revised nomenclature for antigen-nonspecific T cell proliferation and helper factors. J Immunol 123:2928-2929.

Abbas AK, Lichtman AH (2004) Cellular and Molecular Immunology: Elsevier.

Acres RB, Larsen A, Conlon PJ (1987) IL 1 expression in a clone of human T cells. J Immunol 138:2132-2136.

Akeson AL, Woods CW, Hsieh LC, Bohnke RA, Ackermann BL, Chan KY, Robinson JL, Yanofsky SD, Jacobs JW, Barrett RW, Bowlin TL (1996) AF12198, a novel low molecular weight antagonist, selectively binds the human type I interleukin (IL)-1 receptor and blocks in vivo responses to IL-1. The Journal of biological chemistry 271:30517-30523.

Akira S, Takeda K, Kaisho T (2001) Toll-like receptors: critical proteins linking innate and acquired immunity. Nat Immunol 2:675-680.

Allan SM, Tyrrell PJ, Rothwell NJ (2005) Interleukin-1 and neuronal injury. Nature reviews 5:629-640.

Andrade MA, Chacon P, Merelo JJ, Moran F (1993) Evaluation of secondary structure of proteins from UV circular dichroism spectra using an unsupervised learning neural network. Protein engineering 6:383-390.

Andre R, Pinteaux E, Kimber I, Rothwell NJ (2005) Differential actions of IL-1 alpha and IL-1 beta in glial cells share common IL-1 signalling pathways. Neuroreport 16:153-157.

Anforth HR, Bluthe RM, Bristow A, Hopkins S, Lenczowski MJ, Luheshi G, Lundkvist J, Michaud B, Mistry Y, Van Dam AM, Zhen C, Dantzer R, Poole S, Rothwell NJ, Tilders FJ, Wollman EE (1998) Biological activity and brain actions of recombinant rat interleukin-1alpha and interleukin-1beta. European cytokine network 9:279-288.

Arend WP, Malyak M, Smith MF, Jr., Whisenand TD, Slack JL, Sims JE, Giri JG, Dower SK (1994) Binding of IL-1 alpha, IL-1 beta, and IL-1 receptor antagonist by soluble IL-1 receptors and levels of soluble IL-1 receptors in synovial fluids. J Immunol 153:4766-4774.

Argaw AT, Zhang Y, Snyder BJ, Zhao ML, Kopp N, Lee SC, Raine CS, Brosnan CF, John GR (2006) IL-1beta regulates blood-brain barrier permeability via reactivation of the hypoxia-angiogenesis program. J Immunol 177:5574-5584.

Argos P, Rossman MG, Grau UM, Zuber H, Frank G, Tratschin JD (1979) Thermal stability and protein structure. Biochemistry 18:5698-5703.

Arnett TR (2010) Acidosis, hypoxia and bone. Arch Biochem Biophys 503:103-109.

Ashby BS (1966) pH studies in human malignant tumours. Lancet 2:312-315.

Auron PE (1998) The interleukin 1 receptor: ligand interactions and signal transduction. Cytokine & growth factor reviews 9:221-237.

Avacta (2014a) Characterisation of protein aggregation using Optim 1000. Technical note. UK: Avacta Analytical.

Avacta (2014b) Fluorescence data analysis methods using Optim 1000. Technical note. UK: Avacta Analytical.

Ban E, Milon G, Prudhomme N, Fillion G, Haour F (1991) Receptors for interleukin-1 (alpha and beta) in mouse brain: mapping and neuronal localization in hippocampus. Neuroscience 43:21-30.

Ban EM, Sarlieve LL, Haour FG (1993) Interleukin-1 binding sites on astrocytes. Neuroscience 52:725-733.

Banks WA (1999) Characterization of interleukin-1alpha binding to mouse brain endothelial cells. J Pharmacol Exp Ther 291:665-670.

Beissert S, Hosoi J, Stratigos A, Brissette J, Grabbe S, Schwarz T, Granstein RD (1998) Differential regulation of epidermal cell tumor-antigen presentation by IL-1alpha and IL-1beta. The Journal of investigative dermatology 111:609-615.

Ben-Sasson SZ, Hogg A, Hu-Li J, Wingfield P, Chen X, Crank M, Caucheteux S, Ratner-Hurevich M, Berzofsky JA, Nir-Paz R, Paul WE (2013) IL-1 enhances expansion, effector function, tissue localization, and memory response of antigen-specific CD8 T cells. The Journal of experimental medicine 210:491-502.

Berisio R, Sica F, Lamzin VS, Wilson KS, Zagari A, Mazzarella L (2002) Atomic resolution structures of ribonuclease A at six pH values. Acta Crystallogr D Biol Crystallogr 58:441-450.

Bischof JC, He X (2005) Thermal stability of proteins. Annals of the New York Academy of Sciences 1066:12-33.

Blondeau K, Boutur O, Boze H, Jung G, Moulin G, Galzy P (1994a) Development of high-cell-density fermentation for heterologous interleukin 1 beta production in Kluyveromyces lactis controlled by the PHO5 promoter. Appl Microbiol Biotechnol 41:324-329.

Blondeau K, Boze H, Jung G, Moulin G, Galzy P (1994b) Physiological approach to heterologous human serum albumin production by Kluyveromyces lactis in chemostat culture. Yeast 10:1297-1303.

Boch JA, Yoshida Y, Koyama Y, Wara-Aswapati N, Peng H, Unlu S, Auron PE (2003) Characterization of a cascade of protein interactions initiated at the IL-1 receptor. Biochemical and biophysical research communications 303:525-531.

Bodelon G, Palomino C, Fernandez LA (2013) Immunoglobulin domains in Escherichia coli and other enterobacteria: from pathogenesis to applications in antibody technologies. FEMS Microbiol Rev 37:204-250.

Boehmer JL, DeGrasse JA, McFarland MA, Tall EA, Shefcheck KJ, Ward JL, Bannerman DD (2010) The proteomic advantage: label-free quantification of proteins expressed in bovine milk during experimentally induced coliform mastitis. Vet Immunol Immunopathol 138:252-266.

Bomsztyk K, Sims JE, Stanton TH, Slack J, McMahan CJ, Valentine MA, Dower SK (1989) Evidence for different interleukin 1 receptors in murine B- and T-cell lines. Proceedings of the National Academy of Sciences of the United States of America 86:8034-8038.

Borga O, Azarnoff DL, Forshell GP, Sjoqvist F (1969) Plasma protein binding of tricyclic anti-depressants in man. Biochem Pharmacol 18:2135-2143.

Boutin H, Kimber I, Rothwell NJ, Pinteaux E (2003) The expanding interleukin-1 family and its receptors: do alternative IL-1 receptor/signaling pathways exist in the brain? Molecular neurobiology 27:239-248.

Braddock M, Quinn A (2004) Targeting IL-1 in inflammatory disease: new opportunities for therapeutic intervention. Nature reviews Drug discovery 3:330-339.

Brikos C, Wait R, Begum S, O'Neill LA, Saklatvala J (2007) Mass spectrometric analysis of the endogenous type I interleukin-1 (IL-1) receptor signaling complex formed after IL-1 binding identifies IL-1RAcP, MyD88, and IRAK-4 as the stable components. Mol Cell Proteomics 6:1551-1559.

Brough D, Tyrrell PJ, Allan SM (2011) Regulation of interleukin-1 in acute brain injury. Trends in pharmacological sciences 32:617-622.

Buchanan JB, Peloso E, Satinoff E (2008) A warmer ambient temperature increases the passage of interleukin-1beta into the brains of old rats. Am J Physiol Regul Integr Comp Physiol 295:R361-368.

Burstein EA, Vedenkina NS, Ivkova MN (1973) Fluorescence and the location of tryptophan residues in protein molecules. Photochem Photobiol 18:263-279.

Calabrese LH, Rose-John S (2014) IL-6 biology: implications for clinical targeting in rheumatic disease. Nature reviews Rheumatology.
Capitano ML, Nemeth MJ, Mace TA, Salisbury-Ruf C, Segal BH, McCarthy PL, Repasky EA (2012) Elevating body temperature enhances hematopoiesis and neutrophil recovery after total body irradiation in an IL-1-, IL-17-, and G-CSF-dependent manner. Blood 120:2600-2609.
Carroll JA, Garon CF, Schwan TG (1999) Effects of environmental pH on membrane proteins in Borrelia burgdorferi. Infect Immun 67:3181-3187.
Casadio R, Frigimelica E, Bossu P, Neumann D, Martin MU, Tagliabue A, Boraschi D (2001) Model of interaction of the IL-1 receptor accessory protein IL-1RAcP with the IL-1beta/IL-1R(I) complex. FEBS letters 499:65-68.
Chang HK, Mohan SK, Chin Y (2010) 1H, 13C and 15N backbone and side chain resonance assignments of human interleukin 1alpha. Biomol NMR Assign 4:59-60.
Chaudhuri R, Cheng Y, Middaugh CR, Volkin DB (2014) High-throughput biophysical analysis of protein therapeutics to examine interrelationships between aggregate formation and conformational stability. The AAPS journal 16:48-64.
Chen CJ, Kono H, Golenbock D, Reed G, Akira S, Rock KL (2007) Identification of a key pathway required for the sterile inflammatory response triggered by dying cells. Nature medicine 13:851-856.
Chi EY, Krishnan S, Randolph TW, Carpenter JF (2003) Physical stability of proteins in aqueous solution: mechanism and driving forces in nonnative protein aggregation. Pharm Res 20:1325-1336.
Chizzonite R, Truitt T, Kilian PL, Stern AS, Nunes P, Parker KP, Kaffka KL, Chua AO, Lugg DK, Gubler U (1989) Two high-affinity interleukin 1 receptors represent separate gene products. Proceedings of the National Academy of Sciences of the United States of America 86:8029-8033.
Chrunyk BA, Evans J, Lillquist J, Young P, Wetzel R (1993) Inclusion body formation and protein stability in sequence variants of interleukin-1 beta. The Journal of biological chemistry 268:18053-18061.
Chung IY, Benveniste EN (1990) Tumor necrosis factor-alpha production by astrocytes. Induction by lipopolysaccharide, IFN-gamma, and IL-1 beta. J Immunol 144:2999-3007.
Clore GM, Driscoll PC, Wingfield PT, Gronenborn AM (1990) Low resolution structure of interleukin-1 beta in solution derived from 1H-15N heteronuclear three-dimensional nuclear magnetic resonance spectroscopy. J Mol Biol 214:811-817.
Clore GM, Gronenborn AM (1991) Comparison of the solution nuclear magnetic resonance and X-ray crystal structures of human recombinant interleukin-1 beta. J Mol Biol 221:47-53.
Clore GM, Wingfield PT, Gronenborn AM (1991) High-resolution three-dimensional structure of interleukin 1 beta in solution by three- and four-dimensional nuclear magnetic resonance spectroscopy. Biochemistry 30:2315-2323.
Close TE, Cepinskas G, Omatsu T, Rose KL, Summers K, Patterson EK, Fraser DD (2013) Diabetic ketoacidosis elicits systemic inflammation associated with cerebrovascular endothelial cell dysfunction. Microcirculation 20:534-543.
Craig S, Schmeissner U, Wingfield P, Pain RH (1987) Conformation, stability, and folding of interleukin 1 beta. Biochemistry 26:3570-3576.
Cullinan EB, Kwee L, Nunes P, Shuster DJ, Ju G, McIntyre KW, Chizzonite RA, Labow MA (1998) IL-1 receptor accessory protein is an essential component of the IL-1 receptor. J Immunol 161:5614-5620.
Daintith J (2008) Dictionary of Chemistry. Oxford: Oxford.
De Groote D, Zangerle PF, Gevaert Y, Fassotte MF, Beguin Y, Noizat-Pirenne F, Pirenne J, Gathy R, Lopez M, Dehart I, et al. (1992) Direct stimulation of cytokines (IL-1 beta, TNF-alpha, IL-6, IL-2, IFN-gamma and GM-CSF) in whole blood. I. Comparison with isolated PBMC stimulation. Cytokine 4:239-248.
de Marco A, Vigh L, Diamant S, Goloubinoff P (2005) Native folding of aggregation-prone recombinant proteins in Escherichia coli by osmolytes, plasmid- or benzyl alcohol-overexpressed molecular chaperones. Cell stress & chaperones 10:329-339.

DeForge LE, Remick DG (1991) Kinetics of TNF, IL-6, and IL-8 gene expression in LPS-stimulated human whole blood. Biochemical and biophysical research communications 174:18-24.
Del Maschio A, De Luigi A, Martin-Padura I, Brockhaus M, Bartfai T, Fruscella P, Adorini L, Martino G, Furlan R, De Simoni MG, Dejana E (1999) Leukocyte recruitment in the cerebrospinal fluid of mice with experimental meningitis is inhibited by an antibody to junctional adhesion molecule (JAM). The Journal of experimental medicine 190:1351-1356.
Delahunty C, Yates JR, 3rd (2005) Protein identification using 2D-LC-MS/MS. Methods 35:248-255.
Demain AL, Vaishnav P (2009) Production of recombinant proteins by microbes and higher organisms. Biotechnol Adv 27:297-306.
Demczuk S, Baumberger C, Mach B, Dayer JM (1988) Differential effects of in vitro mycoplasma infection on interleukin-1 alpha and beta mRNA expression in U937 and A431 cells. The Journal of biological chemistry 263:13039-13045.
Denes A, Drake C, Stordy J, Chamberlain J, McColl BW, Gram H, Crossman D, Francis S, Allan SM, Rothwell NJ (2012) Interleukin-1 mediates neuroinflammatory changes associated with diet-induced atherosclerosis. J Am Heart Assoc 1:e002006.
Dinarello CA (1991) Interleukin-1 and interleukin-1 antagonism. Blood 77:1627-1652.
Dinarello CA (1996) Biologic basis for interleukin-1 in disease. Blood 87:2095-2147.
Dinarello CA (1998) Interleukin-1, interleukin-1 receptors and interleukin-1 receptor antagonist. International reviews of immunology 16:457-499.
Dinarello CA (2009) Immunological and inflammatory functions of the interleukin-1 family. Annual review of immunology 27:519-550.
Dinarello CA (2010) IL-1: discoveries, controversies and future directions. European journal of immunology 40:599-606.
Dinarello CA (2012) Keep up the heat on IL-1. Blood 120:2538-2539.
Dinarello CA (2014) Interleukin-1alpha neutralisation in patients with cancer. Lancet Oncol 15:552-553.
Dinarello CA, Cannon JG, Mier JW, Bernheim HA, LoPreste G, Lynn DL, Love RN, Webb AC, Auron PE, Reuben RC, et al. (1986) Multiple biological activities of human recombinant interleukin 1. J Clin Invest 77:1734-1739.
Dinarello CA, Goldin NP, Wolff SM (1974) Demonstration and characterization of two distinct human leukocytic pyrogens. The Journal of experimental medicine 139:1369-1381.
Dinarello CA, Renfer L, Wolff SM (1977) Human leukocytic pyrogen: purification and development of a radioimmunoassay. Proceedings of the National Academy of Sciences of the United States of America 74:4624-4627.
Dinarello CA, Simon A, van der Meer JW (2012) Treating inflammation by blocking interleukin-1 in a broad spectrum of diseases. Nature reviews Drug discovery 11:633-652.
Dinarello CA, Wolff SM (1977) Partial purification of human leukocytic pyrogen. Inflammation 2:179-189.
Dixon MM, Brennan RG, Matthews BW (1991) Structure of gamma-chymotrypsin in the range pH 2.0 to pH 10.5 suggests that gamma-chymotrypsin is a covalent acyl-enzyme adduct at low pH. Int J Biol Macromol 13:89-96.
Djoumerska-Alexieva IK, Dimitrov JD, Voynova EN, Lacroix-Desmazes S, Kaveri SV, Vassilev TL (2010) Exposure of IgG to an acidic environment results in molecular modifications and in enhanced protective activity in sepsis. FEBS J 277:3039-3050.
Donovan RS, Robinson CW, Glick BR (1996) Review: optimizing inducer and culture conditions for expression of foreign proteins under the control of the lac promoter. Journal of industrial microbiology 16:145-154.
Dower SK, Kronheim SR, March CJ, Conlon PJ, Hopp TP, Gillis S, Urdal DL (1985) Detection and characterization of high affinity plasma membrane receptors for human interleukin 1. The Journal of experimental medicine 162:501-515.
Drickamer K, Taylor ME (1998) Evolving views of protein glycosylation. Trends Biochem Sci 23:321-324.
Dukovich M, Severin JM, White SJ, Yamazaki S, Mizel SB (1986) Stimulation of fibroblast proliferation and prostaglandin production by purified recombinant murine interleukin 1. Clin Immunol Immunopathol 38:381-389.

Duy C, Fitter J (2006) How aggregation and conformational scrambling of unfolded states govern fluorescence emission spectra. Biophys J 90:3704-3711.
Edye ME, Lopez-Castejon G, Allan SM, Brough D (2013) Acidosis drives damage-associated molecular pattern (DAMP)-induced interleukin-1 secretion via a caspase-1-independent pathway. The Journal of biological chemistry 288:30485-30494.
Eftink MR (1994) The use of fluorescence methods to monitor unfolding transitions in proteins. Biophys J 66:482-501.
Eftink MR (2000) Intrinsic fluorescence of proteins. In: Topics in fluorescence spectroscopy, vol. 6 (Lakowicz, J. R., ed), pp 1-13 New York: Kluwer Academic/Plenum Publishers.
Elias JA, Lentz V (1990) IL-1 and tumor necrosis factor synergistically stimulate fibroblast IL-6 production and stabilize IL-6 messenger RNA. J Immunol 145:161-166.
Epps DE, Yem AW, Deibel MR, Jr. (1989) Characterization of the tryptophan environments of interleukins 1 alpha and 1 beta by fluorescence quenching and lifetime measurements. Arch Biochem Biophys 275:82-91.
Epps DE, Yem AW, McGee JM, Tomich CS, Curry KA, Chosay JG, Deibel MR (1997) Fluorescence and site-directed mutagenesis studies of interleukin 1 beta. Cytokine 9:149-156.
Evans RJ, Bray J, Childs JD, Vigers GP, Brandhuber BJ, Skalicky JJ, Thompson RC, Eisenberg SP (1995) Mapping receptor binding sites in interleukin (IL)-1 receptor antagonist and IL-1 beta by site-directed mutagenesis. Identification of a single site in IL-1ra and two sites in IL-1 beta. The Journal of biological chemistry 270:11477-11483.
Finzel BC, Clancy LL, Holland DR, Muchmore SW, Watenpaugh KD, Einspahr HM (1989) Crystal structure of recombinant human interleukin-1 beta at 2.0 A resolution. J Mol Biol 209:779-791.
Fitzgerald KA, O'Neill LA (2000) The role of the interleukin-1/Toll-like receptor superfamily in inflammation and host defence. Microbes Infect 2:933-943.
Fleer R, Chen XJ, Amellal N, Yeh P, Fournier A, Guinet F, Gault N, Faucher D, Folliard F, Fukuhara H, et al. (1991) High-level secretion of correctly processed recombinant human interleukin-1 beta in Kluyveromyces lactis. Gene 107:285-295.
Fountoulakis M, Gentz R (1992) Effect of glycosylation on properties of soluble interferon gamma receptors produced in prokaryotic and eukaryotic expression systems. Biotechnology (N Y) 10:1143-1147.
Fountoulakis M, Juranville JF, Manneberg M (1992) Comparison of the Coomassie Brilliant Blue, Bicinchoninic Acid and Lowry Quantitation Assays, Using Nonglycosylated and Glycosylated Proteins. J Biochem Bioph Meth 24:265-274.
Freifelder D (1982) Physical Biochemistry. Applications to biochemistry and molecular biology. United States of America: W.H. Freeman and Company.
Frokjaer S, Otzen DE (2005) Protein drug stability: a formulation challenge. Nature reviews Drug discovery 4:298-306.
Ganatra MB, Vainauskas S, Hong JM, Taylor TE, Denson JP, Esposito D, Read JD, Schmeisser H, Zoon KC, Hartley JL, Taron CH (2011) A set of aspartyl protease-deficient strains for improved expression of heterologous proteins in Kluyveromyces lactis. FEMS Yeast Res 11:168-178.
Garidel P, Hegyi M, Bassarab S, Weichel M (2008) A rapid, sensitive and economical assessment of monoclonal antibody conformational stability by intrinsic tryptophan fluorescence spectroscopy. Biotechnology journal 3:1201-1211.
Garlatti V, Martin L, Gout E, Reiser JB, Fujita T, Arlaud GJ, Thielens NM, Gaboriaud C (2007) Structural basis for innate immune sensing by M-ficolin and its control by a pH-dependent conformational switch. The Journal of biological chemistry 282:35814-35820.
Gasser JA, Hulter HN, Imboden P, Krapf R (2014) Effect of chronic metabolic acidosis on bone density and bone architecture in vivo in rats. American journal of physiology Renal physiology 306:F517-524.
Gay NJ, Keith FJ (1991) Drosophila Toll and IL-1 receptor. Nature 351:355-356.
Gellissen G, Melber K, Janowicz ZA, Dahlems UM, Weydemann U, Piontek M, Strasser AW, Hollenberg CP (1992) Heterologous protein production in yeast. Antonie Van Leeuwenhoek 62:79-93.

Glick BR, Pasternak JJ (2003) Molecular Biotechnology. Priciples and Applications of recombinant DNA. Washington D.C.: ASM Press.
Goldberg DS, Bishop SM, Shah AU, Sathish HA (2011) Formulation development of therapeutic monoclonal antibodies using high-throughput fluorescence and static light scattering techniques: role of conformational and colloidal stability. J Pharm Sci 100:1306-1315.
Graves BJ, Hatada MH, Hendrickson WA, Miller JK, Madison VS, Satow Y (1990) Structure of interleukin 1 alpha at 2.7-A resolution. Biochemistry 29:2679-2684.
Gray PW, Glaister D, Chen E, Goeddel DV, Pennica D (1986) Two interleukin 1 genes in the mouse: cloning and expression of the cDNA for murine interleukin 1 beta. J Immunol 137:3644-3648.
Greenfeder SA, Nunes P, Kwee L, Labow M, Chizzonite RA, Ju G (1995a) Molecular cloning and characterization of a second subunit of the interleukin 1 receptor complex. The Journal of biological chemistry 270:13757-13765.
Greenfeder SA, Varnell T, Powers G, Lombard-Gillooly K, Shuster D, McIntyre KW, Ryan DE, Levin W, Madison V, Ju G (1995b) Insertion of a structural domain of interleukin (IL)-1 beta confers agonist activity to the IL-1 receptor antagonist. Implications for IL-1 bioactivity. The Journal of biological chemistry 270:22460-22466.
Greenfield NJ (2006a) Using circular dichroism collected as a function of temperature to determine the thermodynamics of protein unfolding and binding interactions. Nat Protoc 1:2527-2535.
Greenfield NJ (2006b) Using circular dichroism spectra to estimate protein secondary structure. Nat Protoc 1:2876-2890.
Grinstein S, Swallow CJ, Rotstein OD (1991) Regulation of cytoplasmic pH in phagocytic cell function and dysfunction. Clin Biochem 24:241-247.
Gronenborn AM, Wingfield PT, McDonald HR, Schmeissner U, Clore GM (1988) Site directed mutants of human interleukin-1 alpha: a 1H-NMR and receptor binding study. FEBS letters 231:135-138.
Gubler U, Chua AO, Stern AS, Hellmann CP, Vitek MP, DeChiara TM, Benjamin WR, Collier KJ, Dukovich M, Familletti PC, et al. (1986) Recombinant human interleukin 1 alpha: purification and biological characterization. J Immunol 136:2492-2497.
Gursky O, Badger J, Li Y, Caspar DL (1992) Conformational changes in cubic insulin crystals in the pH range 7-11. Biophys J 63:1210-1220.
Hauser C, Saurat JH, Schmitt A, Jaunin F, Dayer JM (1986) Interleukin 1 is present in normal human epidermis. J Immunol 136:3317-3323.
He F, Razinkov VI, Middaugh CR, Becker GW (2013) High-throughput biophysical approaches to therapeutic protein development. In: Biophysics for therapeutic protein development vol. 4 (Narhi, L. O., ed), pp 7-31 New York: Springer Science+Business Media.
Henderson B, Pettipher ER (1988) Comparison of the in vivo inflammatory activities after intra-articular injection of natural and recombinant IL-1 alpha and IL-1 beta in the rabbit. Biochem Pharmacol 37:4171-4176.
Hoffmann MK, Mizel SB, Hirst JA (1984) IL 1 requirement for B cell activation revealed by use of adult serum. J Immunol 133:2566-2568.
Horai R, Asano M, Sudo K, Kanuka H, Suzuki M, Nishihara M, Takahashi M, Iwakura Y (1998) Production of mice deficient in genes for interleukin (IL)-1alpha, IL-1beta, IL-1alpha/beta, and IL-1 receptor antagonist shows that IL-1beta is crucial in turpentine-induced fever development and glucocorticoid secretion. The Journal of experimental medicine 187:1463-1475.
Horuk R, Huang JJ, Covington M, Newton RC (1987) A biochemical and kinetic analysis of the interleukin-1 receptor. Evidence for differences in molecular properties of IL-1 receptors. The Journal of biological chemistry 262:16275-16278.
Howard M, Mizel SB, Lachman L, Ansel J, Johnson B, Paul WE (1983) Role of interleukin 1 in anti-immunoglobulin-induced B cell proliferation. The Journal of experimental medicine 157:1529-1543.

Huang J, Gao X, Li S, Cao Z (1997) Recruitment of IRAK to the interleukin 1 receptor complex requires interleukin 1 receptor accessory protein. Proceedings of the National Academy of Sciences of the United States of America 94:12829-12832.
Huang MT, Larbi KY, Scheiermann C, Woodfin A, Gerwin N, Haskard DO, Nourshargh S (2006) ICAM-2 mediates neutrophil transmigration in vivo: evidence for stimulus specificity and a role in PECAM-1-independent transmigration. Blood 107:4721-4727.
Hunt JF, Fang K, Malik R, Snyder A, Malhotra N, Platts-Mills TA, Gaston B (2000) Endogenous airway acidification. Implications for asthma pathophysiology. American journal of respiratory and critical care medicine 161:694-699.
Jana S, Deb JK (2005) Strategies for efficient production of heterologous proteins in Escherichia coli. Appl Microbiol Biotechnol 67:289-298.
Jensen LE, Muzio M, Mantovani A, Whitehead AS (2000) IL-1 signaling cascade in liver cells and the involvement of a soluble form of the IL-1 receptor accessory protein. J Immunol 164:5277-5286.
Jo HJ, Noh JS, Kong KH (2013) Efficient secretory expression of the sweet-tasting protein brazzein in the yeast Kluyveromyces lactis. Protein Expr Purif 90:84-89.
John GR, Chen L, Rivieccio MA, Melendez-Vasquez CV, Hartley A, Brosnan CF (2004) Interleukin-1beta induces a reactive astroglial phenotype via deactivation of the Rho GTPase-Rock axis. J Neurosci 24:2837-2845.
Jones S, Thornton JM (1996) Principles of protein-protein interactions. Proceedings of the National Academy of Sciences of the United States of America 93:13-20.
Juric DM, Carman-Krzan M (2001) Interleukin-1 beta, but not IL-1 alpha, mediates nerve growth factor secretion from rat astrocytes via type I IL-1 receptor. Int J Dev Neurosci 19:675-683.
Kaplanski G, Farnarier C, Kaplanski S, Porat R, Shapiro L, Bongrand P, Dinarello CA (1994) Interleukin-1 induces interleukin-8 secretion from endothelial cells by a juxtacrine mechanism. Blood 84:4242-4248.
Kasza A (2013) IL-1 and EGF regulate expression of genes important in inflammation and cancer. Cytokine 62:22-33.
Katsuki H, Nakai S, Hirai Y, Akaji K, Kiso Y, Satoh M (1990) Interleukin-1 beta inhibits long-term potentiation in the CA3 region of mouse hippocampal slices. Eur J Pharmacol 181:323-326.
Kawashima H, Yamagishi J, Yamayoshi M, Ohue M, Fukui T, Kotani H, Yamada M (1992) Structure-activity relationships in human interleukin-1 alpha: identification of key residues for expression of biological activities. Protein engineering 5:171-176.
Kelly SM, Jess TJ, Price NC (2005) How to study proteins by circular dichroism. Biochim Biophys Acta 1751:119-139.
Kheddo P, Tracka M, Armer J, Dearman RJ, Uddin S, van der Walle CF, Golovanov AP (2014) The effect of arginine glutamate on the stability of monoclonal antibodies in solution. Int J Pharm 473:126-133.
Kilian PL, Kaffka KL, Stern AS, Woehle D, Benjamin WR, Dechiara TM, Gubler U, Farrar JJ, Mizel SB, Lomedico PT (1986) Interleukin 1 alpha and interleukin 1 beta bind to the same receptor on T cells. J Immunol 136:4509-4514.
Kimura H, Inukai Y, Takii T, Furutani Y, Shibata Y, Hayashi H, Sakurada S, Okamoto T, Inoue J, Oomoto Y, Onozaki K (1998) Molecular analysis of constitutive IL-1alpha gene expression in human melanoma cells: autocrine stimulation through NF-kappaB activation by endogenous IL-1alpha. Cytokine 10:872-879.
Kobayashi Y, Yamamoto K, Saido T, Kawasaki H, Oppenheim JJ, Matsushima K (1990) Identification of calcium-activated neutral protease as a processing enzyme of human interleukin 1 alpha. Proceedings of the National Academy of Sciences of the United States of America 87:5548-5552.
Korherr C, Hofmeister R, Wesche H, Falk W (1997) A critical role for interleukin-1 receptor accessory protein in interleukin-1 signaling. European journal of immunology 27:262-267.
Krakauer T (1985) Biochemical characterization of interleukin 1 from a human monocytic cell line. Journal of leukocyte biology 37:511-518.

Kranz J, AlAzzam F, Saluja A, Svitel J, Al-Azzam W (2013) Techniques for higher-order structure determination. In: Biophysics for therapeutic protein development, vol. 4 (Narhi, L. O., ed), pp 33-82 New York: Springer Science+Business Media

Kurt-Jones EA, Beller DI, Mizel SB, Unanue ER (1985) Identification of a membrane-associated interleukin 1 in macrophages. Proceedings of the National Academy of Sciences of the United States of America 82:1204-1208.

Labriola-Tompkins E, Chandran C, Kaffka KL, Biondi D, Graves BJ, Hatada M, Madison VS, Karas J, Kilian PL, Ju G (1991) Identification of the discontinuous binding site in human interleukin 1 beta for the type I interleukin 1 receptor. Proceedings of the National Academy of Sciences of the United States of America 88:11182-11186.

Labriola-Tompkins E, Chandran C, Varnell TA, Madison VS, Ju G (1993) Structure-function analysis of human IL-1 alpha: identification of residues required for binding to the human type I IL-1 receptor. Protein engineering 6:535-539.

Lang D, Knop J, Wesche H, Raffetseder U, Kurrle R, Boraschi D, Martin MU (1998) The type II IL-1 receptor interacts with the IL-1 receptor accessory protein: a novel mechanism of regulation of IL-1 responsiveness. J Immunol 161:6871-6877.

Lardner A (2001) The effects of extracellular pH on immune function. Journal of leukocyte biology 69:522-530.

Larsen GL, Henson PM (1983) Mediators of inflammation. Annual review of immunology 1:335-359.

Latypov RF, Harvey TS, Liu D, Bondarenko PV, Kohno T, Fachini RA, 2nd, Rosenfeld RD, Ketchem RR, Brems DN, Raibekas AA (2007) Biophysical characterization of structural properties and folding of interleukin-1 receptor antagonist. J Mol Biol 368:1187-1201.

Laue T (2001) Biophysical studies by ultracentrifugation. Curr Opin Struct Biol 11:579-583.

Levitt MA, Sullivan JB, Jr., Owens SM, Burnham L, Finley PR (1986) Amitriptyline plasma protein binding: effect of plasma pH and relevance to clinical overdose. Am J Emerg Med 4:121-125.

Lewis C, Mazzei G, Shaw A (1990) Monoclonal antibodies reacting with the interleukin 1 receptor define a multi-molecular complex. European journal of immunology 20:207-213.

Lin LL, Lin AY, DeWitt DL (1992) Interleukin-1 alpha induces the accumulation of cytosolic phospholipase A2 and the release of prostaglandin E2 in human fibroblasts. The Journal of biological chemistry 267:23451-23454.

Liu C, Takao T, Hashimoto K, Souza EBD (1996) Interleukin-1 Receptors in the Nervous System. In: Cytokines in the Nervous System (Rothwell, N. J., ed), pp 21-40 Austin Texas, USA: R.G. Landes Company.

Lobley A, Whitmore L, Wallace BA (2002) DICHROWEB: an interactive website for the analysis of protein secondary structure from circular dichroism spectra. Bioinformatics 18:211-212.

Luheshi NM, Giles JA, Lopez-Castejon G, Brough D (2012) Sphingosine regulates the NLRP3-inflammasome and IL-1beta release from macrophages. European journal of immunology 42:716-725.

Luheshi NM, McColl BW, Brough D (2009a) Nuclear retention of IL-1 alpha by necrotic cells: a mechanism to dampen sterile inflammation. European journal of immunology 39:2973-2980.

Luheshi NM, Rothwell NJ, Brough D (2009b) Dual functionality of interleukin-1 family cytokines: implications for anti-interleukin-1 therapy. British journal of pharmacology 157:1318-1329.

Luheshi NM, Rothwell NJ, Brough D (2009c) The dynamics and mechanisms of interleukin-1alpha and beta nuclear import. Traffic 10:16-25.

Malinowsky D, Lundkvist J, Laye S, Bartfai T (1998) Interleukin-1 receptor accessory protein interacts with the type II interleukin-1 receptor. FEBS letters 429:299-302.

Mann M, Hendrickson RC, Pandey A (2001) Analysis of proteins and proteomes by mass spectrometry. Annual review of biochemistry 70:437-473.

March CJ, Mosley B, Larsen A, Cerretti DP, Braedt G, Price V, Gillis S, Henney CS, Kronheim SR, Grabstein K, et al. (1985) Cloning, sequence and expression of two distinct human interleukin-1 complementary DNAs. Nature 315:641-647.

Marion D (2013) An introduction to biological NMR spectroscopy. Mol Cell Proteomics 12:3006-3025.
Martin MU, Wesche H (2002) Summary and comparison of the signaling mechanisms of the Toll/interleukin-1 receptor family. Biochim Biophys Acta 1592:265-280.
Martin SR, Schilstra MJ (2008) Circular dichroism and its application to the study of biomolecules. Methods in cell biology 84:263-293.
Martinez D, Vermeulen M, Trevani A, Ceballos A, Sabatte J, Gamberale R, Alvarez ME, Salamone G, Tanos T, Coso OA, Geffner J (2006) Extracellular acidosis induces neutrophil activation by a mechanism dependent on activation of phosphatidylinositol 3-kinase/Akt and ERK pathways. J Immunol 176:1163-1171.
Mason JL, Suzuki K, Chaplin DD, Matsushima GK (2001) Interleukin-1beta promotes repair of the CNS. J Neurosci 21:7046-7052.
Matsushima K, Akahoshi T, Yamada M, Furutani Y, Oppenheim JJ (1986) Properties of a specific interleukin 1 (IL 1) receptor on human Epstein Barr virus-transformed B lymphocytes: identity of the receptor for IL 1-alpha and IL 1-beta. J Immunol 136:4496-4502.
Mcmahan CJ, Slack JL, Mosley B, Cosman D, Lupton SD, Brunton LL, Grubin CE, Wignall JM, Jenkins NA, Brannan CI, Copeland NG, Huebner K, Croce CM, Cannizzarro LA, Benjamin D, Dower SK, Spriggs MK, Sims JE (1991a) A Novel Il-1 Receptor, Cloned from B-Cells by Mammalian Expression, Is Expressed in Many Cell-Types. Embo Journal 10:2821-2832.
McMahan CJ, Slack JL, Mosley B, Cosman D, Lupton SD, Brunton LL, Grubin CE, Wignall JM, Jenkins NA, Brannan CI, et al. (1991b) A novel IL-1 receptor, cloned from B cells by mammalian expression, is expressed in many cell types. The EMBO journal 10:2821-2832.
Merico A, Capitanio D, Vigentini I, Ranzi BM, Compagno C (2004) How physiological and cultural conditions influence heterologous protein production in Kluyveromyces lactis. J Biotechnol 109:139-146.
Mosley B, Urdal DL, Prickett KS, Larsen A, Cosman D, Conlon PJ, Gillis S, Dower SK (1987) The interleukin-1 receptor binds the human interleukin-1 alpha precursor but not the interleukin-1 beta precursor. The Journal of biological chemistry 262:2941-2944.
Muller WA, Weigl SA, Deng X, Phillips DM (1993) PECAM-1 is required for transendothelial migration of leukocytes. The Journal of experimental medicine 178:449-460.
Murphy PA, Chesney PJ, Wood WB, Jr. (1974) Further purification of rabbit leukocyte pyrogen. The Journal of laboratory and clinical medicine 83:310-322.
Nakae S, Asano M, Horai R, Iwakura Y (2001a) Interleukin-1 beta, but not interleukin-1 alpha, is required for T-cell-dependent antibody production. Immunology 104:402-409.
Nakae S, Naruse-Nakajima C, Sudo K, Horai R, Asano M, Iwakura Y (2001b) IL-1 alpha, but not IL-1 beta, is required for contact-allergen-specific T cell activation during the sensitization phase in contact hypersensitivity. International immunology 13:1471-1478.
Nakashima H, Nishikawa K, Ooi T (1986) The folding type of a protein is relevant to the amino acid composition. J Biochem 99:153-162.
Nemoto EM, Frinak S (1981) Brain tissue pH after global brain ischemia and barbiturate loading in rats. Stroke 12:77-82.
Nestler EJ, Hyman SE, Malenka RC (2009) Molecular Neurpharmacology. A foundation for clinical neuroscience. New York: Mc Graw Hill Medical.
New-England-Biolabs (2007) K. lactis Protein Expression Kit. Instruction manual. p 28.
Niki Y, Yamada H, Kikuchi T, Toyama Y, Matsumoto H, Fujikawa K, Tada N (2004) Membrane-associated IL-1 contributes to chronic synovitis and cartilage destruction in human IL-1 alpha transgenic mice. J Immunol 172:577-584.
Niu J, Gilliland MG, Jin Z, Kolattukudy PE, Hoffman WH (2014) MCP-1and IL-1beta expression in the myocardia of two young patients with Type 1 diabetes mellitus and fatal diabetic ketoacidosis. Experimental and molecular pathology 96:71-79.
O'Neill LA (2008) The interleukin-1 receptor/Toll-like receptor superfamily: 10 years of progress. Immunological reviews 226:10-18.
O'Neill LA, Bowie AG (2007) The family of five: TIR-domain-containing adaptors in Toll-like receptor signalling. Nature reviews 7:353-364.

Ohmori Y, Strassman G, Hamilton TA (1990) cAMP differentially regulates expression of mRNA encoding IL-1 alpha and IL-1 beta in murine peritoneal macrophages. J Immunol 145:3333-3339.
Oliva A, Llabres M, Farina JB (2001) Comparative study of protein molecular weights by size-exclusion chromatography and laser-light scattering. J Pharm Biomed Anal 25:833-841.
Palleros DR, Welch WJ, Fink AL (1991) Interaction of hsp70 with unfolded proteins: effects of temperature and nucleotides on the kinetics of binding. Proceedings of the National Academy of Sciences of the United States of America 88:5719-5723.
Parnet P, Amindari S, Wu C, Brunke-Reese D, Goujon E, Weyhenmeyer JA, Dantzer R, Kelley KW (1994) Expression of type I and type II interleukin-1 receptors in mouse brain. Brain research Molecular brain research 27:63-70.
Parra B, Hinton DR, Lin MT, Cua DJ, Stohlman SA (1997) Kinetics of cytokine mRNA expression in the central nervous system following lethal and nonlethal coronavirus-induced acute encephalomyelitis. Virology 233:260-270.
Pinteaux E, Trotter P, Simi A (2009) Cell-specific and concentration-dependent actions of interleukin-1 in acute brain inflammation. Cytokine 45:1-7.
Platko JD, Deeg M, Thompson V, Al-Hinai Z, Glick H, Pontius K, Colussi P, Taron C, Kaplan DL (2008) Heterologous expression of Mytilus californianus foot protein three (Mcfp-3) in Kluyveromyces lactis. Protein Expres Purif 57:57-62.
Priestle JP, Schar HP, Grutter MG (1988) Crystal structure of the cytokine interleukin-1 beta. The EMBO journal 7:339-343.
Priestle JP, Schar HP, Grutter MG (1989) Crystallographic refinement of interleukin 1 beta at 2.0 A resolution. Proceedings of the National Academy of Sciences of the United States of America 86:9667-9671.
Rajalingam D, Kacer D, Prudovsky I, Kumar TK (2007) Molecular cloning, overexpression and characterization of human interleukin 1alpha. Biochemical and biophysical research communications 360:604-608.
Rausch UP, Jordan M, Rodel F, Aigner T, Otterness IG, Beuscher N, Rollinghoff M, Beuscher HU (1994) Transcriptional and translational regulation of IL-1 alpha and IL-1 beta account for the control of IL-1 in experimental yersiniosis. Cytokine 6:504-511.
Rider P, Carmi Y, Guttman O, Braiman A, Cohen I, Voronov E, White MR, Dinarello CA, Apte RN (2011) IL-1alpha and IL-1beta recruit different myeloid cells and promote different stages of sterile inflammation. J Immunol 187:4835-4843.
Rivieccio MA, John GR, Song X, Suh HS, Zhao Y, Lee SC, Brosnan CF (2005) The cytokine IL-1beta activates IFN response factor 3 in human fetal astrocytes in culture. J Immunol 174:3719-3726.
Rogers HW, Tripp CS, Schreiber RD, Unanue ER (1994) Endogenous IL-1 is required for neutrophil recruitment and macrophage activation during murine listeriosis. J Immunol 153:2093-2101.
Romanovsky AA, Almeida MC, Aronoff DM, Ivanov AI, Konsman JP, Steiner AA, Turek VF (2005) Fever and hypothermia in systemic inflammation: recent discoveries and revisions. Front Biosci 10:2193-2216.
Rosenwasser LJ, Dinarello CA, Rosenthal AS (1979) Adherent cell function in murine T-lymphocyte antigen recognition. IV. Enhancement of murine T-cell antigen recognition by human leukocytic pyrogen. The Journal of experimental medicine 150:709-714.
Rothwell N (2003) Interleukin-1 and neuronal injury: mechanisms, modification, and therapeutic potential. Brain, behavior, and immunity 17:152-157.
Ryan GB, Majno G (1977) Acute inflammation. A review. Am J Pathol 86:183-276.
Schmidt JA, Mizel SB, Cohen D, Green I (1982) Interleukin 1, a potential regulator of fibroblast proliferation. J Immunol 128:2177-2182.
Schreuder H, Tardif C, Trump-Kallmeyer S, Soffientini A, Sarubbi E, Akeson A, Bowlin T, Yanofsky S, Barrett RW (1997) A new cytokine-receptor binding mode revealed by the crystal structure of the IL-1 receptor with an antagonist. Nature 386:194-200.
Schreuder HA, Rondeau JM, Tardif C, Soffientini A, Sarubbi E, Akeson A, Bowlin TL, Yanofsky S, Barrett RW (1995) Refined crystal structure of the interleukin-1 receptor antagonist.

Presence of a disulfide link and a cis-proline. European journal of biochemistry / FEBS 227:838-847.
Sheehan D (2000) Physical biochemistry. Principles and applications. Great Britain: John Wiley and Sons Ltd.
Shin J, Lee W, Lee W (2008) Structural proteomics by NMR spectroscopy. Expert Rev Proteomics 5:589-601.
Sieff CA, Tsai S, Faller DV (1987) Interleukin 1 induces cultured human endothelial cell production of granulocyte-macrophage colony-stimulating factor. J Clin Invest 79:48-51.
Sims JE (2002) IL-1 and IL-18 receptors, and their extended family. Curr Opin Immunol 14:117-122.
Sims JE, Acres RB, Grubin CE, McMahan CJ, Wignall JM, March CJ, Dower SK (1989) Cloning the interleukin 1 receptor from human T cells. Proceedings of the National Academy of Sciences of the United States of America 86:8946-8950.
Sims JE, Gayle MA, Slack JL, Alderson MR, Bird TA, Giri JG, Colotta F, Re F, Mantovani A, Shanebeck K, et al. (1993) Interleukin 1 signaling occurs exclusively via the type I receptor. Proceedings of the National Academy of Sciences of the United States of America 90:6155-6159.
Sims JE, March CJ, Cosman D, Widmer MB, MacDonald HR, McMahan CJ, Grubin CE, Wignall JM, Jackson JL, Call SM, et al. (1988) cDNA expression cloning of the IL-1 receptor, a member of the immunoglobulin superfamily. Science 241:585-589.
Sims JE, Smith DE (2003) Regulation of interleukin-1 activity is enhanced by cooperation between the interleukin-1 receptor type II and interleukin-1 receptor accessory protein. European cytokine network 14:77-81.
Sims JE, Smith DE (2010) The IL-1 family: regulators of immunity. Nature reviews 10:89-102.
Slack J, McMahan CJ, Waugh S, Schooley K, Spriggs MK, Sims JE, Dower SK (1993) Independent binding of interleukin-1 alpha and interleukin-1 beta to type I and type II interleukin-1 receptors. The Journal of biological chemistry 268:2513-2524.
Sorensen HP, Mortensen KK (2005a) Advanced genetic strategies for recombinant protein expression in Escherichia coli. J Biotechnol 115:113-128.
Sorensen HP, Mortensen KK (2005b) Soluble expression of recombinant proteins in the cytoplasm of Escherichia coli. Microb Cell Fact 4:1.
Sreerama N, Woody RW (2000) Estimation of protein secondary structure from circular dichroism spectra: comparison of CONTIN, SELCON, and CDSSTR methods with an expanded reference set. Anal Biochem 287:252-260.
Steinkasserer A, Spurr NK, Cox S, Jeggo P, Sim RB (1992) The human IL-1 receptor antagonist gene (IL1RN) maps to chromosome 2q14-q21, in the region of the IL-1 alpha and IL-1 beta loci. Genomics 13:654-657.
Stults JT, Arnott D (2005) Proteomics. Methods Enzymol 402:245-289.
Subramaniam S, Stansberg C, Cunningham C (2004) The interleukin 1 receptor family. Developmental and comparative immunology 28:415-428.
Sugiki T, Shimada I, Takahashi H (2008) Stable isotope labeling of protein by Kluyveromyces lactis for NMR study. J Biomol NMR 42:159-162.
Sullivan B, Magliery T (2010) Operating the OSU Chemistry Jasco J-815 Circular Dichroism Spectrometer. (Magliery, T., ed) http://chemistry.osu.edu/files/page/2918/Operating the Jasco CD_2.pdf.
Swaim CL, Anton BP, Sharma SS, Taron CH, Benner JS (2008) Physical and computational analysis of the yeast Kluyveromyces lactis secreted proteome. Proteomics 8:2714-2723.
Tacheny A, dos Santos S, Huet AC, van Steenbrugge M, Michiels C, Holvoet P, Raes M (2002) Effects of homocysteine on the cellular responses of murine endothelial cells cultured in vitro. Annals of the New York Academy of Sciences 973:550-554.
Takeda K, Kaisho T, Akira S (2003) Toll-like receptors. Annual review of immunology 21:335-376.
Teodorescu M, McAfee M, Skosey JL, Wallman J, Shaw A, Hanly WC (1991) Covalent disulfide binding of human IL-1 beta to alpha 2-macroglobulin: inhibition by D-penicillamine. Mol Immunol 28:323-331.

Tewari A, Buhles WC, Jr., Starnes HF, Jr. (1990) Preliminary report: effects of interleukin-1 on platelet counts. Lancet 336:712-714.
Thery C, Mallat M (1993) Influence of interleukin-1 and tumor necrosis factor alpha on the growth of microglial cells in primary cultures of mouse cerebral cortex: involvement of colony-stimulating factor 1. Neurosci Lett 150:195-199.
Thomas C, Bazan JF, Garcia KC (2012) Structure of the activating IL-1 receptor signaling complex. Nat Struct Mol Biol 19:455-457.
Thornberry NA, Bull HG, Calaycay JR, Chapman KT, Howard AD, Kostura MJ, Miller DK, Molineaux SM, Weidner JR, Aunins J, et al. (1992) A novel heterodimeric cysteine protease is required for interleukin-1 beta processing in monocytes. Nature 356:768-774.
Thornton P, McColl BW, Greenhalgh A, Denes A, Allan SM, Rothwell NJ (2010) Platelet interleukin-1alpha drives cerebrovascular inflammation. Blood 115:3632-3639.
Tokunaga M, Ishibashi M, Tatsuda D, Tokunaga H (1997) Secretion of mouse alpha-amylase from Kluyveromyces lactis. Yeast 13:699-706.
Torres E, Gutierrez-Lopez MD, Mayado A, Rubio A, O'Shea E, Colado MI (2011) Changes in interleukin-1 signal modulators induced by 3,4-methylenedioxymethamphetamine (MDMA): regulation by CB2 receptors and implications for neurotoxicity. Journal of neuroinflammation 8:53.
Trebec-Reynolds DP, Voronov I, Heersche JN, Manolson MF (2010) IL-1alpha and IL-1beta have different effects on formation and activity of large osteoclasts. Journal of cellular biochemistry 109:975-982.
Trevani AS, Andonegui G, Giordano M, Lopez DH, Gamberale R, Minucci F, Geffner JR (1999) Extracellular acidification induces human neutrophil activation. J Immunol 162:4849-4857.
Tsai AM, van Zanten JH, Betenbaugh MJ (1998) I. Study of protein aggregation due to heat denaturation: A structural approach using circular dichroism spectroscopy, nuclear magnetic resonance, and static light scattering. Biotechnol Bioeng 59:273-280.
Tsakiri N, Kimber I, Rothwell NJ, Pinteaux E (2008) Differential effects of interleukin-1 alpha and beta on interleukin-6 and chemokine synthesis in neurones. Molecular and cellular neurosciences 38:259-265.
Turner M, Chantry D, Buchan G, Barrett K, Feldmann M (1989) Regulation of expression of human IL-1 alpha and IL-1 beta genes. J Immunol 143:3556-3561.
Uciechowski P, Saklatvala J, von der Ohe J, Resch K, Szamel M, Kracht M (1996) Interleukin 1 activates jun N-terminal kinases JNK1 and JNK2 but not extracellular regulated MAP kinase (ERK) in human glomerular mesangial cells. FEBS letters 394:273-278.
van Ooyen AJJ, Dekker P, Huang M, Olsthoorn MMA, Jacobs DI, Colussi PA, Taron CH (2006) Heterologous protein production in the yeast Kluyveromyces lactis. Fems Yeast Research 6:381-392.
Vela JM, Molina-Holgado E, Arevalo-Martin A, Almazan G, Guaza C (2002) Interleukin-1 regulates proliferation and differentiation of oligodendrocyte progenitor cells. Molecular and cellular neurosciences 20:489-502.
Vermeulen M, Giordano M, Trevani AS, Sedlik C, Gamberale R, Fernandez-Calotti P, Salamone G, Raiden S, Sanjurjo J, Geffner JR (2004) Acidosis improves uptake of antigens and MHC class I-restricted presentation by dendritic cells. J Immunol 172:3196-3204.
Vigers GP, Anderson LJ, Caffes P, Brandhuber BJ (1997) Crystal structure of the type-I interleukin-1 receptor complexed with interleukin-1beta. Nature 386:190-194.
Vigers GP, Caffes P, Evans RJ, Thompson RC, Eisenberg SP, Brandhuber BJ (1994) X-ray structure of interleukin-1 receptor antagonist at 2.0-A resolution. The Journal of biological chemistry 269:12874-12879.
Vigers GP, Dripps DJ, Edwards CK, 3rd, Brandhuber BJ (2000) X-ray crystal structure of a small antagonist peptide bound to interleukin-1 receptor type 1. The Journal of biological chemistry 275:36927-36933.
Vogt G, Woell S, Argos P (1997) Protein thermal stability, hydrogen bonds, and ion pairs. J Mol Biol 269:631-643.

Wang D, Zhang S, Li L, Liu X, Mei K, Wang X (2010) Structural insights into the assembly and activation of IL-1beta with its receptors. Nat Immunol 11:905-911.
Wang P, Guan PP, Wang T, Yu X, Guo JJ, Konstantopoulos K, Wang ZY (2014) Interleukin-1beta and cyclic AMP mediate the invasion of sheared chondrosarcoma cells via a matrix metalloproteinase-1-dependent mechanism. Biochim Biophys Acta 1843:923-933.
Wang T, Joshi SB, Kumru OS, Telikepalli S, Middaugh CR, Volkin DB (2013a) Case studies applying biophysical techniques to better characterize protein aggregates and particulates of varying size. In: Biophysics for therapeutic protein development, vol. 4 (Narhi, L. O., ed), pp 205-243 New York: Springer Science+Business Media.
Wang T, Kumru OS, Yi L, Wang YJ, Zhang J, Kim JH, Joshi SB, Middaugh CR, Volkin DB (2013b) Effect of ionic strength and pH on the physical and chemical stability of a monoclonal antibody antigen-binding fragment. J Pharm Sci 102:2520-2537.
Ward LD, Matthews JM, Zhang JG, Simpson RJ (1995) Equilibrium denaturation of recombinant murine interleukin-6: effect of pH, denaturants, and salt on formation of folding intermediates. Biochemistry 34:11652-11659.
Ward LD, Zhang JG, Checkley G, Preston B, Simpson RJ (1993) Effect of pH and denaturants on the folding and stability of murine interleukin-6. Protein Sci 2:1291-1300.
Wei-xu H, Qin X, Zhu W, Yuan-yi C, Li-feng Z, Zhi-yong L, Dan H, Xiao-mu W, Guo-zhu H (2014) Therapeutic potential of anti-IL-1beta IgY in guinea pigs with allergic asthma induced by ovalbumin. Mol Immunol 58:139-149.
Weickert MJ, Doherty DH, Best EA, Olins PO (1996) Optimization of heterologous protein production in Escherichia coli. Curr Opin Biotechnol 7:494-499.
Werman A, Werman-Venkert R, White R, Lee JK, Werman B, Krelin Y, Voronov E, Dinarello CA, Apte RN (2004) The precursor form of IL-1alpha is an intracrine proinflammatory activator of transcription. Proceedings of the National Academy of Sciences of the United States of America 101:2434-2439.
Wesche H, Henzel WJ, Shillinglaw W, Li S, Cao Z (1997a) MyD88: an adapter that recruits IRAK to the IL-1 receptor complex. Immunity 7:837-847.
Wesche H, Korherr C, Kracht M, Falk W, Resch K, Martin MU (1997b) The interleukin-1 receptor accessory protein (IL-1RAcP) is essential for IL-1-induced activation of interleukin-1 receptor-associated kinase (IRAK) and stress-activated protein kinases (SAP kinases). The Journal of biological chemistry 272:7727-7731.
Wesche H, Neumann D, Resch K, Martin MU (1996) Co-expression of mRNA for type I and type II interleukin-1 receptors and the IL-1 receptor accessory protein correlates to IL-1 responsiveness. FEBS letters 391:104-108.
Wesche H, Resch K, Martin MU (1998) Effects of IL-1 receptor accessory protein on IL-1 binding. FEBS letters 429:303-306.
Woody RW (1994) Contributions of tryptophan side chains to the far-ultraviolet circular dichroism of proteins. Eur Biophys J 23:253-262.
Woody RW (1995) Circular dichroism. Methods Enzymol 246:34-71.
Wuthrich K (1989) Protein structure determination in solution by nuclear magnetic resonance spectroscopy. Science 243:45-50.
Yamasaki Y, Matsuura N, Shozuhara H, Onodera H, Itoyama Y, Kogure K (1995) Interleukin-1 as a pathogenetic mediator of ischemic brain damage in rats. Stroke 26:676-680; discussion 681.
Yamayoshi M, Ohue M, Kawashima H, Kotani H, M II, Kawata S, Yamada M (1990) A human IL-1 alpha derivative which lacks prostaglandin E2 inducing activity and inhibits the activity of IL-1 through receptor competition. Lymphokine Res 9:405-413.
Yang T, Roder KE, Abbruscato TJ (2007) Evaluation of bEnd5 cell line as an in vitro model for the blood-brain barrier under normal and hypoxic/aglycemic conditions. J Pharm Sci 96:3196-3213.
Yoon JH, Johnson E, Xu R, Martin LT, Martin PT, Montanaro F (2012) Comparative proteomic profiling of dystroglycan-associated proteins in wild type, mdx, and Galgt2 transgenic mouse skeletal muscle. J Proteome Res 11:4413-4424.

Zhang Y, Center DM, Wu DM, Cruikshank WW, Yuan J, Andrews DW, Kornfeld H (1998) Processing and activation of pro-interleukin-16 by caspase-3. The Journal of biological chemistry 273:1144-1149.

Appendix 1: Plasmids and sequences

pET-15b

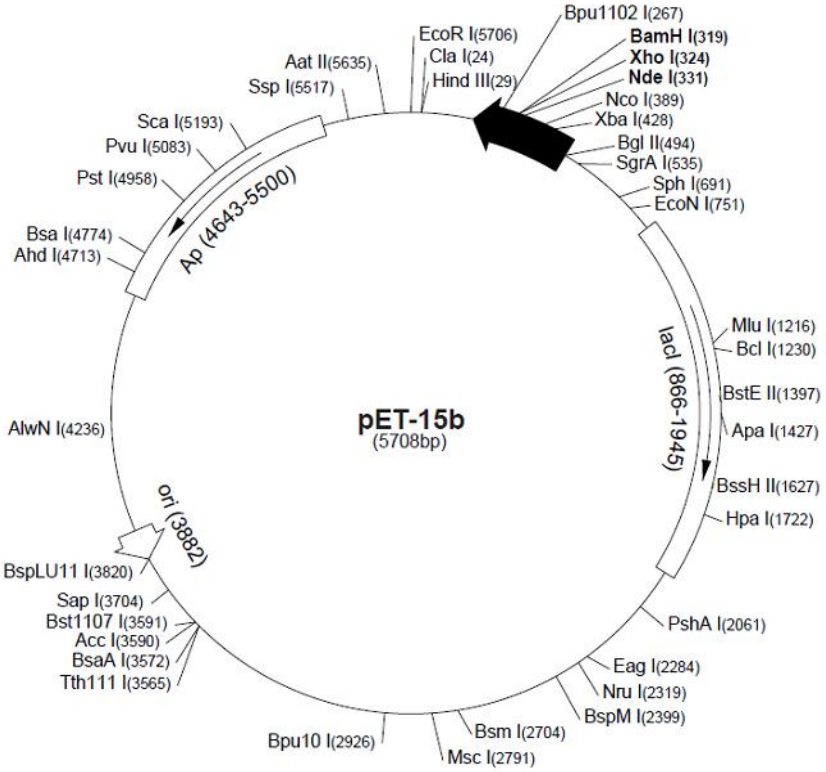

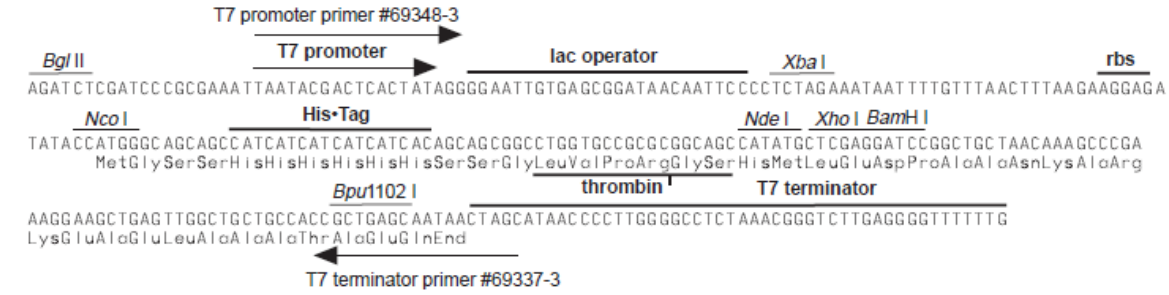

pET-15b cloning/expression region

pQE-30 vector

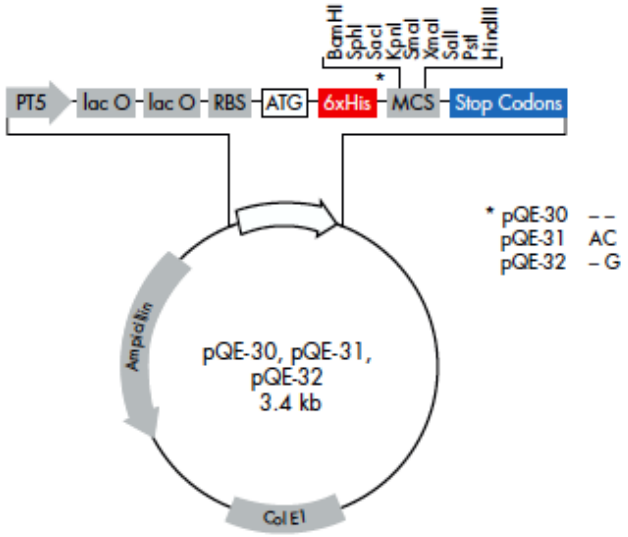

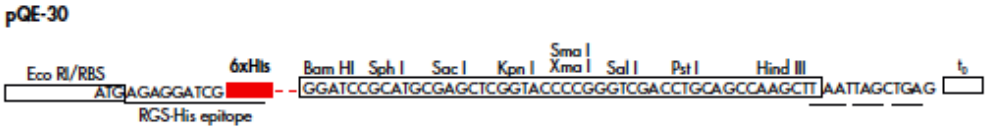

pKLAC2 vector

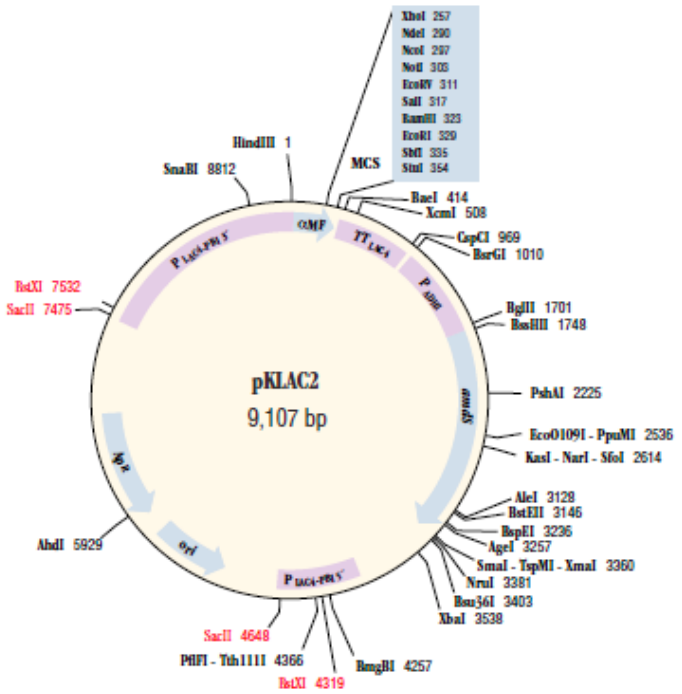


```
9009   GAATTGTGAGCGGATAACAAGCTCAACACTTGAAATTTAGGAAAGAGCAGAATTTGGCAA   9068

                                                      HindIII
9069   AAAAAATAAAAAAAAAAATAAACACACATACTCATCGAGAAGCTTGAAAAAAATGAAATTC     22
                                                        M  K  F

  23   TCTACTATATTAGCCGCATCTACTGCTTTAATTTCCGTTGTTATGGCTGCTCCAGTTTCT     82
       S  T  I  L  A  A  S  T  A  L  I  S  V  V  M  A  A  P  V  S

  83   ACCGAAACTGACATCGACGATCTTCCAATATCGGTTCCAGAAGAAGCCTTGATTGGATTC    142
       T  E  T  D  I  D  D  L  P  I  S  V  P  E  E  A  L  I  G  F

 143   ATTGACTTAACCGGGGATGAAGTTTCCTTGTTGCCTGTTAATAACGGAACCCACACTGGT    202
       I  D  L  T  G  D  E  V  S  L  L  P  V  N  N  G  T  H  T  G

                                                            XhoI
 203   ATTCTATTCTTAAACACCACCATCGCTGAAGCTGCTTTCGCTGACAAGGATGATCTCGAG    262
       I  L  F  L  N  T  T  I  A  E  A  A  F  A  D  K  D  D  L  E

                                  NdeI     NcoI     NotI     EcoRV  SalI
 263   AAAAGAGAGGCTGAAGCTAGAAGAGCTCATATGTCCATGGGCGGCCGCGATATCGTCGAC    322
       K  R  E  A  E  A  R  R  A  H  M  S  M  G  G  R  D  I  V  D

       BamHI  EcoRI  SbfI                  StuI
 323   GGATCCGAATTCCCTGCAGGTAATTAAATAAAGGCCTTGAATCGAGAATTTATACTTAGA    382
        G  S  E  F  P  A  G  N  *

 383   TAAGTATGTACTTACAGGTATATTTCTATGAGATACTGATGTATACATGCATGATAATAT    442

 443   TTAAACGGTTATTAGTGCCGATTGTCTTGTGCGATAATGACGTTCCTATCAAAGCAATAC    502
```

Full-length sequences of IL-1 proteins. Sequences used for protein constructs used in this work are underlined.

Interleukin-1 alpha pro-protein (*Homo sapiens*)

NCBI Reference Sequence: NP_000566.3

MAKVPDMFEDLKNCYSENEEDSSSIDHLSLNQKSFYHVSYGPLHEGCMDQSVSLSI
SETSKTSKLTFKESMVVVATNGKVLKKRRLSLSQSITDDDLEAIANDSEEEIIKPR
SAPFSFLSNVKYNFMRIIKYEFILNDALNQSIIRANDQYLTAAALHNLDEAVKFDM
GAYKSSKDDAKITVILRISKTQLYVTAQDEDQPVLLKEMPEIPKTITGSETNLLFF
WETHGTKNYFTSVAHPNLFIATKQDYWVCLAGGPPSITDFQILENQA

Interleukin-1 beta pro-protein (*Homo sapiens*)

NCBI Reference Sequence: NP_000567.1

MAEVPELASEMMAYYSGNEDDLFFEADGPKQMKCSFQDLDLCPLDGGIQLRISDHH
YSKGFRQAASVVVAMDKLRKMLVPCPQTFQENDLSTFFPFIFEEEPIFFDTWDNEA
YVHDAPVRSLNCTLRDSQQKSLVMSGPYELKALHLQGQDMEQQVVFSMSFVQGEES
NDKIPVALGLKEKNLYLSCVLKDDKPTLQLESVDPKNYPKKKMEKRFVFNKIEINN
KLEFESAQFPNWYISTSQAENMPVFLGGTKGGQDITDFTMQFVSS

Interleukin-1 Receptor type I (*Homo sapiens*)

UniProtKB/Swiss-Prot: P14778.1

MKVLLRLICFIALLISSLEADKCKEREEKIILVSSANEIDVRPCPLNPNEHKGTIT
WYKDDSKTPVSTEQASRIHQHKEKLWFVPAKVEDSGHYYCVVRNSSYCLRIKISAK
FVENEPNLCYNAQAIFKQKLPVAGDGGLVCPYMEFFKNENNELPKLQWYKDCKPLL
LDNIHFSGVKDRLIVMNVAEKHRGNYTCHASYTYLGKQYPITRVIEFITLEENKPT
RPVIVSPANETMEVDLGSQIQLICNVTGQLSDIAYWKWNGSVIDEDDPVLGEDYYS
VENPANKRRSTLITVLNISEIESRFYKHPFTCFAKNTHGIDAAYIQLIYPVTNFQK
HMIGICVTLTVIIVCSVFIYKIFKIDIVLWYRDSCYDFLPIKASDGKTYDAYILYP
KTVGEGSTSDCDIFVFKVLPEVLEKQCGYKLFIYGRDDYVGEDIVEVINENVKKSR
RLIIILVRETSGFSWLGGSSEEQIAMYNALVQDGIKVVLLELEKIQDYEKMPESIK
FIKQKHGAIRWSGDFTQGPQSAKTRFWKNVRYHMPVQRRSPSSKHQLLSPATKEKL
QREAHVPLG

Interleukin-1 Receptor Accessory Protein

UniProtKB/Swiss-Prot: Q9NPH3.2

MTLLWCVVSLYFYGILQSDASERCDDWGLDTMRQIQVFEDEPARIKCPLFEHFLKF
NYSTAHSAGLTLIWYWTRQDRDLEEPINFRLPENRISKEKDVLWFRPTLLNDTGNY
TCMLRNTTYCSKVAFPLEVVQKDSCFNSPMKLPVHKLYIEYGIQRITCPNVDGYFP
SSVKPTITWYMGCYKIQNFNNVIPEGMNLSFLIALISNNGNYTCVVTYPENGRTFH
LTRTLTVKVVGSPKNAVPPVIHSPNDHVVYEKEPGEELLIPCTVYFSFLMDSRNEV
WWTIDGKKPDDITIDVTINESISHSRTEDETRTQILSIKKVTSEDLKRSYVCHARS
AKGEVAKAAKVKQKVPAPRYTVELACGFGATVLLVVILIVVYHVYWLEMVLFYRAH
FGTDETILDGKEYDIYVSYARNAEEEEFVLLTLRGVLENEFGYKLCIFDRDSLPGG
IVTDETLSFIQKSRRLLVVLSPNYVLQGTQALLELKAGLENMASRGNINVILVQYK
AVKETKVKELKRAKTVLTVIKWKGEKSKYPQGRFWKQLQVAMPVKKSPRRSSSDEQ
GLSYSSLKNV

Appendix 2: *E. coli* Strains and media

M1. Characteristics of *E. coli* strains used in this work

Strain	Genotype	Antibiotic resistance
Origami[1]	Δ(*ara–leu)7697* Δ*lacX74* Δ*phoA PvuII phoR araD139 ahpC galE galK rpsL* F'[lac^+ *lacI q pro*] *gor522*::Tn*10 trxB*	Kan, Str, Tet
Rosetta-gami 2[1]	Δ(*ara–leu)7697* Δ*lacX74* Δ*phoA PvuII phoR araD139 ahpC galE galK rpsL* F'[lac^+ *lacI q pro*] *gor522*::Tn*10 trxB* pRARE2	Cam, Str, Tet
Shuffle T7 Express[2]	*fhuA2 lacZ::T7 gene1 [lon] ompT ahpC gal λatt::pNEB3-r1-cDsbC* ($Spec^R$, $lacI^q$) *ΔtrxB sulA11 R(mcr-73::miniTn10*--Tet^S*)2 [dcm] R(zgb-210::Tn10* --Tet^S*) endA1 Δgor Δ(mcrC-mrr)114::IS10*	Str, Spc
Shuffle T7 Express Lys Y[2]	*MiniF lysY (*Cam^R*) / fhuA2 lacZ::T7 gene1 [lon] ompT ahpC gal λatt::pNEB3-r1-cDsbC* ($Spec^R$, $lacI^q$) *ΔtrxB sulA11 R(mcr-73::miniTn10*--Tet^S*)2 [dcm] R(zgb-210::Tn10* --Tet^S*) endA1 Δgor Δ(mcrC-mrr)114::IS10*	Cam, Str, Spc
DH5α[3]	F- Φ80*lac*Z(M15 ((*lac*ZYA-*arg*F)U169 *deo*R *rec*A1 *end*A1 *hsd*R17 (r_κ^-, m_κ^+) *pho*A *sup*E44 *thi*-1 *gyr*A96 *rel*A1 λ^-	_____

[1] Novagen, UK; [2] New England Bioloabs, UK; [3] Invitrogen

M2. Antibiotics concentrations used for plasmid and strains selection

Antibiotic	Name	[µg/mL]
Amp	Ampicillin	50
Cam	Chloramphenicol	34
Carb	Carbenicilin	50
Kan	Kanamycin	15
Spc	Spectinomycin	50
Str	Streptomycin	25
Tet	Tetracycline	12.5

M3. Luria-Bertani broth medium (LB):

10 g	Tryptone
5 g	Yeast extract
10 g	NaCl

M4. Yeast-peptone Glu/Gal media (2 L)

Yeast extrac	20 g
Peptone	40 g
MQ-H_2O	1900 mL
Glu/Gal	100 mL[1]

[1] From 40% stock

M5. Yeast Carbon-Based Agar Medium (500 mL)

Tris-HCl (1M)	15 mL
YCB powder	5.85 g
Agar	10 g
MQ-H_2O	495 mL
Acetamide (100 x)	5 mL

APPENDIX 3: Buffers and solutions

SDS-PAGE

M1. Sample/loading Buffer

3.55 mL	dH_2O
1.25 mL	0.5 M Tris-HCl, pH 6.8
2.5 mL	Glycerol
2.0 mL	10% (w/v) SDS
0.2 mL	0.5% (w/v) Bromophenol Blue
9.5 mL	Total volume

M2. 4 x Lower (resolving) buffer

1.5 M	Tris-HCl, pH 8.8	181.65 g
0.4 %	SDS w/v	

M3. 4 x Upper (stacking) buffer

0.5 M	Tris-HCl, pH 6.8	60.55 g
0.4 %	SDS w/v	

M4. 10x Running buffer (1L)

30.3 g	Tris base
144.0 g	Glycine
10.0 g	SDS

M5. Gel strength

Percent gel	dH_2O (mL)	Acrylamide (mL)	4xbuffer (mL)
4%	6.2	1.3	2.5
5%	5.8	1.7	2.5
6%	5.5	2.0	2.5
7%	5.2	2.3	2.5
8%	4.8	2.7	2.5
9%	4.5	3.0	2.5
10%	4.2	3.3	2.5
11%	3.8	3.7	2.5
12%	3.5	4.0	2.5
13%	3.2	4.3	2.5
14%	2.8	4.7	2.5
15%	2.5	5.0	2.5
16%	2.2	5.3	2.5
17%	1.8	5.7	2.5

To prepare, mix the volumes shown above in a universal and then as before add 50 µl of 10% APS plus 20 µl of TEMED and pour the gels as before.

BIS-Tris SDS-PAGE

M1. 3.5 x gel buffer

Bis-Tris	1.25 M
pH 6.8 adjust with HCl	

M2. 5 x High molecular weight Running Buffer

MOPS	250 mM
Tris	250 mM
EDTA	5 mM
SDS	0.5%
Sodium bisulfite	5 mM

M3. 5 x Low molecular weight Running Buffer

MES	250 mM
Tris	250 mM
EDTA	5 mM
SDS	0.5%
Sodium bisulfite	5 mM

M4. Bis-Tris gel strength

	Upper gel	**Lower gel**			
	4%	**8%**	**10%**	**12%**	**15%**
H_2O	5.2 mL	3.1 mL	2.2 mL	1.2 mL	-
Acrylamide[1]	1.3 mL	2.7 mL	3.3 mL	4 mL	5 mL
Bis-acrylamide	580 µl	1.2 mL	1.5 mL	1.8 mL	2.2 mL
3.5 x gel buffer	2.9 mL	2.9 mL	2.9 mL	2.9 mL	2.9 mL
APS	50 µl	50 µl	50 µl	50 µl	50 µl
TEMED	20 µl	25 µl	25 µl	25 µl	25 µl
Bromophenol blue	25 µl	-	-	-	-
TOTAL VOLUME	10 mL	10 mL			

[1] 30% Acrylamide solution 29:1 (0.8% bis-acrylamide)

Purification Buffers

M1. Buffers for IL-1α IMAC Purification pH 8

	Lysis	Wash/Equilibration	Elution
NaH_2PO_4	20 mM	20 mM	20 mM
Na_2HPO_4	20 mM	20 mM	20 mM
NaCl	300 mM	300 mM	300 mM
Arg + Glu	50 mM	50 mM	50 mM
Imidazole	20 mM	20 mM	300 mM
β-mercaptoethanol	5 mM	5 mM	5 mM
Triton X-100	0.5%	-	-
DNAse	10 μg/mL	-	-
RNAse	10 μg/mL	-	-
Mg_2Cl	5 mM	-	-

M2. Buffers for IL-1β IMAC Purification pH 7

	Lysis	Wash/Equilibration	Elution
Tris	50 mM	50 mM	50 mM
NaCl	150 mM	150 mM	150 mM
Arg + Glu	50 mM	50 mM	50 mM
Imidazole	10 mM	20 mM	300 mM
Triton X-100	0.5%	-	-
DNAse	10 μg/mL	-	-
RNAse	10 μg/mL	-	-
Mg_2Cl	5 mM	-	-

M3. Cation Exchange buffers for purification trials

Buffer	pKa	pH	[mM]	Buffer A	Buffer B
Formic acid	3.75	4	50		
Acetic acid	4.74	4.5	50		
Acetic acid	4.75	5	50	0	1M
Acetic acid	4.75	5.5	50	NaCl	NaCl
MES	6.27	6	50		
MES	6.27	6.5	50		

M4. Anion Exchange buffers for purification trials

Buffer	pKa	pH	[mM]	Buffer A	Buffer B
MOPS	7.15	7	50		
HEPES	7.55	7.5	50		
HEPES	7.55	8	50	0 NaCl	1M NaCl
Tris	8.07	8	50		
Tris	8.07	8.5	50		

M5. NMR buffer

20 mM	Phosphates
50 mM	Arg + Glu
50 mM	β-mercaptoethanol
10 mM	EDTA
10 mM	DTT
50 mM	NaCl

APPENDIX 4: Supplementary material

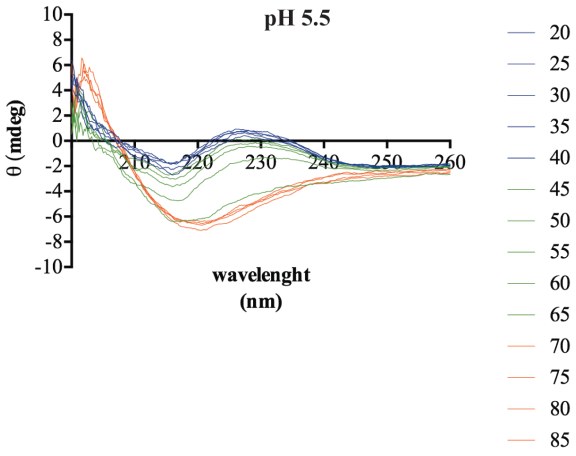

IL-1α pH 5.5 Dichroweb analysis

T (°C)	α-helix	β-sheets	coil
20	0.04	0.48	0.48
25	0.04	0.48	0.48
30	0.04	0.48	0.48
35	0.04	0.48	0.48
40	0.04	0.48	0.48
45	0.04	0.48	0.48
50	0.04	0.48	0.48
55	0.04	0.48	0.48
60	0.04	0.48	0.48
65	0.05	0.48	0.48
70	0.04	0.48	0.48
75	0.03	0.49	0.47
80	0.04	0.48	0.48
85	0.03	0.49	0.47

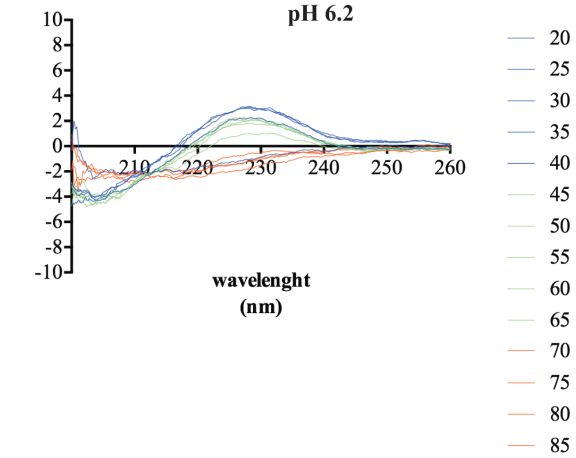

IL-1α pH 6.2 Dichroweb analysis

T (°C)	α-helix	β-sheets	coil
20	0.06	0.46	0.48
25	0.08	0.48	0.44
30	0.08	0.48	0.44
35	0.08	0.48	0.44
40	0.08	0.48	0.44
45	0.08	0.48	0.44
50	0.08	0.48	0.44
55	0.08	0.48	0.44
60	0.08	0.48	0.44
65	0.09	0.48	0.44
70	0.1	0.44	0.46
75	0.07	0.45	0.48
80	0.06	0.46	0.48
85	0.07	0.45	0.48

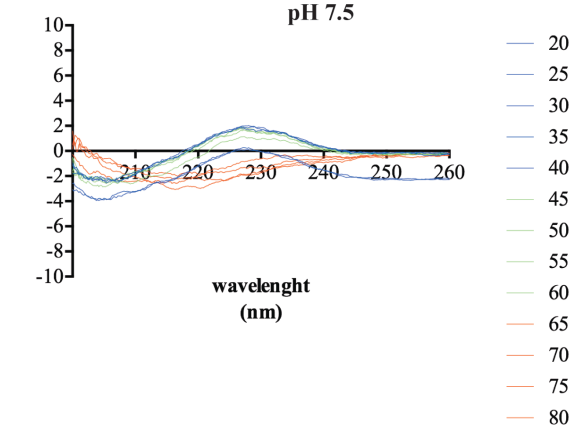

IL-1α pH 7.5 Dichroweb analysis

T (°C)	α-helix	β-sheets	coil
20	0.08	0.48	0.44
25	0.08	0.48	0.45
30	0.09	0.47	0.44
35	0.09	0.47	0.44
40	0.08	0.48	0.44
45	0.08	0.48	0.44
50	0.09	0.48	0.44
55	0.08	0.48	0.44
60	0.08	0.48	0.44
65	0.07	0.45	0.48
70	0.05	0.47	0.48
75	0.05	0.47	0.48
80	0.05	0.47	0.48
85	0.04	0.48	0.48

Figure A4-1. IL-1α Circular dichroism at increasing temperatures and different pH. The far UV spectra of IL-1α between 200-260 nm at each temperature tested is shown in the left panels for each pH used. Right panels show the Dichroweb analysis using the algorithm K2D.

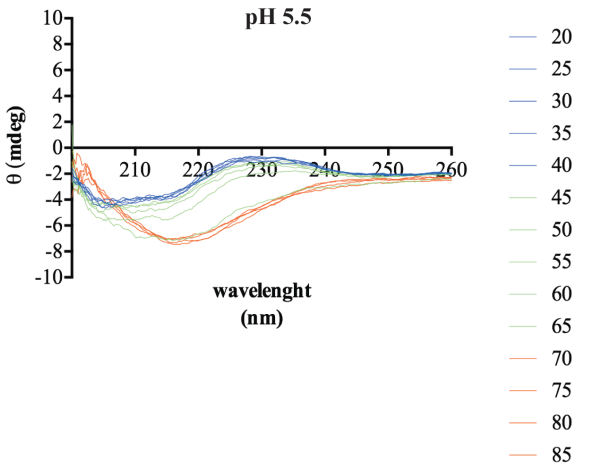

IL-1β pH 5.5 Dichroweb analysis

T (°C)	α-helix	β-sheets	coil
20	0.08	0.48	0.44
25	0.08	0.48	0.45
30	0.09	0.47	0.44
35	0.09	0.47	0.44
40	0.08	0.48	0.44
45	0.08	0.48	0.44
50	0.09	0.48	0.44
55	0.1	0.41	0.48
60	0.12	0.38	0.5
65	0.15	0.32	0.53
70	0.17	0.31	0.52
75	0.16	0.33	0.51
80	0.16	0.33	0.5
85	0.16	0.32	0.52

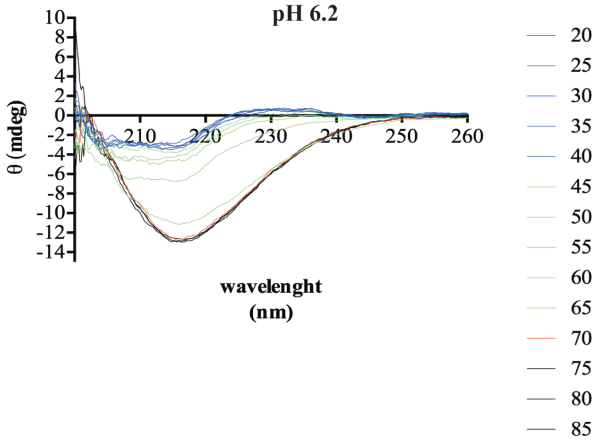

IL-1β pH 6.2 Dichroweb analysis

T (°C)	α-helix	β-sheets	coil
20	0.07	0.45	0.48
25	0.11	0.44	0.45
30	0.07	0.45	0.48
35	0.08	0.44	0.48
40	0.08	0.44	0.48
45	0.09	0.44	0.48
50	0.12	0.42	0.47
55	0.12	0.41	0.47
60	0.11	0.4	0.49
65	0.24	0.24	0.52
70	0.27	0.2	0.53
75	0.27	0.2	0.53
80	0.27	0.21	0.53
85	0.28	0.22	0.5

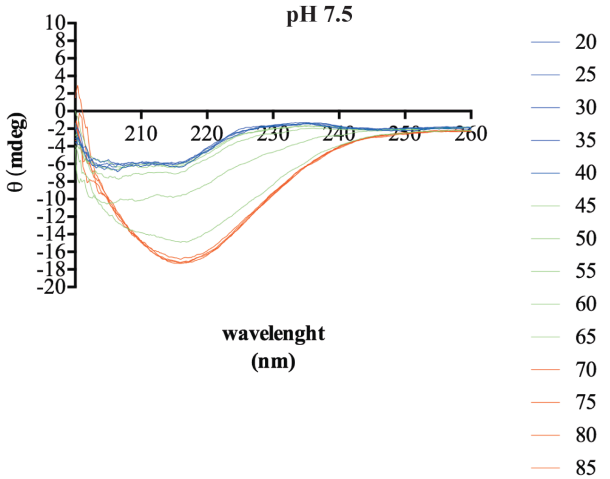

IL-1β pH 7.5 Dichroweb analysis

T (°C)	α-helix	β-sheets	coil
20	0.1	0.41	0.49
25	0.1	0.41	0.49
30	0.1	0.42	0.48
35	0.1	0.41	0.49
40	0.1	0.41	0.49
45	0.1	0.4	0.5
50	0.12	0.38	0.5
55	0.11	0.39	0.51
60	0.12	0.33	0.55
65	0.3	0.11	0.58
70	0.31	0.1	0.59
75	0.31	0.1	0.59
80	0.31	0.11	0.59
85	0.31	0.12	0.57

Figure A4-2. IL-1β Circular dichroism at increasing temperatures and different pH. The far UV spectra of IL-1α between 200-260 nm at each temperature tested is shown in the left panels for each pH used. Right panels show the Dichroweb analysis using the algorithm K2D.

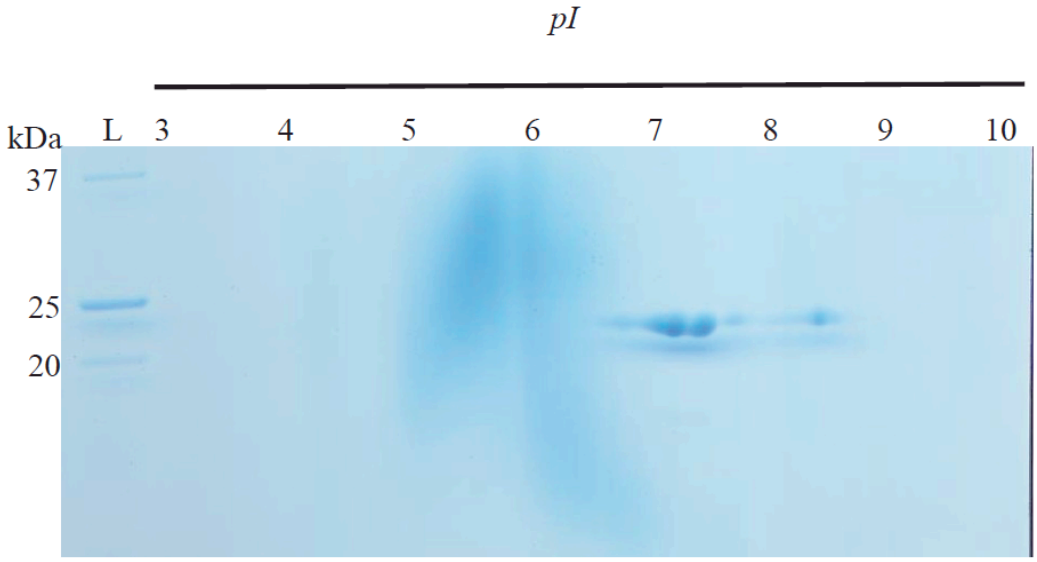

Figure A4-3 IL-1β 2D-SDS-PAGE. IL-1β purified from *E. coli* was analysed by isoelectrofocusing followed by SDS-PAGE. Three 20 kDa bands with *pI* values of 6.9, 7 and 8.2 were analysed by LC-MS/MS and identified as human IL-1β